

Antarctic Meteorites XXIV

Papers presented to the
Twentyfourth Symposium
on Antarctic Meteorites



June 1-3, 1999

南極隕石研究センター

NATIONAL INSTITUTE OF POLAR RESEARCH,
TOKYO

国立極地研究所

Tuesday, June 1, 1999

0900 - 1200 Registration Auditorium (6th Floor)
0925 - 0930 Opening Address **Yasuhiko Naito**
Chief Research Officer
National Institute of Polar Research

*Speaker

Chairmen: Tomeoka K. and Hiroi T.

Page

1	0930 - 0945	Kojima H.* , Kaiden H., and Yada T. Meteorite search of JARE in 1998-99 season	81
2	0945 - 1000	Yada T.* and Kojima H. The collection of micrometeorites in Yamato meteorite ice field of Antarctica in 1998	190
3	1000 - 1015	Itoh D.* and Tomeoka K. Dark inclusions in four CO3 carbonaceous chondrites	56
4	1015 -1030	Ohnishi I.* and Tomeoka K. Dark inclusions in the Mokoia CV3 chondrite: Record of aqueous alteration, thermal metamorphism and shock metamorphism	145
5	1030 - 1045	Yamanouchi T.* and Fujimaki H. Petrological comparison between chondrules of Sahara 97096 (EH3) and Allende (CV3)	192
6	1045 - 1100	Weisberg M. K.* and Prinz M. Zoned metal in the CR clan chondrites	187
7	1100 - 1115	Tomiyama T.* and Kitamura M. Relation between grain size distributions and the petrologic types of ordinary chondrites	177
8	1115 - 1130	Komatsu M.* and Miyamoto M. Behavior of minor elements in olivine and orthopyroxene during metamorphism in LL chondrites	85
9	1130 - 1145	Fujita T.* Formation condition of fine phosphides in metals of Yamato-790126 (L) chondrite	21
10	1145 - 1200	Ozaki H.* , Kallemeyn G. W., and Ebihara M. Weathering effects on the chemical composition of Antarctic UOCs	154
	1200 - 1300	Lunch Time	

Chairmen: Kimura M. and Kojima T.		Page
11	1300 - 1315 Kojima T.*, Yatagai T., and Tomeoka K. A dark inclusion in the Manych LL (3.1) ordinary chondrite: A product of strong shock metamorphism of unequilibrated chondritic material	82
12	1315 - 1330 Ruzicka A.*, Snyder G. A., and Taylor L. A. Origins of large, igneous-textured inclusions in ordinary chondrites	160
✓ 13	1330 - 1345 Kimura M.*, El Goresy A., Suzuki A., and Ohtani E. Heavily shocked Antarctic H-chondrites: Petrology and shock history	67
14	1345 - 1400 Funaki M.*, Tunyi I., Orlicky O., and Porubcan V. Stability of natural remanent magnetization and shock remagnetization of Rumanova (H5) chondrite	26
✓ 15	1400 - 1415 Hirata N.*, Yamaguchi A., and Sekine T. Shock deformation of silica spherules in Cu-powder pressure media: Implication for the chondrule flattening	31
16	1415 - 1430 Newton J.*, Franchi I. A., and Pillinger C. T. An oxygen isotope study of enstatite meteorites	136
17	1430 - 1445 Miura Y. N.*, Nagao K., and Okazaki R. Noble gases in five aubrites, Cumberland Falls, Mayo Belwa, Mt. Egerton, Norton County and Peña Blance Spring	108
18	1445 - 1500 Hutson M.* and Ruzicka A. A simple three-step model for the origin of the enstatite chondrites	40
	1500 - 1530 Tea Time	
-- Special Talk (I) --		
19	1530 - 1630 Lindstrom M. M.* Lunar and martian meteorites: Suites, pairing, and implications	90
	1700 - 1900 Reception Lecture room (2F)	

Wednesday, June 2, 1999

Chairmen: Ikeda Y. and Ebihara M.		Page
20	0930 - 0945 Nakamuta Y.* and Aoki Y. Carbon minerals in ureilites: Implications for the genesis of diamond	127
21	0945 - 1000 Okazaki R.*, Nakamura T., Takaoka N., and Nagao K. Crush-released noble gases from ureilites	148
22	1000 - 1015 Ikeda Y.*, Prinz M., Nehru C. E., Boesenberg J. S., and Kita N. T. Petrology of the Dar al Gani (DAG) 319 polymict ureilite	43
23	1015 - 1030 Kita N. T.*, Ikeda Y., Prinz M., Nehru C. E., Weisberg M. K., Morishita Y., and Togashi S. In-situ SIMS oxygen isotopic analyses of clasts from DAG 319 polymict ureilite	72
24	1030 - 1045 Buchanan P. C., Lindstrom D. J.*, and Lindstrom M. M. Variations in source areas and proportions of partial melting and fractional crystallization as indicated by recent eucrite analyses	4
25	1045 - 1100 Takeda H.*, Saiki K., and Ishii T. Mineralogy of Y791192, HED breccia and its cratering history on a Vesta-like body	172
26	1100 - 1115 Satoh H.* Oxygen isotope microanalysis of a zoned orthopyroxene megacryst in A-881526 diogenite	163
27	1115 - 1130 Floss C.*, Crozaz G., Yamaguchi A., and Keil K. Trace element constraints on the origins of highly metamorphosed Antarctic eucrites	18
28	1130 - 1145 Warren P. H.* Differentiation of siderophile elements in the Moon and the HED parent asteroid	185
29	1145 - 1200 Sugiura N.* and Hoshino H. H isotopic compositions in ALH84001	168
30	1200 - 1215 Hiroi T.* and Sasaki S. Space weathering of olivine as a key to understanding S/A/R/V asteroids and lunar soils	34
	1215 - 1315 Lunch Time	

Chairmen: Nagahara H. and Hiyagon H.		Page
31	1315 - 1330 Hanamoto T., Tsuchiyama A.*, Kawabata T., Koezuka T., Tsujimoto Y., and Wasson J. T. Three dimensional structure of pallasite Esquel by X-ray computed tomography	28
32	1330 - 1345 Tsukamoto K.*, Satoh H., Takamura Y., and Kuribayashi K. A new approach for the formation of olivine-chondrules by aero-acoustic levitation	179
33	1345 - 1400 Kawabata T.*, Tsuchiyama A., and Kondo M. Three dimensional structure of chondrule texture: Possibility of a spinning chondrule	64
34	1400 - 1415 Nagahara H.*, Kita N. T., Ozawa K., and Morishita Y. Chondrule formation by condensation of major elements	113
35	1415 - 1430 Tachibana S.* and Tsuchiyama A. The possibility of Mg/Si fractionation by incongruent evaporation of enstatite	169
36	1430 - 1445 Hiyagon H.* and Hashimoto A. An ion microprobe study of oxygen isotopes in various types of inclusions in Yamato-791717 (CO3) chondrite: Oxygen isotopes vs fayalite content in olivine	37
37	1445 - 1500 Jabeen I.*, Kusakabe M., Nakamura T., and Nagao K. Parent body processes in Allende: Evidence from oxygen isotope study of the Allende chondrules	59
	1500 - 1530 Tea Time	
38	1530 - 1545 Kobatake H.*, Satoh H., Tsukamoto K., and Fujimaki H. The distribution of oxygen isotopes and cations in Allende matrix	78
39	1545 - 1600 Imai H.* and Yurimoto H. Distribution of oxygen isotopes in a type-C CAI of the Allende meteorite	53
40	1600 - 1615 Ushikubo T.*, Hiyagon H., Sugiura N., and Ul'yanov A. A. Mg isotopic anomaly of two types of anorthite in CAIs	182
41	1615 - 1630 Mostefaoui S.*, Kita N. T., Nagahara H., Togashi S., and Morishita Y. A short period of chondrule formation: The ²⁶ Al- ²⁶ Mg evidence from two type II chondrules in a highly unequilibrated ordinary chondrite	111
--Special Talk (II) --		
42	1630 - 1730 MacPherson, G. J.* Mg-chondrules, Al-chondrules, and CAI: Connections	93

Thursday, June 3, 1999

Chairmen: Nagao K. and Tsuchiyama A.		Page
43	0930 - 0945 Kimura S., Kaito C.*, and Wada S. Structure of quenched carbonaceous composite (QCC) and formation of micro-diamond by heat treatment of QCC	69
44	1945 - 1000 Naraoka H.* Molecular and isotopic distributions of polyaromatic hydrocarbons (PAHs) in three Asuka carbonaceous chondrites (CM2) from Antarctica	133
45	1000 - 1015 Kiuchi H., Tachibana S.*, and Tsuchiyama A. Evaporation experiments on naphthalene (C ₁₀ H ₈) by thermogravimetry (TG)	75
46	1015 - 1030 Nagai H., Kokubo M., Kobayashi T., and Honda M.* Cosmogenic ¹⁰ Be and ²⁶ Al in iron meteorites and the inclusions	116
47	1030 - 1045 Jull A. J. T.*, Klandrud S. E., Cielaszyk E., and Cloudt S. Carbon-14 terrestrial ages of meteorites from the Yamato region, Antarctica	62
48	1045 - 1100 Ninagawa K.*, Toyoda S., Imae N., and Kojima H. Thermoluminescence of Japanese Antarctic meteorites III	139
49	1100 - 1115 Zaizen S.*, Nakasyo E., Maruoka T., and Matsuda J. Purely physical separation of the phase enriched in noble gases from the Allende meteorite	195
50	1115 - 1130 Nakasyo E.*, Maruoka T., and Matsuda J. The influence of hot water alteration on noble gas composition in the Allende meteorite	130
51	1130 - 1145 Matsuda J.*, Namba M., Maruoka T., and Kurat G. On the primordial composition of the noble gases in Canyon Diablo	99
52	1145 - 1200 Asame K.*, Kawano S., Matsuda J., Maruoka T., and Kurat G. Nitrogen isotopic signatures of metal and graphite in Canyon Diablo	1
53	1200 - 1220 Nakamura N.*, Sawada S., Tamaki M., Kondorosi G., Imae N., Kojima H., Clayton R. N., and Mayeda T. K. Consortium studies of five Antarctic Rumuruti-group chondrites: A progress report	121
	1220 - 1320 Lunch Time & Poster Session	

Chairmen: Noguchi T. and Nakamura T.		Page
54	1320 - 1335 Schnabel C., Herzog G. F.*, Taylor S., Field M. P., and Sherrell R. M. Magnesium isotope abundances in stony Antarctic micrometeorites	166
Special Session: Antarctic Micrometeorites from the Dome Fuji Station		
55	1335 - 1350 Noguchi T.*, Imae N., Nakamura T., Nozaki W., Terada K., Mori T., Nakai I., Kondo N., Sasaki M., Murakami T., Fukuoka T., Nogami K., Oomori R., and Ohashi H. Antarctic micrometeorites recovered from the Dome Fuji Station: A combined study of mineralogy, bulk chemistry, and isotopic compositions	143
56	1350 - 1405 Nakai I.*, Kondo N., Sasaki M., Terada Y., Terada K., Noguchi T., and Nakamura T. Characterization of cosmic dust samples by synchrotron radiation X-ray fluorescence analysis	119
57	1405 - 1420 Imae N.*, Noguchi T., Nakamura T., and Nozaki W. X-ray microprobe analyses of Antarctic micrometeorites from the Dome Fuji Station	50
58	1420 - 1435 Noguchi T.* and Nakamura T. Mineralogy of Antarctic micrometeorites recovered from the Dome Fuji Station	141
59	1435 - 1450 Nakamura T.*, Noguchi T., and Nakamura Y. Relative mineral abundance of individual micrometeorites collected at the Dome Fuji Station	125
60	1450 - 1505 Nakamura T. and Takaoka N.* Solar wind in micrometeorites: Characterization by stepped pyrolysis	123
	1505 - 1535 Tea Time	
61	1535 - 1550 Osawa T.*, Nagao K., Nakamura T., and Takaoka N. Noble gas measurement in individual micrometeorites using laser gas-extraction system	151
62	1550 - 1605 Terada K.*, Sano Y., Mori T., Nakamura T., Nozaki W., Noguchi T., Imae N., Fukuoka T., and Japan AMM working group Isotopic studies on Antarctic micrometeorites collected at the Dome Fuji Station in 1996 using SHRIMP	175
63	1605 - 1620 Fukuoka T.*, Tazawa Y., Terada K., Mori T., Sano Y., Nakamura T., Imae N., Noguchi T., Nogami K., Ohmori R., Murakami T., Kondo N., Nakai I., and Ohashi H. Chemical composition of glassy spherules collected at the Dome Fuji Station by the 37th JARE team	24

Postar Session**Page**

- 64** **Bérczi Sz., Gál-Sólymos K., Lukács B., and Martinás K.** 6
Measurements and theoretical studies on the ALHA 77257, 77-4 ureilite: Igneous/primitive dichotomy in its mineralogy and chemistry, paradoxes and solutions in its thermal history
- 65** **Bérczi Sz., Holba Á., and Lukács B.** 9
Splitting of the two Wiik lines in the Urey-Craig field: C-S are related to H-S like as LL-S are related to L-S (Statistical analyses of the NIPR dataset, VII)

Abstract only

- ✓ **66** **Chikami J. and Miyamoto M.** 12
The opaque mineral assemblage of matrix in L chondrites
- 67** **Detre C. H., Tóth I., Don G., Kiss A. Z., Uzonyi I., Bodó P., and Schléder Z.** 15
The Permian-Triassic supernova event
- 68** **Imae N., Nakamura N., and Kojima H.** 47
Mineralogical studies in five Rumuruti chondrites: Y-75302, Y-791827, Y-793575, Y-82002, and A-881988
- 69** **Kondorosi G., Hirota Y., Hori K., Nakamura N., Morikawa N., and Misawa K.** 88
Trace element studies of leachates and residues from the lherzolitic shergottite Y-793605
- 70** **Marakushev A. A., Bobrov A. V., and Chaplygin O. V.** 96
Antarctic chondrites in the oxygen isotopic system
- 71** **Mikouchi T., Miyamoto M., and McKay G. A.** 102
Olivine megacrysts in the basaltic Martian meteorites Dar al Gani 476 and EETA79001: Cooling rates deduced from Fe-Mg zoning of olivine
- 72** **Mitreikina O. B. and Zinovieva N. G.** 105
Differentiation of the matrix material in the Kainsaz (CO) carbonaceous chondrite
- 73** **Pinault L. J., Scott E. R. D., Bogard D. D., and Keil K.** 157
Portales Valley, a metal-veined H6 chondrite with evidence of internally-generated partial melting of Fe-Ni-S

ABSTRACTS

Nitrogen isotopic signatures of metal and graphite in Canyon Diablo

Kouichiro Asame¹, Sige Kawano¹, Jun-ichi Matsuda¹, Teruyuki Maruoka¹ and Gero Kurat²

1. Department of Earth and Space Science, Graduate School of Science, Osaka University,
Toyonaka, Osaka 560-0043, Japan

2. Naturhistorisches Museum, Postfach 417, A-1014 Viene, Austria

Introduction

The origin of the large range of nitrogen isotopic compositions in extraterrestrial samples is not well understood. As to the iron meteorites, it has been reported that the bulk Canyon Diablo showed a range of nitrogen isotopic compositions from -69.9‰ to -49.9‰ ($\delta^{15}\text{N}$ compared with air) [1]. One plausible explanation on such a variation would be a mass-dependent fractionation during diffusive loss of nitrogen from shock events in the parent body [2]. However, it is difficult to explain all of such isotopic variations of nitrogen. Prombo et al. [1] and Murty et al. [3] reported a nitrogen isotopic heterogeneity in iron meteorites which could not be explained by the mass-fractionation. Such an isotopic heterogeneity is also observed in co-existing minerals such as troilite, taenite, carbide and graphite, which have $\delta^{15}\text{N}$ values of -73.2‰, -65.3‰, -39.3‰ and -2.1‰, respectively [4]. In this study we analyzed nitrogen isotopic compositions of graphite and metal phases separated from Canyon Diablo (Fig.1) and attempted to understand the origin of the nitrogen isotopic heterogeneity.

Samples preparation and experiments

We prepared two samples from Canyon Diablo (Fig.1), M-bulk (metal-rich fraction; 1.32mg) and C-fraction (graphite-rich fraction; 0.46mg). The M-bulk is a metal-rich phase prepared by hand-picking from a crushed bulk sample. The C-fraction is a graphite-rich residue leached with 12N-HCl at 70 °C for 3 days. Two samples were wrapped in pre-degassed Pt foil and loaded into the ultra-high vacuum extraction and purification system.

Gases were extracted from those samples by a stepwise combustion technique (from 200 °C to 1200 °C in 30 minutes). Amounts and isotopic compositions of extracted nitrogen have been analyzed with the quadrupole mass spectrometer (QMA 400 BALZERS) at Osaka University [5]. Abundance of carbon was quantified with Pirani-gauge (ULVAC GP-1S) attached on the extraction line.

Results and discussion

The amounts of carbon and nitrogen, and nitrogen isotopic composition in C-fraction and M-bulk are presented in Fig.2, 3 and 4, respectively.

As shown in Fig.2, a release curve of carbon from C-fraction clearly has the highest peak at 800-850 °C. The peak at the same temperature was also observed for nitrogen release

from C-fraction (Fig.3). Therefore, the nitrogen released at 800–850 °C should be derived from graphite. The release peak of nitrogen at 1100–1200 °C was observed for M-bulk. This should be responsible for trapped nitrogen in metal. The isotopic ratio of metal, $-55 \pm 1 \%$ at 1100–1200 °C, was similar to that of graphite, $-52 \pm 2 \%$ at 800–850 °C, as shown in Fig.4. It shows that graphite and metal in this bulk of Canyon Diablo were produced in an equilibrium condition. However, this result is not consistent with Franchi et al. [2] and Sugiura [4]. As the metal was incorporated as a vein (Fig.1), it obtained the nitrogen equilibrium with the surrounding graphite.

We observed the release peak of nitrogen at 1100 °C in C-fraction. It might be derived from cohenite (Fe_3C) resided in C-fraction. This mineral ordinarily exists in Canyon Diablo [4] and is a carrier of nitrogen [3, 4]. In Fig.4, the $\delta^{15}\text{N}$ values of this phase was $-7 \pm 3 \%$. Nitrogen isotopic composition of cohenite was apparently different from that of co-existing graphite and metal. Therefore, these observations require the reservoirs with different isotopic compositions of nitrogen. This graphite nodule should not be heated up to the temperature that caused the isotopic homogenization between graphite and cohenite.

References

- [1] Prombo C. A. and Clayton R. N. (1993) *Geochim. Cosmochim. Acta.* 57, 3749–3761. [2] Franchi I. A., Wright I. P. and Pillinger C. T. (1993) *Geochim. Cosmochim. Acta.* 57, 3105–3121. [3] Murty S. V. S. and Marti K. (1993) *Geochim. Cosmochim. Acta.* 58, 1841–1848. [4] Sugiura N. (1998) *Meteorit. Planet. Sci.* 33, 393–409. [5] Yamamoto T., Hashizume K., Matsuda J. and Kase T. (1998) *Meteorit. Planet. Sci.* 33, 857–870. [6] Ponganis K. V. and Marti K. (1998) *Meteorit. Planet. Sci.* 33, A125.

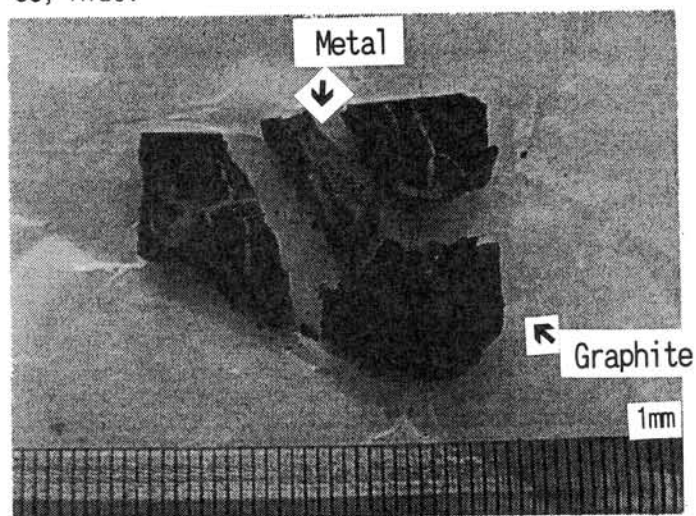


Fig.1 This Canyon Diablo iron meteorite mostly consisted of the graphite bulk and a few veins of metal.

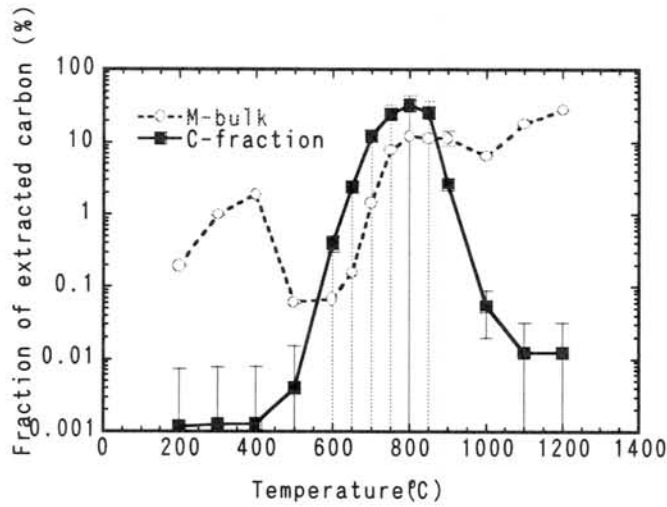


Fig.2 Fraction of extracted carbon (%) vs. released temperature (°C) in each of M-bulk and C-fraction. Note that a unit of carbon extraction ratio is in a logarithmic scale.

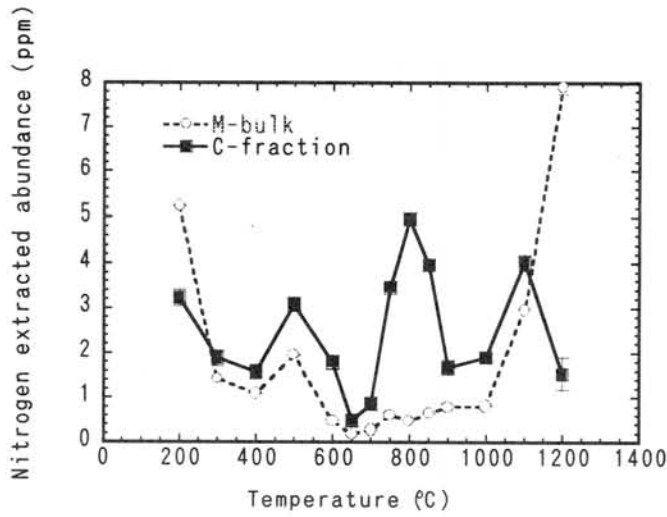


Fig.3 Nitrogen extracted abundance (ppm) vs. release temperature (°C) in each of M-bulk and C-fraction. The first combustion time at 1200 °C is 120 minutes from prediction of M-bulk releasing much nitrogen abundance. Note that a unit of nitrogen abundance is in a linear scale.

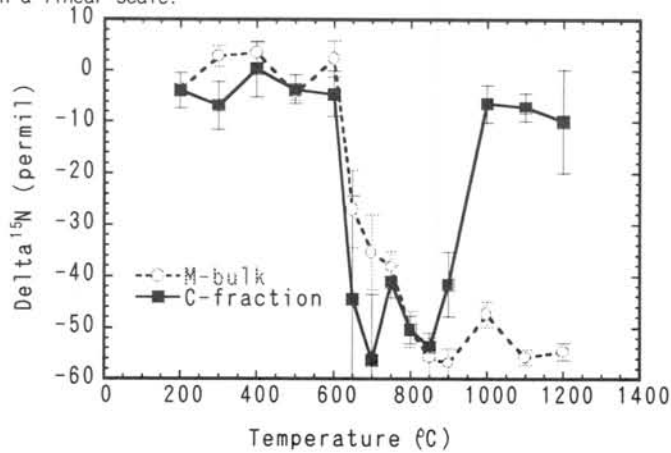


Fig.4 Isotopic composition of extracted nitrogen (‰) vs. release temperature (°C) in each of M-bulk and C-fraction.

VARIATIONS IN SOURCE AREAS AND PROPORTIONS OF PARTIAL MELTING AND FRACTIONAL CRYSTALLIZATION AS INDICATED BY RECENT EUCRITE ANALYSES. P. C. Buchanan¹, D. J. Lindstrom¹, and M. M. Lindstrom¹. ¹Mail Code: SN2, NASA Johnson Space Center, Houston, Texas 77058 USA.

Introduction: Stolper (1977) determined that 'main group' eucrites (e.g., Juvinas) are similar in composition to near-primary melts of a primitive source composed of olivine, plagioclase, Cr spinel, and metal. He suggested that these 'main group' eucrites were formed by 15-20% partial melting of this primitive source. In contrast, the composition of the meteorite Stannern is enriched in incompatible elements relative to 'main group' eucrites and is consistent with 5-10% partial melting of the same source area (Stolper, 1977). A third meteorite, Nuevo Laredo, is more Fe-rich than 'main group' eucrites or Stannern and is similar in composition to a residual melt formed by 30-40% fractional crystallization of pigeonite and plagioclase from a 'main group' eucrite melt (Stolper, 1977). These relationships are clearly seen on a plot of La vs. Sc (Fig. 1). Compositions of 'main group' eucrites plot as a cluster. In contrast, the composition of Stannern plots at much higher La abundance and the composition of Nuevo Laredo plots at much higher Sc abundance. The goal of this study is to discuss recent data for eucritic materials acquired since Stolper's study and how these data fit into his petrogenetic model.

Samples and Analyses: The data include our recent compositional analyses by INAA for clast A/B from the polymict eucrite Macibini, for clast A from the polymict eucrite Petersburg, and for several clast samples from the monomict eucrite Piplia Kalan (Fig. 1). All of these meteorites are falls and, hence, should be unaffected by weathering. Because all of these clast samples are relatively small (~100mg), it is important to evaluate the extent to which sample heterogeneities may have affected these analyses. On the plot of La vs. Sc (Fig. 1), an excess of plagioclase in the sample will move the composition toward lower La and Sc. An excess of pigeonite will move the composition toward higher Sc and lower La; an excess of phosphate will move the composition to higher La at approximately the same Sc. Composition of Macibini clast A/B (Buchanan et al., 1999) plots along the partial melting trend defined by 'main group' eucrites and Stannern. Compositions of samples of Piplia Kalan (Shukla et al., 1997; Buchanan et al., 1997) plot along the fractional crystallization trend defined by 'main group' eucrites and Nuevo Laredo. These data suggest that both materials were not affected by significant heterogeneities caused by sampling.

Discussion: *Fractional Crystallization Trend* - Plotting along the fractional crystallization trend between the 'main group' eucrites and Nuevo Laredo are the meteorites Lakangaon (Warren and Jerde, 1987) and Vetluga (Lindstrom and Mittlefehldt, 1992). Samples of lithic clasts from the meteorite Piplia Kalan range along this trend from the 'main group' eucrites toward Vetluga. These data suggest that Lakangaon was affected by ~30% fractional crystallization, whereas Vetluga was affected by 20-25% fractional crystallization. Samples of Piplia Kalan apparently represent proportions of fractional crystallization ranging from 0-20%. Hence, these data fill in the gap between the 'main group' eucrites and Nuevo Laredo. In fact, the division between the 'main group' eucrites and eucrites grouped with Nuevo Laredo is arbitrary.

Partial Melting Trend - Compositional data for several eucrites and eucritic clasts fall along the partial melting trend (Fig. 1) that is defined by the 'main group' eucrites and Stannern. The meteorite Bouvante (Christophe Michel-Levy et al., 1987) plots close to, but at slightly higher La than, Stannern. Macibini clast A/B, which is a relatively unmetamorphosed eucritic material similar to Y 75011,84 (e.g., Takeda et al., 1994), plots between 'main group' eucrites

and Stannern. These compositions suggest that Bouvante formed by a lower proportion of partial melting than Stannern, whereas Macibini clast A/B formed by ~10-15% partial melting (see also Consolmagno and Drake, 1977). Hence, these new data fill in the gap between 'main group' eucrites and Stannern in terms of proportions of partial melting.

Source Area Variations - There is also some evidence for source area variations among eucrites. The meteorite Pomozdino (Warren et al., 1990) and Petersburg clast A (Buchanan and Reid, 1996) are distinctly more magnesian than 'main group' eucrites and Stannern. Warren et al. (1990) interpreted Pomozdino as a partial cumulate. Mittlefehldt and Lindstrom (1997) suggested that anomalously magnesian eucritic materials may be impact melts of howardites or polymict eucrites. However, these interpretations are more difficult for Petersburg clast A because it is so rich in incompatible trace elements (e.g., Sm) that it would require a eucritic component that is much more REE-rich than anything yet reported.

Conclusions: Recent data acquired for monomict eucrites and lithic clasts from polymict eucrites and howardites have begun to fill in gaps in the partial melting and fractional crystallization trends first observed by Stolper (1977). These data demonstrate a continuous variation in proportions of partial melting between 'main group' eucrites and Stannern and a continuous variation in proportions of fractional crystallization between 'main group' eucrites and Nuevo Laredo. These data also suggest compositional variations in source areas from which eucrites were derived.

References: Buchanan P. C. and Reid A. M. (1996) *GCA* **60**, 135-146. Buchanan P.C. et al. (1997) *Meteoritics and Planetary Science* **32**, supplement, A22-A23. Buchanan P.C. et al. (1999) *Lunar and Planetary Science* **XXX**, 1647. Christophe Michel-Levy M. et al. (1987) *Bull. minéral.* **110**, 449-458. Consolmagno G. J. and Drake M. J. (1977) *GCA* **41**, 1271-1282. Lindstrom M. M. and Mittlefehldt D. W. (1992) *Meteoritics* **27**, 250. Mittlefehldt D. W. and Lindstrom M. M. (1997) *GCA* **61**, 453-462. Shukla A. D. et al. (1997) *Meteoritics and Planetary Science* **32**, 611-615. Stolper E. (1977) *GCA* **41**, 587-611. Takeda H. et al. (1994) *EPSL* **122**, 183-194. Warren P. H. and Jerde E. A. (1987) *GCA* **51**, 713-725. Warren P. H. et al. (1990) *Proc. 20th LPSC*, 281-297.

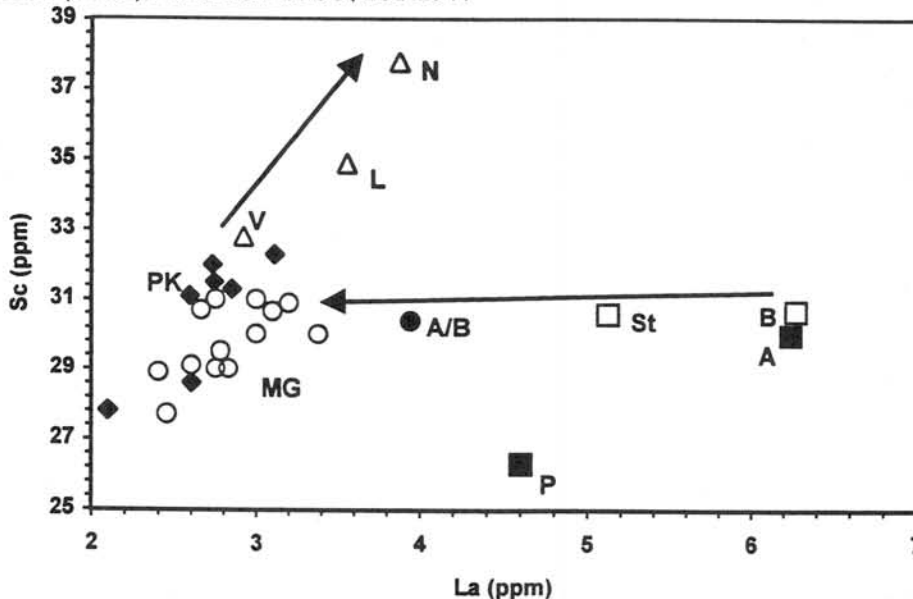


Fig. 1. La (ppm) vs. Sc (ppm) for eucrites and eucritic clasts. St=Stannern, B=Bouvante, N=Nuevo Laredo, L=Lakangaon, V=Veluga, MG=main group (open circles), PK=Piplia Kalan (diamonds), P=Pomozdino, A/B=Macibini clast A/B, A=Petersburg clast A. Data sources in text.

MEASUREMENTS AND THEORETICAL STUDIES ON THE ALHA 77257,77-4 UREILITE: IGNEOUS/PRIMITIVE DICHOTOMY IN ITS MINERALOGY AND CHEMISTRY, PARADOXES AND SOLUTIONS IN ITS THERMAL HISTORY

Bérczi Sz.,¹ Gál-Sólymos K.,² Lukács B.,³ Martinás K.⁴

1 Eötvös University, Dept. G. Technology, Cosmic Mat. RSG. H-1117 Budapest, Pázmány s. 1/a.

2 Eötvös University, Dept. Petrology, Geochem., H-1088 Budapest, Múzeum krt. 4/a., Hungary

3 Central Research Institute for Physics, CRIP-RMKI, H-1525 Budapest-114, P.O.B. 49., Hungary

4 Eötvös University, Dept. Atomphysics, H-1117 Budapest, Pázmány Péter sétány 1/a., Hungary

ABSTRACT

The ALHA 77257,77-4 thin section of the NIPR collection exhibits all characteristics of an olivine-pigeonite-carbon/metal-vein compositional ureilitic sample. Inter-grain regions are filled with carbonaceous and partly metallic (FeNi and troilite) material. The large olivine-pigeonite grains have transitional outer rims toward the carbonaceous veins, which contain reduction-exsolved metal blebs. On the basis of their metamorph/primitive dichotomy in mineralogy and geochemistry, the loss of first iron (I. order primitive achondrite) and loss of light silicates (II. order primitive achondrite) we consider ureilites to be a II order primitive achondrites. We formulate several paradoxes of ureilitic mineral assemblage and start to resolve them with thermodynamic explanation for their origin by using mainly solid state physical laws (diffusion, lattice rearrangement by movement of vacancies) in the thermal evolution of parent body.

INTRODUCTION: TEXTURE, MINERALOGY, GEOCHEMISTRY; MEASUREMENTS

The ALHA 77257,77-4 thin section of the NIPR collection is a 4mm X 7mm surface, on loan for studies on the Eötvös University (Pict.1/a.). The thin section nicely exhibits characteristic features of the ureilitic mineralogy and texture. (Yanai, Kojima, 1987) Our carbon distribution map shows that ALHA 77257,77-4 ureilite veins are rich in carbon (Pict. 1/d.). The large olivine and pigeonite grains frequently have triple junctions with 120 degrees. Most inter-grain boundary regions are filled with carbonaceous veins, but many with metal ones. Outer rims of the olivine and clinopyroxene contain reduction-exsolved metal blebs which form transitional semi-opaque boundaries around the minerals. Some veins are alternately filled with carbon and metal. While Ol/px assemblage is more igneous/metamorphic and may be classified together with terrestrial mantle rocks (i.e. lherzolites), the other component, the veins are the remnants of the carbonaceous matrix (Janssens et al, 1987): they are last survivors and preservers of chondritic primitive components. Survival of such a primitive component allows us to call ureilites primitive achondrites, although in II. order, because they are very much metamorphosed if compared to acapulcoites and lodranites. (Igneous origin of ureilites was also summarized, e.g. Goodrich et al, 1986, Goodrich, 1992)

Microprobe compositional investigations were carried out by an AMRAY 1830I/T6 SEM instrument equipped with an EDAX PV 9800 ED system. Accelerating voltage was 15 keV and we used 1-2 nA beam current. Measurements on olivine and clinopyroxene gave the conventional Fe content range: Fs 15-22 %, Fa 13-25 %. There are 2 kinds of olivine, the darker with 50.54 % MgO, 41.32 % SiO₂ 41.32 %, FeO 6.48 %, the lighter with MgO 44.80, SiO₂ 40.05, FeO 13, 51 %. Both olivines have Cr₂O₃ bw. 0.69-0.76 %. We found Cr sulfide spherules in olivines; their Cr content varies bw. 9.50 and 24.86 weight %. This high-Cr spherules together with the previously mentioned primary magmatic carbon grains in ureilites (Goodrich & al., 1986), shows that mafic silicate minerals also contain probably primitive chondritic components (see Pict. 1/b, 1/c and 1/e). If we compare them with other reducing inclusions in chondrules (Hanon et al., 1998) we have another probably primordial inclusions in ureilites.

In order to understand ureilite genesis we place ureilites into the thermal metamorphic (thermal evolution) sequence from chondrites to different achondrites. We can find their place between the primitive achondrites and the more evolved (partly depleted) mantle rocks. Primitive achondrites preserve their main mafic chondritic silicate mineralogy, but lost (at least partly, or began to lose) their iron. Ureilites lost not only main mass of their iron component but lost their most mobile light silicate components assemblage (Tomeoka, Takeda, 1990), too (although they kept a surprisingly fair amount of water). But because of their preserved primitive component we shall classify them as II. order primitive achondrites.

Petrolog. type of V Schm-W.	1	2	3	4	5	6	7 Primit. Achondr. I. order	Primitiv. Achondr. II. order	Basaltic Achondrites
E			+	+	+	+		Aubrites?	Aubrites?
Between E and H (BEH)			+	+	+	+	Acapulco Lodran Winona	Some of LODRA NITES	
H			+	+	+	+	e.g. Port Valley	?	Eucrite, How, Dio
C	+	+	+	+	+	+	?	UREI- LITES	
L			+	+	+	+	+	?	
LL		+	+	+	+	+	+	?	

UREILITES: II. ORDER PRIMITIVE ACHONDRITES

According to these textural characteristics ureilitic mineral assemblage seems to belong to the II. order primitive achondritic stage. We distinguish I. order primitive achondritic stage by **iron loss** and II. order primitive achondritic stage by **both iron and light silicate loss**. (It seems and can be reasoned that the second never precedes the first.) Iron loss causes minor changes in the chondritic chemistry and mineralogy (petrologic type 7 in chondritic metamorphic range, with Acapulco, Lodran, Winona and silicate inclusions of some irons). However, when partial melts of the mobile light silicates move out from the originally chondritic assemblage (Tomeoka, Takeda, 1990) further loss of chondritic character can be observed. This stage was named however, to II. order primitive achondrite, because it preserved not only the carbon, but volatiles and oxygen isotopic ratios from the ancient carbonaceous chondritic matrix. In bulk chemistry II. order primitive achondrites can be characterized by increased Mg/Si ratios. Flowing out of basaltic melts left behind a more mafic silicate content of primitive mantle rocks, then that of chondrites themselves.

PARADOXES: RESOLUTIONS, CONCLUSIONS: SOLUTIONS FROM THERMAL HISTORY

There are several paradoxical geochemical and mineralogical composition characteristics of ureilites we intend to reconcile and explain from the viewpoint of thermodynamics: We note that Goodrich (1992) when trying to classify ureilites either as metamorphic or as primitive, ran into contradictions, which clearly imply paradoxical features.

1) *Only one type of ureilite exists although we need at least five for the 5 chondrite groups.* This was mentioned in the Table. There also aubrites were tentatively mentioned as analogons of ureilites for E chondrites (Bérczi, Holba, Lukács, 1999). Now, observe Fig. 1, where we displayed the FeO distributions of chondrites, HEDs and ureilites of the NIPR Catalog (Yanai, Kojima & Haramura, 1995). The Figure demonstrates that after iron loss the remaining Fe content has already a single peak, so it is possible that the different ordinary chondrites would result in similar primitive achondrites of order II. (i.e. ureilites)

2) *It contains more Mg than the average chondrites.* From statistical data (NIPR dataset, Yanai, Kojima, Haramura, 1995) it seems that the Mg/Si ratio for ureilites is higher than this ratio for chondrites and even for carbonaceous chondrites. However this property may have a natural explanation. Losing the partial melts can explain this increasing MgO content. Observe the process from the "chair" of the Mg silicates sitting deep in the mantle of the ureilitic parent body asteroid. Originally both olivine and pyroxene might be present in the chondritic mineral assemblage. Partial melting in the peritectic $2\text{MgO} \cdot \text{SiO}_2 - \text{SiO}_2$ system produces first melts of $\text{MgO} \cdot \text{SiO}_2$ (together with most Na, Ca, Al, silicates) and left more $2\text{MgO} \cdot \text{SiO}_2$ olivine than $\text{MgO} \cdot \text{SiO}_2$ pyroxene, so the relative weight of olivine increased. This is a similar process in every planetary mantle chondritic/peridotitic assemblages, and that is why we can observe the parallel trends for peridotite-basalt sequence both for smaller (asteroidal) and larger (the terrestrial) evolutionary sequences (Lukács, Bérczi, 1997, 1998).

The remaining three paradoxes are much more interwoven:

3) *Low Na content is present with rather high water content.* The low Na concentration is no problem, observe that the bulk composition of ALH-77257 is extremely poor also on Al. This simply would mean a deep-mantle residue. However then one would expect water loss too, which is the real problem.

4) How could it be that water, much carbon and a small amount of metal are in equilibrium. This clearly implies that under the special circumstances carbon does not dissolve water.

5) Contrary to their great diffusion-lengths, which means long staying in a hot environment water and carbon is present in considerable amounts. Contrary to the previous item this means physical properties: both C and H₂O diffuse very easily under familiar circumstances. Note that the fact that carbon has been collected in the inter-grain veins may be explained by diffusion and solid state vacancies transport. The grain boundaries are the zones of weakness in a solid state. Not only diffusion drives incompatible elements (and all other elements not-easily forming crystals) into the veins but the transport effects of vacancies, too. Carbonaceous intergrain regions mean that ureilites were hot for long time. Their presence does not need melting, only long time of hot staying below the melting point. (Between Tamann temperature = 0.52x T (melting) and T (melting)). Because the number of vacancies below melting point is 0.23 % during a long time heated state diffusion can rearrange texture into a very "igneous"-like metamorphic one.

We admit that we do not have satisfactory explanations for the last 3 problems. However, we suggest possibility, which may or may not be true, but with it they are no more paradoxes.

Assume a carbon phase on large pressure and/or high temperature, which is of great molecular weight and almost inert. Then the parts of points 4 & 5 regarding C get explanation: this allotrope of C will not evaporate easily from the lattice and will not dissolve water. We do not know which modifications may be stable or metastable at the ureilite locality (deep mantle?), but an *example* is the buckminsterfullerene C₆₀. It is a large molecule, forming negative ions, so not a concurrent of H for O (Hauffer L. E. & al., (1990); Ohsawa V. & Saji T., (1992)).

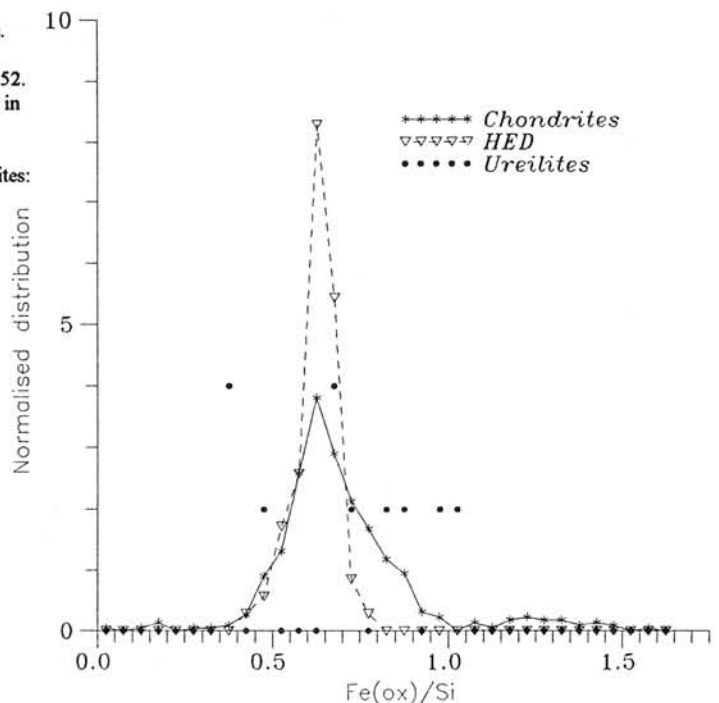
Then what would remain would be only something binding water in the lattice more strongly than usual; and we note the enormous Mg in ureilite. Now, silicates of C chondrites are slightly more "mafic" than of ordinary chondrites, and they retain more water at comparable petrologic types, too.

Finally we note that for C there is another possibility, too. Deep mantle C may have diffused out of the iron core: C diffuses easily in Fe, and we guess that the diffusion length in a million year may have gone to several km's.

ACKNOWLEDGEMENTS Partly supported by T 026660 OTKA program.

REFERENCES

- Bérczi, Holba, Lukács, (1999): LPSC XXX. #1014.
 Goodrich C.A., Berkley J.L. (1986): Primary magmatic carbon in ureilites. GCA, 50, 681-691.
 Goodrich C.A. (1992): Ureilites: A critical review. Meteoritics, 27, 327-352.
 Hanon, P., Robert, F., Chaussidon, M. (1998): High carbon concentration in meteoritic chondrules. GCA 62, 903-913.
 Hauffer L. E. & al., (1990): J. Phys. Chem. 94, 8634
 Janssens M-J., Hertogen J., Wolf R., Ebihara M., Anders E. (1987): Ureilites: Trace elements clues to their origin. GCA, 51, 2275-2283.
 Lukács B., Bérczi Sz. (1997): Statistical analysis of NIPR meteorite compositions, II.: Comparison of sequences of differentiated rocks from an asteroidal sized body and Earth. Antarctic Meteorites XXII. 94.
 Lukács B., Bérczi Sz. (1998): Barometric height formula type fractionation in the stony-planetary bodies. (Stat. analys. of NIPR meteorite compositions II.) LPSC XXIX. #1223
 Ohsawa V. & Saji T., (1992): J. Chem. Soc. Chem. Comm. 781
 Saito, J., Takeda H. (1991): Mineralogical studies of metals at grain boundaries of magnesian ureilites. 16th Symposium on Antarctic Meteorites, Tokyo, 1991. 13-1.
 Takeda H., Saito J., Hiroi T. (1991): Mineralogy of MAC88177 and Comparison with Augite-bearing Lodranite Yamato 74357. LPSC XXII, 1375.
 Tomeoka K., Takeda H. (1990): Fe-S-Ca-Al bearing carbonaceous vein in the Yamato 74130 ureilite: Genetic link to carbonaceous chondrites. GCA, 54, 1475-1481.
 Yanai K., Kojima H., (1987): Photographic Catalog of Antarctic Meteorites, NIPR, Tokyo
 Yanai K., Kojima H., Haramura H., (1995): Catalog of Antarctic Meteorites. NIPR, Tokyo



**SPLITTING OF THE TWO WIIK LINES IN THE UREY-CRAIG FIELD:
C-S ARE RELATED TO H-S LIKE AS LL-S ARE RELATED TO L-S.
(STATISTICAL ANALYSES OF THE NIPR DATASET, VII)**

Sz. Bérczi^{1,3}, *Á. Holba*², *B. Lukács*²

¹ Eötvös University, Cosmic Mat. Res. Gr. Dept. G. Technology, H-1117 Budapest, Pázmány P.s. 1/a.

² Hungarian Academy of Sci. Central Res. Inst. Phys. RMKI, H-1525 Budapest 114. P.O.Box 49.

³ Eötvös University, Dept. Petrology, Geochem., H-1088 Budapest, Múzeum krt 4/a, Hungary

ABSTRACT

From the NIPR meteorite chemical composition dataset we formed multicomponent functions to see thermal evolution (metamorphism) trends of chondrite parent bodies. We have found that the two Fe-compound supergroups of Wiik split into two subgroups of (H and C) and (L and LL) in an evolutionary process along the van Schmus-Wood metamorphic sequence.

**FORMULATION OF THE PROBLEM: WHERE ARE THE ANCESTORS OF L'S?
WITH WIIK'S SET (30), CANNOT, WITH NIPR SET (500) MAY BE ANSWERED**

The Catalog of Antarctic Meteorites (Yanai, Kojima, Haramura, 1995) with its more than 550 "points" made it possible to restudy the possibility of the common origin of chondrites grouped by Urey & Craig (1953) and Wiik (1956) into two main total iron content lines. One line was split by Fredrickson and Keil to L and LL but the common origin for H and C supergroup was less emphasized. Since Fe-compounds belong to initial condition type parameters of chondrites, we considered the changes in mutual ratio of Fe-compounds as modifications by thermal evolution along the sequence milestone by petrologic types.

Going back to Wiik (1956), his developments on the Urey & Craig (1953) results was the following. Since chondrites seemed to form only 2 disjoint groups, H(igh) and L(ow) for total Fe content, Wiik selected 30 very careful measurements. He suggested to find ancestors of the developed chondrite groups. Explicitly he wanted to answer the question: what would be connection of the the H and L groups with the "primitive" C's. H found that all measured C's belonged to the H group. So he could conclude that C's may be the "ancestors" of H's (and E's?), but not of L's.

However, this was not the only and not a necessary conclusion. If all chondrite groups (at that time H and L) were independent, then it was also possible that L-s might have had other ancestor. If he concluded this direction then he could have put a question: If in an evolutionary scheme (where Fe/Si content is initial condition) why only H's can have precursors (Bérczi & Lukács, 1998), but precursors of L's can not be seen. After more than 4 decades answers can be formulated using the NIPR dataset (Fig. 1).

**HOW CAN WE STEP FORWARD FROM THE DEBATE BETWEEN THE GRADISTIC VS:
CLADISTIC VIEWS IN EVOLUTIONARY CLASSIFICATION**

GRADISTIC VIEW: In evolution of biological systems gradistic viewpoint is traditional, when the gradual changes can be observed. Comparing grades (stages in a sequence) in an evolutionary process, "undeveloped", "primitive" stage is the initial one and for example for chondrites: volatile loss, equilibration of matrix and chondrules, fading of chondrule boundaries are the "gradually higher evolutionary stages". Different initial conditions (for other clades) may result in slightly different appearance of grades or different rate of approach to the grades similar. For example: diffusion will result in higher temperature for H than L having higher Mg content and so higher melting point for the olivine and pyroxene.

CLADISTIC VIEW: In evolution of biological systems cladistic viewpoint means that we originally define initial conditions and sort objects to that initial condition. Later the clades develop according gradual processes, and new objects develop by branchings (bifurcations) of the clades. The evolution of clades (with different initial conditions) cannot merge. But if the clades were defined originally in an ambivalent way, confusion may arise and the branchings (the bifurcated "main groups") want to mix for gradistic steps.

We think that the problem with the ancestor of L's is at least partly a consequence of mixing the gradistic and cladistic viewpoints in meteoritics. In a gradistic viewpoint in a chondritic evolutionary process we compare grades so, that C is synonymous with the name of the "undeveloped" or "primitive" stage, (with many volatiles, especially C), then H (E) and L (LL) are the "higher evolutionary stages". In the cladistic view C may have gone "as far" as the others did from the startpoint, and then C3 (the "olivine-pigeonite chondrites", Brooks & Shaw, 1970) is comparable to H3 or LL3, or C6 (equilibrated) is comparable to H6; and the different initial conditions (for at least Fe and Mg; Bérczi & Lukács, 1997) support this view, because *evolutions with different initial conditions cannot merge*. At the same time, the cladistic/gradistic debate still lingers, because the main chondrite groups still have preserved their notations according to their traditional gradistic meaning, too.

OXIDATION/REDUCTION RACE HELPS TO UNIFY THE TWO EVOLUTIONARY VIEWPOINTS

Now we would like to see the consequences of a common ancestor, split regional ancestor hypothesis. If two groups have common ancestor, but the volatile ratios are different, splitting of the evolutionary paths can be observed. We can get this structure of main chondrite group representatives along the van Schmus-Wood petrologic types, with Fe-compound ratios. Earlier we found such process when studied the oxidation/reduction race. (Lukács, Bérczi, 1996.) Unfortunately, the NIPR Catalog does not give C data, so we had to use a smaller statistics of Hayes (1974) and of Otting, Zähringer (1967) and we also accept the suggestion of Hutchison et al. (1987) and take Semarkona and Bishunpur as LL2. The average C, H₂O and Fe^o contents are shown on Fig. 2, as the widths of the representative strips, valence weighted (Fe=2, H=1 and C=4); the vertical position is total Fe/Si. The scales are independently normalized for each group. Fig. 3 is a similar graph for metallic, oxide and sulphide irons. Fig. 2 contains H, C, L and LL; on Fig. 3 we, from technical reasons, omitted C, but between PT 3 and 6 it would be practically almost only the metallic component. Fig. 4 is a more detailed Figure for C according to Hayes, Otting & Zähringer and Hutchison & al.

THE MESSAGES OF FIGS. 2 & 3

It would be more proper to use colour graphs, impossible in the present Volume. However the message is clear enough. See first Fig. 2. We, according to Wiik's observations, have 2 supergroups differing in total Fe/Si content, one H(igh), H and C (and maybe E, H3-4, the C1, Y-82162 of the Catalog, all even higher), and one L(ow), L and LL. Now, in both subgroups there are 2 different trends of the evolution. H and L both are finally dominated by Fe^o, both C and H₂O finally secondaries in the race. On the other hand, in both the H and in the L supergroups there exists the other trend too (C and LL), when all the three racing components more or less die out towards PT 6. In this sense L is the Low counterpart of H, while LL is of C. At this moment we do not see the reasons of such symmetric trends, but they are present. Fig. 3 shows that comparing now the possible fates of Fe, from PT 3 upwards the sulfide is of secondary importance (not, however, for E, not shown here), and oxide Fe finally dominate the metallic one in the sequence H<L<LL<C. This arrangement is quite different than that of Fig. 2, and not symmetric.

Partly supported by OTKA T/026660.

REFERENCES

- Bérczi Sz. & Lukács B., Antarctic Meteorites **XXII**, 6-8 (1997);
 Bérczi Sz. & Lukács B., Antarctic Meteorites **XXIII**, 4-6 (1998);
 Bérczi Sz. & Lukács B., this Volume (1999);
 Brooks J. & Shaw G., *Origin and Development of Living Systems*, Academic Press, London, (1973);
 Hayes, J.M. GCA, **31**, 1395, (1967);
 Hutchison R. & al, GCA **51**, 1875, (1987);
 Jarosewich E., Meteoritics **25**, 323-337 (1990);
 Krot A.N. & al., GCA **61**, 219, (1997);
 Otting W. & Zähringer J. GCA, **31**, 1949, (1967);
 Urey H.C. & Craig H., GCA **4**, 36 (1953);
 Wiik H.B., GCA **9**, 279, (1956);
 Yanai K. et al., *Catalog of the Antarctic Meteorites*, NIPR, Tokyo, (1995);
 Zolensky M.E. & al., GCA **61**, 5099, (1997);

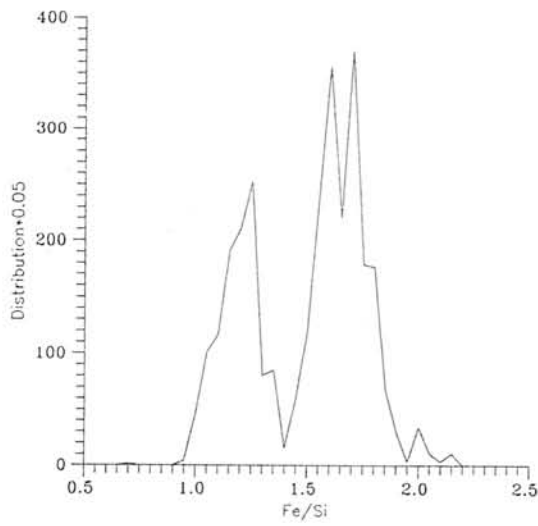


Fig. 1.

The distribution of Fe/Si in NIPR chondrites

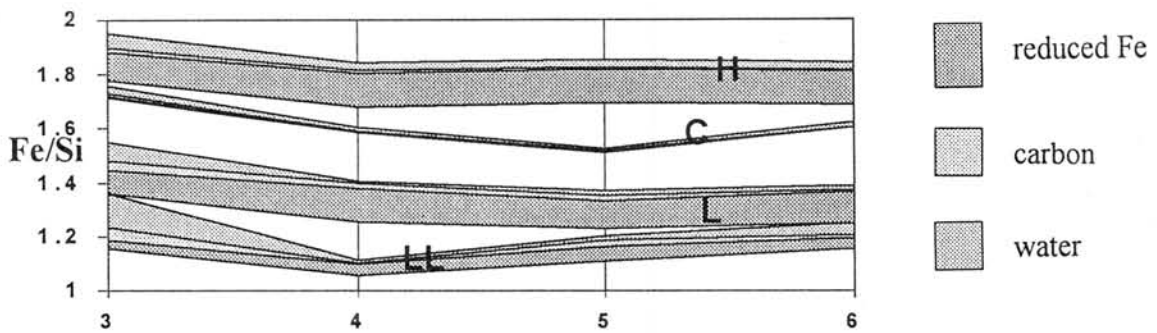


Fig. 2.

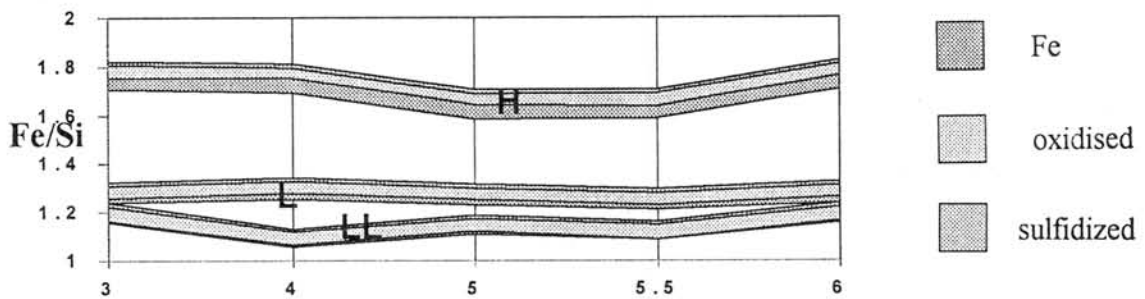


Fig. 3.

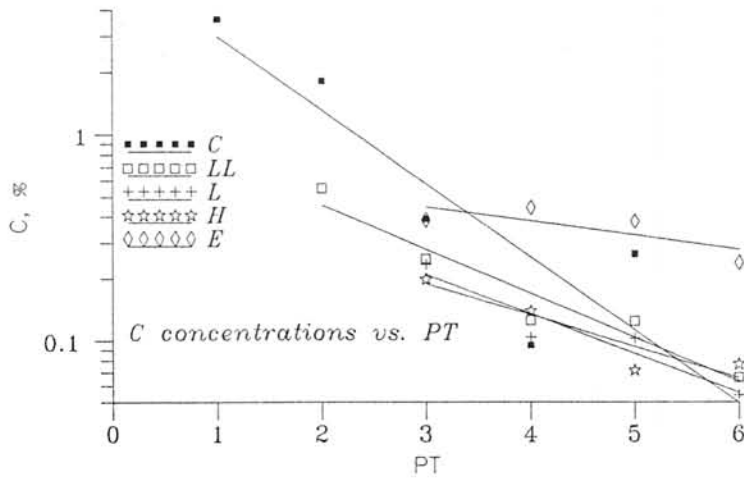


Fig. 4.

The opaque mineral assemblage of matrix in L chondrites.

Jun Chikami* and M. Miyamoto

Mineralogical Institute, Graduate School of Science, University of Tokyo, Hongo 7-3-1, Bunkyo-ku, Tokyo, 113-0033, JAPAN, chikami@min.s.u-tokyo.ac.jp

* present address: Fachgebiet Strukturforschung, Fachbereich 21, Materialwissenschaft, Technische Universität Darmstadt, Petersenstrasse 23, 64287 Darmstadt, Germany, chikami@hrzpub.tu-darmstadt.de

Introduction:

We proposed that Zn content in spinel group minerals which has spinel structure mineral might be an indicator for differentiation process in the early solar system (Chikami et al., 1999). The ZnO content of spinel group in meteorites increases from unequilibrated chondrites and equilibrated chondrites to primitive achondrites and ureilites. This fact might indicate that spinel group in primitive achondrites and ureilites reequilibrated with Zn-rich melt which was partial melt of unequilibrated chondrites. The ZnO content in spinel group decreases in the order: primitive achondrites and ureilite to HED and Martian meteorites. It suggested that Zn was depleted from molten magma during the formation of HED and Martian meteorites.

From our recent study it has been found that ZnO content in chromites of LL chondrites, one group of ordinary chondrites, does not show any trend over different petrologic type, although Zn content in daubreelite, one kind of thiospinel, of enstatite chondrites decreases from lower to higher petrologic types (Chikami and Miyamoto, 1999). In both LL chondrites and enstatite chondrites bulk Zn content is almost constant in different petrologic types (Kallemeyn et al., 1989, Kallemeyn and Wasson, 1986). Different Zn behavior in different petrologic types between enstatite chondrites and LL chondrites suggests that they have different formation process.

Our previous result of LL chondrites showed that ZnO wt% of chromite in one thin section of LL chondrites is not constant. The range of variable ZnO wt% is from 0.1 to 0.25 wt% in each thin section and the average of ZnO wt% of chromite is also different in thin sections. It is amazing that ZnO wt% of chromite core is variable even in LL6 and LL7 chondrites although McSween and Patchen (1984) suggested that equilibration temperatures recorded by type 6 and 7 LL chondrites are 900-960 °C and 1150 °C, respectively, based on the composition of clinopyroxene. We proposed three possibilities to explain variable ZnO content in LL chondrites chromites. 1) Assuming that Zn diffusion rate in chromite is very low, the core composition of chromites might be variable. But no systematic difference between core and rim does not support this idea. 2) Disequilibrium in LL4 chondrites might cause the variable ZnO content in LL4 chondrites. 3) We may have analyzed both primary and secondary chromites might cause the variable ZnO content of our result. Although we have proposed three possibilities to explain variable ZnO content in LL chondrites chromite, it is still controversial.

In this study, we compare the Zn behavior in L chondrite chromite with that in LL chondrite in order to consider how ZnO content of chromite in ordinary chondrite is variable. We focus on the relationship between ZnO content in chromite and opaque mineral assemblage containing chromites in L chondrites in order to consider the reason of variable Zn content in LL chondrites.

Analytical techniques:

We studied thin sections of Y81070 (L4), Y791710 (L4), Y791630 (L4), Y791635 (L4), Y790723 (L5), Y75102 (L6), Y82178 (L6) and ALH77269 (L6) using an optical microscopy and an electron microprobe analyzer. We measured 13 oxides (SiO₂, TiO₂, Al₂O₃, MnO, FeO, MgO, CaO, Na₂O, K₂O, Cr₂O₃, V₂O₃, NiO and ZnO) using the electron microprobe analyzer (JEOL 733-mkII at the Geological Institute, University of Tokyo) with an accelerating voltage of 15 kV and a beam current of 12 nA. The Bence-Albee correction was used for chromites in L chondrites. Counting time at peak wavelength were 10 seconds. Counts were accumulated 4 times. The background intensity was measured for each element at both sides of the peak wavelength. The detection limit of ZnO in chromite is 0.02 wt%.

Results:

Y81070 (L4): The mineral assemblages with chromites are as follows. 1) chromite, metal, silicate and troilite, 2) chromite, metal and silicate, 3) chromite, troilite and silicate, 4) chromite and silicate. Except one grain ZnO content in chromite core is lower than that at chromite rim in three chromite grains. There is no correlation between Zn content in chromite and mineral assemblage. For example, ZnO content in the chromite core is variable (0.30-0.53 wt%) although the mineral assemblage (chromite, troilite and silicate) is the same. The range of Zn content in chromite core of Y81070 is from 0.30 to 0.58 w% ZnO.

Y791710 (L4): The mineral assemblages with chromite grains in Y791710 are 1) chromite, troilite and silicate or 2) chromite, metal, troilite and silicate. ZnO content at chromite rim (0.46 wt%) is higher than that in chromite core (0.41 wt%). Furthermore, the ZnO content of chromite coexisting with metal, troilite and silicate (0.62 wt%) is higher than that of chromite with troilite and silicate (0.41-0.46 wt%). We can not conclude anything from this result in Y791710 L4 chondrite, because it is a comparison of only two grains. ZnO content in chromite core is from 0.41 to 0.62 wt% in Y791710 thin section.

Y791630 (L4): Chromite grains coexist with metal and silicate. The chromite core shows a little bit lower ZnO content (0.59 wt%) than that at chromite rim (0.62 wt%).

Y791635 (L4): The mineral assemblages with chromite grains are as follows. 1) chromite and troilite, 2) chromite and silicate, 3) chromite, metal and silicate, 4) chromite, troilite and silicate. 4 chromite grains show that ZnO content at chromite rim is lower than that in chromite core. 2 chromite grains show the opposite trend, that is, ZnO content at chromite rim is higher than that in chromite core. We could not find any correlation between mineral assemblage and ZnO content in chromite in Y791635. ZnO content in chromite core varies from 0.44 to 0.64 wt%.

Y790723 (L5): The mineral assemblages of chromites are 1) chromite, troilite, silicate and metal, 2) chromite, metal and silicate, 3) chromite and silicate 4) chromite, troilite and silicate. In one chromite grain ZnO content shows higher at rim than in core. There is no relationship between ZnO content in chromite and mineral assemblage. Chromite core in Y790723 shows the variable ZnO content ranging from 0.10 to 0.19 wt%.

Y75102 (L6): The mineral assemblage of chromites are 1) chromite, troilite, silicate and metal, 2) chromite, troilite and silicate and 3) chromite and silicate. ZnO content at chromite rim is higher than that in chromite core in three chromite grains of Y75102. ZnO content in chromite of Y75102 is not connected with mineral assemblage containing chromite. ZnO wt% in chromite core is from 0.29 to 0.58 wt%.

Y82178 (L6): Chromite grains coexist with 1) silicate, 2) metal and silicate and 3) troilite and silicate. 6 chromite grains showed that ZnO content at chromite rim is higher than chromite core. On the other hand, 2 grains showed the opposite trend. We could not find any correlation between ZnO content in chromite and mineral assemblage. We found the variable ZnO content ranging from 0.30 to 0.49 wt%.

ALH77269 (L6): Chromite grains coexist with 1) chromite, metal and silicate and 2) chromite and silicate. The ZnO content in chromite core is higher than chromite rim in 2 chromite grains. ZnO content in chromite is not connected with mineral assemblage. Even chromite cores coexisting with only silicate show variable ZnO content (0.30-0.43 wt%). ZnO content in chromite core varies from 0.30 to 0.45 wt%.

Discussion:

It is important to know whether the ordinary chondrites groups are isochemical independent of petrologic type because some models attribute the properties of the different types to progressive thermal metamorphism of uniform materials. Such models, as espoused by Dodd and Van Schmus (1967) and Wasson (1972) imply closed system evolution for all but the most volatile element. In the other chief class of models, such as two-component model of Anders (1964), thermal metamorphism is envisioned to occur under closed system conditions. Variation in the contents of highly volatile elements are attributed to chemical isolation from the nebular at different time periods, during each of these epochs the temperature dropped only a minor portion of the range within which 99% of the condensation of these elements occurred.

With the exception of highly volatile Br, no significant differences in abundance are observed among the petrologic types of each group (Kallemeyn et al., 1989). This conflict with earlier conclusions

that intertype differences are present. The absence of a relationship between composition and petrologic type is consistent with models calling for the progressive thermal metamorphism of primitive unequilibrated materials to produce the observed spectrum of petrographic grades, and places narrow limits on the relative accretion efficiency of nebular components in those models calling for the sequential accretion of nebular materials. Because volatile elements may be easily volatilized in type 6 or 7 LL chondrites in the open system of the sequential accretion model. On the other hand, the progressive thermal metamorphism model assumes that high petrologic type chondrites are present in the core of LL chondrite parent body. In the pseudo-closed system in the core of LL chondrite parent body volatile elements may be mostly retained. Concentrations of most volatile elements are relatively constant in ordinary chondrites, independent of group or type.

Ebihara et al. (1993) suggested that Zn and Cu abundances in ordinary chondrites are not widely variable in unequilibrated ordinary chondrites and equilibrated ordinary chondrites. There are at least three stages for controlling elemental abundances in meteoritic materials, nebular fractionation, shock metamorphism and thermal metamorphism. Abundances of Cu and Zn in ordinary chondrites seem to have been mostly controlled by the nebular fractionation, possibly at the condensation stage (Ebihara et al., 1993). There is a small but apparent differences in Zn abundance between equilibrated ordinary chondrites and unequilibrated ordinary chondrites. In H chondrites similar tendencies can be noticed. To explain these features in volatile elements Ebihara et al. (1993) propose a model invoking the transportation of volatiles induced by thermal metamorphism on the parent body. Our result about L chondrites also supports the idea of Ebihara et al. (1993). ZnO content in chromite is decreasing from L4 (0.30-0.64 wt%) to L5 (0.10-0.19 wt%) and then it is increasing from L5 to L6 (0.29-0.58 wt%). This result suggests the transportation of volatiles induced by thermal metamorphism on L chondrite parent body.

Yabuki et al. (1983) found that a remarkable feature is the high Zn content (up to 2.3 wt% ZnO) and the positive clear-cut relationship between Zn and Al contents of the spinels in many chondrules in L3, L4 and L5 chondrites and some LLs. They considered these features as important genetic signature of the chondrule formation processes. The simultaneous enrichment in the refractory Al and the volatile Zn is indicative of a distinct chondrule precursor component enriched in both elements. Grossman and Wasson (1983), however, do not find any significant correlation between lithophile Zn with the non-volatile lithophile elements in the Semarkona (LL3) chondrite. In contrast to the result of Yabuki et al. (1983) our results did not show such a high ZnO content in L chondrites chromite although we measured ZnO content in chromite of L chondrite matrix not in chondrule. However, we suggested before that Zn content in daubreelite, one kind of thiospinel, of enstatite chondrite chondrule is lower than that in enstatite chondrite matrix. As Yabuki et al. (1983) suggested the positive relationship between Zn and Al of spinel, the high Zn content (up to 2.3 wt% ZnO) might be contained in spinel (Al-rich), although chromite (Al-poor. Chromite in L chondrites matrix contains 6 wt% Al_2O_3 .) does not contain so much ZnO. It would suggest that the partition coefficient between spinel and liquid may be higher than that between chromite and liquid.

Conclusions:

- 1) ZnO content in chromite core is lower than that at chromite rim in many chromite grains. On the other hand, some chromite grains show that ZnO content in chromite core is higher than that at chromite rim.
- 2) There is no correlation between ZnO content in chromite and mineral assemblage.

References:

- Anders E. (1964) *Space Sci. Rev.*, 3, 583-714.
Chikami J. et al. (1999) *Antarctic Meteorites Research*, 12, in press
Chikami J. and Miyamoto M. (1999) *LPSC*, XXX, CD
Dodd R. T. and Van Schumus W. R. (1967) *GCA*, 31, 747-765.
Ebihara M. et al. (1993) *Meteoritics*, 28, 343.
Grossman N. L. and Wasson J. T. (1983) *GCS*, 47, 759-772.
Kallemeyn G. W. and Wasson J. T. (1986) *GCA*, 50, 2153-2164.
Kallemeyn G. W. et al. (1989) *GCA*, 53, 2247-2767.
McSween H. Y. and Patchen A. D. (1984) *Meteoritics*, 24, 219-226.
Wasson J. T. (1972) *Rev. Geophy. Space Phys.*, 10, 711-759.
Yabuki H. et al. (1983) *Meteoritics*, 18, 426-427.

The Permian-Triassic supernova event

Csaba H. Detre¹, Imre Tóth², György Don¹, Árpád Z. Kiss³, Imre Uzonyi³, Péter Bodó⁴, Zsolt Schléder⁴

¹ Geological Institute of Hungary, Stefánia út 14., H-1143 Budapest, Hungary

² Konkoly Observatory, P.O.Box 67, H-1525 Budapest, Hungary

³ Institute for Nuclear Research, ATOMKI, P.O.Box 51, H-4001 Debrecen, Hungary

⁴ Eötvös L. University, Dept of Petrology and Geochemistry, Múzeum krt 4/a, H-1088 Budapest, Hungary

The boundary separating the Permian from the Triassic divides at the same time the old world of life from an entirely new one - save the unbroken existence of a few archaic species. This Permian-Triassic boundary (P/Tr) can be dated by coming into sight new living creatures born at the onset of the Triassic age, but the global crisis itself which has almost totally exterminated the life of the Paleozoic era needed approximately 200 million years for running its course. Although there were periods of renewals or „renaissances” which from time to time tried to break the march of the terrible destruction by bringing rejuvenations of the life, they were checked again and again by a mysterious process which by its repeated blows annihilated immense sectors of the Earth’s biosphere. Thus instead of using the term „P/Tr boundary” that of „Late or Upper Permian transitional period” or „transitional period at the end of the Permian” seems to be rather expedient as it describes the character of this event more expressively. The well known P/Tr boundary in its proper geological and biostratigraphical sense pegs out the very end of this period subsequently to which in the Lower- or Early Triassic already the new species of a regenerated biosphere are present.

Let us consider briefly the point at issue. Namely, the end of the Permian has been one of the most tranquil epochs of the Earth’s history; from that time no powerful orogenic movements, no volcanism of considerable importance - save the effusion of the Siberian plateau-basalts - are known and also there are no traces of the impact of some bigger celestial body like a great meteorite, a core of a comet or some micro-planet, of a disaster also which might be compared to that one causing the notorious Cretaceous-Tertiary boundary event (K/T). The papers published up to now are speaking of Permian-Triassic boundary event, although this crisis took place in the late period of the Permian, defined geologically as the „upper” part of this age. The Permian-Triassic boundary as it is understood in traditional sense was the time of the renaissance of organic life : then the living world had got the crisis over, and the development of a new, quite different world of creatures took its course. The crisis lasted approximately 20 million years; it commenced some 250 My ago and came to end 230 My ago. At first the overwhelming majority of the terrestrial plants (the giant ferns for example) and a lot of the plankton organisms disappeared: e.g. the radiolarians became extinct. This was the first phase of the crisis. The lasting „quiet and sneaking” character of the destructive process suggest the thought that these organisms may have been entirely defenseless against the increased level of the high-frequency electromagnetic and corpuscular radiations. During this time a gradual process of destruction evolving through several million years can be detected by the profound changes in the spectrum of the sessile benthic population (i.e. in that of the organisms living fixed to the sea floor); the brachiopods became extinct practically as a whole, moreover classes which had been outstandingly characteristic components of the Paleozoic fauna like the trilobites and several classes of the crinoids disappear as well. The list of such losses can be continued still for long (see Erwin, D.H. 1984, 1993; Hallam, A.-Wignall, P.B. 1997; Kozur, H. 1998). The tremendous destruction of the terrestrial plants, marine plankton and sessile benthic organisms triggered far reaching and hardly detectable „domino-effects” resulting in further steps of the ongoing extinction. Contrary to these events the ruin of the nektonic, i.e. free swimming organisms was of far less

dimensions, e.g. it is hardly perceptible in the fossil record of the fish. Obviously for these animals the way of escape was given by fleeing into greater depths sheltering them from the downpouring radiation.

The characteristic phenomena of the Upper Permian are the enrichment of the ^{13}C isotope in a measure unprecedented in the Earth's entire history together with the fall of the amount of the oxygen in the atmosphere from 35% to 10-12% causing in this manner the „superanoxy at the end of the Permian” (see Detre, Cs.H. et al. 1998). Both phenomena are known since some 20 years, and according to several opinions just these ones could have been the causes of extinction. But the potential causes responsible just for them were not found by the scientists. If we change however the facts occupying in this connection the positions of the cause and effect : that is to say by interpreting the superanoxia as an effect of the decaying biomass, then more than sufficient explanation can be found for the observed reality. In brief : the rotting biomass extracts tremendous amounts of oxygen from the atmosphere and from the seas. The extinction of more than 90% of the species resulted inevitably in the accumulation of enormous amounts of dead biomass. The characteristic lithologies of the Upper Permian are worldwide sedimentary rocks having very high organic matter content : their organic components originate from the decaying biosphere. As for example the exposures of Upper Permian black, bituminous limestone at Nagyvisnyó village in the Bükk Mountains can be mentioned. At the beginning of the Upper Permian the biosphere had suffered a kind of tremendous blow from the effects of which it could not recover even up to now : the available estimations - although their figures are broadly scattered - all conclude in pointing out that the amount of the recent biomass should be only a fraction of that existing 250 million years ago. The oxygen content of the recent atmosphere amounts to 21%; thus being far from that 35% which characterized it 250 million years ago. The golden age of the biosphere, its most widespread extension may have been in the Upper Carboniferous - Lower Permian time some 300-250 million years ago : the volume of it together with the rich diversity of its forms reached a peak never approached since then. It can be taken as granted however that the destructive supernova event of the Upper Permian had been the precondition of those evolutionary dynamics which led to the appearance of higher forms of the life ; first of all to that of the Man. The bulk of coal measures sedimented during the Upper Carboniferous - Lower Permian is many times as voluminous as the productive biomass of the recent time. (The quantification gives dispersed figures here too, but the significant mass-difference is unambiguous). From the outset of the Triassic the formation of carbonate rocks is on a leap-like increase : the rate of their Post-Triassic accumulation is approximately by an order of magnitude higher as it has been before. It seems to be a satisfactory explanation for this development, that the amount of C consumed earlier by living organisms accumulated henceforth in the lithosphere.

The spherules of interstellar origin, which can be found in the Late Permian deposits provide a rather solid argument for seeing in them the interstellar dust swept together by the shock wave front of a supernova explosion. Having diameters between 3-20 μm , they are composed preponderantly of iron (in excess of 90%) containing also some percents of Ni, Ti and Si (see Miono, S. et al. 1998). Their dimensions and elementary composition are remarkably similar in all occurrences. They were found in Hungary (in the Bükk Mountains), in Japan and South China, several occurrences of them are known in Central Asia, moreover in South Africa, Canada and the Antarctica too. These micron-sized particles which could have survived the penetration into the Earth's atmosphere became sedimented in the Upper Permian soil or on the sea-floor of that time. We have to mention here also the theory put forward by Ruderman and Truran some time ago (see Ruderman, M.-Truran, J.W. 1980). According to them it should have been possible as well that the shock wave front of a nearby supernova

explosion blew off a certain amount of dust from the Moon's surface : later these particles took part in the accumulation of geological deposits. In our case however we have to deal with spherules of interstellar origin. The crisis at the end of the Permian can be traced fundamentally by paleontological methods concerning micro- and macrofossils, biomass, superanoxia and so on. Based on the facts got known in this way and as an obvious explanation for their occurrence a nearby supernova explosion can be reconstructed. The spherules derived from the interstellar dust are additional evidences. It is also a fact however that the „supernova theory” of the great extinction evolving towards the end of the Permian can not be refuted - and this is a very good status for a scientific theory.

The event of the Upper Permian which during its course has dealt repeated but slow blows to the biosphere decimating but not exterminating it, moreover led to the sedimentation of the spherules may have been the result of the explosion of a supernova being then within 10 parsecs approximately from the Sun. In this event the interstellar material swept together by the explosion moreover the radiation space (as the supernova remnant) have had a decisive role. The explosion may have been neither too close, nor too far: the researchers are unanimous in estimating the extension of the danger zone at 10 parsecs approximately. The geological, paleontological and biostratigraphical evidences are all indicating that this explosion may have preceded the classical boundary between the Permian and the Triassic by some 20 million years. In the space measured by a radius of some 500 parsecs around the Sun a supernova event occur statistically in every 100 million years approximately, while in that one having the radius of 10 parsecs the occurrence of these events is reduced to several hundred million years already. Thus during the 4.6 thousand million year long history of the Solar System several nearby supernova explosions being within the 10 parsec range may have occurred (see Table 1.). During the time of the Upper Permian the Solar System may have crossed the closeness of a zone of star formation where the density of the interstellar material consisting of gases and dust surpassed the average one and where several big stars may have been in the course of formation, some of them at the outset of a supernova-type development.

Table 1.

Mass extinctions in the Earth's history caused probably by a nearby supernova explosion.

Geological boundary	Age in million years	Cosmic event
End of the Cambrian	500	SN
End of the Permian	250	SN
End of the Triassic	180	SN

References

- Detre, Cs.H., Tóth, I., Gucsik, A., Kiss, Á., Uzonyi, I., and Bérczi, Sz., 1998. *29th LPSC Conference*, p. 1030 (Houston, TX).
- Erwin, D.H., 1984. *Nature* **367**, 231.
- Hallam, A., and Wignall, P.B., 1997. *Mass Extinctions and Their Aftermath (Oxford University Press, 1997)*
- Kozur, H., 1998. *Palaeogeog., Palaeoclimat., Palaeoec.* **143.**, pp.227-272.
- Miono, Sh., Detre, Cs.H., Bérczi, Sz., Don, Gy., Dosztály, L., Solt, P., Tóth, I., Uzonyi, I., and Lukács, B., 1998. *29th LPSC Conference*, p. 1029 (Houston, TX).
- Ruderman, M.A., Truran, J.W., 1980. Possible transfer of lunar material to Earth from a nearby supernovae *Nature* **284**, pp.328-329.

TRACE ELEMENT CONSTRAINTS ON THE ORIGINS OF HIGHLY METAMORPHOSED ANTARCTIC EUCRITES

C. Floss¹, G. Crozaz¹, A. Yamaguchi², K. Keil³.

¹McDonnell Center for the Space Sciences and the Department of Earth and Planetary Sciences, Washington University, St. Louis, MO 63130, U.S.A.

²Antarctic Meteorite Research Center, National Institute of Polar Research, 1-9-10 Kaga, Itabashi, Tokyo 173-8515, Japan.

³Hawai'i Institute of Geophysics and Planetology, University of Hawai'i at Manoa, Honolulu, HI 96822, U.S.A.

Introduction: Although eucrites formed as crustal rocks through the eruption of basaltic lavas on the surface of their parent body, many of them have experienced varying degrees of metamorphism [e.g., 1]. Studies of non-cumulate eucrites [2] have nevertheless shown that most exhibit systematic trace element variations in pyroxene and plagioclase, which provide information about their petrogenetic histories and relationships to one another. For example, most non-cumulate eucrites have similar ratios of light rare earth elements (LREE) to heavy rare earth elements (HREE) for plagioclase and pigeonite, respectively (Fig. 1). Although highly metamorphosed eucrites such as Ibitira [2,3] and EET90020 [4,5] have experienced redistribution of the rare earth elements (REE) from Ca-phosphates to plagioclase and pigeonite, in at least some instances other trace elements do not appear to have been affected by inter-mineral redistribution [e.g., 5].

Here we have used the ion microprobe to examine the distributions of the REE and selected other trace elements in individual minerals from four unusual equilibrated eucrites from Antarctica. Petrologic observations have been reported by [6] and are briefly summarized below.

Yamato 86763: this eucrite has a subophitic texture resembling that of EET90020. Pigeonite crystals are large and contain closely spaced thin augite lamellae, classifying this eucrite as a type 5 [7]. Plagioclase grains have a narrow compositional range and the laths are mostly clear, although some contain minor inclusions. Recrystallized mesostasis is present as finer-grained intergrowths of tridymite, pyroxene and plagioclase. Oxide minerals in Y-86763 are often surrounded by thin rims of compositionally variable pyroxene and Fe-rich olivine, similar to those observed in EET90020 [8].

We measured trace element abundances in the cores and rims of both pigeonite and plagioclase. Plagioclase is LREE-enriched ($La = 7 \times CI$) with a positive Eu anomaly. Pigeonite is enriched in the HREE ($Yb = 11 \times CI$; $Yb/Sm = 2.3$) with a negative Eu anomaly. Both minerals have uniform REE abundances, within as well as between individual grains. One merrillite grain has a LREE-enriched pattern with abundances intermediate between those of non-cumulate eucrites and Ibitira.

Asuka 87272: this is a monomict eucrite, which contains both coarse-grained regions with relict subophitic texture and fine-grained recrystallized granulitic areas. Pigeonites have retained some remnant Ca-zoning and contain heterogeneously spaced augite lamellae. Plagioclase grains have uniform compositions and are largely free of inclusions. This meteorite is highly shocked. The pyroxenes are extensively fractured and mosaicized; although plagioclase grains are less fractured, many have been maskelynitized.

Plagioclase REE abundances are uniform, with La concentrations about a factor of two lower than those in Y-86763. Pyroxene REE compositions are variable and abundances increase with increasing Ca abundances, reflecting heterogeneous sampling of augite lamellae during analyses. Furthermore, all pyroxene REE patterns exhibit positive Ce anomalies whose magnitudes (expressed as Ce/Ce^* where Ce^* is the interpolated value between CI-normalized La and Pr abundances) range from 2.5 to 8.2. Both positive and negative Ce anomalies have been

observed in numerous Antarctic meteorites [2,9-12]. In eucrites they are found in both plagioclase and pyroxene and have been attributed to remobilization of the REE through terrestrial weathering of phosphates, during which Ce^{3+} is oxidized to the more insoluble Ce^{4+} [10,13]. Ce anomalies are most pervasive in the presence of networks of shock-induced fractures and microcracks along which the REE may be mobilized [2,10]. The extensive fracturing of pyroxene in A-87272, but not of plagioclase, probably accounts for the presence of Ce anomalies in the former and their absence in the latter. Because redistribution of the REE in pyroxene may be accompanied by alteration-induced variations of other elements, these data cannot be used to interpret the origin of A-87272. However, plagioclase compositions appear to have been unaffected by terrestrial weathering.

Asuka 881467 and Asuka 881388: these eucrites are granulitic with highly recrystallized textures. Both pigeonite and augite are present as well as plagioclase. The pigeonites contain thin closely spaced augite lamellae, but separate augite grains generally do not contain inclusions or exsolved phases. Pyroxene compositions are slightly more magnesian in A-881388 than in A-881467. Plagioclase compositions are homogeneous within each eucrite, but differ slightly between the two [6]. In A-881388 most plagioclase grains are clear, but those in A-881467 contain abundant inclusions of pyroxene and silica. Trace element measurements are presently underway for A-881467 and results will be presented at the meeting. In A-881388, plagioclase REE compositions are uniform, with abundances similar to those in A-87272 plagioclase. Both pigeonite and augite also have uniform REE compositions, with REE patterns typical for these minerals.

Discussion: Figure 1 shows the relationship between HREE and LREE in plagioclase and pigeonite from non-cumulate eucrites. Most fall along a single correlation line, which for plagioclase also represents the abundances expected for crystallization from melts with chondritic proportions of the REE [2]. However, Hsu and Crozaz [2] found that in highly metamorphosed eucrites, such as Ibitira, pigeonite and plagioclase REE compositions are LREE-enriched and fall to the right of these lines. They noted that REE concentrations of Ibitira

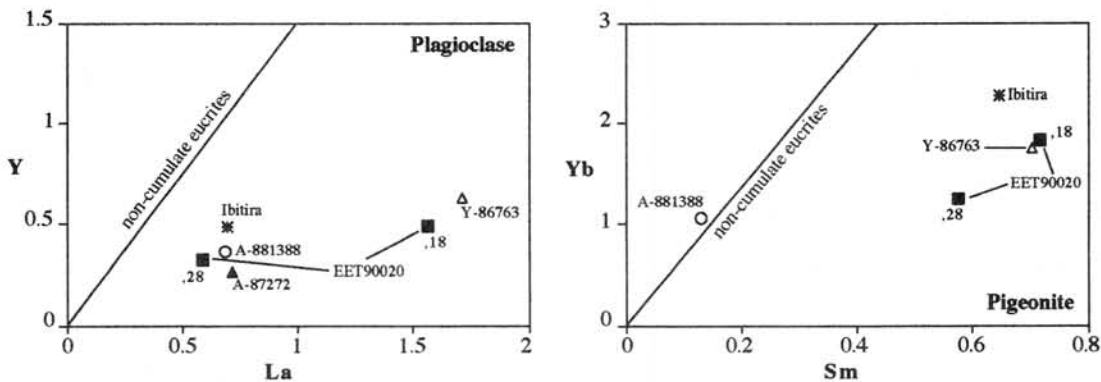


Fig. 1 HREE vs. LREE abundances (ppm) in plagioclase and pigeonite. Adapted from [2].

merrillite were lower than in other non-cumulate eucrites, and suggested that partial melting of the mesostasis, which contains phosphates, and interaction of this melt with pigeonite and plagioclase produced the LREE-enriched signature [2,3]. Merrillite would ultimately crystallize from the partial melt with lower REE concentrations. Floss and Crozaz [4,5] examined the trace element distributions in another highly metamorphosed eucrite, EET90020 and found evidence for a heterogeneous redistribution of the REE. Both plagioclase and pyroxene exhibit greater degrees of LREE-enrichment in a portion of the eucrite which, texturally, appears to have undergone more extensive heating and/or partial melting [5]. In addition to extensive thermal metamorphism, Yamaguchi *et al.* [8] have suggested that EET90020, as well as Ibitira, experienced an episode of rapid reheating and cooling, based on the presence of compositionally variable phases with the well-equilibrated host material of both of these eucrites. They

suggested that deep burial and extended heating of these eucrites [1], followed by excavation during a large impact event could account for the observations.

Plagioclase in the eucrites studied here exhibits LREE-enrichments similar to those previously observed in Ibitira and EET90020 (Fig. 1). A-87272 and A-881388 have LREE/HREE ratios similar to those of Ibitira and EET90020,28 whereas Y-86763 exhibits a much higher degree of LREE-enrichment, similar to that displayed by EET90020,18. LREE/HREE ratios for pigeonite from Y-86763 are similar to those observed in Ibitira and EET90020. However, pigeonite from A-881388 falls along the non-cumulate eucrite trend.

We analyzed one merrillite grain from Y-86763 with REE abundances lower than those of other non-cumulate eucrites; Ca-phosphates are present in the other eucrites, but none large enough to analyze by ion microprobe have been found. It is likely that a mechanism similar to that postulated for Ibitira and EET90020 is responsible for the LREE-enrichments observed in plagioclase and pigeonite from these eucrites. Furthermore, Y-86763 contains compositionally variable rims on oxide grains similar to those observed in EET90020 and Ibitira and, thus, may have experienced a similar thermal history.

The fact that pigeonite from A-881388 falls along the non-cumulate eucrite trend, whereas plagioclase is LREE-enriched (Fig. 1) suggests that pyroxene may be less affected by redistribution of the REE than plagioclase. Although this appears counterintuitive, it may be significant that those eucrites which exhibit the largest LREE-enrichments in plagioclase (Y-86763 and EET90020,18) have pyroxenes whose LREE/HREE ratios do not differ significantly from Ibitira. An alternative explanation is suggested by the fact that this eucrite contains, in addition to pigeonite, augite thought to have formed during thermal metamorphism [6]. The LREE may have been preferentially incorporated into augite relative to pigeonite during recrystallization and subsolidus growth. A similar process has been suggested for augite derived from the inversion of primary pigeonite [14]. Results from analysis of A-881467, which also contains both pigeonite and augite, may help resolve this question.

Although REE distributions in plagioclase and pigeonite from these eucrites do not offer clues to their petrogenetic origins, the distributions of several other trace elements appear to provide links to the non-cumulate eucrites. Abundances of Ti and Zr in A-881388 pigeonite fall in the non-cumulate eucrite field (Fig. 2), although Y-86763 pigeonite show enrichments of these elements similar to those observed for Ibitira and EET90020. Furthermore, abundances of Na, K, Sr and Ba in plagioclase from all three of these eucrites fall within the fields defined for non-cumulate eucrites [2,3].

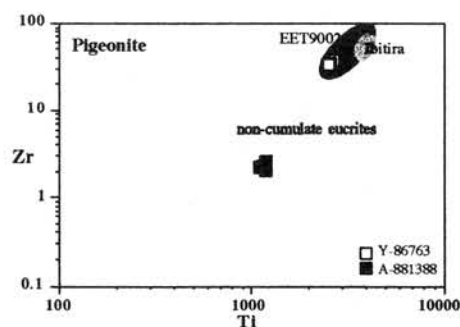


Fig. 2 Abundances (in ppm) of Ti vs. Zr in pigeonite. Data for non-cumulate eucrites and Ibitira from [2].

References: [1] Yamaguchi *et al.* (1996) *Icarus* **124**, 97-112. [2] Hsu and Crozaz (1996) *Geochim. Cosmochim. Acta* **60**, 4571-4591. [3] Hsu and Crozaz (1997) *Geochim. Cosmochim. Acta* **61**, 1293-1302. [4] Floss and Crozaz (1997) *Met. Planet. Sci.* **32**, A41-A42. [5] Floss and Crozaz (1998) *Lunar Planet. Sci. XXIX*, Abstract #1239. [6] Yamaguchi *et al.* (1997) *Antarct. Meteorite Res.* **10**, 415-436. [7] Takeda and Graham (1991) *Meteoritics* **26**, 129-134. [8] Yamaguchi *et al.* (1997) *Met. Planet. Sci.* **32**, A144-A145. [9] Lundberg *et al.* (1990) *Geochim. Cosmochim. Acta* **54**, 2535-2547. [10] Floss and Crozaz (1991) *Earth Planet. Sci. Lett.* **107**, 13-24. [11] Harvey *et al.* (1993) *Geochim. Cosmochim. Acta* **57**, 4769-4783. [12] Wadhwa *et al.* (1994) *Geochim. Cosmochim. Acta* **58**, 4213-4229. [13] Mittlefehldt and Lindstrom (1991) *Geochim. Cosmochim. Acta* **55**, 77-87. [14] James *et al.* (1998) *Lunar Planet. Sci. XXIX*, Abstract #1292.

Formation condition of fine phosphides in metals of Yamato-790126 (L) chondrite

Takashi Fujita

Department of Geology and Mineralogy, Graduate School of Sciences, Kyoto University, Sakyo, Kyoto 606-8502.

Introduction

It has been reported that reduction of phosphate in chondrite increased phosphor content in metals or formed phosphides (Begemann and Wlotzka, 1969; Taylor and Heymann, 1971). Schreibersite, a common iron-nickel phosphides in meteorites shows various morphologies (platy or rod-like texture) depending on its composition and thermal histories experienced by the host meteorite (Doan and Goldstein, 1969). Therefore, variety of phosphide texture may be used as an indicator of thermal condition experienced by the meteorite.

In shock-melted chondrites, metal-troilite aggregates often contain phosphide as schreibersite layer observed at a metal-troilite contact (Begemann and Wlotzka, 1969; Taylor and Heymann, 1971). Such occurrence accompanies negative zoning relation of P and Ni in adjacent metals, and was explained by crystallization of the schreibersite from Fe-Ni-P liquid (Taylor and Heymann, 1971).

In Yamato-790126, metals include numerous fine phosphides of rod-like (so called "rhabdite") texture although the texture of host metal-troilite aggregate resembles to those containing layered schreibersite. In the present study, observation and microprobe analysis (using Jeol-8800) of metal-troilite aggregate and host meteorite of Y-790126 were carried out in order to distinguish the different conditions reflected in the phosphide texture.

Texture of host meteorite (Fig.1)

Texture of host meteorite in Y-790126 experienced severe reprocessing after the accretion. Silicate portion is well separated from metals and is composed of coarse phenocrysts of euhedral pyroxene and dusty olivine embedded in matrix mainly composed of granular olivines and interstitial glass. Metal-troilite forms a coarse aggregate in which globular metals are embedded in troilite. As like as similar textures reported previously (Begemann and Wlotzka, 1969; Taylor and Heymann, 1971, Scott,1982), such texture can be interpreted as a product of secondary melt formed on the parent body (possibly by impact).

Metal and phosphide

In the metal-troilite aggregate, globular metals of hundreds μms in sizes are embedded in troilite. Metals are richer in Ni in their edges (Ni~20), while some

coarse grains have Ni-rich core. These metal grains include numerous phosphides of micron to submicron sizes (Fig.2). The crystal morphology of the phosphide, show fine rod-like texture which resembles natural "rhabdite" (Doan and Goldstein, 1969) and artificial precipitate from phosphor rich iron (Suzuki, 1992). Results of broad beam analysis of metals plotted against distance from the rim (Fig3) show a positive correlation of phosphor content with Ni.

Formation condition of fine phosphide

Texture of both opaque phase and silicate portion resemble to those reported as products of impact melts (Begemann and Wlotzka, 1969; Taylor and Heymann, 1971; Miyamoto et al.,1984). The clear separation of metals from silicate, so-called eutectic texture of the metal-troilite aggregate, and Fe-Ni zoning pattern of metals indicates the formation of the opaque aggregate from liquid immiscibly separated from silicate on the parent body.

As it has been discussed in the previous studies, high P content in the opaque phase may be a result of reduction of phosphate originally included in the chondritic texture. On the other hand, we need different explanation for different occurrence of phosphide and different zoning pattern of metals. Taylor and Heymann (1971) explained the negative relation of Ni and P of metals, and occurrence of schreibersite layer in opaque aggregate in Orvinio chondrite by crystallization of metal and schreibersite from Fe-Ni-P liquid. While, this interpretation can not be used to explain the positive correlation of Ni and P in metals in Y-790126. In the present specimen, occurrence of fine phosphide implies a solid state precipitation from metal. In such a case, as P in phosphide is originally a solution in the metal, positive correlation of Ni and P must be formed in crystallization process of the metal. If a metal crystallize from Fe-Ni-P-S system without an occurrence of phosphide, enrichment of both Ni and P content in the rim of the metal grain may be expected (cf. Zayzev et al., 1994). High Ni content in the metals requires a relatively low eutectic temperature at which metal completed crystallization. In such condition, low diffusion rate of P and Ni in metal prevents formation of schreibersite layer (Doan and Goldstein, 1969), but allowed precipitation of phosphide in situ.

As a cause for the difference in occurrence of phosphide in opaque phase, different composition of the original liquid, and different cooling rate of the aggregate can be considered. Because the Ni and P content in the metals of Orvinio and Y-790126 show no significant difference, a plausible explanation is that in Y-790126, phosphide layer didn't solidified from melt because of a relatively faster cooling rate, but subsequent annealing resulted in precipitation of fine phosphide from metals. Because the phosphide grains fixed Ni content in situ, zoning pattern of the Ni may be preserved during such annealing condition.

References

- Begemann, F. and Wlotzka, F. (1969) *Geochim. Cosmochim. Acta*, **33**, 1351-1370.
 Doan, A.S. Jr., and Goldstein, J.I. (1969) *Meteorite Research*, edited by Millman, P.M., D.Reidel Dordrecht, Holland, p.763-779.
 Miyamoto, M., Takeda, H. and Ishii, T. (1984): *J. Geophys. Res.*, **89**, 11581-11588.
 Scott, E.R.D. (1982): *Geochim. Cosmochim. Acta*, **46**, 813-823.
 Suzuki, S. (1992): *Z. Metallkd.*, **83**, 153-156.
 Taylor, G.J. and Heymann, D. (1971): *J. Geophys. Res.*, **76**, 1879-1893.
 Zaitsev, A.I., Litvina, A.D., Dobrokhotova, Zh.V., and Mogutnov, V.M. (1994): *Inorganic Materials*, **30**, 1264-1270.

Fig1

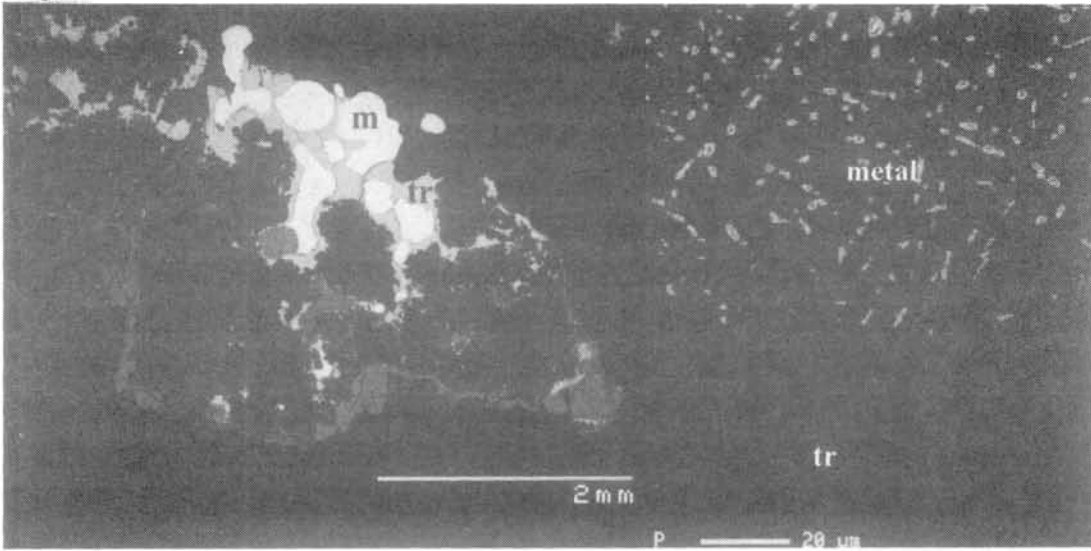


Fig.2

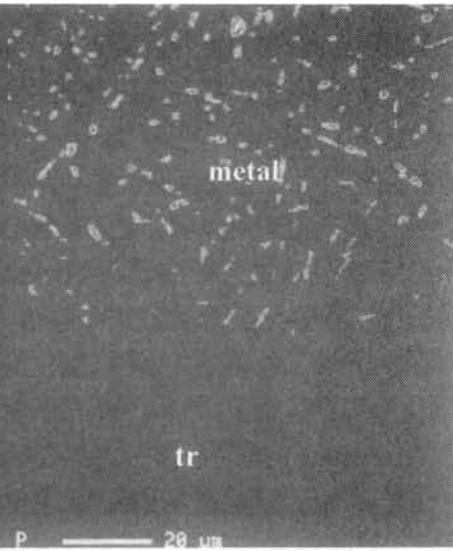


Fig.3

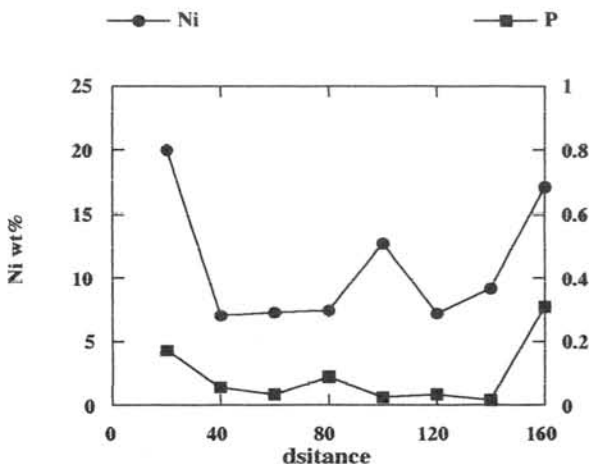


Fig.1 Backscattered electron image of Yamato-790126. Metal-troilite forms a coarse aggregate. m: metal, tr: troilite.

Fig.2 X-ray map of phosphorus at a metal-troilite boundary region. Fine phosphides occur in the metal.

Fig.3 Weight content of Ni and P plotted against distance (μm) in a metal globule.

CHEMICAL COMPOSITION OF GLASSY SPHERULES COLLECTED AT THE DOME FUJI STATION BY THE 37TH JARE TEAM

Takaaki Fukuoka¹, Yuji Tazawa², Kentaro Terada³, Takeshi Mori³, Yuji Sano³, Tomoki Nakamura⁴, Naoya Imae⁵, Takaaki Noguchi⁶, Ken-ichi Nogami⁷, Rie Ohmori⁷, Toshio Murakami⁸, Nahoko Kondo⁹, Izumi Nakai⁹, and Hideo Ohashi¹⁰

¹ Dept. of Environmental Systems, Fac. of Geo-Environmental Sci., Rissho Univ., 1700 Magechi, Kumagaya, Saitama 360-0194, ² Dept. of Phys., Fac. of Sci., Kyoto Univ., Sakyo, Kyoto 606-8502, ³ Dept. of Earth and Planet. System Sci., Fac. of Sci., Hiroshima Univ., 1-3-1 Kagamiyama, Higashi-Hiroshima 739-8526,

⁴ Dept. of Earth and Planetary Sci., Fac. of Sci., Kyushu Univ., Hakozaki, Fukuoka 812-8581, ⁵ Nat. Inst. of Polar Res., 1-9-10 Kaga, Itabashi, Tokyo 173-8515, ⁶ Dept. of Materials and Biological Sci., Ibaraki Univ., 2-1-1 Bunkyo, Mito 310, ⁷ Dept. of Physics, Dokkyo Univ., School of Medicine, Mibu, Tochigi 321-0293, ⁸ Computer Center, Gakushuin Univ., 1-5-1 Mejiro, Toshima, Tokyo 171-8588, ⁹ Dept. of Applied Chemistry, Fac. of Sci., Sci. Univ. of Tokyo, Kagurazaka, Shinjuku, Tokyo 162-0825, ¹⁰ Dept. of Ocean Sci., Tokyo Univ. of Fisheries, Kounan, Minato, Tokyo 108

Glassy spherules have been separated from deposit in the water tanks of the dome Fuji station, Antarctica which was collected by the 37th Japanese Antarctic Research Expedition team. The water tanks were used as reservoir of water for the daily life of the residents. 400 liters of water were prepared every day from accumulated snow around the station. Shapes of glassy spherules are sphere, droplets, and sometimes dumb-bells. They are mainly yellow, rarely brown. They contain a lot of babbles.

Chemical composition (28 elemental compositions) of five glassy spherules have been analyzed by instrumental neutron activation analysis (INAA). Chemical composition of 12 glassy spherules have also been analyzed by EPMA and by SHRIMP. The results of INAA are shown in Table 1. The results of INAA show that high Ca and Al contents with low Si, Fe, Mg, Na contents. The C1 chondrites normalized REE pattern show fractionated patterns with higher La values. Siderophiles such as Ir and Au which are typical extraterrestrial elements could not be detected. The results of EPMA and SHRIMP are similar to those of INAA with one exception. Only one glassy spherule has a flat pattern which is typical REE pattern for extraterrestrial sample.

Dosztaly and Don (1977) found glassy spherules in a number of stratigraphic levels from Upper Permian formations to recent fluvial sediments. Their shapes, color etc are similar to the dome Fuji glassy spherules. The chemical compositions of those are surprisingly similar to the dome Fuji spherules except one glassy sample which was analyzed by EPMA and SHRIMP.

How to explain similar physical and chemical features and different locality. At present, we don't have good answer.

Tabel I. Chemical abundances of glassy spherules separated from deposit in the water tanks of the dome Fuji station, Antarctica

		1	2	3	4	5	JB-1	Error*
								(%)
Wt	μ g	16.8	13.2	12.6	20.1	29.2	45.3	
Al ₂ O ₃	%	15.2	15.5	15.8	14.5	14.9	=14.5	0.5
FeO ¹⁾	%	0.32	0.28	0.33	0.30	0.36	=8.11	6-7
MgO	%	6.9	6.3	6.2	4.5	6.2	=7.7	16-24
CaO	%	37.9	38.7	39.8	35.2	38.7	=9.24	5
Na ₂ O	%	0.201	0.193	0.205	0.195	0.213	=2.79	0.4-1
K ₂ O	%	0.35	0.28	0.32	0.33	0.36	=1.42	6-9
TiO ₂	%	1.12	1.00	0.89	2.10	0.77	=1.34	13-45
MnO	%	0.16	0.22	0.17	0.15	0.17	=0.16	<3
Cr	ppm	39	25	27	26	30	=414	3-4
V	ppm	1.45	0.22	—	0.136	0.124	=212	5-25
Rb	ppm	6.5	—	6.3	16.9	12.3	=41.2	30-86
Sr	ppm	480	590	450	400	530	=435	17-22
Ba	ppm	760	830	730	690	760	=490	12-16
Sc	ppm	21.2	22.0	22.0	21.1	21.9	=28.9	0.5
La	ppm	51.5	50.9	53.0	50.1	55.5	=38.8	1
Ce	ppm	94.6	97.6	94.5	91.0	100.3	=63	1
Nd	ppm	46.8	46.2	48.4	46.1	51.3	=27	3
Sm	ppm	10.12	9.89	10.39	9.77	10.84	=5.02	0.4
Eu	ppm	2.97	2.86	3.04	2.90	3.22	=1.59	1.2-1.7
Tb	ppm	1.69	1.71	1.77	1.63	1.79	=0.70	5
Yb	ppm	7.7	7.3	8.0	7.3	8.2	=2.4	2-3
Lu	ppm	1.22	1.17	1.27	1.19	1.30	=0.37	3-3.5
Zr	ppm	300	200	410	380	300	=143	26-50
Hf	ppm	5.7	5.8	5.7	5.8	5.9	=3.4	3-4
Th	ppm	13.1	12.7	13.1	13.0	13.3	=9.2	2
U	ppm	8.2	8.2	8.4	8.0	8.7	=1.7	3-4
Ta	ppm	0.31	0.25	0.20	0.27	0.80	=3.6	20-100
Co	ppm	12.1	5.1	1.6	1.7	1.8	=39.1	2-10

* Errors for INAA are due to counting statistics.

1) Total iron as FeO.

Stability of natural remanent magnetization and shock remagnetization of Rumanova (H5) chondrite

M. Funaki¹, I. Tunyi², O. Orlicky² and V. Porubcan³

1: National Institute of Polar Research, Tokyo, Japan

2: Geophysical Institute of Slovak Academy of Sciences, Bratislava, Slovak Republic

3: Astronomical Institute of Slovak Academy of Sciences, Bratislava, Slovak Republic

Rumanova (H5) chondrite showed evidence of recrystallized features in the chondrules and matrix which we ascribe to shock heating, and impact deformation is further characterized by the presence of Neumann bands on kamacite grains (Rojkovic et. al., 1995). We have investigated the basic magnetic properties of Rumanova, with the purpose of evaluating criteria which might be related to the impact disturbance.

The natural remanent magnetization (NRM) stability of Rumanova was examined by AF demagnetization out to 50mT in steps of 5mT, as shown in Fig. 1. The original NRM intensity $5.755 \times 10^{-2} \text{Am}^2/\text{kg}$ decreased gradually and its direction shifted smooth out to 45mT. The magnetization at 50mT is insignificant because of the abrupt change in the direction between 45 to 50mT and the weak residual magnetization. When the sample acquired the saturation isothermal remanent magnetization (SIRM) due to a field of 0.8T, the intensity increased to $7.921 \times 10^{-1} \text{Am}^2/\text{kg}$. The REM value (NRM/SIRM) of 0.072 may suggest weak magnetic contamination by a hand magnet etc. (Wasilewski and Dickinson, 1998).

The 1st run thermomagnetic curve (Fig. 2) was measured in a magnetic field of 1.0T of the external magnetic field under 10^{-3} Pa atmospheric pressure. The curve yielded the clearly defined Curie point of taenite (γ -phase) at 450°C and the phase transition from kamacite (α -phase) to γ -phase at 760°C and from γ -phase to α -phase at 630°C . No tetrataenite (γ' -phase) may be present in the sample due to absence of the apparent Curie point around 550°C . Fine-grained magnetic minerals are probably present due to relatively large coercive force (H_C)=17.1mT, and remanent coercive force (H_{RC})=75.2, which were identified by the magnetic hysteresis loop. Another possibility for the large coercivity is shock hardening which remains to be evaluated.

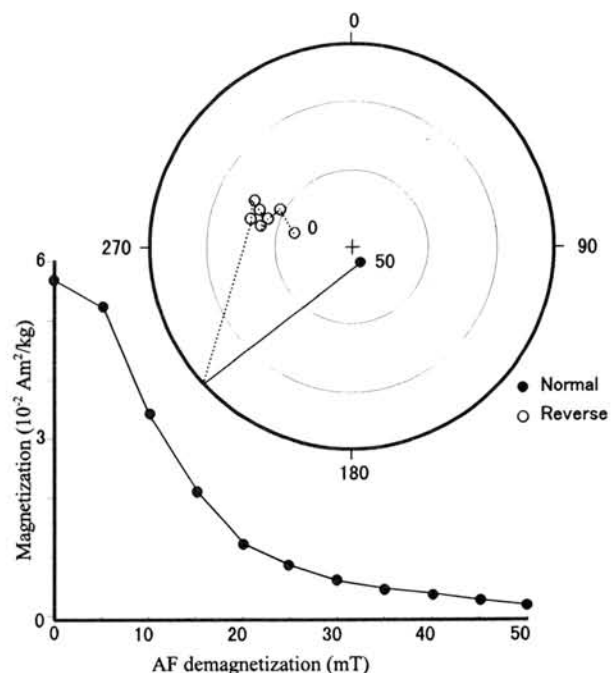


Fig. 1 AF demagnetization curves of NRM for Rumanova

A polished section was etched by NO_2 and then it was observed by reflected light microscopy. The results indicated that the metallic grains consisted of α , γ , plessite ($(\alpha+\gamma)$ -phase), and cloudy taenite (fine-grained $(\alpha+\gamma)$ -phase). Deformed Neumann bands decorate on the α -phase. When magnetic fluid was painted on the surface, the fluid accumulated on the cloudy taenite, but no accumulation was observed on the periphery of the cloudy taenite. The γ' -phase, when present, is formed along the periphery of taenite and cloudy taenite, and we therefore conclude that tetrataenite is absent by these microscopical observations.

The presence of Neumann bands suggest the shock level could not be lower than 1GPa. However, from the partial melting of silicate phase (Rojkovic et al., 1995), the maximum local temperature suggests local shock levels much higher. If the shock level exceeds about 13GPa, the transformation microstructure is observed, but we did not observe this microstructure. This NRM of Rumanova has high directional stability and may be indicative of shock related demagnetization. We suggest the NRM of Rumanova was acquired in the cloudy taenite and plessite in the presence of the internal local magnetic field of the parent body during shock impact.

References

- Rojkovic, I., V. Porubcan and P. Siman (1995): Nalez meteoritu pri obci Rumanova. *Mineralia Slovaca*, **27**, 331-342.
- Wasilewski, P., and Dickinson, T. (1998): The role of magnetic contamination in meteorites. submitted to *Meteorit . Planet. Sci.*

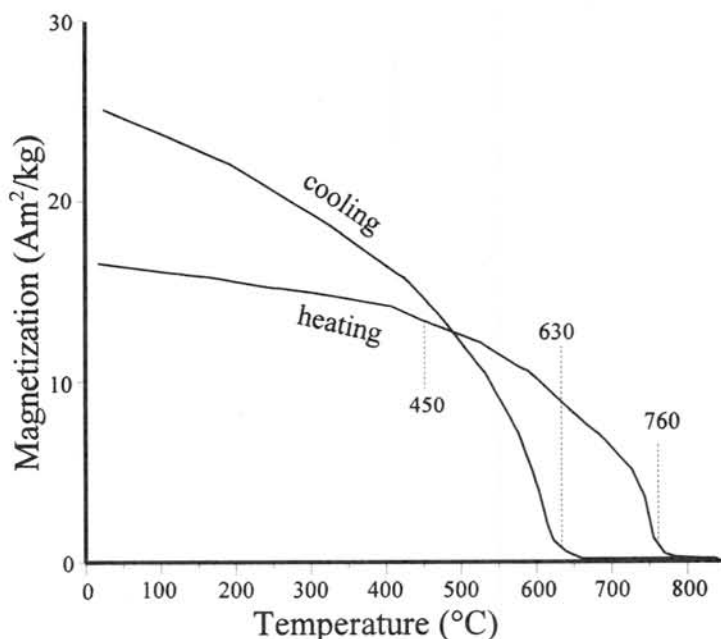


Fig. 2 Thermomagnetic curve (1st run) of Rumanova. $H=1.0T$

THREE DIMENSIONAL STRUCTURE OF PALLASITE ESQUEL BY X-RAY COMPUTED TOMOGRAPHY

HANAMOTO Takashi¹, TSUCHIYAMA Akira^{1*}, KAWABATA Toshiharu¹, KOEZUKA Takayasu², TSUJIMOTO Yoshikazu², and WASSON John T.³

1) Department of Earth and Space Science, Osaka University, Toyonaka 560-0043, JAPAN, *akira@ess.sci.osaka-u.ac.jp, 2) Nara National Cultural Properties Research Institute, Nara, 630-8002, JAPAN, 3) Institute of Geophysics and Planetary Physics, University of California, Los Angeles, CA 90095-1567, USA

Introduction: It is widely accepted that main group pallasites formed at an asteroidal core-mantle boundary because of their mineral compositions (olivine and metal). Two different origins of pallasites have been proposed; pallasites were formed by (1) impact fragmentation of olivine and injection of metal from the crystallizing core [1,2], and (2) incomplete buoyant separation of mantle olivine from the adjacent molten metallic core under static conditions [3,4]. The fragmentation origin is accepted by the observation that most pallasitic olivine is angular, and thus attention has focused on formation by mixing of metal and olivine during violent events. In the present study, a three dimensional structure of Esquel meteorite, which is a typical main-group pallasite and has angular olivine, was examined by X-ray computed tomography (CT) to obtain new perspectives on pallasite formation.

Experiments: Esquel has four lithologies [1]: (1) “pallastic” matrix consisting of olivine fragments embedded in metal, (2) large olivine nodules, (3) massive metal, and (4) rare zones dominated by FeS and fine olivine. The sample used in the present study has a “pallastic” matrix lithology, which consists of 60.6% olivine, 37.9% metal and 1.5% others (troilite, schreibersite and chromite) [1]. A parallelepiped (8x6.5x13 cm) of the sample was imaged by X-ray CT for three dimensional analysis.

An X-ray CT scanner for industrial use (HITACHI HiXCT-1M) at Nara Cultural Properties Research Institute was used. This scanner has a linear accelerator as an X-ray source (950 keV). The transition-rotation method was used to obtain X-ray projections, and images were reconstructed from the projections by the filtered back projection method. Each image of a slice has 512x512 pixels, and each pixel has 8-bit gray scale of CT value, which is related to the X-ray attenuation coefficient of the sample. The size of the pixel is 0.4x0.4 mm, which determines the horizontal spatial resolution. The slice thickness is 2.0 mm, and successive images were taken with every 0.8 mm intervals. This determines the vertical spatial resolution. Successive images of 100 slices were taken to reconstruct the three dimensional structure.

Image analysis: Some artifacts were observed in the images; beam hardening, ring artifacts, and artifacts by X-ray scattering. Correction for the beam hardening was made by adding a linear CT value function (from the edge to the center of a rectangular sliced sample), which was determined empirically from the images. No correction was made for the other artifacts. The outer parts of the sample (air) and the sample edges, which are diffused due to the spatial resolution, were removed for further analysis. Olivine and metal were distinguished by using a threshold CT value (180), which was determined to match the modal olivine in the sample.

In order to detect individual olivine particles in the three dimensional structure, a specific algorithm, named seeding and olivine/metal interface (SOMI) algorithm, was developed in the present study. In this algorithm, “seeds” (1 boxel in size) of olivine particles were found by erosion of the olivine images first. The seeds were dilated spherically by N_i times, where N_i is the number of the erosion for a finding seed- i . If a seed- j was included in a sphere with a seed- k , olivine with the seed- j was removed and merged into olivine with the seed- k . Then, olivine particles were detected by using the seeds temporally. Many of these particles were in contact with each other. If the proportion of the surface area of the olivine-olivine interface exceeded a threshold (0.4), this particle was merged into a neighbor particle with less olivine-olivine interface. By repeating the above process, olivine particles were finally determined.

Results and discussion: Fig.1a shows the three dimensional structure of the images with the gray scale. Grains with dark contrasts are olivine embedded in metal with bright contrasts. If some olivine grains are isolated, the olivine-metal system did not reach a gravitational equilibrium. The olivine grains seem to be touching each other within the present spatial resolution (≥ 1 mm) except for one small grain (Fig.2). More isolated olivine grains may be detected if the spatial resolution is enhanced. We also observed planer metal which divides olivine grains three dimensionally (Fig.3) and small metal inclusions in olivine. These textures suggest fragmentation of a dunite with metal injection followed by some degree of annealing.

Olivine particles detected by the SOMI algorithm are shown in Fig.1b. The olivine particles generally have complex shapes (Fig.4). Relation between the volumes and surface areas of the particles (Fig. 5) shows that the fractal dimension of the particle shapes is 2.34. Size frequency distribution of the olivine particles (Fig.6) does not show a power law distribution, which is expected from simple fragmentation. This distribution may be caused by fragmentation of a dunite along olivine grain boundaries although a simple cumulate model cannot be excluded by the size distribution alone. The fractal-like shape of the olivine particles may be explained by deformation of a dunite before metal injection.

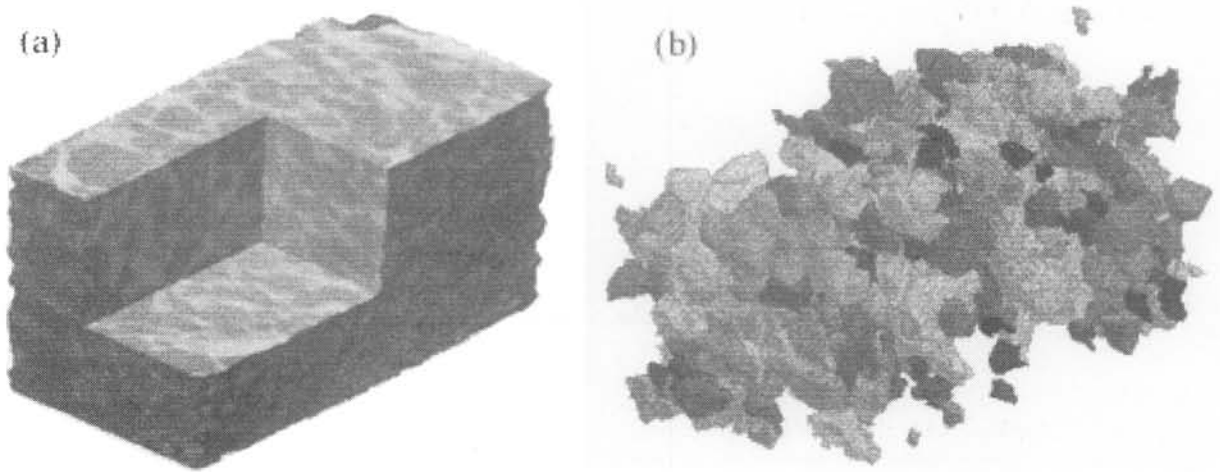


Figure 1. Three dimensional structure of pallasite Esquel (8x6.5x13 cm). (a) Olivine (gray) and metal (dark). (b) Olivine particles detected by the SOMI algorithm. Particles touching the border are removed.

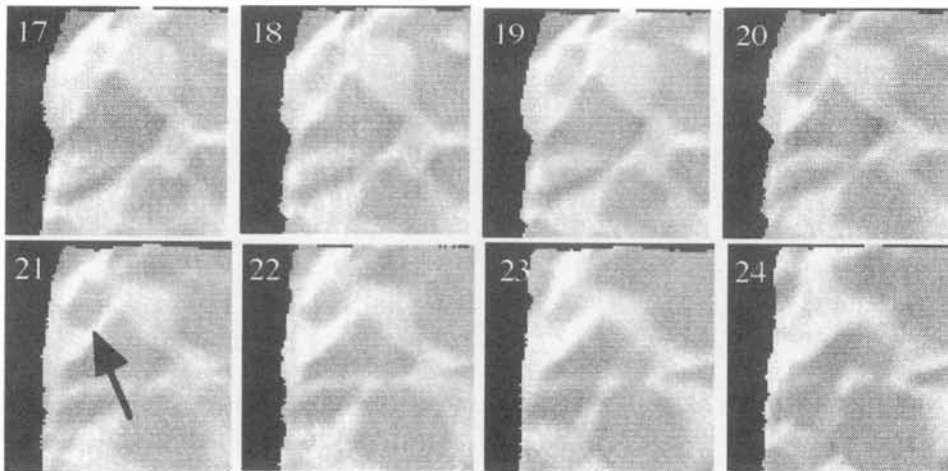


Figure 2. An isolated olivine grain in successive images with 0.8 mm interval. The width of each image is about 3.5 cm.

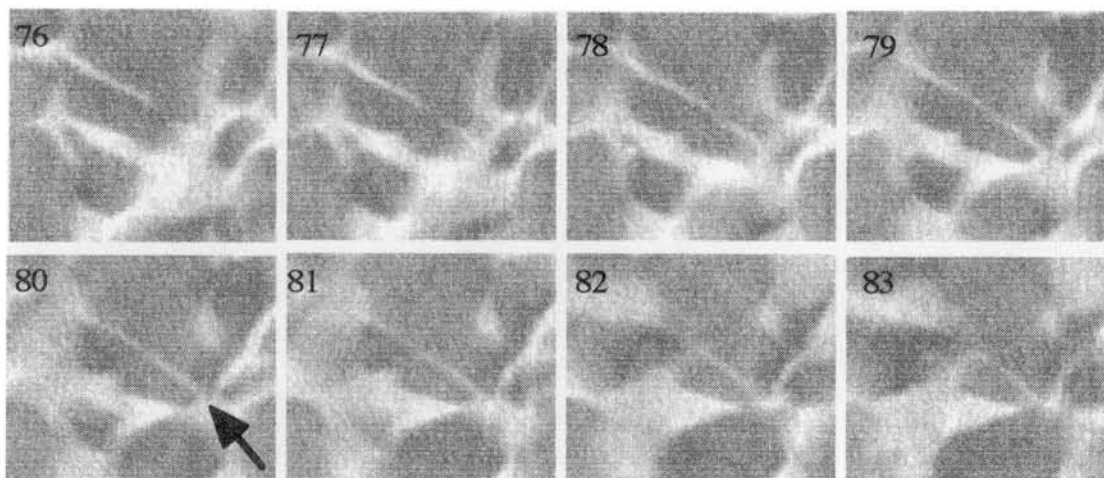


Figure 3. Planer metal dividing olivine grain in successive images with 0.8 mm interval. The width of each image is about 3.8 cm.



Figure 4. A stereograph of an olivine particle showing complex shape (about 3 cm in size).

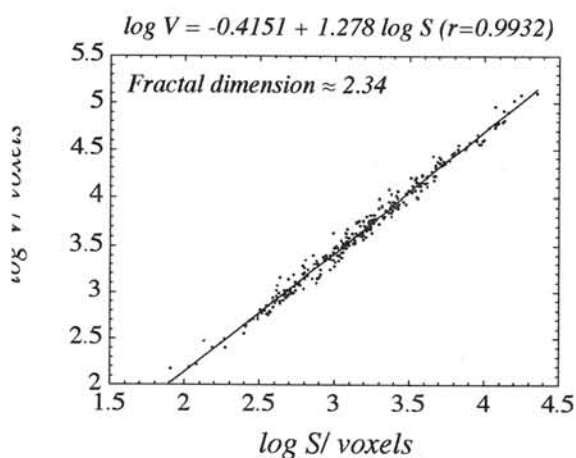


Figure 5. Logarithms of the volumes, V , plotted against those of the surface areas, S , for the olivine particles. The relation gives the fractal dimension of 2.34.

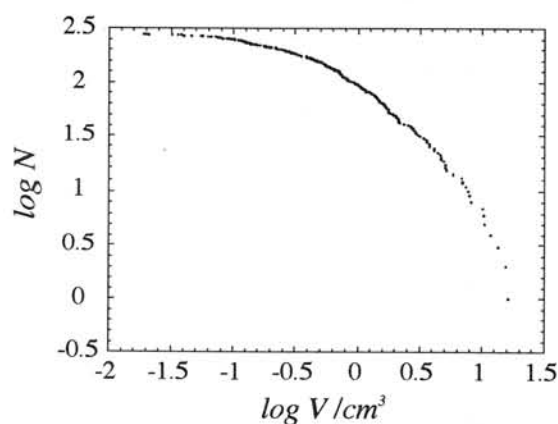


Figure 6. Size frequency distribution of the olivine particles. N is the number of particles with volumes of less than V . The mean volume is 1.40 cm^3 (mean diameter is 1.14 cm).

Acknowledgement: The authors thank Dr. Tsukasa Nakano of Geological Survey of Japan for helping us with the beam hardening correction and examination of olivine grain connection.

References: [1] Scott E.R.D. (1977) *G.C.A.*, **41**, 693-710. [2] Ulf-Møller F., Choi B-G., Rubin A., Tran J., Wasson J.T. (1998) *Meteor. Planet. Sci.*, **33**, 221-227. [3] Buseck P.R. (1977) *G.C.A.*, **41**, 711-740. [4] Wood J.A. (1978) *LP.S.*, **IX**, 1273-1274.

Shock deformation of silica spherules in Cu-powder pressure media: Implication for the chondrule flattening

Naru HIRATA¹, Akira YAMAGUCHI² and Toshimori SEKINE³

¹National Space Development Agency of Japan, 2-1-1 Sengen, Tsukuba, Ibaraki 305-8505, Japan

Correspondence author's e-mail address: naru@hope.tksn.nasda.go.jp

²National Institute of Polar Research, 1-9-10 Kaga, Itabashi, Tokyo 173-8515, Japan

³National Institute for Research in Inorganic Materials, 1-1 Namiki, Tsukuba, Ibaraki 305-0044, Japan

Introduction

Impact is one of the most common phenomena in the early solar system. Effects of impacts are imprinted on meteorites as various shock metamorphic features, caused by high pressure and temperature and they provide an important information of the early history of meteorite parent bodies. Preferred orientation of flattened chondrules is one of the impact-induced deformation features seen in some chondrites [1-2]. Nakamura et al. [3] reproduced chondrule flattening by shock experiments of Allende CV3 carbonaceous chondrite, and they showed that the degree of chondrule flattening is proportional to the shock intensity. However, it is still uncertain about other factors controlling shock deformation of chondrules. We began series of shock-recovery experiments on chondrite analogs to clarify the shock deformation process of chondrule. In this abstract, we will present a preliminary report of these experiments.

Methods

Shock experiments were conducted by using a 30-mm bore single-stage propellant gun at National Institute for Research in Inorganic Materials. We employed the mixture of copper powder and silica beads as starting material. The grain size of copper powder is about 10 μm , and the diameter of silica beads is about 200 μm . The volume ratio of copper powder and silica beads was 2:1. The sample powder was packed into a stainless steel SUS304 container of 12-mm internal diameter. The initial porosities were $13 \pm 2 \%$. The sample container was set in a steel holder. We used two types of holder to control a deformation mode of a sample container; a normal type holder and a tunnel type (Fig. 1). The container in the tunnel type holder is expected to be restrained from deformation perpendicular to the shock compression axis. Shock pressures were 14, 22 and 31 GPa. Recovered samples were cut and polished along the direction of shock wave propagation and examined by a scanning electron microscope (JEOL JSM-5400).

Results

Fig. 2 shows the texture of the pre-shocked sample. The initial average aspect ratio of silica beads is 0.91, indicating that most beads are spherical. Pore spaces exist in the matrix of copper powder. Fractures in the matrix were formed when the pressure by which the starting material was charged into the container was released.

Fig. 3 - 5 show the textures of shocked samples. The deformation mode of sample containers do not differ between experiments using normal type holders and those using tunnel type holders. Copper matrices are well compacted, and all pores disappear. Average axial ratios (minor axis/major axis) of silica beads in the pre-shocked material and the shocked samples are shown in Fig. 6. In the samples shocked at 14 and 22 GPa, axial ratios of silica beads are 0.90 and 0.89, respectively. They do not differ from the initial value. In the sample shocked

at 14 GPa, some beads are heavily fractured, and some are deformed by collision with other beads or wall of sample container (Fig. 3). However, axial ratios of such beads do not significantly differ from the initial value. At 22 GPa, some beads are pear-shaped, but the average axial ratio remains unchanged.

At 31 GPa, deformation of beads become apparent (Fig. 4). Most beads are pear-shaped, with the average axial ratio of 0.72. Fig. 5 shows a close-up image of a pear-shaped bead. The calyx-side of the bead is faced to "the upstream-side" of the FIRST shock wave propagation, and the flat-side is faced to "the downstream-side" of that. All beads with such shape are placed in the same arrangement. Fracturing is not evident, but small irregular fractures are seen within deformed beads. Some beads are collided each other, and were deformed irregularly. In this case, the damage of beads at the downstream-side is greater than that of beads at the upstream-side. Most beads on the wall of downstream-side are shattered.

Discussion

The results of our experiments are slightly different from those on the Allende CV3 meteorite [3]. Although the sample shocked at 22 GPa contains pear-shaped beads, the flattening of silica beads become evident at > 31 GPa. On the other hand, chondrules in the shocked Allende are flattened at 11 GPa. The degree of silica beads flattening in our experiments is lower than that of chondrule flattening in shocked Allende at the same pressure. If chondrules are flattened by squeezing into pores of matrix, the initial porosity is an important factor for shock deformation [3]. The initial porosity of the starting material is about 13 %, while that of Allende is 38 %. This porosity difference probably affects to the degree of flattening.

It is inferred that the mechanical properties also control the shock deformation of chondrules and beads. The contrast of strength between silica beads and chondrule may also affect the degree of deformation. Formation of the pear-like beads is a characteristic feature of in our experiments. The shape of chondrules in shocked Allende is simple elliptical shape [4]. Generally, the damage of beads become greater in the downstream-side of the sample. It probably relates to the mode of the shock wave propagation and a flow within the sample.

Referneces

[1] Martin and Mills (1980) *Earth Planet. Sci. Lett.*, **51**, 18-25. [2] Sneyd et al. (1988) *Meteoritics*, **23**, 139-149. [3] Nakamura et al. (1995) *Meteoritics*, **30**, 344-347.

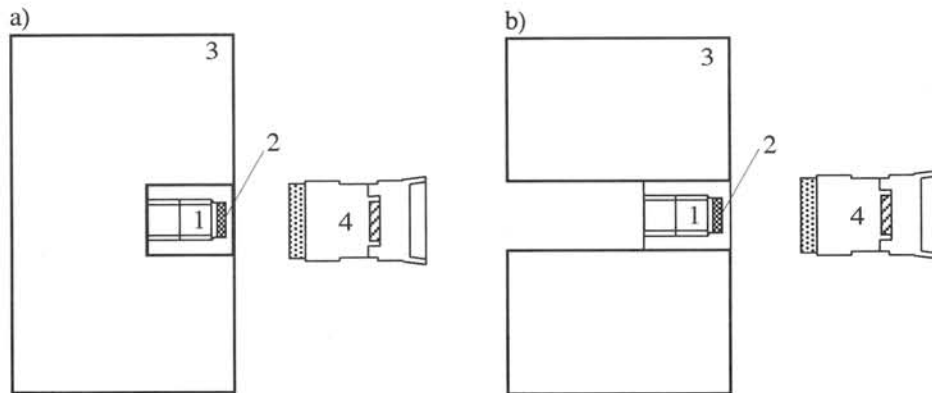


FIG. 1. Schematic cross-section of sample assemblies with a) normal type and b) tunnel type holder: 1. sample container, 2. sample, 3. holder. A hole penetrate a tunnel type holder. Flyers are also shown on a same scale (4).

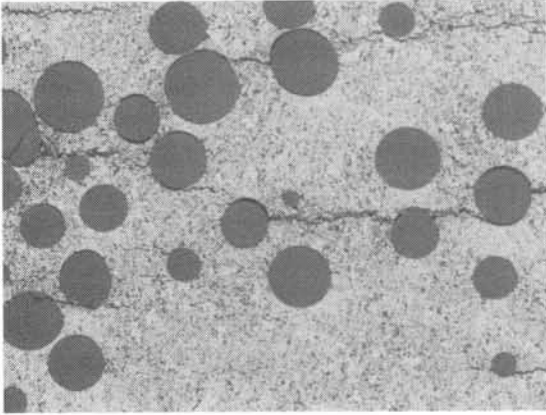


FIG. 2. The pre-shocked sample. Gray = silica bead; White = copper; Black = pore space (epoxy). Width of view = 1.8 mm.

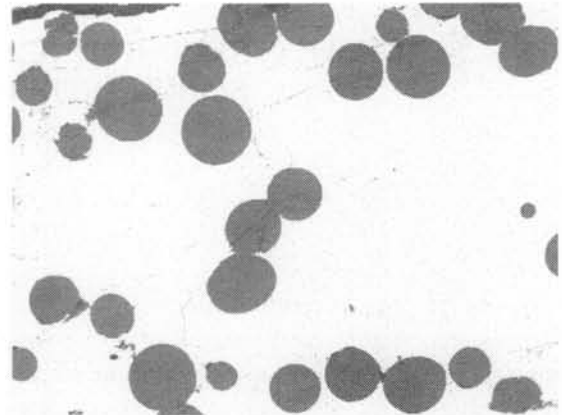


FIG. 3. The sample shocked at 14 GPa, cutting along the direction of shock wave propagation. Width of view = 1.8 mm.

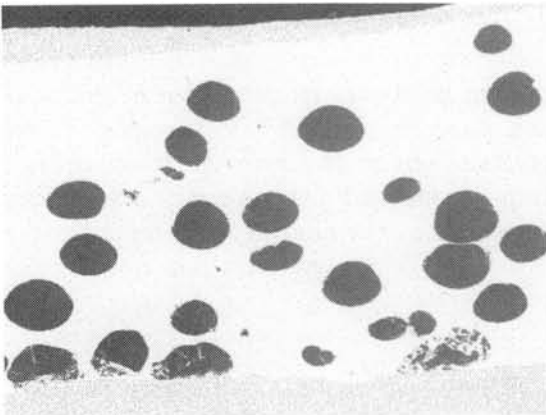


FIG. 4. The sample shocked at 31 GPa. Width of view = 1.8 mm.

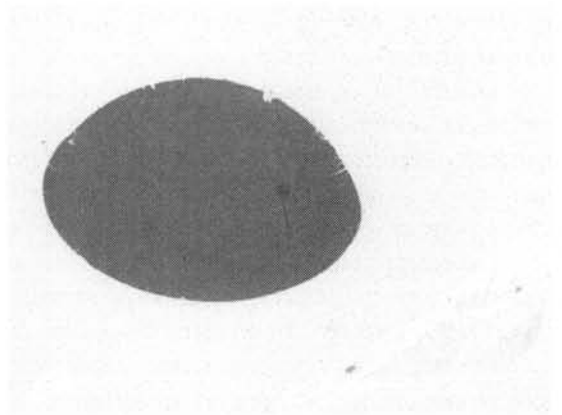


FIG. 5. A pear-shaped silica bead in the sample shocked at 31 GPa. Width of view = 390 μm .

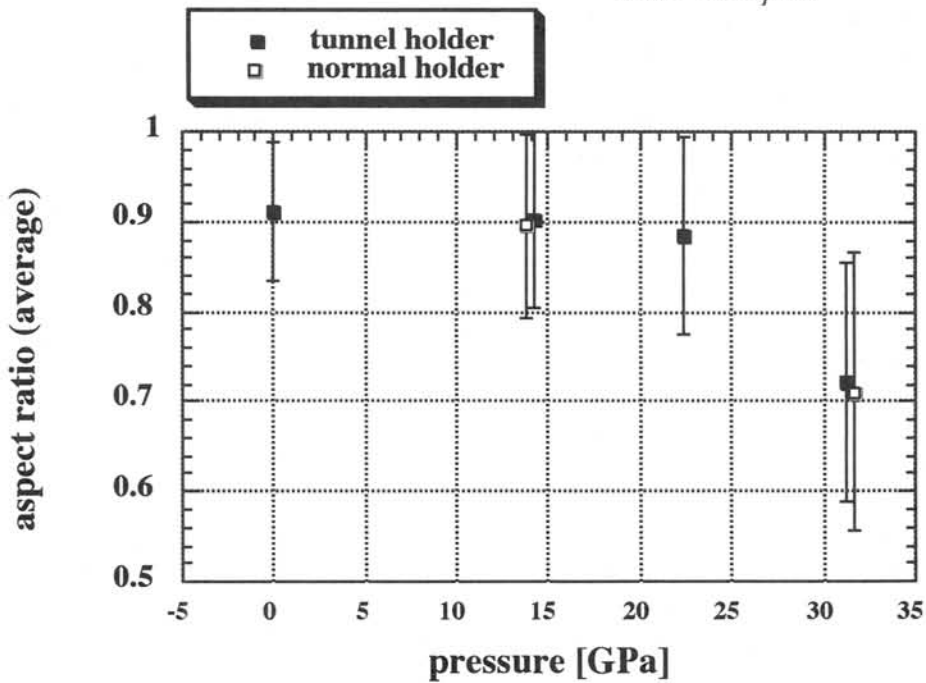


FIG. 6. Average axial (minor axis/major axis) ratio of silica beads plotted against shock pressure.

SPACE WEATHERING OF OLIVINE AS A KEY TO UNDERSTANDING S/A/R/V ASTEROIDS AND LUNAR SOILS

Takahiro Hiroi¹ and Sho Sasaki²

¹*Dept. of Geological Sci., Brown University, Providence, RI 02912, U. S. A.*

²*Geological Inst., School of Sci., Univ. of Tokyo, Hongo, Tokyo 113-0033*

Introduction

Existence, cause, and process of space weathering on the S asteroids have been often discussed in the absence of any likely candidate shown experimentally or by meteorite studies. A trend was shown that S asteroids larger than about 120 km show much shallower absorption bands than the others [1], which could be due to space weathering. However, nothing more informative could be pointed out from the trend.

A simulation of space weathering process by irradiating laser beam to minerals and meteorites have been performed [2, 3]. However, the problem was that apparent reddening was mainly caused by glass or olivine formation and no exact S-type spectral change could be observed. Furthermore, it was discouraging to suggest that the S-type reddening could be realized only by drastically changing olivine/pyroxene ratios, making identification of modal mineralogy difficult.

Recently, an extensive series of such simulation was performed for pyroxene and olivine samples [4], and the laser-irradiated olivine sample showed a very similar spectrum to some of olivine-rich S/A asteroids [5], while pyroxene sample did not show much spectral change after the same amount of laser irradiation. In this paper, importance of olivine in S-asteroid space weathering is further examined, and preliminary study on the nature of laser-irradiated olivine samples is reported.

Space Weathering Trend of Olivine

Shown in Fig. 1 are comparison of reflectance spectra of laser-irradiated olivine samples [4] and an olivine-rich asteroid 354 Aeternitas [8, 9] and a Copernicus central peak on the moon [10]. Laser-irradiated olivine samples show similar spectral profiles and depths to 354 Aeternitas although they show a little redder profile in the 2- μm region. On the other hand, laser-irradiated olivine samples are very different in the 1- μm

band depth and the 2- μm profile from the Copernicus central peak. Difference between the asteroidal and lunar space weathering of olivine may be due to difference in either space environment such as frequency of micrometeorite impacts and average regolith age or minor mineral composition such as spinel-group minerals.

Importance of Olivine

Shown in Fig. 2 is a plot of 2- μm /1- μm absorption band area ratios vs. 1- μm band continuum slope for the S/A/R/V asteroids [1], laser-irradiated olivine and pyroxene samples [4], and fresh olivine and pyroxene powders. Smaller value in the area ratio (x axis) indicates higher

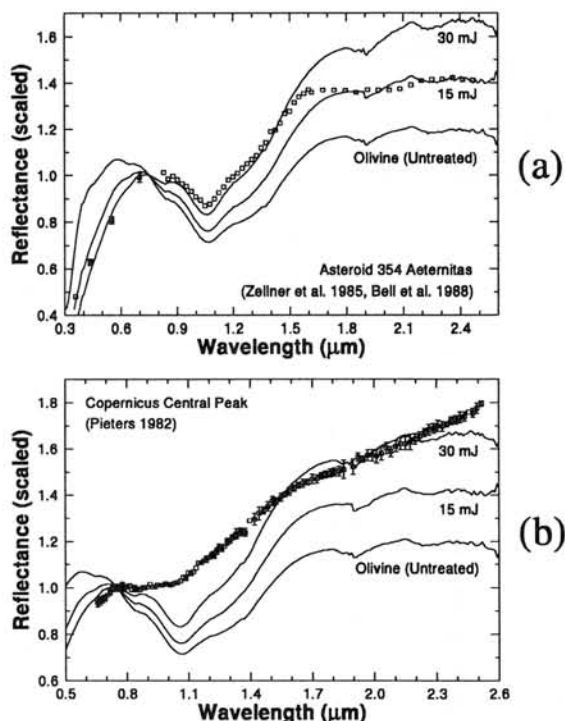


Fig. 1. Comparison of reflectance spectra between laser-irradiated olivine samples and (a) an olivine-rich asteroid 354 Aeternitas [8, 9] and (b) a Copernicus central peak on the moon [10].

olivine abundance, and larger value indicate higher pyroxene abundance. Larger value in 1- μm band continuum slope indicates redder spectrum which is believed to have more space weathering.

As is shown by a broken line, the highest degree of space weathering of the S/A/R/V asteroids depends on olivine / pyroxene ratio: higher olivine abundance can lead to higher space weathering degrees. Therefore, from both observations of S-asteroid reflectance spectra and laser-irradiation experiments of olivine and pyroxene, it is suggested that olivine become more easily space-weathered than pyroxene in terms of their Vis-NIR reflectance spectra.

The only problem here is that even fresh olivine and pyroxene have various degrees of red 1- μm slope as shown in the plot. Because we don't know what kind of reflectance spectra olivine and pyroxene on these asteroids should show when they were fresh, the choice of right kind of olivine and pyroxene is important. As more quantitative analyses of absorption bands become developed for these asteroids, this problem may become solved.

Nature of Laser-Irradiated Olivine

In order to study what kind of process is taking place when olivine sample was irradiated by la-

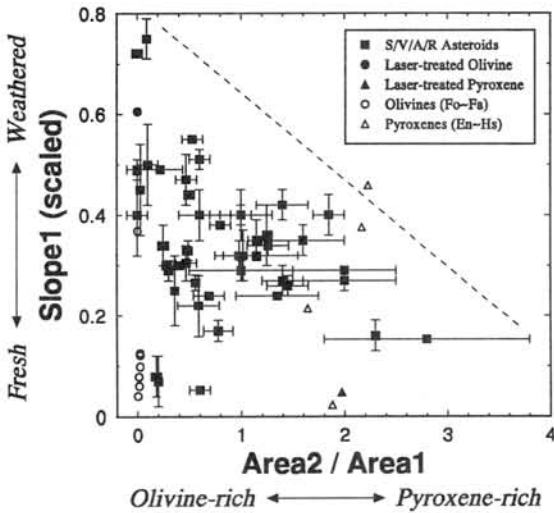


Fig. 2. A plot of area ratio between the 1- μm and 2- μm bands vs. continuum slope of the 1- μm band of the S/V/A/R asteroids [1], laser-irradiated olivine and pyroxene powders [4], and fresh olivine and pyroxene powders.

ser, reflectance spectra of olivine samples were deconvolved according to the Modified Gaussian Model [6, 7]. The results are shown in Fig. 3.

As seen in Fig. 3 (a), this olivine spectrum show some water bands around 1.4 and 1.9 μm which are also evidence in the residual error spectrum in the top part of the plot. Although it is not clear whether this water can be structural, adsorbed, or atmospheric, it would be cautious not to take this level or residual error (0.01 in natural log reflectance) as significant. With such a threshold assumed, all the fits in Fig. 3 are excellent in the limitation that the wavelength range

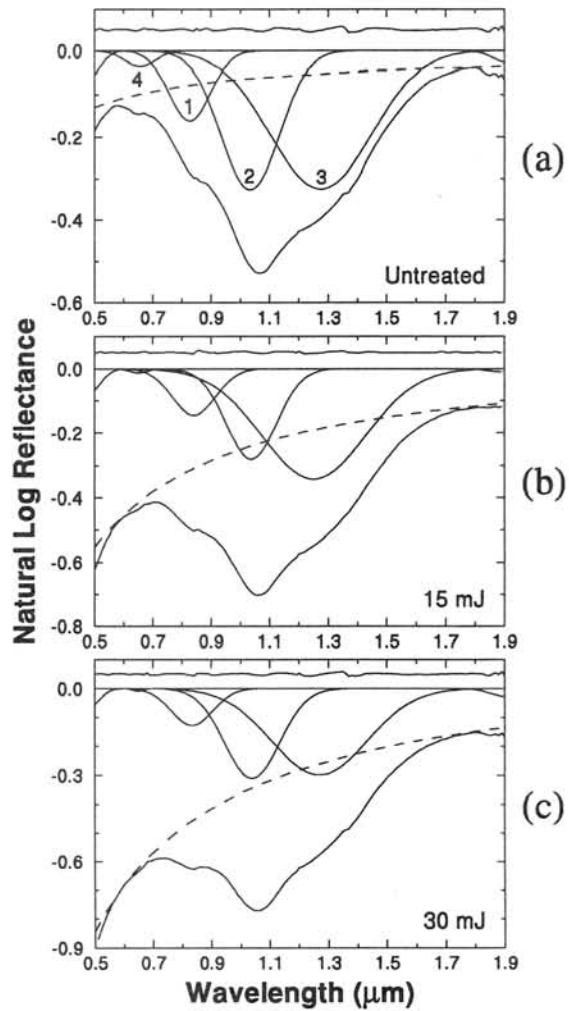


Fig. 3. Modified Gaussian model fits of untreated and laser-irradiated olivine powders. Natural log reflectance spectrum and modified Gaussians are shown in solid lines, and continuum spectrum is shown in a broken line in each plot. Residual error spectrum is shown in a solid line in the top part of each plot with an appropriate offset for clarity.

was limited to 0.5 to 1.9 μm and only six bands were assumed to exist. The overall results show mostly expected trend that continuum becomes redder and absorption bands become weaker.

In order to address the effects of laser irradiation more precisely, three parameters (center, width, and strength) of modified Gaussians are plotted in Fig. 4.

Shown in Fig. 4 (a) is a plot of band centers vs. width. The major three bands (1~3) consistently retain similar band center and width values while the band 4 becomes narrower (an weaker from Fig. 4 (b)) as more laser-irradiation is performed. Because the band 4 is a small band and

near the edge of calculated wavelength range, this trend may not reflect any real physical change. However, experience from space weathering of lunar rocks and soils tells us that disappearance of minor short-wavelength bands by space weathering may be universal.

Shown in Fig. 4 (b) is a plot of laser energy vs. band strength. Note that the strength is always negative and negatively larger values indicate stronger bands. As mentioned above, the bands 4 and 1 consistently become weaker as more energy is put by laser irradiation, but the bands 2 and 3 show a little complex trend. At laser energy 15 mJ, the band 2 becomes very weak and the band 3 becomes stronger, and then at 30 mJ they become similar in the order of strength to that of untreated sample. Although it is not clear whether this trend is due to some real physical change or an artifact of fitting calculations, it is unlikely that this strange trend is caused by formation of any major amount of glass because glass spectrum usually show a very broad asymmetric band.

Conclusions

It is likely that olivine on the S/A/R/V asteroids is more subject to space weathering than pyroxene. Olivine seems to retain most of its absorption band characteristics without any signature of glass formation although the spectrum becomes redder and darker as it is space-weathered.

Acknowledgment: Reflectance spectra of fresh olivine and pyroxene powder samples were taken from the RELAB database. RELAB is a NASA-funded multiuser facility at Brown University.

References: [1] Gaffey M. J. *et al.* (1993) *Icarus* 106, 573-602. [2] Moroz L. V. *et al.* (1996) *Icarus* 122, 366-382. [3] Wasson J. T. *et al.* (1997) *Lunar Planet. Sci. XXVIII*, 1505-1506. [4] Yamada M. *et al.* (1998) *Antarct. Meteorites* 23, 173-176. [5] Yamada M. *et al.* (1999) *Earth, Planets & Space* (in review). [6] Sunshine J. M. *et al.* (1990) *J. Geophys. Res.* 95, 6955-6966. [7] Sunshine J. M. and Pieters C. M. (1998) *J. Geophys. Res.* 103, 13675-13688. [8] Zellner B. *et al.* (1985) *Icarus* 61, 355-416. [9] Bell J. F. *et al.* (1988) *Lunar Planet. Sci. XIX*, 57-58. [10] Pieters C. M. (1982) *Science* 215, 59-61.

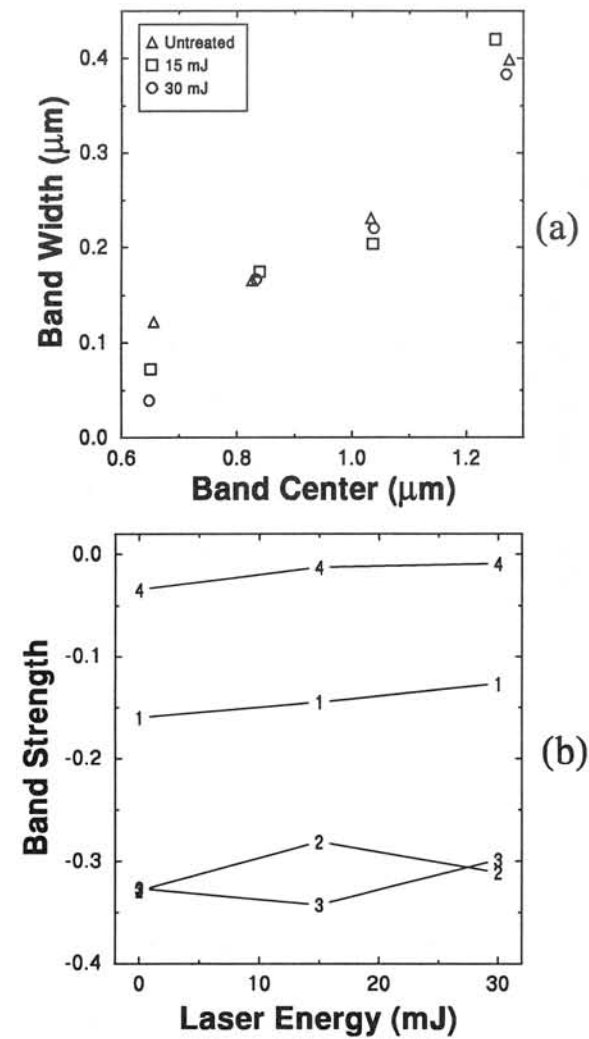


Fig. 4. Changes in band center, width, and strength of absorption bands 1~4 caused by laser irradiation. Numbers connected with solid lines in (b) correspond to the band numbers specified in Fig. 3 (a).

An ion microprobe study of oxygen isotopes in various types of inclusions in Yamato-791717 (CO3) chondrite: Oxygen isotopes vs fayalite content in olivine.

¹Hajime Hiyagon and ²Akihiko Hashimoto

1. Department of Earth and Planetary Physics, The University of Tokyo, Bunkyo-ku, Tokyo 113-0033, Japan.
2. Department of the Earth and Planetary Sciences, Hokkaido University, Sapporo 060-0810, Japan.

1. Introduction

Recently, we discovered olivine-rich inclusions (OIs) [1], which have large ^{16}O excesses similar to those found in spinel grains in CAIs in Allende and other carbonaceous chondrites [2-4]. This indicates that the oxygen isotopic anomalies of $\delta^{17,18}\text{O} = -40\text{‰}$ to -50‰ relative to SMOW (standard mean ocean water) are characteristic not only of highly refractory CAI minerals but also of olivine, a much abundant mineral in chondrites, and hence such anomalies were more extensive in the early solar system than previously thought. This was further confirmed in our recent work [4], in which OIs were also found in two CO chondrites, Yamato-82050 and ALH-77307, and most of the OIs as well as amoeboid-olivine-aggregates (AOAs) in these two CO chondrites showed large oxygen isotopic anomalies with $\delta^{17,18}\text{O}$ from -30‰ to -47‰ . Enstatite in a CAI in Yamato-77307 was also found to have a high oxygen isotopic anomaly of $\delta^{17,18}\text{O} \sim -40\text{‰}$ [5]. These observations have expanded our knowledge about distribution of oxygen isotopes in various components in chondrites.

In the present study, we conducted *in situ* ion microprobe analyses on AOAs, OIs and CAIs in Yamato-791717 (CO3.3) chondrite. Our particular interest is in the relationship between oxygen isotopic composition and fayalite content of olivine in these inclusions, which may give important constraints on the origin of the oxygen isotopic anomalies. Analytical procedures and conditions were similar to those described in [1].

2. Inclusions and mineral phases

Inclusions #2, #5, #8, #59 and #70 are AOAs, and inclusions #15 and #16 are probably OIs. They consist mostly of olivine with variable amounts of the fayalite component ($\text{Fa} = \text{Fe}/(\text{Fe}+\text{Mg})$ atomic ratio in %) from $\text{Fa} = 2$ (inclusion #2) up to $\text{Fa} \sim 50$ (inclusions #41 and #42). Inclusion #47 is a CAI ($80\mu\text{m} \times 120\mu\text{m}$ in size) consisting of fassaitic to diopside pyroxene with some nepheline in the core and Fe-rich olivine ($\text{Fa} = 50-57$) in the rim; both pyroxene-rich core and olivine rim were analyzed. Inclusion #31 is a CAI with the melilite-rich core and the pyroxene (diopside) mantle; both phases were analyzed. Inclusion #33 is a CAI, consisting of the nepheline-rich core with minor amounts of

fassaite and hercinite, and of the diopside rim; the core was analyzed. Inclusion #39 (190 μ m x 230 μ m in size) is a round-shaped aggregate of spinel (hercinite ~50%), nepheline and ilmenite; a spinel-rich spot was analyzed. Inclusion #63 is an irregularly-shaped object (260 μ m x 330 μ m in size) consisting mostly of Fe-rich spinel (hercinite = 59-63%); two analyses were made on the spinel.

3. Results

The results are presented in the three-isotope diagram (Fig.1). All of the analyses made on the olivine grains and olivine-rich spots in AOAs, OIs and a CAI rim (inclusion #47) show the $\delta^{17,18}\text{O}$ values from ~-40‰ to ~-50‰. Figure 2 shows the $\Delta^{17}\text{O}$ value (departure in $\delta^{17}\text{O}$ of the analyses from the terrestrial fractionation line; $\Delta^{17}\text{O} = \delta^{17}\text{O} - 0.52 \times \delta^{18}\text{O}$ [‰]) versus the fayalite content. There is no correlation between them. This observation indicates that there is no difference in the oxygen isotopes between the Fe-rich and Fe-poor olivine unlike those in Allende [3].

A key question is how Fe was introduced into the olivine without changing slightly its oxygen isotopic composition. Planetary processes (e.g. reactions of Fe-poor minerals with an Fe-rich fluid) are unlikely, because they would have modified the oxygen isotopic composition toward the terrestrial one. Alternatively, Fe could have been introduced into olivine by nebular processes. Many olivine grains in AOAs show zoning in Fe content, from low Fe in the center to high Fe near the grain boundary. This suggests that forsteritic olivine formed first and became Fe-rich by later reactions with Fe-rich gas, or by direct condensation of increasingly Fe-rich olivine from the nebula. If the solar nebula was the place where the Fe-rich olivine formed, however, its canonical (hence close to normal) oxygen isotopic composition would have affected the oxygen isotopic composition of the olivine, just as expected in the planetary processes.

A possible explanation might be that the environment in which these inclusions formed as a whole was anomalous with respect to oxygen isotopes (viz. $\delta^{17,18}\text{O} \sim -40\text{‰}$). In other words, a region having locally anomalous oxygen isotopes existed in the solar nebula. However, such a model seems to have difficulties in explaining the uniform and extreme oxygen isotopic anomalies (always $\sim -40\text{‰}$), because we would expect intermediate anomalies to be observed in some inclusion population as a result of the mixing of materials (both gas and dust) in the nebula.

Another alternative explanation would be that some kind of mass-independent fractionation process [e.g., 6, 7] was involved in the formation of CAIs, AOAs and OIs, and their Mg-rich to Fe-rich olivine grains as well. Thus far, the laboratory experiments have not been successful in generating similar effects in solids.

References: [1] Hiyagon H. and Hashimoto A., *Science* **283**, 828-831, 1999; [2] Clayton R. N., Grossman L. and Mayeda T. K., *Science* **182**, 485-488, 1973; [3] Clayton R. N., Onuma N., Grossman L., and Mayeda T. K., *Earth Planet. Sci. Lett.* **34**, 209-224, 1977; [4] Clayton R. N. and Mayeda T. K., *Earth Planet. Sci. Lett.* **67**, 151-161, 1984; [5] Hiyagon H. and Hashimoto A., *Lunar Planet. Sci.* **XXX**, Abstr.#1319, LPI, Houston (CD-ROM); [6] Thiemens M. H. and Heidenreich III, J. E., *Science* **219**, 1073-1075, 1983; [7] Thiemens M. N., in *Chondrules and the Protoplanetary Disk* (eds. Hewins R. H., Jones R. H. and Scott E. R. D.) 107-118, Cambridge Univ. Press, Cambridge, 1996.

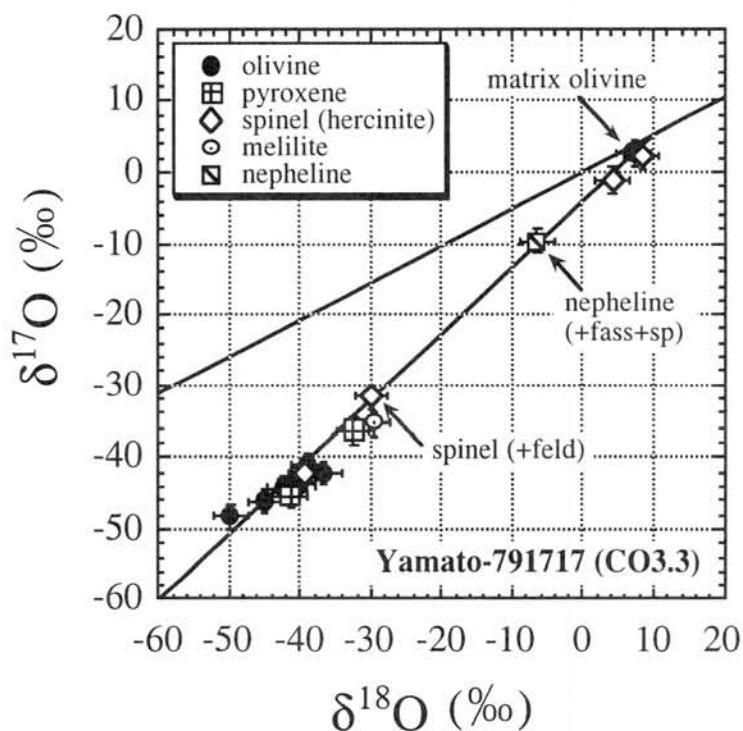


Fig.1 Three isotope diagram of oxygen isotopes in various inclusions in Yamato-791717 (CO) chondrite. Also plotted are the terrestrial fractionation (TF) line (slope ~ 0.5) and the carbonaceous chondrite anhydrous mineral (CCAM) line (slope ~ 1).

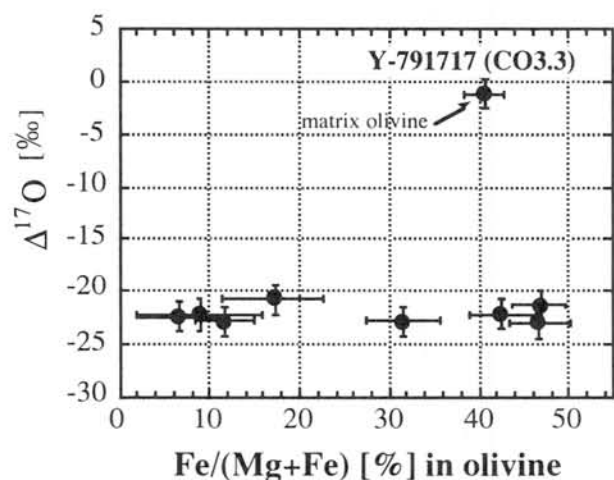


Fig.2 Oxygen isotopic composition vs fayalite content in olivine in AOAs, OIs and a CAI-rim. $\Delta^{17}\text{O} = \delta^{17}\text{O} - 0.52 \times \delta^{18}\text{O}$.

A SIMPLE THREE-STEP MODEL FOR THE ORIGIN OF THE ENSTATITE CHONDRITES. Melinda Hutson¹ and Alex Ruzicka²

¹Portland Community College, P.O. Box 19000, Portland, OR, 97280, U.S.A. ²Department Geological Sciences, University of Tennessee, Knoxville, TN, 37996, U.S.A.

The enstatite chondrites are a unique class of meteorites, consisting of highly reduced phase assemblages. Several models to account for the origin of the enstatite chondrites have been proposed, including condensation with slow nucleation kinetics [1]; condensation at high pressures (>1 bar) [2,3]; formation in a region of the nebula with low H₂O/H₂ ratio [4] or high C/O ratio [5]; increasing the amount of a “tar” component in the nebula [6]; and condensation with partial isolation of solids [7]. However, none of the previous models adequately explained the mineralogy and bulk compositions of enstatite chondrites. We considered chemical perturbations of the solar or cosmic composition [8] as a possible way to explain the unusual character of enstatite chondrites. Chemical perturbations can occur at condensation fronts, where there is both excess condensate and a sunward depletion of the vapor phase involved in the condensation reaction [9-11]. The free-energy-minimization program PHEQ [6] was used to examine three types of plausible models: sulfur enrichment, water depletion, and refractory-element fractionation. A representative nebular gas pressure of 10⁻⁵ bar [6,12] was assumed in the calculations. We found that a combination of water depletion and refractory element fractionation can explain the bulk chemical composition and modal mineralogy of the unequilibrated enstatite chondrites (UECs), which experienced less metamorphism than other enstatite chondrites and presumably reflect their original formation conditions.

Sulfur enrichment. The enstatite chondrites contain a number of unusual sulfide minerals, suggesting that they may have been sulfidized [e.g., 13,14]. One way to accomplish this sulfidation is to partially vaporize solids near the troilite “condensation front”. As troilite is produced by reaction of Fe-metal with sulfur-bearing gas, the only difference compared to the cosmic case is that the gas produced by vaporizing the solids at the troilite condensation front will have an excess of S. Thus, to simulate this process, the abundance of S was increased relative to other elements, with the maximum S content set equal to the Fe content. Relative to the nominal cosmic composition, sulfur enrichment causes: 1) the abundance of troilite and pyrrhotite to increase; 2) a large amount of the unobserved mineral Na₂SiO₃ to form at the expense of enstatite at T ≤ 900K; and 3) the rare (in enstatite chondrites) mineral nepheline to form at T ≤ 850K. Notably, certain phases present in many UECs, such as oldhamite (CaS) and niningerite (MgS), do not form at any temperature with the sulfur-enrichment model. Thus, this model cannot explain the enstatite chondrites.

Water-vapor depletion. Depleting the water content of a gas, as might be expected sunward of the water condensation front [9-11], has the effect of increasing the C/O ratio of the gas. We define “cosmic water” as the abundance of water present at high temperature for a cosmic composition. Various degrees of water depletion (0-100% in 5% increments) relative to the cosmic case were assumed. For 0-80% water depletion, the only effect is a lowering of the condensation temperatures for the silicates, and an enstatite-chondrite-like mineralogy is not produced. The condensation temperatures and mineralogy change significantly with 85% water depletion. Differences from the cosmic case involve: 1) decreasing the proportion of enstatite produced at high (≥ 1000K) temperatures; and 2) the stable appearance of oldhamite and niningerite at temperatures around 900K. The assemblage at 900K and 85% water depletion

resembles that of enstatite chondrites, except that it lacks silica minerals and albite and contains too much graphite. Additional water depletion causes a greater mismatch with UECs. Consequently, water depletion alone does not explain the observed mineralogy of UECs.

Refractory element fractionation. The models discussed above do not match the observed bulk chemistry of the enstatite chondrites. Larimer and Wasson [15] concluded that the EH and EL chondrites had lost various proportions of Al, Ca, Si, and Mg in a refractory-element fractionation. Indeed, our trial-and-error calculations show that the bulk composition of enstatite chondrites can best be approximated by the removal of 56% of the solids in equilibrium with a solar-composition gas at 1270K. However, condensation of the remaining vapor produces a mineral assemblage unlike that of enstatite chondrites, as it includes large amounts of the unobserved phase Na_2SiO_3 (stable up to 900K) and lacks oldhamite and niningerite.

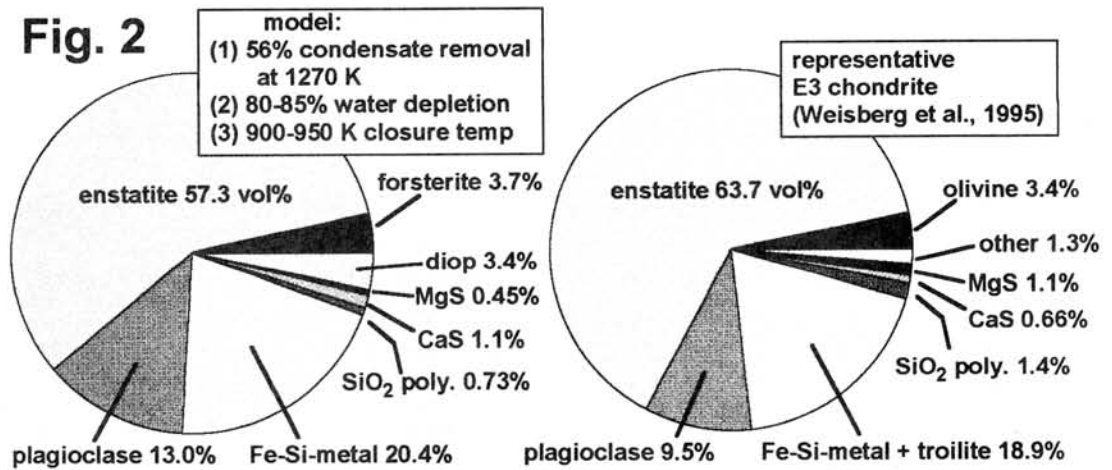
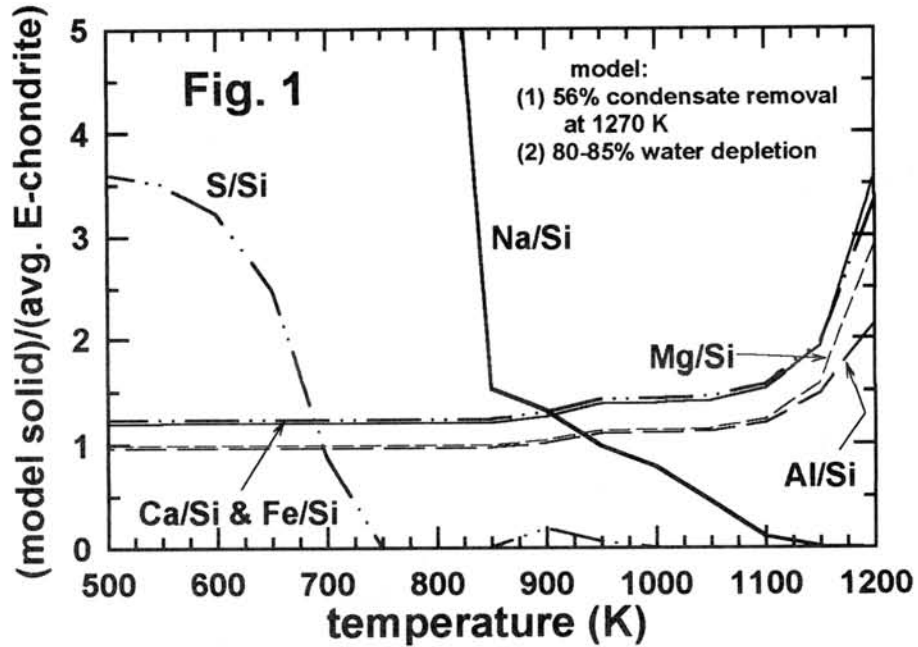
A three-step model. A good match to both the bulk chemistry and modal mineralogy of UECs can be obtained with a model involving 1) initial removal of 56% of the solids at 1270K in a cosmic system, 2) an average of 80-85% water loss in the remaining gas, and 3) two different closure temperatures for solids. To accomplish an average of 80-85% water loss in the second step, we assumed mixing of equal parts of solids produced by 80% water loss and 85% water loss, which could correspond to a small amount of radial mixing in the nebula.

Figure 1 shows the Si-normalized major-element abundances in the equilibrium solid assemblage relative to average enstatite chondrite [16] as a function of temperature. Values close to one on the ordinate indicate agreement between the model assemblage and enstatite chondrites. With the exception of S/Si, all the model elemental ratios converge near the enstatite chondrite values at a temperature of ~900-950K. The S/Si ratio approaches the enstatite chondrite value at ~700K. This suggests that, except for sulfur, the enstatite chondrites ceased equilibrating with the solar nebula around 900-950K. Sulfidation of metal must have continued to lower temperatures, ceasing at ~700K. This type of difference in closure temperature is reasonable. Fegley [17] suggested that different minerals ceased equilibrating with the solar nebula at different temperatures due to kinetic effects. Reactions involving extensive solid-state diffusion, such as those involving silicates, are unlikely to reach completion at low temperatures [17], while the formation of troilite by sulfidation of metal is a rapid process, even at low temperatures [e.g., 18,19].

Figure 2 shows the modal mineralogy of the condensates produced by the three-step model at 900-950K compared to that of a representative E3 chondrite (average of EH3 and EL3 chondrites) [14]. In the models, troilite does not form at 900-950K. However, as troilite forms by the sulfidation of Fe-metal, the two phases have been lumped together in Fig. 2 for the E3 chondrites for comparison with the model. There is remarkable agreement between the modal mineralogy predicted by the three-step model and that observed in E3 chondrites. The agreement in the modes is even more striking considering that the model predictions generally fall within the abundance ranges reported by Weisberg et al. [14]. The only discrepancy is that the model predicts more diopside (3.4 vol%) than is actually observed (<0.5%) [14].

References: [1] Blander, M. (1971) GCA 35, 61-76. [2] Herndon J. M. and Suess, H.E. (1976) GCA 40, 395-399. [3] Sears, D.W. (1980) Icarus 43, 184-202. [4] Baedeker, P. A. and Wasson, J. T. (1975) GCA 39, 735-765. [5] Larimer, J. W. and Bartholomay, M. (1979) GCA 43, 1455-1466. [6] Wood, J. A. and Hashimoto, A. (1993) GCA 57, 2377-2388. [7] Petaev, M. I. and Wood, J. A. (1998) MAPS 33, 1123-1137. [8] Anders E. and Grevesse N. (1989) GCA 53, 197-214. [9] Morfill, G. E. (1985) in Birth and Infancy of Stars, 693-792. [10] Stevenson, D. J. and Lunine, J. I. (1988) Icarus 75, 146-155. [11] Cyr, K. E. et al (1998) Icarus 135, 537-548. [12] Wood, J. A. and

Morfill, G. E. (1988) in MESS, 329-347. [13] Rubin, A. E. (1983) EPSL 64, 201-212. [14] Weisberg, M. K. et al. (1995) LPSC XXVI, 1481-1482. [15] Larimer, J. W. and Wasson, J. T. (1988) in MESS, 394-415. [16] Hutson, M. L. (1996) Ph.D. dissertation. [17] Fegley, B. (1988) in LPI Tech. Rep. No. 88-04, 51-60. [18] Lauretta, D. S. et al. (1996) Proc. NIPR Symp. Ant. Met. 9, 111-126. [19] Lauretta, D. S. et al. (1998) MAPS 33, 821-833.



PETROLOGY OF THE DAR AL GANI (DAG) 319 POLYMICT UREILITE

Y. Ikeda¹, M. Prinz², C.E. Nehru², J. S. Boesenberg² and N. T. Kita³

¹Dept. Material & Biol. Sci., Ibaraki Univ., Mito 310, Japan. ²Dept. Earth Planet. Sci., Am. Museum Nat. Hist., NY, NY 10024, USA. ³Geol. Survey Japan, Tsukuba 305-8567, Japan

The DAG 319 polymict ureilite is a complex polymict ureilite consisting of a wide variety of lithic and mineral clasts. Our goal is to sort out all of the types of materials which contribute to the mixture. In this preliminary study we classify the various types of components and distinguish seven major groups, and characterize them mineralogically and petrologically. A further phase of this study includes oxygen isotopic analyses of some of these components, utilizing a Cameca 1270 ion microprobe [1].

A preliminary classification of the different groups is presented in Table 1. It includes: **(A) Coarse-grained mafic lithic clasts** of (A1) typical ol-pigeonite-C (Fo74-78) monomict ureilite (Type I) and (A2) unusual ol-opx -aug-no C (Fo84-87) monomict ureilite clasts (Type II), similar to Hughes 009 and FRO 90054 [2,3]. The type I ureilite is the dominant lithic clast type, has reduction features along grain margins and fractures, and contains Si-bearing kamacite with 9-11% Si and sulfides, whereas the type II ureilite has melt inclusions in the olivines, no reduction along grain margins, and contains Si-poor kamacite with <0.1%Si and schreibersite, as well as sulfides. **(A3) Magnesian ureilitic clasts** consist mainly of olivine with Fo91-97, orthopyroxene and minor diopside. **(B) Fine-grained mafic lithic clasts.** These consist of (B1) ol-pyx and (B2) pyx-rich clasts, and the former seems to be fragments of shocked, reduced, and recrystallized ureilites and the latter may be lithic fragments of some monomict ureilites including fine-grained pyroxene aggregates replacing original pigeonites. Granular ol (Fo74-84)-rich clasts (B3) have minor opx and alkali-free glass and may be, in part, shocked, reduced and/or recrystallized lithic fragments. **(C) Felsic lithic clasts.** This group includes plagioclase-predominant trachytic-textured (C1) type and porphyritic (C2) and glassy (C3,C4) types, and some felsic clasts can be impact melts and other can represent the fractionates of the missing basaltic components which were lost during the formation of monomict ureilites. The troctolitic assemblage (C5) consists of coarse-grained olivine (Fo93) and plagioclase (An81) and may be a plutonic rock type. **(D) Dark Inclusions.** There are numerous hydrated DIs, up to several mm across, which contain mainly Fe-rich olivine and/or phyllosilicate phases, FeS, magnetite (sometimes as framboids) and Ca-Fe-Mn carbonates. These are similar to the DIs found in Nilpena and North Haig, described in Brearley and Prinz [4]. **(E) Sulfide- or metal-rich clasts.** There are several sulfide-rich or metal-rich clasts and these are difficult to relate to the other groups of components. **(F) Chondrules and chondritic fragments.** Several whole chondrules were found, and a number of chondritic fragments, and these are listed in Table 1. It is interesting to note that the compositions of the chondrules and fragments are not of the common Mg-rich type 1 chondrules found in all carbonaceous chondrites, and are more like the chondrules in ordinary chondrites. **(G) Isolated mineral clasts.** The olivine clasts (G1.1) appear to be related to the ureilitic lithic clasts, but the source of the forsterite

(G1.3) is uncertain, although it may be related to the Mg-rich enstatite clasts (G2.5). Some of the pyroxene clasts (G2) appear to be related to the ureilitic clasts, especially to type I ureilites, but the source of the fassaite (G2.7) is uncertain. The enstatite (G2.5) is a persistent isolated mineral clast type, associated with the $Fo > 99$, and seems to represent a small percentage of a highly reduced rock type, but not an E chondrite or aubrite. Plagioclase clasts (G3) range from about An5 to An97, but the number of clasts found as yet is small. It is not clear whether these represent distinct groupings or are a continuum. Chromite, ilmenite, apatite, whitlockite, sulfides, and metallic clasts occurring as isolated minerals are also found in lithic clasts, suggesting that they derived from such lithic clasts by disaggregation. The Si-bearing kamacite, suessite and perryite, perhaps the bladed graphite, may be related to type I ureilites or the small fragments of highly Mg-rich enstatite and forsterite.

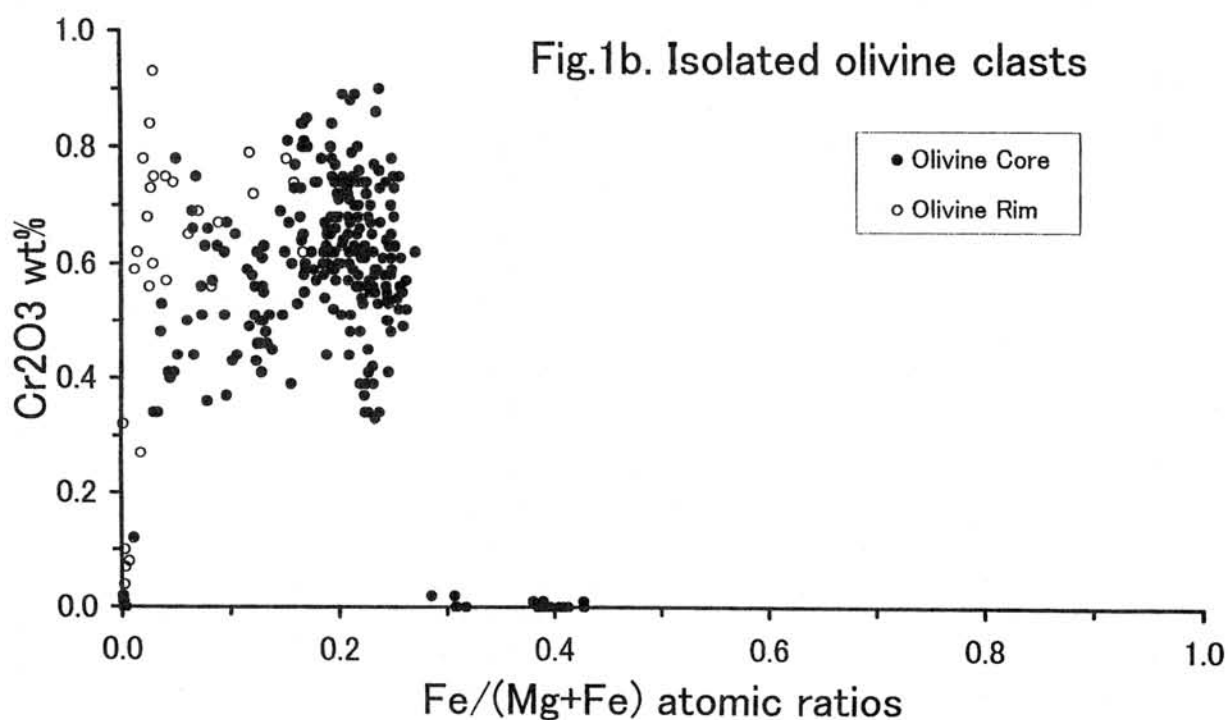
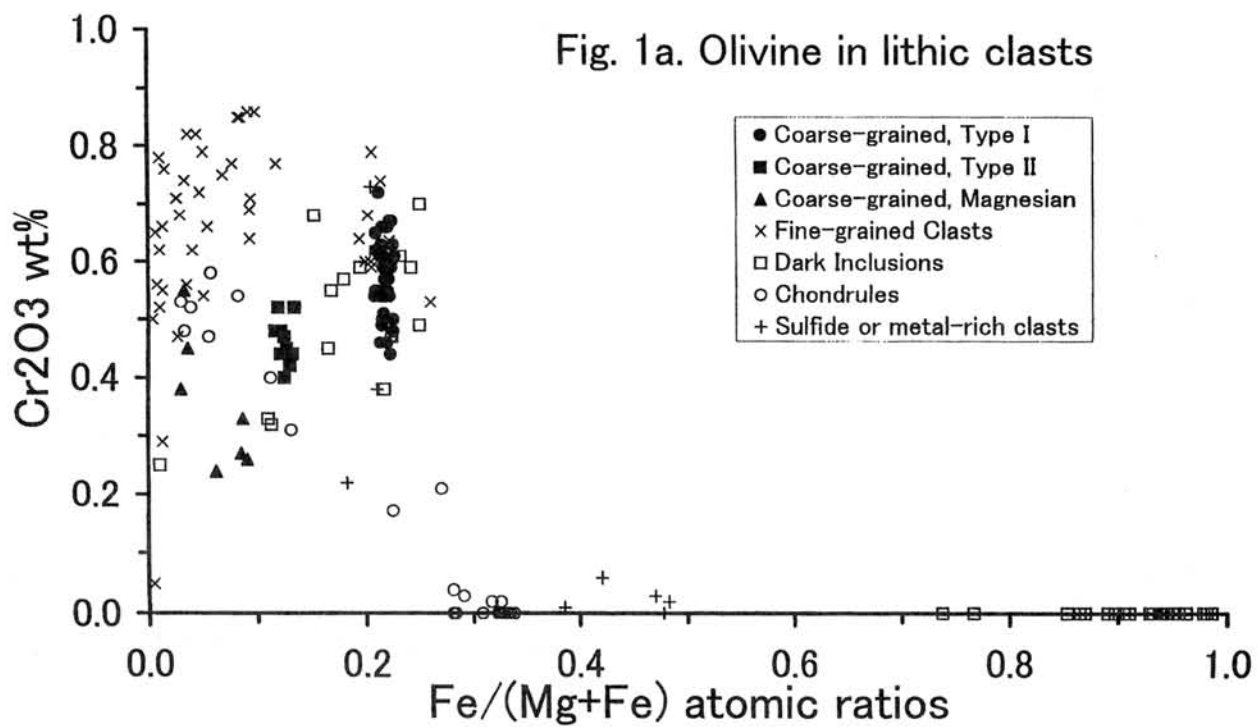
The olivine compositions in the lithic and mineral clasts are shown in Figs. 1a and b, where Cr_2O_3 is plotted against $Fe/(Mg+Fe)$. Fig 1a shows the coarse-grained mafic lithic clasts have high Cr_2O_3 contents typical of ureilitic olivine. The fine-grained mafic lithic clasts are generally more reduced because of their smaller grain size, and most are probably type I or magnesian ureilite type. The dark inclusions are mainly Fe-rich, with no Cr, and the sulfide or metal-rich clasts have no distinct pattern. The magnesian olivines from chondrules also have high Cr, typical of ureilitic ol, as well as some type I chondrules from some carbonaceous chondrites. Fig. 1b shows the compositions of isolated mineral clasts of olivines and indicates more clearly that they are mainly from type I ureilite and, to a lesser extent, from type II ureilite and magnesian ureilite types. Note that some olivines are extremely Mg-rich and have low Cr, and there are some olivine grains which are more Fe-rich and have no Cr.

The petrologic significance of these findings is at a preliminary stage. The complexity of these lithic and mineral clasts, as evidenced by Table 1, makes it difficult to relate each of the fragments to one or more coherent petrologic processes at this stage. We are therefore undertaking a more extensive study, which will also include reevaluation of clasts in Nilpena and North Haig. Since plagioclase-bearing lithic clasts in ureilites are rare, being found only in polymict ureilites, their relationship to the ureilitic clasts is of great interest. A large plagioclase clast (An47, G3.2), about 5 mm across, contains many magmatic inclusions, about $100 \mu m$ in diameter, consisting of sodic plagioclase and augite with minor glass of rhyolitic compositions. The melt inclusions in olivine of type II ureilite clasts are also of great interest in terms of determining the composition of the melts involved in olivine crystallization. Oxygen isotope analyses of minerals in these clasts is crucial to an understanding of their relationships and is currently being pursued. Clearly, polymict ureilites represent one of the best opportunities to develop a better understanding of the origin of ureilites.

References: [1] Kita et al. (1999), Proc.NIPR Symp.Ant.Met., this vol. [2] Goodrich et al. (1999), LPSC 30, #1026 & 1027. [2] Traubadino et al. (1997), Met.Planet.Sci. 32,671-678. [4] Brearley and Prinz (1992), GCA 56, 1373-1386.

Table 1. Clast Classification in The DAG 319 Polymict Ureilite

A. Coarse-grained mafic lithic clasts	
A1. Ol-pigeonite monomict ureilite; Fo74-78 (Type I)	
A2. Ol-Opx-Aug monomict ureilite; Fo84-87 (Type II)	
A3. Magnesian Ol-Pyx monomict ureilite; Fo91-97	
B. Fine-grained mafic lithic clasts	
B1. Ol-Pyx; Fo91-99	
B2. Pyx-rich; En83-90	
B3. Granular Ol-rich, with Opx and glass; Fo74-84 (normal zoning)	
C. Felsic lithic clasts	
C1. Trachytic-textured, with Pl, Aug and glass; An31-53	
C2. Porphyritic, Pl and Pyx, with merrihueite and whitlockite; An1-60	
C3. Glassy type having rhyolitic comp., with En and Di	
C4. Glassy type having alkali-poor comp., with Ol, Opx and Aug, mg(Opx) 55-80	
C5. Troctolitic type, with Ol (Fo93) and Pl (An81); coarse-grained	
D. Dark Inclusions	
Fe-rich olivine and/or phyllosilicates (serpentine, chlorite; mg, 50-84), with sulfide, magnetite (sometimes framboids) and carbonates (dolomite, magnesite, calcite)	
E. Sulfide- or metal-rich clasts	
E1. Sulfide-rich type, Fe-rich Ol-bearing; Fo47-83	
E2. Metal-rich type, En-bearing, with Pl and silica; mg En>98	
F. Chondrules and chondritic fragments	
F1. Barred Ol chondrule; Fo71	
F2. Porphyritic Ol chondrule; Fo72-96 (normal zoning)	
F3. Porphyritic En-Di chondrule; En92-99 (normal zoning)	
F4. Radial Pyx chondrule (complete); En98-99	
F5. Chondritic; with Ol, Opx and minor Ab, Fo82, and Fo66	
G. Isolated mineral clasts	
G1. Olivine	G3. Plagioclase
G1.1 Ureilitic Ol, mg73-97	G3.1 Calcic Pl, An>90
G1.2 Fe-rich Ol, Fo< 72	G3.2 Intermediate Pl, An47; melt pockets
G1.3 Forsterite, mg>99	G3.3 Sodic Pl, 5<An<40
G2. Pyroxene	G4. Chromite and ilmenite
G2.1 Orthopyroxene, mg76-97	G5. Apatite and whitlockite
G2.2 Pigeonite, mg76-92	G6. Bladed graphite
G2.3 Inverted pigeonite (pig-opx)	G7. Sulfides, troilite and Pyrrh+Pent
G2.4 Fe-rich pigeonite, mg<70	G8. Metallic clasts
G2.5 Enstatite, mg>99	G8.1 Kamacite, <1%Si to 12.5%Si
G2.6 Augite (diopside)	G8.2 Suessite, perryite
G2.7 Fassaite, Al ₂ O ₃ 5 wt %	G8.3 Phosphides, schreib. and barring.
	G8.4 Taenite, up to 28% Ni



Mineralogical studies in five Rumuruti chondrites:
Y-75302, Y-791827, Y-793575, Y-82002, and A-881988

¹Naoya Imae, ²Noboru Nakamura, and ¹Hideyasu Kojima

¹*Antarctic Meteorite Research Center, National Institute of Polar Research, Kaga 1, Itabashi,
Tokyo 173-8515, Japan*

²*Department of Earth and Planetary Sciences, Kobe University, Nada Kobe 657-8501, Japan*

Rumuruti (R) chondrites have been previously called Carlisle Lakes-type chondrite (Weisberg et al., 1991) or tentatively “unique” in the catalog by Yanai and Kojima (1995). They were first classified by Rubin and Kallemeyn (1989), which are characterized by a highly oxidized anhydrous silicates, a low abundance of chondrule, a higher ¹⁷O, and the brecciation texture (Weisberg et al., 1991; Nakamura et al., 1993; Rubin and Kallemeyn, 1994; Bischoff et al., 1994; Schulze et al., 1994; Kallemeyn et al., 1996).

In the present study, we studied five R chondrites, which are Y-75302, Y-791827, Y-793575, Y-82002 and A-881988 found from the bare ice region in Queen Maud Land by Japanese Antarctic Research Expedition.

Three oxygen isotopes of these five chondrites have been analyzed all suggesting R chondrites (Kojima et al., 1998 and this volume by N. Nakamura et al.). Bulk chemical composition by wet chemistry has been determined except Y-75302 by H. Haramura (Kojima et al., 1998). According to the analyses, Mg/Si molar ratio is nearly 1. FeO/Si (mol) and (FeS+Fe+Fe₂O₃)/Si (mol) plot called Urey-Craig diagram looks like forming a relationship for R chondrites (Fig. 1). Polished thin sections were used for the mineralogical studies: Y-75302, 51-1 (the surface area of the PTS = 46 mm²), Y-791827, 51-2 (30 mm²), Y-793575, 51-1 (19 mm²), Y-82002, 61-1 (17 mm²) and A-881988, 51-1 (94 mm²). An optical microscope was used for the observation of textures. JXA-733 electron microprobe analyzer was used only for the random analyses of silicates. JXA-8800M electron microprobe analyzer was used for the determination of the chemical composition of constituting minerals and for the observation of the textures. Analytical condition was 15kV and 11nA for both apparatus.

From EPMA random analyses data (Kojima et al., 1998), the mean fayalite content (Fa) was determined to be sequentially 37.9, 38.3, 38.6, 38.2, and 35.1 mol% with single peak. Matrices are all thus recrystallized. Y-75302, Y-791827, Y-793575, Y-82002, and A-881988 are then petrologically classified into 3.8, ≥4, ≥4, ≥4, and ≥4, respectively. Average chondrule size is nearly 400, 300, 400, 500, and 600 μm, in the same sequence.

Main constituting minerals are olivine and sulfides. Most olivines contain small amount of Ni (0.1~1 wt%). As opaque minerals, sulfides of pyrrhotite with minor amount of Ni (Fe_{1-x}S), pentlandite ((Fe,Ni)₉S₈), Ni-containing pyrrhotite (Fe,Ni)_{1-x}S and small amount of oxide (chromite) can be also found (Fig. 2 and Fig. 3). Opaque mineral assemblages (OAs) of sulfides and oxide mainly occur in matrices and chondrule rim. The grain size of OAs in matrices has several tens μm, which is a bit smaller than the mean chondrule size. For sulfides in matrices, pyrrhotite and pentlandite often coexist (Fig. 3). Sulfide often coexists with oxide (chromite). No FeNi metals were found in the studied PTSs. As accessory minerals, augite (Y-30275, Y-82002 and A-881988), diopside (Y-791827, Y-793575), pigeonite (Y-75302), Ca-poor pyroxene (Y-75302, Y-791827, Y-82002, A-881988), plagioclase (Y-791827, Y-793575, Y-82002) can be found. Ferrosilite composition of small number of Ca-poor

pyroxenes is heterogeneous between grains, being different from the small variation of Fa.

A-881988 has clearly different several features from other four R chondrites from Yamamo bare ice: (1) Average chondrule size is largest among five Rumuruti chondrites, (2) bulk chemical composition is characteristic of lower FeO, higher H₂O(-), higher FeS, and lower total Fe among studied five R chondrites (Kojima et al., 1998) and (3) the mean Fa composition is lowest among studied five and other R-chondrites appeared in Kallemeyn et al. (1996) and (4) sulfide constitutes pyrrhotite with richer Ni. While other four R chondrites seem to look like each other.

Rubin and Kallemeyn (1994) pointed out the possibility of the oxidation in the solar nebula rather than on the parent body based on the lack of the oxidized agents. This idea is on the assumption of closed system. However, when the system is open, H₂O and O₂ (and S) fluid may incorporate into the initially constituting minerals of R chondrites to form oxidized minerals, anhydrously oxidation might occur on the parent body at high temperature (Dohmen et al., 1998). This oxidation reaction is also thermodynamically expected. Oxidation of silicates and FeNi metals with nebular oxidizing gases might be also kinetically inhibited in the solar nebula (e.g., Fegley and Prinn, 1989). We thus prefer the parent body oxidation model rather than the nebular oxidation model.

References:

- A. Bischoff, et al. (1994): *Meteoritics* 29, 264-274.
- A. Dohmen, et al. (1998): *Am. Min.*, 83, 970-984.
- B. Fegley Jr. and R. G. Prinn (1989): In: Weaver H. A. and Danley L. (ed.) *The formation and evolution of Planetary Systems*. Cambridge Univ. Press, Cambridge, pp. 171-211.
- G. W. Kallemeyn et al. (1991): *Geochim. Cosmochim. Acta* 55, 881-892.
- G. W. Kallemeyn, et al. (1996): *Geochim. Cosmochim. Acta* 60, 2243-2256.
- H. Kojima, et al. (1997): *Antarctic Meteorites* 23, 54-57.
- T. Nakamura, et al. (1993): *Proc. NIPR Symp. on Antarctic Met.* 6, 171-185.
- A. E. Rubin and G. W. Kallemeyn (1989): *Geochim. Cosmochim. Acta* 53, 3035-3044.
- A. E. Rubin and G. W. Kallemeyn (1994): *Meteoritics* 29, 255-264.
- H. Schulze, et al. (1994): *Meteoritics* 29, 275-286.
- M. K. Weisberg, et al. (1991): *Geochim. Cosmochim. Acta* 55, 2657-2669.
- K. Yanai and H. Kojima (1995): *Catalog of the Antarctic Meteorites*.

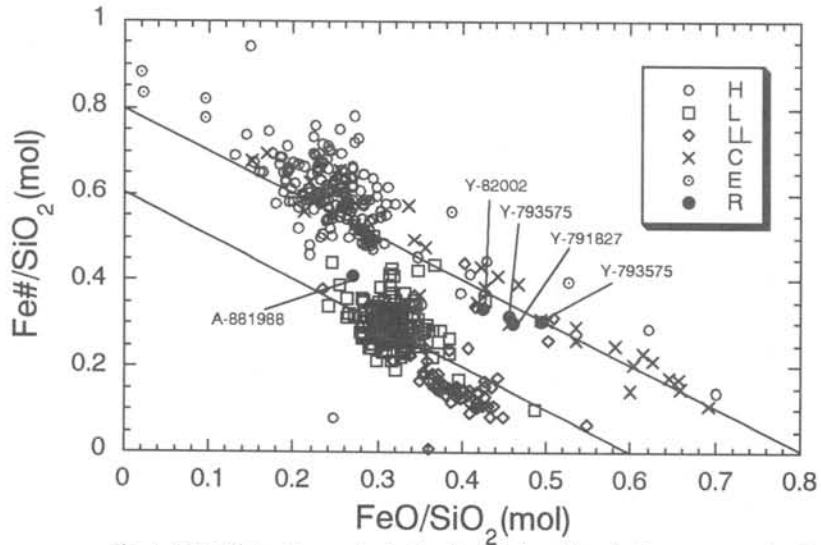


Fig. 1. Urey-Craig diagram including four R chondrites in the present study. Fe# shows (FeS + Fe + Fe₂O₃). The graph includes all data of chondrites from Yanai and Kojima (1995).

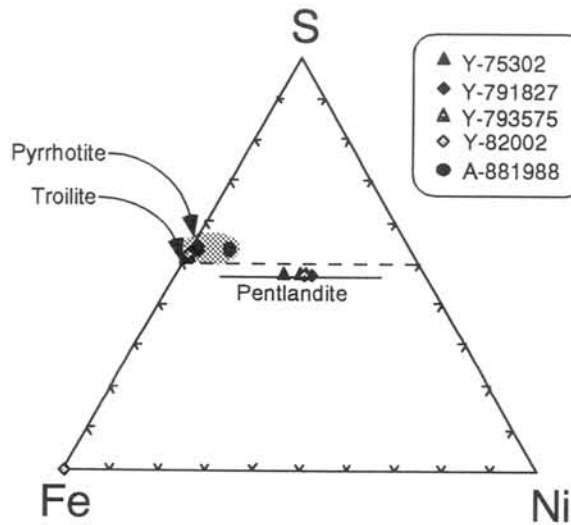


Fig. 2. Chemical composition of sulfides in five R-chondrites.

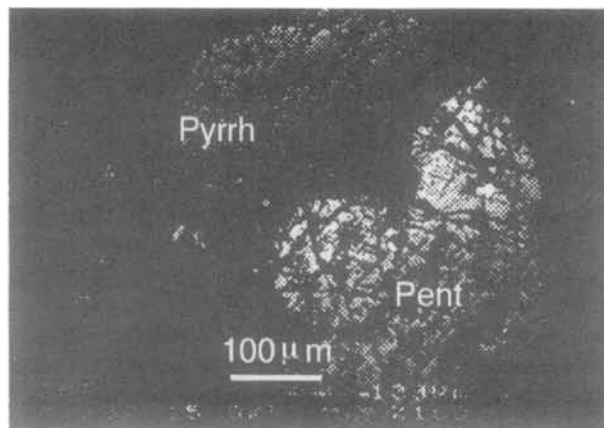


Fig. 3. An example of opaque mineral assemblages in R chondrite (Y-753575). Pyrrh=pyrrhotite, Pent=penlandite.

X-ray microprobe analyses of Antarctic micrometeorites from the Dome Fuji Station

¹Naoya Imae, ²Noguchi Takaaki, ³Tomoki Nakamura and ³Wataru Nozaki

¹*Antarctic Meteorite Research Center, National Institute of Polar Research, Kaga 1, Itabashi, Tokyo 173-8515, Japan.*

²*Department of Materials and Biological Science, Ibaraki University, Bunkyo 2-1-1, Mito, Ibaraki 310-8512, Japan.*

³*Kyusyu University 33, Hakozaki, Fukuoka, 812-8581, Japan.*

Extraterrestrial materials are divided into meteorites, cosmic dusts and lunar samples at present. Cosmic dusts have been believed to have new information of planetary system formation which has not been deduced from meteorites, due to their sizes, than ~1mm, while meteorites are more than ~1mm. Because of their small sizes, it will make easy to reach the Earth from all around the planetary bodies from a dynamical point of view (Brownlee, 1997). It is also expected that some cosmic dusts are cometary materials which we can not acquire as meteorites. Moreover, cosmic dusts are more common than meteorites, whose flux is estimated to be 4×10^4 ton/year from the analyses attacked the surface of artificial satellites (Love and Brownlee, 1993). Sampling sites of cosmic dusts are divided into two: on Earth surface (in polar ice or in deep sea sediments) and above Earth surface (mainly stratosphere). 100~200 μm size particles which are most frequent among the population of cosmic dusts are collected from on Earth surface but not stratosphere. Especially, samples collected from polar ice are usually less altered than those from deep sea sediments, and contain various kinds of dusts including cosmic dusts unmelted by frictional heating during the atmospheric entry.

Most important problems for cosmic dust are that (1) the classification is not satisfactory, and (2) the genetic relationship between interplanetary dust particles (IDPs) from stratosphere and Antarctic micrometeorites have not been understood. Different from IDPs, the cosmic dusts from polar ice are much abundant and much larger size than IDPs. Therefore, properties of cosmic dusts may become clear when Antarctic micrometeorites are investigated.

The initial non-destructive analyses for the identification and construction of cosmic catalog of 231 samples (irregular 80%, sphere 20%) by the cosmic dust research team in Japan have been carried out (Noguchi et al., 1999). From the catalog data (Murakami et al., 1998), we can see the size distribution. The most frequent size is the range of 100-150 μm . Noble gas analysis of a cosmic dust-rich fraction of Dome Fuji particles indicates that Ne in the cosmic dust are dominated by solar-wind derived component and almost absent from spallation-induced one, suggesting that the cosmic dust were present as small particles in space and exposed to solar winds for short duration (Nakamura and Takaoka, 1999).

In the present study, we have observed textures under optical microscopy and scanning electron microscopy, and determined major elements of constituting minerals of about 80 samples from these by electron probe microanalyzer and tentatively classified these. These 80 dusts have been those of tentatively classified as group 2 and 3 based on the bulk S/Si ratio (Noguchi et al., 1999). Sample was each mounted into micromolds and embedded by epoxy resin, and polished sections were made. Analyzed elements were Mg, Si, Fe, S, Al, Ca, Fe, Ni, Ti, Cr, Na, K and Mn for the electron microprobe analyzer. Major relict minerals which can be analyzed by EPMA were anhydrous silicates (olivine and low-Ca pyroxene), sulfides and FeNi metals. Phyllosilicates could be analyzed in one micrometeorite.

As a result of the X-ray microprobe analyses combing with morphological features, the Antarctic cosmic dust was broadly classified into eight. Our classification in the Antarctic micrometeorites from the Dome Fuji Station is summarized as follows:

•Type 1 (~8%): spherule experienced total melting,

- Type 2 (~6%): scoriaceous particles with nearly rounded shape, which experienced high melting degrees, with a small amount of relict minerals,
- Type 3 (~40%): scoriaceous particles containing materials with serpentine-like composition, serpentine does not survive,
- Type 4 (~8%): scoriaceous particles containing materials with saponite-like composition, saponite does not survive,
- Type 5 (~15%): partially melted particles including coarse anhydrous relict minerals,
- Type 6 (~6%): partially melted particles, which probably contained both hydrous and anhydrous minerals before atmospheric entry, only hydrous phyllosilicates were decomposed and melting during the entry,
- Type 7 (~3%): particles suffered partial subsolidus alteration of hydrous phyllosilicates into anhydrous minerals or amorphous materials, and
- Type 8 (~20%): unique and rare (CV3 matrix like etc.).

In addition, as most primitive dust, there are also cosmic dusts that there are no evidence having experienced alteration in the atmospheric entry. This is not reported here, but will be presented by Noguchi et al. (1999) and Nakamura et al. (1999). Degree of atmospheric entry heating is broadly type 1 > type 2 > type 5 > type 4 ~ type 3 ~ type 6 > type 7 (> type 8) in the higher sequence. That most frequent dust is type 3 is inconsistent with the case of IDPs, because IDPs with serpentine is poorer. Representative morphological feature and the chemical feature (type 3) are shown in Fig. 1 and Fig. 2, respectively.

When we exclude the effect of the atmospheric entry heating, that is, before into atmospheric heating, based on the major minerals, the dust is classified as (1) serpentine dominant, (2) saponite dominant, (3) hydrous and anhydrous mixtures (serpentine+olivine) dominant, and (4) anhydrous (olivine) dominant. And the majority is hydrous phyllosilicates dominant, inconsistent with meteorites, whose majority is ordinary chondrites consisting with anhydrous minerals. However, we should take into consideration that the frequency of each type includes the artificial selection effect in our picking up cosmic dusts from vast various dusts. In the classification, we can not take into account or discuss the origin in the solar system such as the body in the solar system which originated the dust at present. Mg/Si ratio from the electron microprobe seems to suggest that bulk Mg/Si atomic ratio of a lot of dusts tends to be ≤ 1 . On the other hand, it is well known that most chondritic meteorites show Mg/Si atomic ratio being nearly 1 or slightly higher. Since both Mg and Si are refractory elements, it is expected that the change of Mg/Si is small due to the atmospheric entry heating alteration of the dust. Thus the feature of the Mg/Si (atomic ratio) ≤ 1 might be one of the inherent character of Antarctic micrometeorite. This character is consistent with that of interplanetary dust (Rietmeijer, 1998).

References:

- D. E. Brownlee et al. (1996): *Meteoritics & Planet. Sci.*, 32, 157-175.
 S. G. Love and D. E. Brownlee (1993): *Science*, 262, 550-553.
 T. Nakamura et al. (1999): *Antarct. Met. Res.*, 12 (In press).
 T. Nakamura et al. (1999): This volume.
 T. Nakamura and N. Takaoka (1999): This volume.
 T. Noguchi et al. (1999): This volume.
 T. Murakami et al. (1998): *Antarct. Met.* 23, 95-98.
 F. J. M. Rietmeijer (1998): *Review in Mineralogy Vol. 36, Chapt. 2.*

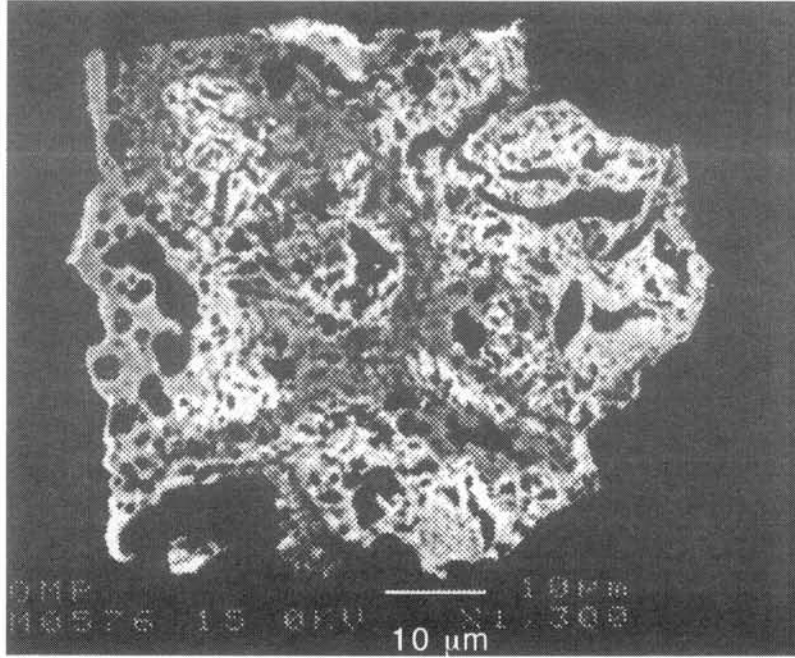


Fig. 1. Antarctic micrometeorites classified as type 3 with most high frequency in the present study which is considered to have been mainly composed of serpentine. Dark part is dehydrated relic, and white part is melted (F96DK021).

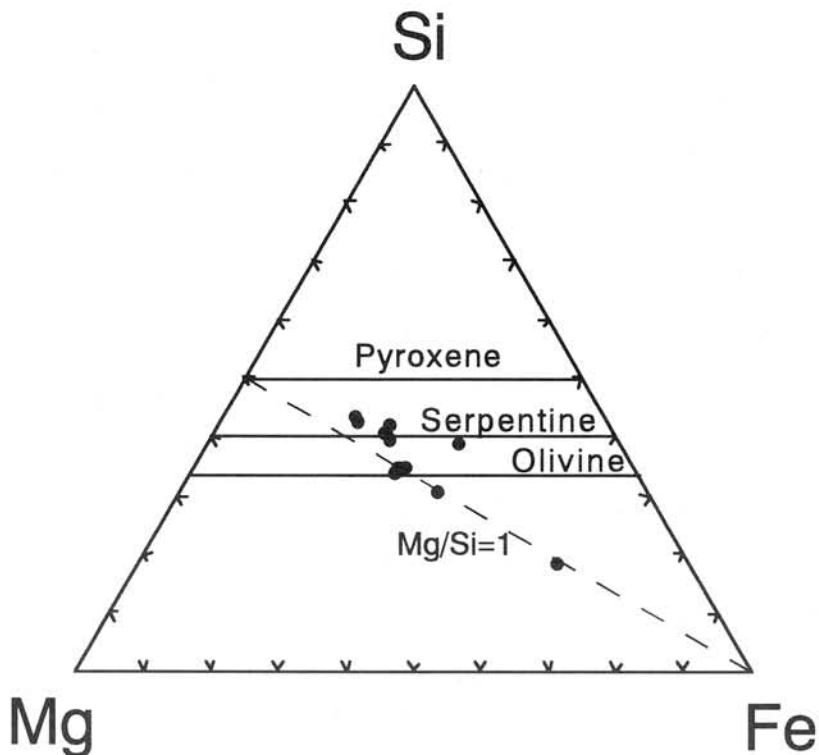


Fig. 2. The chemical composition of F96DK021 shown as Si-Mg-Fe plot. Point analyses suggest serpentine as a major mineral in origin but decomposed at present. Melting part became Fe-richer due to the decomposition of serpentine. Si-rich phase produced by the decomposition of serpentine can not be detected, which might suggest the evaporation of the phase during the heating in the air or the reaction with FeNi metal having been included in the dust. The bulk Mg/Si of the dust seems to be ≤ 1 .

Distribution of oxygen isotopes in a type-C CAI of the Allende meteorite

H. Imai and H. Yurimoto

Department of Earth and Planetary Sciences, Tokyo Institute of
Technology, Meguro, Tokyo 152-8551, Japan.

1. Introduction

Since oxygen isotope anomaly was observed in Calcium-Aluminium-rich inclusions (CAIs) [1], the inter-mineral distribution of O isotopes has been established for type A and B coarse grained CAIs [2]. Recently the inter-mineral distribution of micro-scale level has been determined for Type B CAIs [3, 4]. However distributions of oxygen isotopes have not been observed for all typical types of coarse grained CAIs.

In this study, distribution of oxygen isotopes among and in minerals of a type-C CAI from the Allende meteorite has been measured by secondary ion mass spectrometry (SIMS). The oxygen isotope ratios homogeneously distributed in each CAI minerals. The oxygen isotope ratios among the minerals distributed heterogeneously the carbonaceous chondrite anhydrous mineral (CCAM) mixing line.

2. Experimental Procedure

The sample used was a polished thin section named TTA1 from the Allende meteorite. The sample surface was coated with 20 nm carbon film and then examined by scanning electron microscope, JEOL JSM-5310LV, equipped with energy dispersive X-ray spectroscopy, Oxford LINK ISIS.

After the petrological and mineralogical studies the coated film was removed and then gold film of 30nm thick was coated onto the sample surface. In-situ oxygen isotope analysis were performed by the TiTech ims CAMECA 1270 SIMS instrument. The primary ion beam was mass filtered positive $^{133}\text{Cs}^+$ ions accelerated to 20 keV and the beam spot size was $\sim 3\mu\text{m}$ in diameter. Negative secondary ions of the ^{16}O -tail, ^{16}O , ^{17}O , ^{16}OH and ^{18}O were analyzed at a mass resolution power of ~ 6000 , sufficient to completely eliminate hydride interference. In order to correct instrumental mass fractionation, a Russian spinel with known O isotope ratios [3] was used for standardization.

3. Results and Discussion

A type-C CAI, TTA1-01 is subrounded in shape and 4x3 mm in size on thin section (Fig.1).

TTA1-01 consists of anorthite (~27vol%), melilite (~16vol%), fassaite (~15vol%), spinel (~9vol%) and alteration area (~33vol%). Spinel grains are enclosed poikilitically by melilite. This is against from the calculated equilibrium order for solid condensates [5]: melilite → spinel. Therefore, melilite is thought to be crystallized from liquid and then enclosed spinel. Anorthite represents like lath shape. This shape implies that anorthite also crystallized from liquid [6]. Fassaite compositions of TTA1-01 are similar to those of type B CAIs [8]. Alteration area mainly consists of nepheline. Some hedenbergite grains are observed in the alteration area. The texture of TTA1-01 are similar to those of type-B CAIs thought to be crystallized from liquid [7].

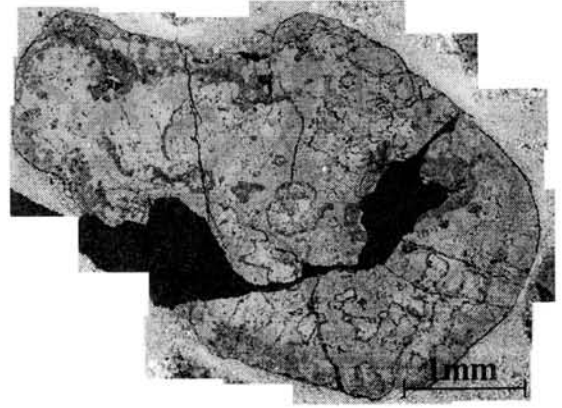


Fig. 1 Backscattered electron image of TTA1-01, CAI.

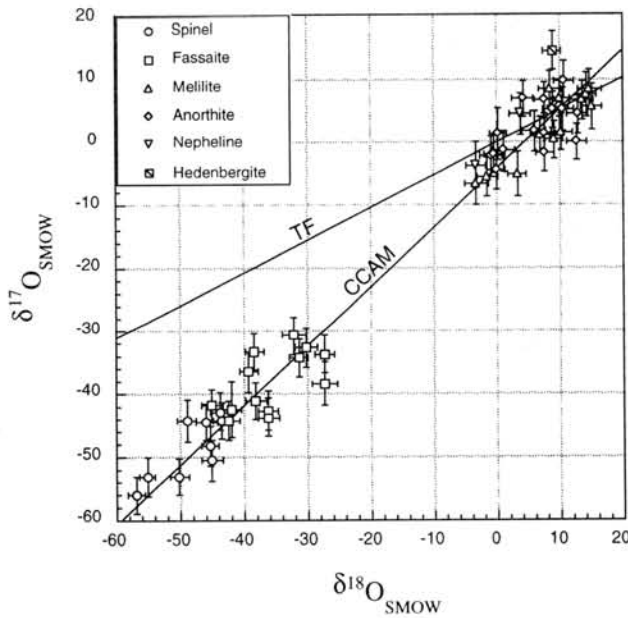


Fig. 2 Oxygen isotope compositions of TTA1-01 CAI from the Allende meteorite. TF: Terrestrial fractionated line. CCAM: Carbonaceous chondrite anhydrous mineral mixing line.

Distribution of oxygen isotopes of minerals in TTA1-01 are shown in Fig. 2. The values of oxygen isotopic ratios ($\delta^{17}\text{O}$, $\delta^{18}\text{O}$) fall on the carbonaceous chondrite anhydrous minerals (CCAM) line. No systematic O isotopic zonings within crystals have been observed for each minerals. The mean values of ($\delta^{17}\text{O}$, $\delta^{18}\text{O}$) for spinel, fassaite, anorthite and melilite are (-48.5‰, -48.3‰), (-38.5‰, -35.8‰), (+5.2‰, +8.4‰) and (+2.5‰, +8.4‰), respectively.

The distribution of oxygen isotopes among minerals in TTA1-01 is similar to those of typical type-B CAI [2].

From the petrological and oxygen

isotopical similarities, origin and formation processes are thought to be similar between type-C and type-B CAIs in spite of difference of their bulk compositions. The values of oxygen isotopic ratios of each minerals in CAI are thought of result of mixing between ^{16}O -rich endmember thought to be precursors of CAI and ^{16}O -poor endmember though to be the solar nebula gas [9]. The exchange of oxygen isotopes was not proved by diffusion after solidification [3], but occurs in melting stages of CAI precursor[4]. Spinels poikilitically enclosed in other minerals are thought has not experienced melting stages and its values of oxygen isotopic ratios (-48.5‰, -48.3‰) represents the values of TTA1-01 precursor. From textures, anorthite and melilite are thought have experienced melting stages and their values of oxygen isotopic ratios (+2.5~+5.2‰, +8.4‰) may close to the values of solar nebula.

References

- [1] Clayton, R. N., Grossman, L. and Mayeda, T. K. (1973) *Science* **182**, 485-488. [2] Clayton, R. N. (1993) *Annu. Rev. Earth Planet. Sci.* **21**, 115-149. [3] Yurimoto, H., Nagasawa H., Mori Y., and Matsubaya O. (1994) *Earth and Planetary Science Letters* **128**, 47-53. [4] Yurimoto, H., Ito M., and Nagasawa H. (1998) *Science* **282**, 1874-1877. [5] Grossman, L. (1972) *Geochimica et Cosmochimica Acta* **36**, 597-619. [6] Stolper, E. and Paque, J. M. (1986) *Geochimica et Cosmochimica Acta* **50**, 1785-1806. [7] MacPherson, G. J. and Grossman, L. (1981) *Earth and Planetary Science Letters* **52**, 16-24. [8] Grossman, L. (1975) *Geochimica et Cosmochimica Acta* **39**, 433-454. [9] Clayton, R. N., Onuma N., Grossman L., and Mayeda T. K. (1977) *Earth and Planetary Science Letters* **34**, 209-224.

DARK INCLUSIONS IN FOUR CO3 CARBONACEOUS CHONDRITES

Daisuke Itoh and Kazushige Tomeoka

Department of Earth and Planetary Sciences, Faculty of Science, Kobe University, Nada,
Kobe 657-8501, Japan

INTRODUCTION

Dark inclusions (DIs) in carbonaceous chondrites have been a subject of great interest in recent years. They are lithic clasts consisting largely of extremely fine grains of Mg-Fe silicates, mainly olivine. They may give us a wealth of information regarding the processes of the solar nebula [e.g., 1, 2] or the processes of the meteorite parent bodies [e.g., 3-6]. DIs are common in CV3 chondrites and have been mainly described from this type of chondrites. No DI has been reported from CO3 chondrites. We performed an extensive survey of dark inclusions in the four non-Antarctic CO3 chondrites, Kainsaz, Ornans, Lancé and Warrenton, and found a total of 129 unusual inclusions that are dark to brownish translucent in transmitted light. We here present the results of detailed mineralogical and petrographic study of these dark inclusions. Kainsaz, Ornans, Lancé and Warrenton were classified into 3.1, 3.3, 3.4 and 3.6, respectively [7], spanning a wide range of petrologic types. One of our purposes was, if any sign of a secondary process was found from DIs, to determine relationship between the secondary process and the metamorphism of the host CO3 chondrites.

RESULTS

31, 35, 31 and 32 dark inclusions were found from Kainsaz, Ornans, Lancé and Warrenton, respectively. Most of them are rounded to oval in shape; angular or irregularly-shaped inclusions are rather uncommon. They range in size from 40 to 1200 μm , but most are 100-200 μm , thus are comparable with most chondrules. These morphological and dimensional characteristics are distinct from DIs in CV3 chondrites; the latter are generally more angular or irregular in morphology and much larger (1-20 mm) in size. The small sizes may be a main reason of why DIs in CO3 chondrites have been overlooked in the past compared to DIs in CV3 chondrites despite the relatively abundant occurrence. Most inclusions are porous aggregates composed mainly of fine grains (1-20 μm in diameter) of Fe-rich olivine (Fa50-80) and minor diopside, Fe-Ni metal, Fe sulfide, Na-Al-Si-rich phase (probably nepheline) and Ca phosphate. The nepheline-like phase occurs widely as submicrometer-size grains in interstices between fine olivine grains. We found that most DIs in each meteorite have similar mineralogical and textural characteristics, and in general, DIs in Kainsaz resemble those in Lancé, and DIs in Ornans resemble those in Warrenton. Thus DIs in Kainsaz and Lancé are described together in the following. So are DIs in Ornans and Warrenton.

Dark inclusions in Kainsaz and Lancé

Most DIs contain rounded to oval-shaped sections (typically 10-40 μm in diameter); some are composed entirely of assemblages of these sections. Each section is commonly enclosed by a thin rim (~1 μm in thickness) of Fe-rich olivine and consists of a stack of thin lath-shaped grains (1-3 μm in thickness and 10-15 μm in length) of olivine that are oriented almost parallel to each other. The sections are most clearly discernible in crossed polarized light. The olivine grains in each section exhibit parallel extinction, indicating that they have a common crystallographic orientation. The sections in the Kainsaz DIs commonly have coarse-grained cores of Fe-poor olivine (Fa5-25), which show strong Fe-Mg zoning, mantled by fine grains of Fe-rich olivine. On the other hand, the sections in the Lancé DIs do not show such cores. The DIs in both Kainsaz and Lancé contain rounded to oval-shaped aggregates of Fe-Ni metal and minor Fe sulfide, Fe-rich olivine and Ca phosphate; metal is commonly replaced

partially by olivine and Ca phosphate. They are nearly opaque in transmitted light, resembling opaque nodules in chondrules.

Remarkable characteristic is that some DIs contain narrow veins that range in width from 1 to 6 μm and in length from 10 to 50 μm . They are filled with fine grains of Fe-rich olivine and occasionally Fe-Ni metal; these grains tend to be elongated along the veins. The veins filled with Fe-Ni metal extend from large grains of Fe-Ni metal. Vein minerals commonly show symmetrical distribution; olivine forms walls of the veins, and the central zone is hollow, exhibiting a pipe-like appearance. Most veins occur between the rounded to oval-shaped sections but some penetrate them. The veins always terminate at the boundaries between DIs and the host meteorite, indicating that they formed prior to incorporation to the present location.

Some DIs in Lancé contain aggregates (40-80 μm in diameter) of relatively coarse grains (5-20 μm) of Fe-rich olivine, in which coarse grains (20-30 μm) of nepheline and tiny grains (<3 μm) of Fe sulfide are contained. Coarse grains (5-20 μm) of diopside are common in Kainsaz DIs, whereas they are less common and smaller in size in Lancé DIs.

Dark inclusions in Ornans and Warrenton

DIs in Ornans and Warrenton are distinctly different in texture from those in Kainsaz and Lancé. Most DIs in Ornans and Warrenton consist predominantly of fine straight needle-like grains (<1-2 μm in width and 5-20 μm in length) of Fe-rich olivine. Those fine olivine needles are nearly randomly oriented throughout each DI, and neither discrete section nor vein-like feature, as observed in the DIs in Kainsaz and Lancé, is present. Diopside is much less common and occurs in smaller grains than in Kainsaz and Lancé. One of the DIs in Ornans is by far the largest of all the DIs studied (1200×500 μm). This DI is elliptical in shape and consists entirely of fine needle-like grains of Fe-rich olivine. In this DI and some other DIs in Ornans, irregularly shaped aggregates (20-50 μm in diameter) of kirschsteinite and Ca phosphate occur. Some DIs in Ornans contain rounded grains (5-30 μm in diameter) of Fe-poor olivine (Fa5-20) that show Fe-Mg zoning, whereas DIs in Warrenton do not contain such Fe-poor olivine.

DISCUSSION

The DIs found in Kainsaz and Lancé show peculiar textures, i.e. assemblages of rounded to oval-shaped sections, each consisting of fine grains of Fe-rich olivine. Most of the fine olivine grains in each section have a common crystallographic orientation. These textural and mineralogical characteristics closely resemble those of chondrule pseudomorphs in a type B DI in Allende [4], and suggest that the rounded to oval-shaped sections had been originally large single crystals of Fe-poor olivine and were later replaced by fine grains of Fe-rich olivine during some secondary process. We believe that, as in the case of DIs in Vigarano and Allende [3, 4], the rounded to oval-shaped sections were originally phenocrysts in porphyritic chondrules. The coarse-grained cores of forsteritic olivine common in the Kainsaz DIs may be unaltered relicts of phenocrysts.

The DIs in Kainsaz and Lancé show another peculiar texture, i.e., abundant veins filled with Fe-rich olivine and Fe-Ni metal. Veins consisting mainly of Fe-rich olivine [4, 8] and Ca-Fe-rich pyroxene [6] were found from Allende DIs. The previous authors [4, 6] suggested that the veins in the Allende DIs were formed during aqueous alteration that occurred on the meteorite parent body. We suggest that the veins in the DIs in Kainsaz and Lancé were also formed during aqueous alteration. The DIs probably experienced dehydration after aqueous alteration. Thus hydrous phases such as phyllosilicates are now absent in the DIs. From these results, we suggest that the DIs in Kainsaz and Lancé are CO chondrite clasts that experienced extensive aqueous alteration and subsequent dehydration on the meteorite parent body, thus are similar in formation history to the type B DIs in CV3 chondrites.

The DIs in Ornans and Warrenton consist mostly of randomly oriented fine needle-like

grains of Fe-rich olivine and contain neither chondrules nor chondrule pseudomorphs. These characteristics are similar to those of the type C DIs in CV3 chondrites [9]. Because of the featureless texture, the formation process of this type of DIs is less clear than that of type A-B DIs. Recently, Tomeoka and Kojima [10] suggested that fine grains in a type C DI in Vigarano resulted from size-sorting of grains produced by disaggregation and comminution of a type B DI-like material. They suggested that the size-sorting process may have occurred during activity of liquid water on the meteorite parent body. The fine needle-like grains of olivine in the DIs in Ornans and Warrenton are similar in morphology and composition to the thin lath-shaped grains of olivine in the DIs in Kainsaz and Lancé. Thus the former may have resulted from disaggregation and comminution of a material that had a lithology similar to the latter.

Our results suggest that the DIs in CO3 chondrites are clasts that came from different locations in the CO parent body, and the extents of aqueous alteration and thermal metamorphism differed greatly from location to location. Compared to DIs in CV3 chondrites, DIs in CO3 chondrites are much smaller and more uniform in size but more abundant. This suggests that DIs in CO3 chondrites have undergone a mechanical process, probably a brecciation process, that broke the parent rock to smaller and more uniformly-sized fragments than DIs in CV3 chondrites. These results imply that the CO parent body was probably not homogeneous and unprocessed, as implicitly imagined previously, but was heterogeneous in distribution of water and temperature and active in aqueous alteration and thermal metamorphism.

The present study showed that there is a tendency that Mg-rich olivine grains are less common in DIs in meteorites of higher petrologic type. However, the texture of DIs and the degree of secondary processes responsible for the formation of the major part of DIs, i.e. aqueous alteration and subsequent dehydration, have no apparent correlation with the petrologic grades of the host meteorites. Therefore the secondary processes of DIs in the CO3 chondrites may not be directly related to the metamorphism that resulted in the different petrologic grades (3.0-3.9) of the host meteorites. The secondary processes of DIs were probably completed before the metamorphism of the host meteorites took place.

References

- [1] Kurat G., Palme H., Brandstätter F. and Huth J. (1989) *Z. Naturforsch.* 44a, 988-1004.
- [2] Weisberg M. K. and Printz M. (1998) *Meteorit. Planet. Sci.* 33, 1087-1099.
- [3] Kojima T., Tomeoka K. and Takeda H. (1993) *Meteoritics* 28, 649-658.
- [4] Kojima T. and Tomeoka K. (1996) *Geochim. Cosmochim. Acta* 60, 2651-2666.
- [5] Krot A. N., Scott E. R. D. and Zolensky M. E. (1997) *Meteorit. Planet. Sci.* 32, 31-49.
- [6] Krot A. N., Petaev M. I., Zolensky M. E., Keil K., Scott E. R. D. and Nakamura K. (1998) *Meteorit. Planet. Sci.* 33, 623-645.
- [7] Scott E.R.D. and Jones R.H. (1990) *Geochim. Cosmochim. Acta* 54, 2485-2502.
- [8] Krot A. N., Petaev M. I., Scott E. R. D., Choi B-G., Zolensky M. E and Keil K. (1998) *Meteorit. Planet. Sci.* 33, 1065-1085.
- [9] Krot A. N., Scott E. R. D. and Zolensky M. E. (1995) *Meteoritics* 30, 748-776.
- [10] Tomeoka K. and Kojima T. (1998) *Meteorit. Planet. Sci.* 33, 519-525.

Parent Body Processes in Allende: Evidence from Oxygen Isotope Study of the Allende Chondrules

Iffat Jabeen¹, Minoru Kusakabe¹, Tomoki Nakamura² and Keisuke Nagao³

¹Institute for Study of the Earth's Interior, Okayama University, Yamada-827, Misasa-cho, Tottori-ken 682-0193, Japan. ²Department of Earth and Planetary Sciences, Faculty of Science, Kyushu University 33, Hakozaki, Fukuoka 812-8581, Japan. ³Laboratory for Earthquake Chemistry, Graduate School of Science, University of Tokyo, Hongo, Bunkyo-ku, Tokyo 113-0033, Japan.

Introduction

On the three isotope plot of oxygen most of carbonaceous chondrites fall below the terrestrial fractionation line (TF). Among them, CV group shows a wider spread of oxygen isotopic compositions. The spinels in CAI (calcium aluminium rich inclusions) from this type of chondrites have $\delta^{18}\text{O}$ values as low as -40‰ (Clayton, 1993). Oxygen isotopic compositions of anhydrous minerals in CV chondrites fall along a line of slope ~ 1 (Clayton et al. 1977, Young and Russel, 1998). This array has been interpreted as mixing between ^{16}O -enriched solids and ^{16}O -poor nebular gas (Clayton, 1993). The arrays for the CI, CM and CR groups show shallower slopes and reflect the fact that these chondrites have undergone aqueous alteration, probably on asteroidal bodies, during which oxygen isotopic fractionation occurred (Clayton and Mayeda, 1984; Weisberg et al. 1993). In case of Allende, very few studies about oxygen isotopic signatures with respect to secondary characteristics are available. Allende provides a hot topic among the researchers worldwide with regard to the parent body processes. Oxygen isotopes are a key to understand such signatures (Clayton, 1993; Choi et al. 1997; Weinbruch et al. 1993; Jabeen et al. 1998a, Jabeen et al. 1998b). In this study new oxygen isotope data from various chondrules of Allende is added to further explore their hidden signatures.

The $\delta^{17}\text{O}$ and $\delta^{18}\text{O}$ values of the 53 different types of chondrules were determined using the CO_2 laser fluorination-mass spectrometric technique (Jabeen et al. 1998a). These include porphyritic olivine (PO), porphyritic olivine pyroxene (POP), barred olivine (BO), porphyritic pyroxene (PP), cryptocrystalline (CRYPT), glassy chondrule (GC) and mellilite, fassite, sodalite (MSF), chondrules. A collective slope defined through the oxygen isotopic compositions of these chondrules is ~ 0.8 . This line with shallower slope observed among the chondrules could not be the result of mass dependent fractionation (with slope 1/2) or mass independent fractionations (slope 1). This might represent the mixing line between primary and secondary phases. Very recently the CCAM line presented by Clayton et al, 1977 is redefined by Young and Russell, 1998 (in this study we term it as AML). AML (anhydrous mineral line) has a slope of 1.00 ± 0.03 and is based on the in situ UV laser ablation analysis of anhydrous minerals from CAI of Allende.

Oxygen isotopic constraints on alteration processes in Allende

A three stage model is given to explain the oxygen isotopic signatures in Allende: (1) high temperature stage corresponds to early nebular processes, (2) low temperature stage, when the aqueous alteration produced secondary mineralization, and (3) thermal

metamorphism stage, when the signs of low temperature alteration were wiped out to a great extent. These stages are summarized in Fig. 1 and the explanation is given below:

Stage I - High temperature exchange processes

Such processes took place in the early nebular environment. At 1800°C, the high temperature exchange is assumed for solids and nebular gas. The initial solids (S) had isotopic compositions as $\delta^{18}\text{O} = -40.6\text{‰}$ and $\delta^{17}\text{O} = -41.9\text{‰}$ (Young and Russell, 1998). The Allende chondrules line, with slope of ~ 0.8 , crosses the AML at point A. This intersecting point on anhydrous mineral line is taken as isotopic composition of solid precursors of the matrix minerals. This point is defined as A with $\delta^{18}\text{O} = -12.0\text{‰}$ and $\delta^{17}\text{O} = -13.4\text{‰}$. The shifts in solids oxygen isotopic composition of solids from S to A is used to judge the shift in the nebular gas composition from initial (G1) to final (G2).

Stage II - Low temperature aqueous alteration

These processes resulted in the secondary mineralization in Allende by interaction of water with primary materials produced during the high temperature exchange stage. Using the calcite-serpentine geothermometry, the temperature of alteration of 75°C is estimated (This line is termed as HML). At 75°C the G2 condensed to produce L1 (initial liquid). The oxygen isotope data of all Allende chondrules defines a mixing line between hydrous (HML) and anhydrous phases (AML) with a slope of ~ 0.8 . This line is termed as CML. The shift in oxygen isotopic composition from A to M is used to infer the change in water composition from L1 to L2 (final liquid). Using this line as a reference, and considering the temperature of 75°C, the water rock ratio and in turn the initial water composition and initial nebular gas composition (which caused the alteration signatures) are determined. The water/rock ratio (oxygen atomic ratio) of ~ 0.7 is calculated for Allende which indicates that plenty of water was available for interaction with different primary materials. Such an excess of water could only be available in a large planet or asteroidal body. This interpretation is consistent with recent studies (Kojima and Tomeoka, 1996; Choi, et al. 1997; Krot et al. 1998 etc.).

Stage III - Thermal metamorphism

We have observed an increase in the Fa content of olivine in chondrules as we go along the CML line from the residual solids (A) towards the matrix (M). This Fe enrichment is the result of thermal metamorphism as explained by many researchers (Kojima and Tomeoka, 1996; Brearley, 1997; Krot et al. 1998). Dehydration during such metamorphism could have resulted in the mass dependent trends within individual chondrules having the oxygen isotopic data shifting towards higher delta values.

Conclusions

The variations of oxygen isotopic compositions within Allende chondrules are considered to be due to both primary and secondary processes. It could be the different degrees of aqueous alteration followed by thermal metamorphism within different chondrules resulting in the observed oxygen isotopic trends. These chondrules define a mixing line between hydrous and anhydrous phases. The aqueous alteration ($\sim 75^\circ\text{C}$) and

CARBON-14 TERRESTRIAL AGES OF METEORITES FROM THE YAMATO REGION, ANTARCTICA.

A. J. T. Jull, S. E. Klandrud, E. Cielaszyk and S. Cloude. NSF-Arizona Accelerator Mass Spectrometer Laboratory, 1118 East Fourth St., Tucson, AZ 85721, USA

The cold and dry conditions of Antarctic permit storage of meteorites with low rates of weathering and meteorite destruction. Japanese, American and other search parties have recovered many samples from this continent. The terrestrial age (or storage time) of a meteorite on the earth's surface, can be determined by the decay of cosmic-ray-produced radionuclides. The radionuclide ^{14}C ($t_{1/2}=5730$ years) is very useful in most instances for determining these ages. Fireman (1978) did some early measurements on Antarctic meteorites by β -decay counting. However, since Brown et al (1984) used accelerator mass spectrometry (AMS) to measure the ^{14}C terrestrial ages of Antarctic meteorites, all subsequent studies have used much smaller sample sizes (0.1-0.5g) and AMS measurements. Jull et al. (1998) have made a complete summary of this ^{14}C literature in a recent paper.

The longer-lived isotopes ^{81}Kr (e.g. Miura et al., 1993) and ^{36}Cl (summarized by Nishiizumi et al., 1989) can be used to determine longer terrestrial ages. The useful range of ^{14}C which is about 40,000 years. In the case of samples at the limit of ^{14}C age determination, we can sometimes place upper limits on their age by a lower limit determined by the ^{36}Cl age. Nishiizumi et al. (1989), Cresswell et al. (1993), Jull et al. (1993) and Michlovich et al. (1995) have shown that the age distributions of meteorites at the Allan Hills and Yamato collection sites in Antarctica can be very different. Nishiizumi et al. (1989) reported that many meteorites from the Allan Hills Main Icefield have long terrestrial ages, as determined by ^{36}Cl ($t_{1/2} = 301,000$ years). The Yamato site has been known for several years to have much younger meteorite falls (Beukens et al., 1988; Nishiizumi et al., 1989, Cresswell et al., 1993), although ^{81}Kr ages on eucrites show a wide distribution of ages from recent to 300ka (Miura et al., 1993).

In this paper, we investigate the ^{14}C terrestrial ages of a selection of meteorites from the Yamato region. Figure 1 shows results of ^{14}C measurements on a number of Yamato meteorites. We had previously reported on some ^{14}C ages on Yamato achondrites (Jull et al., 1993). In Figure 2, we summarize all terrestrial-age determinations on Yamato meteorites, compared to the Allan Hills Main icefield (see Jull et al., 1998). It is striking that some achondrites appear to survive much longer than chondrites, on the basis of some ^{14}C and ^{81}Kr measurements (Miura et al., 1993). There appear to be very few Yamato chondrites of terrestrial ages $>50,000$ yr. The terrestrial age determinations on meteorites from different sites can vary dramatically, the differences between the ages observed from these sites and some of the factors influencing them will be discussed. Weathering products found on these meteorites show ^{14}C ages younger than the terrestrial age of the meteorites studied. For previous studies at Allan Hills, where the area of collection is known, we can calculate infall rates based on meteorites recovered and their age distributions. Such an analysis gives a minimum infall rate of 40 to 60 meteorites ($>10\text{g}$)/ $10^6\text{km}^2/\text{yr}$ in quite good agreement (Jull et al., 1998) with the infall rates estimated from meteoroid fluxes.

References:

R. G. Cresswell et al. (1993), ^{14}C terrestrial ages of nine Antarctic meteorites using CO and CO_2 temperature extractions, *Proc. NIPR Symp. Ant. Met.*, **6**, 381-390.

E. L. Fireman (1978), Carbon-14 in lunar soil and in meteorites. *Proc. Lunar Planet Sci. Conf. 9th*, 1647-1654.

A. J. T. Jull et al. (1993), AMS ^{14}C ages of Yamato achondritic meteorites, *Proc. NIPR Symp. Ant. Met.*, **6**, 374-380.

A. J. T. Jull et al. (1998), ^{14}C terrestrial ages of meteorites from Victoria Land, Antarctica, and the infall rate of meteorites in "Meteorites: Flux with time and impact effects" (eds. M. M. Grady et al.), Geological Society (London), Special Publication **140**, 75-91.

Y. Miura (1993) ^{81}Kr terrestrial ages and grouping of Yamato eucrites based on noble-gas and chemical compositions., *Geochim. Cosmochim. Acta*, **57**, 1857-1866.

E. Michlovich et al. (1995) Chemical studies of H chondrites 5: Temporal variations of sources. *J. Geophys. Res.*, **100**, 3317-3333.

K. Nishiizumi et al. (1989) Update on terrestrial ages of meteorites. *Earth Planet. Sci. Lett.*, **93**, 299-313.

Yamato Meteorites

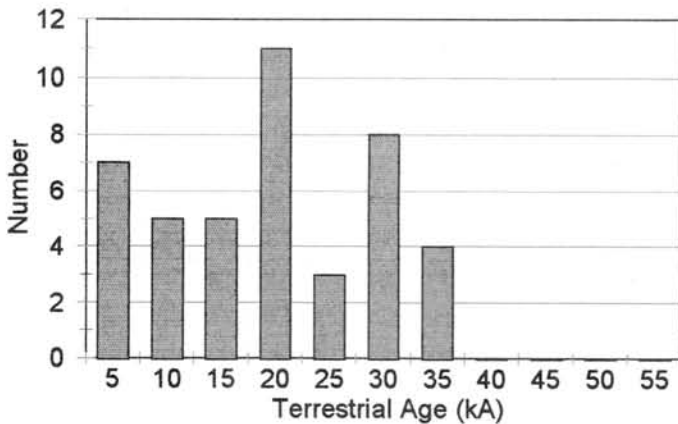


Figure 1: ^{14}C age distribution of Yamato meteorites.

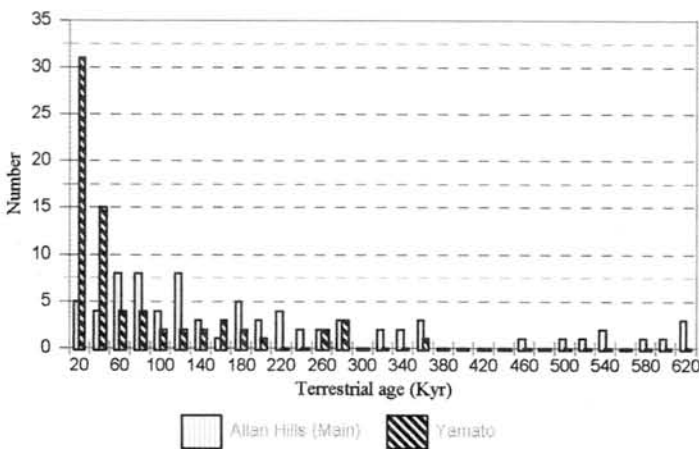


Figure 2: Comparison of Allan Hills (Main) Icefield and Yamato age distributions.

THREE DIMENSIONAL STRUCTURE OF CHONDRULE TEXTURE: POSSIBILITY OF A SPINNING CHONDRULE

KAWABATA Toshiharu*, TSUCHIYAMA Akira, KONDO Masahiko
Department of Earth and Space Science, Osaka University, Toyonaka 560-0043, JAPAN,
*kawabata@ess.sci.osaka-u.ac.jp,

Introduction

Chondrules have been examined extensively by many different methods. However, their three dimensional structures have not been known well. X-ray computed tomography (CT) can give textural information without breaking samples, and provide three-dimensional structures by successive imaging [e.g., 1,2]. Tsuchiyama *et al.* [3] preliminary reported a three dimensional structure of a chondrule obtained by a high resolution X-ray CT. In the present study, we analyzed the three dimensional structure, especially on the external shape of the chondrule and distribution of voids in the chondrule, in order to obtain information on movement of chondrules during their formation.

Experiments and image analysis

The sample used in the study was a large chondrule removed from Allende by the freeze-thaw method. A third generation X-ray CT scanner of Nittetsu Elex [1] was used. This scanner has a micro-focus X-ray source with a tungsten target to give a spatial resolution of up to several μm . Successive images were obtained simultaneously by using an area detector for X-rays (512x512 channeling plate). The accelerating voltage and tube current were 44 keV and 0.1 mA, respectively. Images of cross sections were reconstructed with a filtered back projection method (FBP) by rotating the sample. Each image has 512x512 pixels with CT values of 8-bit gray scale, which are related to the X-ray attenuation coefficients of the sample. The horizontal spatial resolution was about 7 μm , and the slice thickness was 17 μm . Successive images of 104 slices were taken with every 22.6 μm interval to reconstruct the three dimensional structure. In order to compare the CT images, thin sections of the chondrule were made and observed under an optical microscope and a scanning electron microscope (SEM) equipped in an electron probe micro analyzer (EPMA).

A specific algorithm was developed in the present study to analyze the three dimensional structure. In this algorithm, the constituents of the chondrule and their connectivity were examined in the three dimensional image.

Results and discussion

Fig.1a shows one of the X-ray CT images, where materials with high X-ray attenuation coefficients are shown by bright contrasts. As reported by [1,3] the chondrule has a porphyritic texture, where chondrule rim, euhedral phenocrysts, and voids were recognized. SEM/EPMA analysis showed that the euhedral crystals are olivine with FeO-rich rims, and the rest of the silicate part consists of orthopyroxene phenocrysts and mesostasis. The presence of voids in chondrules had been already observed on cutting surfaces of chondrites [4]. However, we cannot eliminate possibility of void formation during the cutting processes. The X-ray CT method confirmed real voids in chondrules from Allende [1].

The three dimensional image of the chondrule reconstructed by stacking the 104 slices is shown in Fig.2. It was found that this chondrule is not a complete sphere, but has a shape similar to an oblate. The major and minor axes are 2.8 and 2.6 mm, respectively. Although deviation of chondrule shapes from complete spheres is generally accepted, this is the first time that a three dimensional chondrule shape was described qualitatively as far as the authors know. The deviation is caused either by (1) spinning of chondrules in a space, (2) an aerodynamic effect during moving in a gas, or (3) compaction by shock loading after accumulation as a chondrite.

Three types of the chondrule constituents, rim, silicate part (olivine, orthopyroxene and mesostasis) and air including voids were distinguished by the image analysis. It was usually found that a void which seems to be located inside the chondrule in a cross section was three

dimensionally connected to the outside air (Fig.1b). The total volume % of the isolated voids ranges from 0.1 to 1.0 depending on the threshold CT value. There are several possibilities for the origin of voids in the chondrule [1], but we cannot specify the accurate origin of the voids at present. The three dimensional distribution of the isolated voids in the chondrule is shown in Fig.3. Most of the voids seem to be aligned nearly along the minor axis of the chondrule oblate. If this is the case, a partially molten silicate droplet was spinning during formation of the chondrule.

Acknowledgement: The authors thank Mrs. A. Koishikawa and K. Hirai of Nittetsu Elex Co. Ltd. For kindly taking the X-ray CT images.

References: [1] Kondo, M *et al.* (1997) *Proc. NIPR Symp. Antarctic Meteorites*, **10**, 437-447. [2] Carlson W.D. and McCoy T.J. (1998) *LPS*, **XXIX**, 1541. [3] Tsuchiyama *et al.* (1997) *LPS*, **XXVIII**, 1453-1454. [4] Zbik. M. and Lmag B. (1983) in "*Chondrules and their Origins*" ed. E.A. King, 319-329

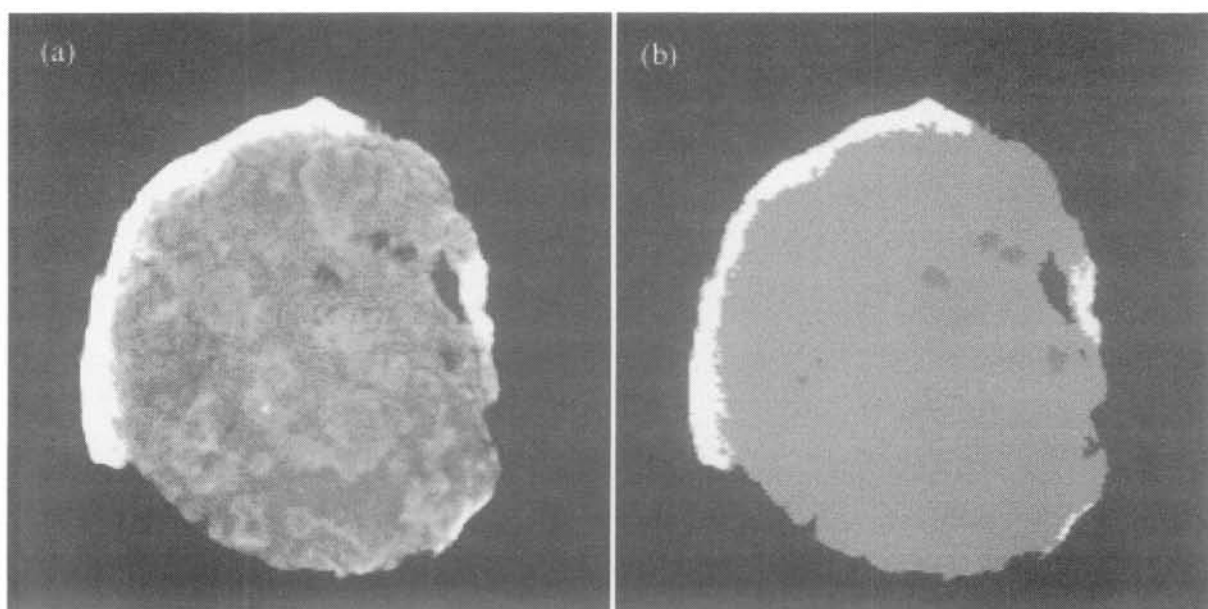


Figure 1. (a) An X-ray CT image of a chondrule removed from Allende. The contrast was enhanced to distinguish olivine phenocrysts (euhedral crystals bounded by bright rims) from other silicates (orthopyroxene and mesostasis). Voids (dark gray to black) and a chondrule rim (white) are also seen. (b) An image showing chondrule constituents; rim (white), silicates (bright gray), isolated voids (dark gray), and voids connecting to the outside air (black). The width of each image is 3.16 cm.

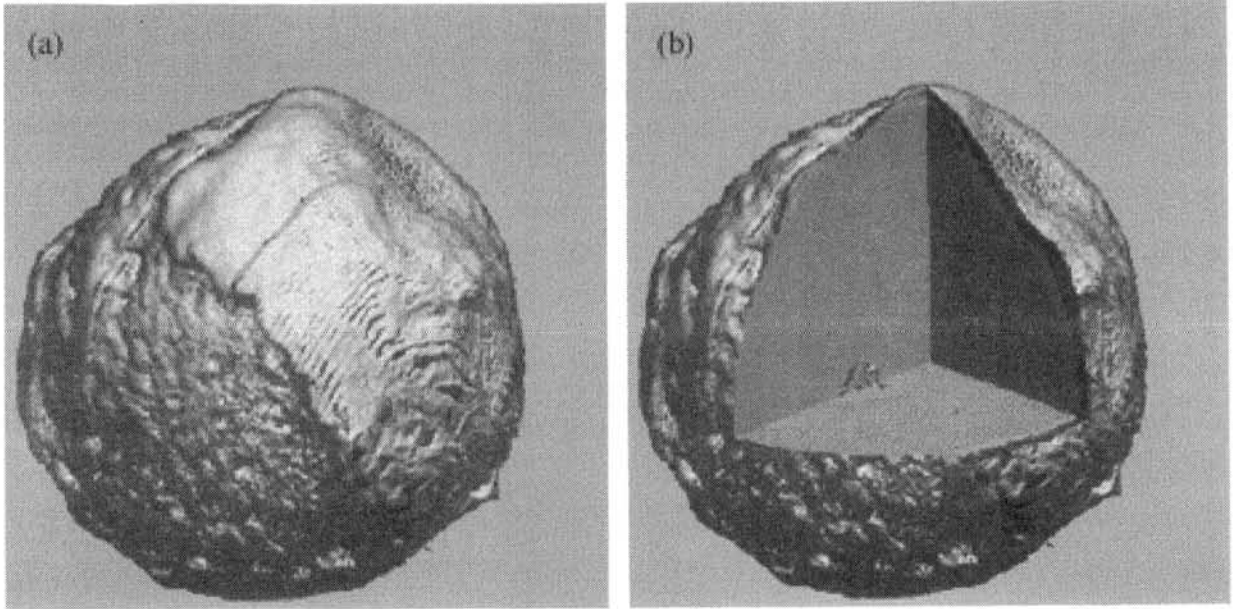


Figure 2. Three dimensional images of the chondrule. (a) An image showing the whole shape. (b) An image showing inside texture.

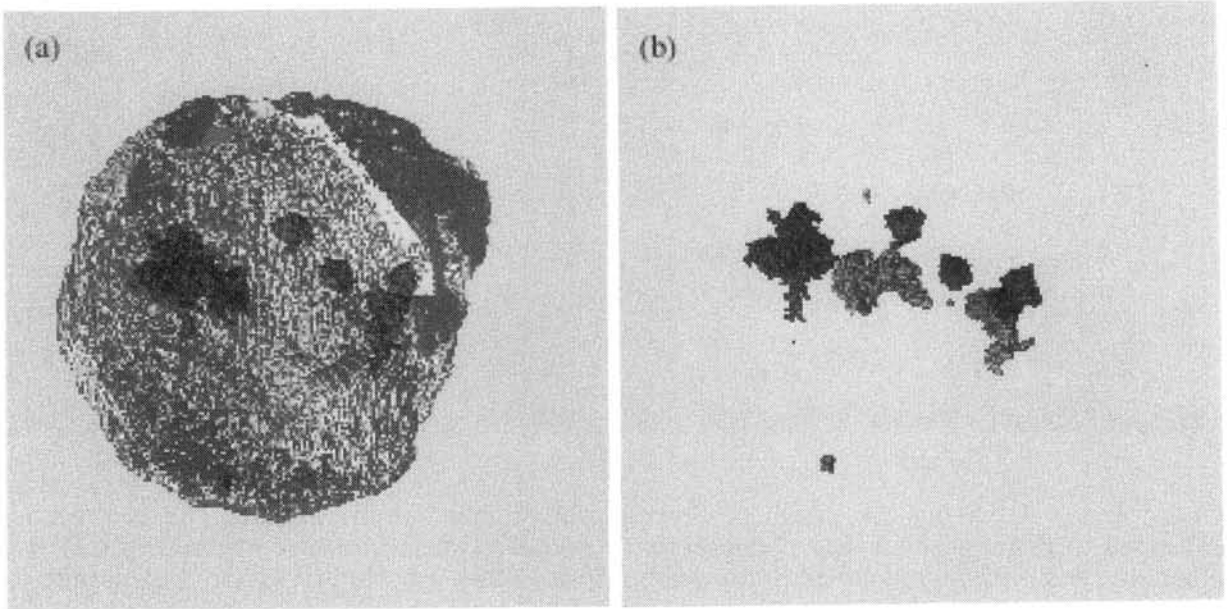


Figure 3. Three dimensional distribution of isolated voids aligned nearly along the minor axis of the chondrule oblate. (a) Voids (dark gray) with a part of the chondrule body. (b) Different void particles with different contrasts.

Heavily Shocked Antarctic H-chondrites: Petrology and Shock history.

Kimura M.¹, El Goresy A.², Suzuki A.³ and Ohtani E.³, ¹Ibaraki University, Mito, Japan, ²Max-Planck-Institut für Chemie, 55128 Mainz, Germany, ³Tohoku University, Sendai, Japan.

1. Introduction

Recent discoveries of high-pressure phases, such as ringwoodite, majorite and magnesiowüstite, from melt veins in heavily shocked L-chondrites, revealed that they experienced shock-induced melting and crystallization processes at very high pressures and temperatures [*e.g.*, 1 and 2]. On the other hand, such phases have not yet been reported from H-chondrites, although some of them show evidence for high degrees of shock-induced melting [*e.g.*, 3 and 4]. In order to explore the shock history of H-chondrites, we conducted petrographical study, with laser micro Raman investigations, of heavily shocked Antarctic H-chondrites (Y-790746, Y-791949, Y-793535 and Y-793537), in comparison with a shocked L-chondrite (Y-74445).

2. Petrography

All the H-chondrites studied here consist of highly deformed chondritic hosts and shock-induced melt regions. A thin section of Y-790746 mostly comprises the melt region. The less shocked hosts show the texture typical of H6, and consist mainly of homogeneous olivine (Fa₁₈₋₂₀) and low-Ca pyroxene (Fs₁₆₋₁₈). Raman spectroscopic data reveal no high-pressure phases in the hosts.

The melt regions mainly comprise two lithologies: 1) fine-grained euhedral to subhedral olivine and low-Ca pyroxene (below ~10m), and 2) coarse-grained rounded to subhedral olivine and pyroxene (~10 to ~100m). The fine-grained olivine and pyroxene usually show normal zoning from their cores (Fa₁₄ and Fs₁₁) to the rims (Fa₂₄ and Fs₂₁). On the other hand, the coarse grains commonly include corroded cores (Fa₁₈₋₂₀ and Fs₁₆₋₁₈), surrounded by the peripheral rims (2-10m in width) which usually show normal zoning like the

fine-grained olivine and pyroxene.

Our Raman spectroscopic investigations indicate that the melt regions contain no high-pressure polymorphs of silicate phases in any lithologies. On the other hand, ringwoodite and majorite occur in Y-74445 (L) melt region, like the other shocked L-chondrites.

The melt regions in the H-chondrites contain numerous metal-troilite spherules (<300m). Rare chondrule ghosts of barred olivine and radial pyroxene types are encountered, like Ramsdorf [5]. Y-791949 melt region includes a few enstatite ($\text{Fs}_{0.5-9.8}$) and forsterite ($\text{Fa}_{2.5-9.7}$) fragments (5-40m).

Broad beam analysis of the melt region in Y-793535 revealed a composition (48.9% SiO_2 , 3.4% Al_2O_3 , 13.4% FeO , 28.1% MgO , 2.4% CaO and 1.2% Na_2O) identical to the bulk silicate compositions of H-chondrites, suggesting *in situ* melting of H-chondrite material.

3. Implications

The absence of high-pressure polymorphs and crystallization of low-Ca pyroxene at low pressures [6] in the melt regions, indicates that the parent body of H-chondrites might have experienced different shock events than L-chondrites. Survival of high-pressure liquidus phases like majorite-pyroxene_{ss} + magnesiowüstite in shocked L-chondrites, indicates that this assemblage and the coarse-grained ringwoodite and majorite were quenched under high-pressures [1]. On the other hand, the petrologic setting in the shocked H-chondrites is indicative of melting and pressure release. We argue that the duration of the shock-induced high-pressure regime in the H-chondrite parent body was much shorter than in the L-chondrite parent body.

References: [1] Chen M. *et al.* (1996a) *Science*, 271, 1570-1573, [2] Chen M. *et al.* (1996b) *MAPS*, 31, A27, [3] Stöffler D. *et al.* (1991) *GCA*, 55, 3845-3867, [4] Chen M. *et al.* (1995) *Meteoritics*, 30, 28-32, [5] Yamaguchi A. *et al.* (1999) *MAPS*, 34, 49-59, [6] Zhang J. and Herzberg C. (1994) *JGR*, 99, 17729-17742.

Structure of Quenched Carbonaceous Composite (QCC) and formation of micro-diamond by heat treatment of QCC

Seiji Kimura¹, Chihiro Kaito¹, Setsuko Wada²

¹ Department of Nanophysics in Frontier Project, Ritsumeikan University,
Kusatsu-shi, Shiga 525-8577, Japan

² Department of Chemistry, University of Electro-Communications,
Chofugaoka, Chofu, Tokyo 182, Japan

Introduction The 217.5nm bump is well known feature caused by interstellar dust. For a candidate of interstellar dust, many types of carbon and other carbonaceous materials have been proposed to explain the 217.5nm bump. For examples, graphite[1], hydrogenated amorphous carbon (HAC)[2], a coagulation of polycyclic aromatic hydrocarbons (PAH)[3], graphite onions[4], and diamond-like carbon[5] are proposed.

A carbonaceous materials produced by condensation from an ejecta of hydrocarbon plasma, which is named Quenched Carbonaceous Composite (QCC) by Sakata et al., shows an absorption peak at 220nm[6,7]. A brown-black carbonaceous materials (dark-QCC) was formed in the center beam of the ejecta from the plasma. By dissolving organic molecules containing in the dark-QCC with acetone, dark-QCC showed an absorption peak at wavelength of 220nm, though the peak was more broader than the observed bump. At the center of the dark-QCC, a black circular spot with 5~7mm in diameter was formed. Sakata called this granular-QCC, which was a thickly condensed carbonaceous material from the ejecta. Sakata et al. measured an absorption spectrum of the granular-QCC and obtained a peak wavelength of 220~224nm. The peak of the granular-QCC was a little broader than that of the dark-QCC. Though the unheated QCC showed an absorption peak at a wavelength of 217~224nm, after heating, the absorption peak shifted to the longer wavelength side. By heating at 500°C, the absorption peak shifts to 225nm.

In previous study using transmission electron microscopy[7], the QCC materials showed a halo-like diffraction pattern that suggested an amorphous structure. We have used high resolution electron microscopic (HREM) technique to observe the structure of other materials that had also been thought to be amorphous materials and have revealed atomic arrangement in the amorphous structure[8]. In this report, by HREM observation we will show that the fundamental structure of QCC which shows a 220nm observation peak. In order to clarify a correlation between QCC structure and a shift of peak position, structural change by heating from room temperature to 500°C was studied by using of in-situ HREM observation. In this paper, formation of micro-diamond produced by heating are discussed with structural change of QCC.

Experimental procedure The experimental apparatus for producing QCC was reported by Sakata et al. QCC is formed from the ejecta of a methane plasma generated by a microwave discharge of 2.45GHz. The ejecta left the plasma tube through a narrow hole and were condensed on a room temperature substrate under vacuum. A brown-black carbonaceous material (named 'dark-QCC') formed around the center of the ejecta. At the center of the ejecta corresponding to the dark-QCC, a black circular spot (Named 'granular-QCC') about 5~7mm in diameter was formed. The QCC samples were collected on a quartz glass. For in-situ HREM observation, the QCC samples were directly mounted on tungsten heater and heated to 500°C in an apparatus of a Hitachi H-9000NAR electron microscope.

Results and discussion Figure 1 shows HREM images of the granular-QCC and the dark-QCC. Onion-like structure exist in both the QCC images in spite of the amorphous-like electron diffraction pattern. Each particle is composed of concentric shells. The fringe spacing is similar to the (002) lattice spacing of the graphite structure. The size of onion-like particles in the dark-QCC and the granular-QCC ranges from 5 to 15nm in diameter. Larger particles more than 10nm in diameter are found in the granular-QCC. A central vacant core 2~3nm in diameter is often observed in the particles, as shown in the top of Fig.1(b). Some cores are very round, although most QCC cores are very distorted rather than spherical. We could not observe any clear structure inside the round-shaped core in spite of the 0.18nm point resolution electron micrograph image. We conclude that the inside of the core is vacant.

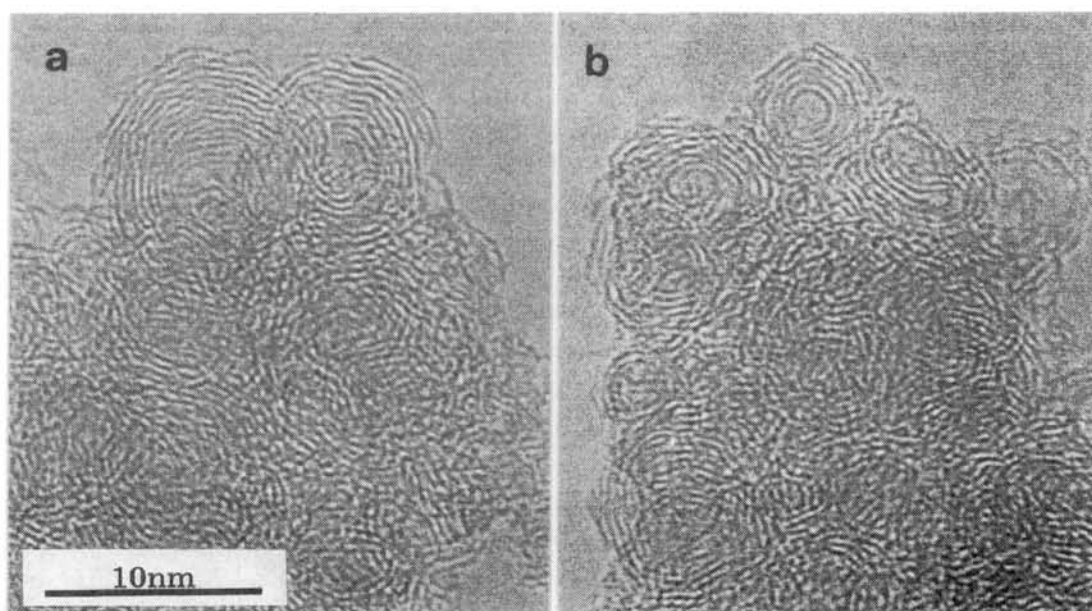


Fig.1. HREM images of (a) the granular QCC and (b) the dark QCC. The images are shown in the same scale.

By the heating of these QCC in electron microscope, a continuous range of (002) fringes of the onion region becomes gradually larger, i.e. graphitization partly took place. In addition to the graphitization by heating at 500°C, the black spots about 1.5nm appeared in the QCC as shown in Fig.2. Since the materials were composed of carbon atoms. The strong contrast of the dark spots shows the different crystal formation. As indicated by arrows, the fringes of 0.206nm which corresponds to (111) reflection of diamond can be seen. The formation of the micro-diamond by heating of the QCC took place lower temperature. Since the QCC was prepared from the CH₄ plasma, the hydrogen may be contained in the QCC. The trigger to the formation of micro-diamond may be due to the contained hydrogen. The change of the QCC itself by the heating will be also shown.

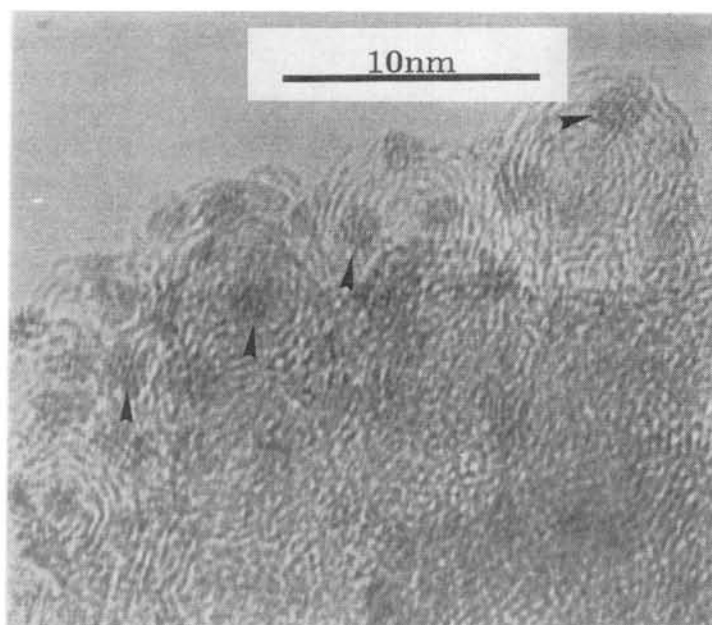


Fig.2. HREM image of the QCC heated at 500°C in vacuum.

References (1) T.P.Stecher and B.Donn, *Astrophys. J.*, 142 (1965) 1681. (2) V.Mennella, L.Colangeli, P.Palumbo, A.Rotundi, W.Schutte and E.Bussoletti, *Astrophys. J.*, 464 (1996) L191. (3) C.Joblin, A.Leger and P.Martin, *Astrophys. J.*, 393 (1992) L79. (4) L.Henrad, A.A.Lucas and PH.Lambin, *Astrophys. J.*, 406 (1993) 92. (5) H.Mutschke, J.Dorschner, Th.Henning and C.Jäger, *Astrophys. J.*, 454 (1995) L157. (6) A.Sakata, S.Wada, Y.Okutsu, H.Shintani and Y.Nakada, *Nature*, 493 (1983) 301. (7) A.Sakata, S.Wada, A.Tokunaga, T.Narisawa, H.Nakagawa and H.Ono, *Astrophys. J.*, 430 (1994) 311. (8) C.Kaito and T.Shimizu, *Jpn. J. Appl. Phys.*, 23 (1984) L7.

IN-SITU SIMS OXYGEN ISOTOPIC ANALYSES OF CLASTS FROM DAG 319 POLYMICT UREILITE

Noriko T. Kita¹, Yukio Ikeda², Martin Prinz³, C.E. Nehru³, Michael K. Weisberg³, Yuichi Morishita¹, and Shigeo Togashi¹.

¹Geological Survey of Japan, 1-1-3 Higashi, Tsukuba 305-8567, Japan. ²Department of Material & Biological Sciences, Ibaraki Univ. Mito 310-8512, Japan. ³Department of Earth and Planetary Sciences, American Museum of Natural History, New York, NY 10024-5192, USA.

Introduction: Polymict ureilites contain a wide variety of mineral and lithic clasts, along with monomict ureilite clasts [1-4]. These clasts may be from different portions of the ureilite parent body, and may include some “missing” basaltic components which are complementary to the ultramafic typical monomict ureilite component. In addition, “chondritic” clasts in polymict ureilites may represent potential candidates for ureilite precursors, or projectile components. In the present study, we have measured the oxygen isotopic compositions of several clasts in the DAG 319 polymict ureilite, described in Ikeda et al. [5], by performing in-situ SIMS analyses. The aim is to identify the origin and relationships of the various clasts in this polymict ureilite.

Samples: From more than a hundred clasts in a polished thin section of DAG 319 (AMNH 4963-1) we selected 14 clasts for oxygen isotopic analyses (Table 1). Because of high Fo content, B4-3 may be similar Type II ureilite, the unusual olivine-opx-augite ureilite clasts in [5], or magnesian ureilite clast. The augite-plagioclase clast C2-2 is a felsic lithic clast in [5] with porphyritic augite and plagioclase. Two olivine-orthopyroxene clasts (H2-1 and F4-2) are similar to chondritic clasts in [5].

Analytical Method: The oxygen isotopic measurements were performed using a secondary ion mass spectrometer (SIMS) Cameca IMS-1270 at the Geological Survey of Japan. Each sample was coated with carbon and exposed with a 0.2-0.3 nA Cs⁺ primary ion (total acceleration of 20 kV) which was shaped to a homogeneous 10 μm spot. O⁻ secondary ions were sputtered from the sample and accelerated with -10kV for isotopic analyses. By optimizing secondary ion optics, mass resolution was set to 5,000 with a total secondary ion transmission of more than 70%. The typical secondary ¹⁶O⁻ ion intensity was 2×10⁸

cps. We obtained two isotopic ratios independently using two detectors; ¹⁸O/¹⁶O ratios were measured using a Faraday cup detector (FC), and ¹⁷O/¹⁸O ratios using an electron multiplier (EM) with pulse counting mode. Each analysis takes one hour, with 80 cycles of switching both magnetic field and detectors. The internal errors of (¹⁸O/¹⁶O)_{FC} and (¹⁷O/¹⁸O)_{EM} ratios were 0.8 ‰ and 0.5 ‰ (2σ), respectively. The ¹⁷O/¹⁶O ratios were obtained by (¹⁷O/¹⁸O)_{EM} × (¹⁸O/¹⁶O)_{FC}. Terrestrial olivine, orthopyroxene and plagioclase standards were used for correction of the instrumental mass fractionation during the SIMS analyses. The external error of the ¹⁸O/¹⁶O ratio from repeated analyses of terrestrial standards was in the range of 1-2 ‰. The average ¹⁷O/¹⁶O ratio in SMOW scale (mass fractionation normalized to ¹⁸O/¹⁶O = 0.0020052, [6]) for terrestrial standards was calculated to be 0.00038289 ± 0.00000007, in good agreement with the literature value of

Table 1. Clasts from DAG-319

Sample	Clast Type	Mineral for SIMS
<u>Ureilite Clast</u>		
B3-1	Type I ureilite Ol	Fo 75
B5-1	Type I ureilite Ol	Fo 76
D1-3	Type I ureilite Ol	Fo 77
D4-1	Type I ureilite Ol	Fo 77
D1-2	Type I ureilite Ol	Fo 83
B4-3	Type II ureilite Ol, or Magnesian ureilite	Fo 88
<u>Ureilite-related Clast</u>		
D5-1	Plagioclase	An 47
D3-2	Plagioclase	An 28-40
C2-2	Augite-plag	An 22
D3-1	Orthopyroxene	En88Wo4
<u>Non-ureilite-related Clast</u>		
H2-1	Olivine-opx	Fo 66-69
F4-2	Olivine-opx	Fo 82
D1-1	Forsterite	Fo 100
D6-1	Forsterite	Fo 100

0.00038309 ± 0.00000034 by McKeegan (1987) [7]. Instrumental mass fractionation corrected isotopic ratios are expressed as permil deviation from the SMOW scale ($\delta^{17}\text{O}$ and $\delta^{18}\text{O}$). Excess ^{16}O in a meteoritic sample is expressed as $\Delta^{17}\text{O} = \delta^{17}\text{O} - 0.52 \delta^{18}\text{O}$. The internal and external errors of $\Delta^{17}\text{O}$ of terrestrial standards are 0.5 ‰ and 0.7 ‰ (2σ), respectively.

Results and Discussion: Oxygen isotopic analyses of the clasts analyzed in DAG 319 are shown in an oxygen three isotopic plot (Fig. 1). The ureilite clasts show both the petrology and oxygen isotopes very similar to monomict ureilites. The remaining clasts can be divided into two groups, as seen in Fig. 1. One consists of the orthopyroxene, plagioclase and augite-plagioclase clast, which plot along the ureilitic trend, and the other consists of the forsterite and olivine-orthopyroxene clasts, which plot further left in Fig. 1, with nearly zero or positive $\Delta^{17}\text{O}$ values.

Ureilite clasts. All the ureilite clasts plot along the ureilite mixing line [8], though our data are systematically on the higher $\delta^{18}\text{O}$ side of this line, to the level of 1-2 ‰. This may indicate that these ureilitic clasts are systematically heavier in oxygen isotopes, or that the present results are systematically shifted to higher $\delta^{18}\text{O}$ values by some artifact. The relationship between the olivine-mg# and the $\Delta^{17}\text{O}$ (Fig. 2) for the ureilitic clasts from DAG-319 is identical to the monomict ureilite data [8]. Many of ureilitic clasts (Type I) from DAG 319 fall on an extension of the monomict ureilite line, on or near the terrestrial fractionation line, in keeping with its low olivine mg#.

Ureilite-related clasts. The similarity in oxygen isotopic compositions between a group of these four clasts (opx, plag and aug-plag clasts) and the monomict ureilites is an indication that they may be genetically related. The absence of mass fractionation between the plagioclase and olivine, at the level of 1 ‰, implies they were fractionated from a common source at high temperature through igneous processes. Thus, the plagioclase- and pyroxene-bearing clasts may represent some of the fractionated “missing” basalt component from the ureilite parent body. Further petrologic and isotopic studies on these clasts are promising for a better understanding of that body.

Non-ureilite-related clasts. This group or groups of clasts do not follow the ureilite mg#- $\Delta^{17}\text{O}$ relationship shown in Fig. 2. These clasts are carbon-free and are petrologically very different from the monomict ureilites and ureilite-related clasts. Their oxygen isotopic compositions appear to be closer to those of chondrites or primitive achondrites. Because of nearly zero $\Delta^{17}\text{O}$ values for both forsterite clasts and some of ureilitic clasts (Type I), forsterite clasts might be derived from ureilite source with significant reduction processes and the fractionation of lighter oxygen isotopes. However, they are more likely to be related to other highly reduced En clasts in DAG 319 [5], and in turn may be genetically related to either enstatite chondrites, Kakangari-type chondrites or aubrites. Clearly, these clasts formed in a much more reducing environment than did the ureilitic components, but they lack the unusual mineralogy of E chondrites and aubrites, and are more similar to Kakangari-type chondrites. Two olivine-orthopyroxene clasts (chondritic clasts in [5]) show positive $\Delta^{17}\text{O}$ values as in the case of ordinary chondrites. The oxygen isotopic composition of the H2-1 plots on an extension of the ordinary chondrite slope 1 line, with a higher $\Delta^{17}\text{O}$ value. The $\Delta^{17}\text{O}$ in H2-1 is slightly lower than that in R chondrites, which have the highest $\Delta^{17}\text{O}$ values among meteoritic samples [9].

Conclusions: In-situ SIMS analyses of oxygen isotopes in clasts in the DAG polymict ureilite, combined with petrologic data, show that different clast types can be distinguished; (1) The ureilitic olivine clasts are similar to monomict ureilites in oxygen isotopic compositions, (2) there are plag- and plag-bearing clasts which may be part of the “missing” basaltic component in the ureilite parent body, and (3) there are clasts which may be related to a chondritic parent body(ies). Further combined petrologic-oxygen isotopic studies of clasts in the DAG 319, as well as other polymict ureilites, is the key to understanding the petrogenesis of the ureilite parent body.

References: [1] Jaques A. L. & Fitzgerald M. J. (1982) GCA 46, 893-900. [2] Prinz M. et al. (1986) LPSC XVII, 681-682. [3] Prinz M. et al. (1987) LPSC XVIII, 802-803. [4] Brearley A.J. & Prinz M. (1992) GCA 56, 1373-1386. [5] Ikeda Y. et al. (1999) this volume. [6] Baertschi P. (1976) EPSL 31, 341-344. [7] McKeegan K.D. (1987) PhD. Thesis, Washington Univ. [8] Clayton R.N. & Mayeda T.K. (1996) GCA 60, 1999-2017. [9] Weisberg M.K. et al. (1991) GCA 55, 2657-2669. [10] Clayton R.N. et al. (1991) GCA 55, 2317-2337. [11] Clayton R.N. (1993) Annu. Rev. Earth Planet. Sci. 21, 115-49.

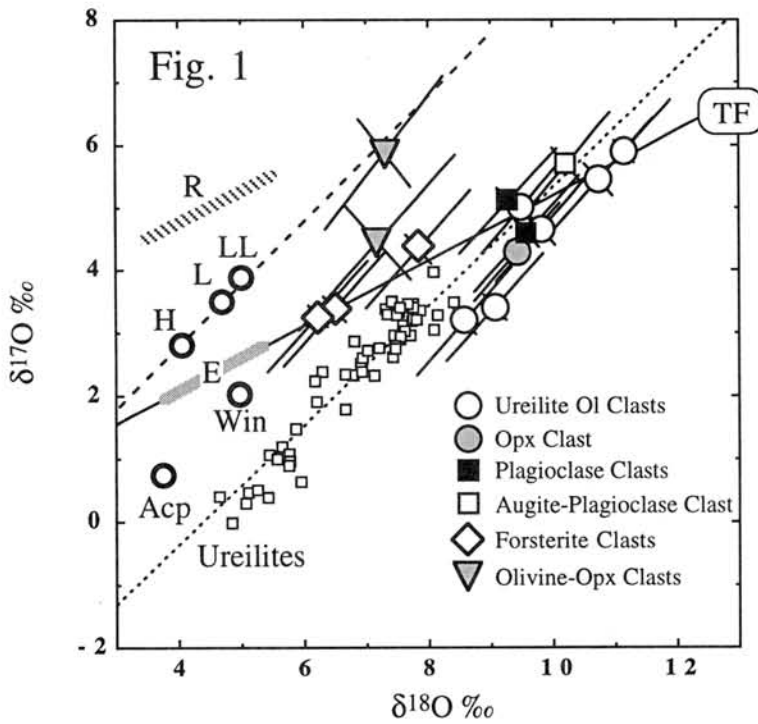


Fig.1. Oxygen isotopic data from DAG319 ureilite clasts. Small squares indicate bulk ureilite data [8]. Other meteorite data; (Data source, 8,10-11)

Acp = acapulcoite
 Win = winonaite
 E = E chondrite
 H = H chondrite
 L = L chondrite
 LL = LL chondrite
 R = R chondrite
 TF indicates the terrestrial fractionation line.

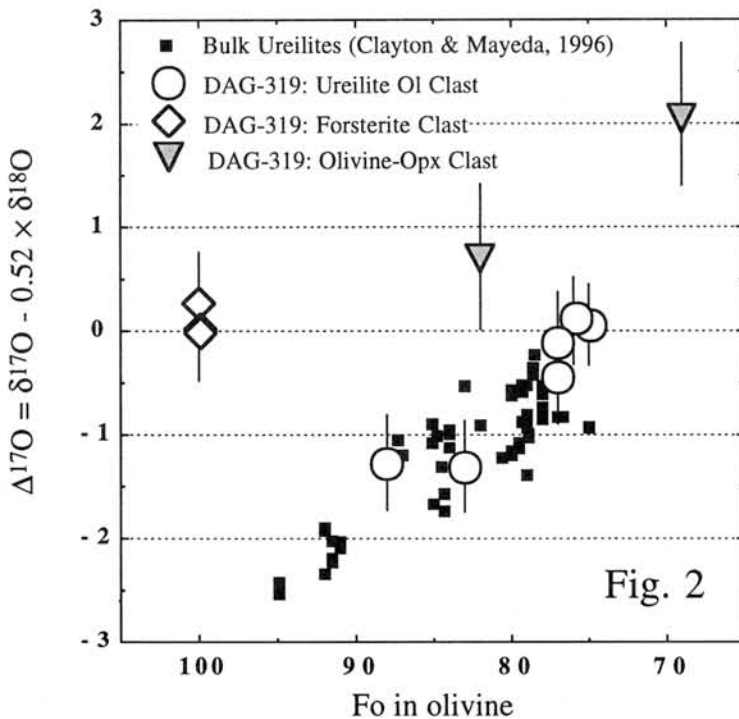


Fig.2. $\Delta^{17}\text{O}$ in DAG319 ureilite and other clasts. Filled squares indicate bulk ureilite data [8]

Evaporation experiments on naphthalene ($C_{10}H_8$) by thermogravimetry (TG)

Hitoshi KIUCHI, Shogo TACHIBANA* and Akira TSUCHIYAMA

Dept. Earth and Space Sci., Osaka Univ., 1-1 Machikaneyama, Toyonaka, Osaka 560-0043, JAPAN

*e-mail: tachi@ess.sci.osaka-u.ac.jp

Introduction:

Organic materials, which were brought from the space to the primitive Earth, might have played an important role on the generation of life on the Earth. Carbonaceous chondrites contain carbon mostly in the form of organic matter [e.g.,1-3]. Murchison (CM2), which fell in Australia in 1969, was the meteorite that contained significant amounts of extraterrestrial organic components including amino acids. Organic components in Murchison have been studied intensively, and given us a lot of information on the organic chemistry of meteorites.

Studier *et al.* [3] reported 24 polycyclic aromatic hydrocarbons (PAHs) in Murchison. Although some PAHs are highly volatile, they still remain in the meteorite. In the present study, in order to discuss the condition under which meteorites can keep volatile PAHs, we carried out evaporation experiments on naphthalene ($C_{10}H_8$), which was one of volatile PAHs, by using thermogravimetry (TG) at 1atm total pressure. We chose naphthalene because it was found in Murchison (320-400ppm, [3]) and safe to handle.

The advantage of a TG method is that we can monitor a weight change of a sample *in situ* during experiments. Hence, this method is useful for evaporation experiments, especially for highly volatile materials, such as naphthalene, which evaporate somewhat even at room temperature.

Experiments:

We established a TG system by using an electric balance and a drying oven (45 x 47.5 x 45cm³ in volume) (Fig.1). Naphthalene powder was pressed into a pellet (5mm in diameter and 2-4mm in height). The pellet was hung in a glass tube settled in the oven by a suspension wire which was hooked to the balance. The sample was heated at constant temperature ranging from 48 to 66°C for about 3hours (*c.f.*, the melting point of naphthalene is 80.2°C). Temperature was controlled by an electric controller equipped with the oven, and it was measured by a chromel-almel thermocouple adjacent to the pellet. The balance and the thermocouple were connected to PCs, respectively, and the weight of the sample and temperature were monitored every 60 seconds. Argon gas was flowed in some runs in order to take evaporated gas away from the glass tube. The flow rate of argon gas was controlled by a flow meter (200-280cm³/min). Some blank experiments (experiments with the suspension wire but without sample) were also done for the performance test of our "handmade" TG system.

Results:

The result of a blank experiment is shown in Fig.2. The weight change (M) of the suspension wire and temperature were plotted against time (t), respectively. Fig.2 shows that both M and temperature were unstable for about half an hour after an experiment started, while M was constant after temperature became stable. Temperature fluctuated at the beginning because we had to open the oven to set a pellet in it. The reason why M also fluctuated with temperature is probably that the change of temperature would cause

convection in the oven and affect the buoyancy on the wire. We use the data at stable temperatures in the further discussion.

Examples of experimental results are shown in Fig.3(a) and (b). It was found that the pellet lost its mass linearly with time. The pellets became harder after experiments due to sintering.

The evaporation rate of the sample was estimated from the slope of the M-t curve taking the change of the sample size due to evaporation into account. Fig.4 is the Arrhenius plot of the evaporation rates. The activation energy for evaporation is ~84kJ/mol without argon gas flow. The ideal Hertz-Knudsen evaporation rate of naphthalene, which is calculated from an equilibrium vapor pressure of naphthalene [4], is also plotted in Fig.4. The ideal evaporation rate is much larger than the experimental evaporation rates by the order of 4 or more.

The evaporation rate of naphthalene under argon gas flow is a few times larger than that without argon gas flow. This means that argon gas worked more or less effectively to remove evaporated gas from the sample although the evaporation rate with argon gas flow is still much smaller than the ideal evaporation rate.

Discussion:

The fact that the experimental evaporation rate of naphthalene is much smaller than the ideal one might indicate large kinetic constraints for the evaporation. However, there is another possibility. Since the experiments were done at 1atm total pressure, the backward reaction (recondensation) cannot be ignored. Moreover, the argon gas flow rate did not seem to be enough to remove evaporated gas although it worked more or less (Fig.4) (we could not use a high gas flow rate because it affected the stability of the valance). Hence, the small evaporation rate of naphthalene is probably the extrinsic one caused by experimental conditions.

However, this evaporation rate can be used to discuss the evaporation of naphthalene from a meteorite after falling. Highly volatile materials like naphthalene might evaporate from a meteorite during its terrestrial age. In this case, evaporation would take place at 1atm total pressure, and thus our experimental results can be applied. The lifetime of naphthalene grain at 1atm total pressure was calculated by using the experimental evaporation rate (Fig.5). In the experimental temperature range, the lifetime is less than an hour. Provided that our results can be extrapolated to lower temperatures, even the lifetime of 100 μ m-sized grain is about a day at room temperature. This implies that naphthalene in fallen meteorites might have evaporated completely soon after meteorites fell if it was trapped loosely in meteorites. Hence, volatile PAHs including naphthalene, which has been found in meteorites so far, should have been trapped firmly inside them. It is important to investigate where and how organic matter is trapped in meteorites.

References:

[1] Cronin J.R. et al. (1988) In *Meteorites and the Early Solar System*, eds. Kerridge J.F. and Matthews M.S., 819-857. [2] Shimoyama A. (1987) In *Science in Antarctica vol.6 Antarctic Meteorites*, 246-275. [3] Studier M.H. et al. (1972) *GCA*, **36**, 189-215. [4] e.g., A.P.I Research Project 44 (1953-1969), *Selected Values of Properties of Hydrocarbons and Related Compounds*.

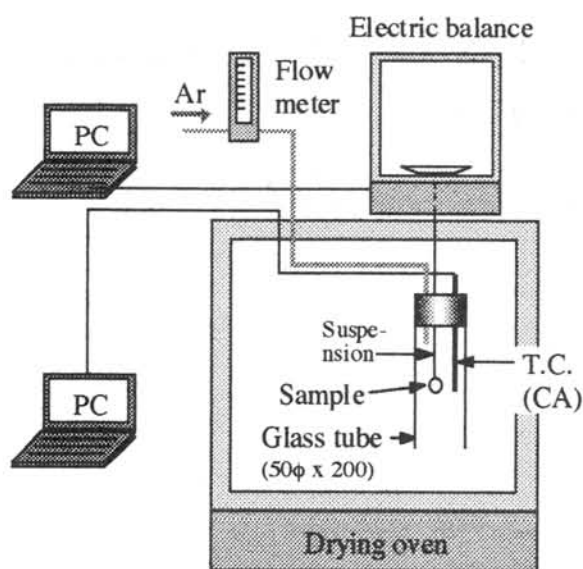


Fig.1 A schematic drawing of a TG system.

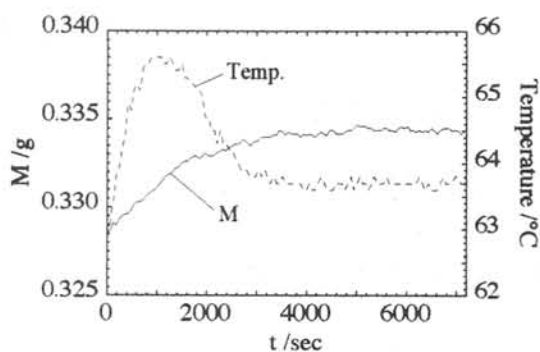


Fig.2 The weight of the suspension wire and temperature vs. time (a blank experiment).

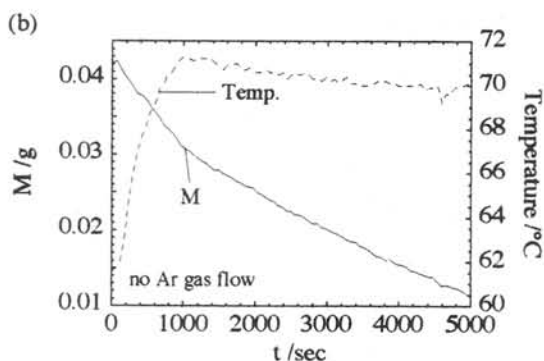
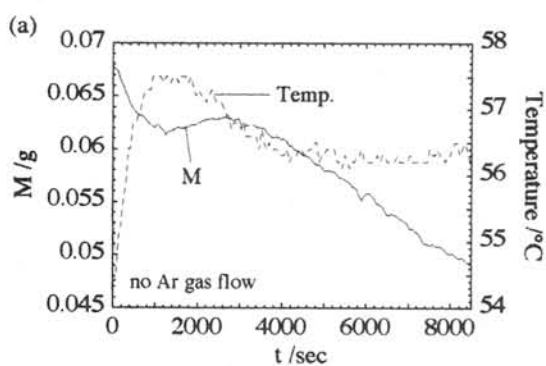


Fig.3 The weight of the sample and temperature vs. time. (a) $T \sim 56^\circ\text{C}$ and (b) $T \sim 70^\circ\text{C}$.

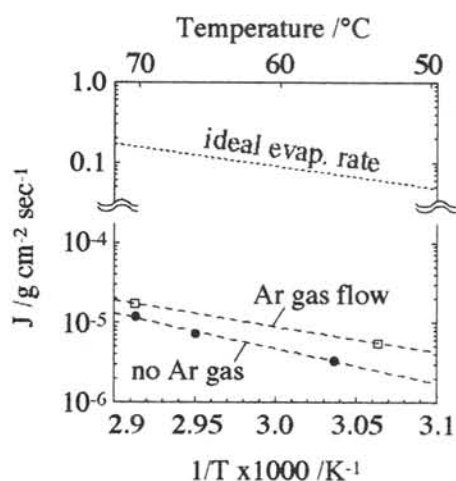


Fig.4 An Arrhenius plot of evaporation rates. The ideal evaporation rate is also plotted.

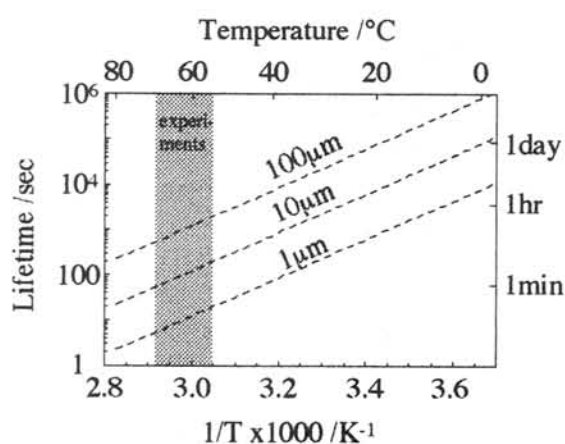


Fig.5 Lifetime of naphthalene grain estimated by the experimental evaporation rate. The experimental temperature range is shaded.

The distribution of oxygen isotopes and cations in Allende matrix

Hidekazu Kobatake¹⁾, Hisao Satoh^{1,2)}, Katsuo Tsukamoto¹⁾ and Hirokazu Fujimaki¹⁾

1) Institute of Mineralogy, Petrology, and Economic Geology, Tohoku University, Aoba, Sendai 980-0845, Japan

2) Geological Survey of Japan, Higashi, Tsukuba 305-8567, Japan

1. Introduction

Stable oxygen isotope studies on Allende CV3 chondrite provide us useful information on physicochemical process in the early solar nebula [1,2,3]. Large oxygen-16 anomalies have already been found in some inclusions: CAIs (Ca-Al rich inclusions; $\delta^{18}\text{O} = -40\text{-few}\%$, $\delta^{17}\text{O} = -42\text{-few}\%$), chondrules ($\delta^{18}\text{O} = -1.99\text{-}2.21\%$, $\delta^{17}\text{O} = -6.37\text{-} -1.64\%$) [4], and AOAs (amoeboid olivine aggregates; $\delta^{18}\text{O} = -13.9\text{and-}7.3\%$, $\delta^{17}\text{O} = -11.2\text{and-}17.0\%$) [5]. These data were mostly obtained by conventional fluorination or by ion microprobe analyses. However, the oxygen isotope value of matrix other than inclusions in Allende meteorite has not been well studied, because of its large heterogeneity and with fine texture. Recently developed laser-fluorination microprobe (LFM) method is best applicable for this kind of studies in sub-millimeter scale [7][8]. The matrix of Allende may preserve the oxygen isotopic signatures from the interaction with inclusions after accumulation at parental asteroid rather than primitive history in the solar nebula. We employed the LFM and the electron microprobe analyses both on Allende inclusions and matrix to visualize 2-dimensional distribution of $\delta^{18}\text{O}$ and Fe.

2. Analytical Procedures and Sample description

As preparation for the analyses, a clast of Allende meteorite (1.0 × 1.2 cm) was cut into thick and thin sections. Inclusions (AOA and chondrules) and matrix in the thick section were broken to microchips (0.3-1.5mg), each of which were individually fluorinated and measured with a MAT-252 mass spectrometer. Prior to the LFM analysis, we had to confirm the analytical potential of LFM in forsterite, which is representative phase in Allende. A number of replicate tests on a working standard of forsterite (TUSF-1: CZ-synthesized crystal) and gave acceptable results of $\delta^{18}\text{O} = 10.69 \pm 0.06\%$. (n=30)

In the thin section sharing the same cut face to the thick section, the texture and the chemical composition were optically observed and analyzed with a JXA-8800 electron microprobe, respectively. Our Allende clast contained many chondrules with a barred olivine (BO), porphyritic olivine (PO) and pyroxene (PP) and several AOA with irregular form. As accessory phases, purple-colored spinels and reddish sodalites could be detected by polarization

microscopy.

3. Results and discussion

The $\delta^{18}\text{O}$ data of analyzed Allende microchip were as follows: AOA: -10.54-3.19‰ (n = 23); BO: 0.53-4.28‰ (n = 4); PO: -0.88-5.86‰ (n = 11); PP: -1.58-2.01‰ (n = 5); matrix: -0.5-6.90‰ (n = 51). Considerable $\delta^{18}\text{O}$ heterogeneity was observed in AOAs, which is enclosed at the center of relatively massive matrix. Their oxygen isotope data show a significantly wide variation in the matrix (~6.85‰) as well as in chondrules (~7.43‰) (Fig. 1). The 2-D distribution of the $\delta^{18}\text{O}$ values in Allende matrix is shown in Fig. 2. Low $\delta^{18}\text{O}$ (0-4‰) values distribute around AOAs in the matrix and high $\delta^{18}\text{O}$ matrix (4-6‰) value distribute far from the low $\delta^{18}\text{O}$ AOAs, indicating that the oxygen isotopic exchange reaction between the matrix and the inclusions after the aggregation was completed.

The low- $\delta^{18}\text{O}$ matrix surrounding these AOAs was found to be enriched in secondary minerals such as nephelines and also sodalites. The elemental mapping of Fe shows that the Fe content of matrix was extensively depleted near these AOAs. Besides, the grain size in the low- $\delta^{18}\text{O}$ matrix was a little larger than those in the other high- $\delta^{18}\text{O}$ matrix. It was reported that AOAs typically consist of dominant fine olivine crystals (~10 μm) with high Fo-content (Fo₉₈), but that nepheline (NaAlSi₃O₈), spinel (MgAl₂O₄), sodalite (Na₄Al₃Si₃O₁₂Cl), and diopside (CaMgSi₂O₆) appear as minor phases [6] Sodalites appear in a strongly altered PP chondrules. The oxygen isotope value of this altered chondrule was $\delta^{18}\text{O}$ =1-2‰, which is similar to those of the low- $\delta^{18}\text{O}$ matrix. The Na-phase bearing matrix clearly shows low $\delta^{18}\text{O}$ values.

It is interesting to note that the distribution of the $\delta^{18}\text{O}$ value by LFM can be correlated to the distribution of elements by chemical mapping. The positive correlation between the $\delta^{18}\text{O}$ value and Fe content in the matrix is clear as can be seen in Fig. 2. The low $\delta^{18}\text{O}$ value matrix distribute around the AOAs, which have the lowest $\delta^{18}\text{O}$ value in this study where Fe is considerably depleted. The matrix enriched in oxygen-18 contains less nepheline. We concluded here two importance from these observations that (1) the Fe depletion in the matrix suggest that the enhancement of cationic exchange occurred in olivine solid solution; (2) the Na-enrichment may be accompanied with the alteration product of Na-minerals. This fact may suggest that the inclusions with low $\delta^{18}\text{O}$ may have chemically and isotopically affected the surrounding matrix to deplete in oxygen-18 and Fe, and to form Na-minerals during or after the formation of parent asteroid.

References:

[1] Clayton et al. (1973) *Science*, 182, 485-488. [2] Yurimoto et al. (1998) *Science*, 282, 1874-1877. [3] Hiyagon and Hashimoto (1999) *Science*, 238, 828-831. [4] Alan. E Rubin et al. (1990) *Earth Planet. Sci.*, 96, 247-255 [5] Clayton et al. (1977) *Earth Planet. Sci. Lett.*, 34, 209-224 [6] Brearley and Jones *Reviews in Mineralogy* 36, 3-38-191. [7] Young et al. (1998) *Science*, 282 452-455 [8] Satoh and Ohmoto, in prep. We acknowledge H. Ohmoto of the Pennsylvania University Astrobiology Research Center for the supply of meteorite specimens.

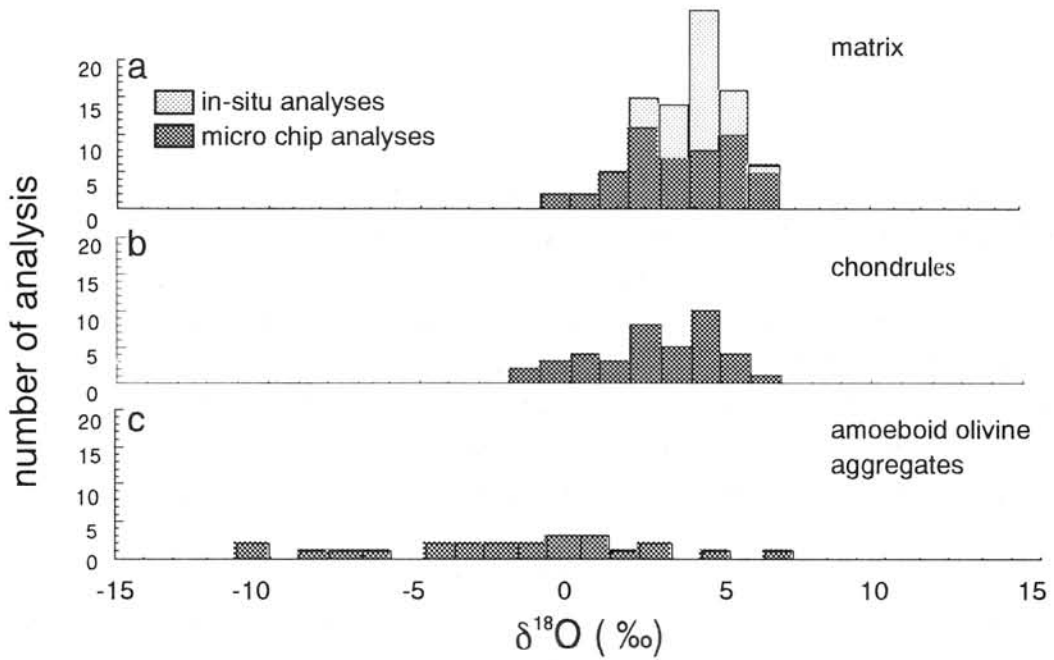


Fig.1 Histogram of $\delta^{18}\text{O}$ values showing the variations in Allende.(a) matrix, (b) chondrules, and (c) amoeboid olivine aggregates (AOA).

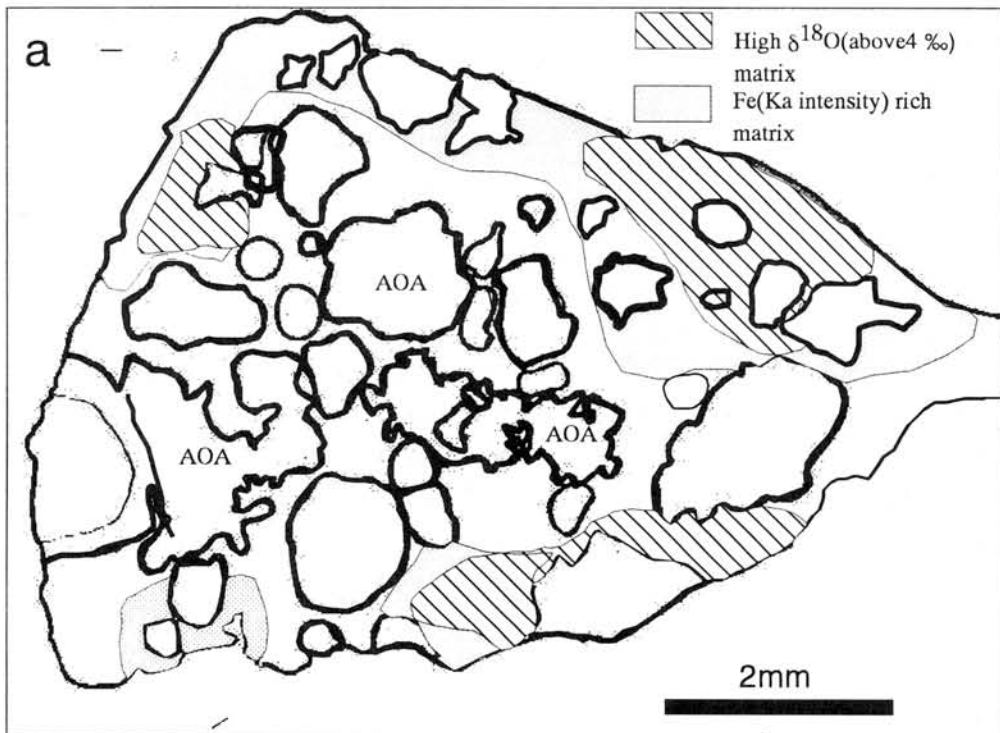


Fig.2 The high $\delta^{18}\text{O}$ and Fe (K_{α} intensity) distribution in Allende matrix. The matrix near AOAs appears to be depleted in oxygen-18.

Meteorite search of JARE in 1998 - 99 season

Kojima H.¹, Kaiden H.² and Yada T.³

1. National Institute of Polar Research, Kaga, Itabashi-ku, Tokyo 173-8515
2. Tokyo Univ., Hongo, Bunkyo-ku, Tokyo 113-0033
3. Dept. Earth & Planet. Sci., Kyushu Univ., Fukuoka 812-8581

Meteorite search party composed of eight men of the 39th Japanese Antarctic Research Expedition (JARE) collected about 4100 meteorites on bare ice areas around the Yamato and Bergica Mountains in 1998 - 99 season.

6000 meteorites have been already collected by 13 times of the expeditions on bare ice fields around the Yamato Mountains. However, we expected to collect additional many meteorites by following two reasons. The gross of bare ice areas around the Yamato Mountains are estimated about 4000 km². Half of the area has been already done meteorite search. However, the other half of the area is still remaining for meteorite search. Meteorite search around the Yamato Mountains has not done for the last twelve years. And more than one meter of ice sheet are estimated to be abraded for the period. Some meteorites are expected to appear from the abraded ice sheet. We have planned to search meteorite both searched and non searched areas.

The party has left Syowa Station with 4 large snow vehicles on 16th of October, 1998 and has reached the Yamato Mountains on 2nd of November after 600km traveling. We have used 3 large snow vehicles and 4 snowmobiles for meteorite search. Collection positions of the all meteorites were recorded by a global positioning system (GPS). The records indicate two concentration regions of meteorites. One is around south Yamato Nunataks and the other is west of JARE IV Nunataks. Approximately 2000 meteorites have been collected at the former region. Approximately 1000 meteorites have been collected at the latter region. Over 4100 meteorites have been collected around the Yamato Mountains. They include many kinds of rare meteorites such as lunar, carbonaceous, diogenite and eucrite. Only three iron are included in the great number of the meteorites..

We also searched meteorites around the Bergica Mountains. 21 Meteorites have been collected. All of them are chondrites.

A DARK INCLUSION IN THE MANYCH LL (3.1) ORDINARY CHONDRITE: A PRODUCT OF STRONG SHOCK METAMORPHISM OF UNEQUILIBRATED CHONDRITIC MATERIAL

Tomoko Kojima, Tomomi Yatagai and Kazushige Tomeoka

Department of Earth and Planetary Sciences, Faculty of Science, Kobe University,
Nada, Kobe 657-8501

Introduction

Dark inclusions (DIs) composed largely of fine-grained Fe-rich olivine commonly occur in CV3 chondrites [e. g., 1, 2]. Recent workers suggested that most DIs are not aggregates of primitive nebular condensates as previously interpreted, but that they are products of aqueous alteration and subsequent thermal metamorphism on the meteorite parent body [e. g., 3-6]. Therefore, DIs may provide important clues to the secondary processes that occurred on the meteorite parent body. Although DIs have been mainly reported from CV3 chondrites, it has been known that some ordinary chondrites contain inclusions that may be related to DIs in CV3 chondrites [7, 8]. We here present the results of detailed mineralogical and petrographic study of a DI in the Manych LL (3.1) chondrite. The DI, hereafter termed MNC-1, has been briefly studied by Zolensky et al. [8]. Our results suggest that MNC-1 has experienced shock-induced igneous processes, thus has an origin quite different from that of DIs in CV3 chondrites.

Results

The Manych LL chondrite consists of densely packed chondrules and opaque nodules embedded in a matrix. Chondrules and opaque nodules are apparently flattened roughly in the same direction, suggesting that Manych experienced shock metamorphism. This is supported by the common presence of undulatory extinction, mosaicism and parallel sets of planar fractures in relatively coarse olivine grains. Matrix is highly compacted. Another remarkable shock indicator is the abundant occurrence of melt pockets and veins along chondrule-matrix and opaque nodule-matrix boundaries; the melt contains numerous opaque globules and subrounded silicate fragments in a glassy groundmass, and is generally rich in Na, Al and Si (6-10 wt.% Na₂O, 16-20 wt.% Al₂O₃, 65-70 wt.% SiO₂). Based on the classification of Stöffler et al. [9], the shock stage of Manych is estimated to be S3 or S4.

MNC-1 is approximately 1.7 x 3.5 mm in size but might have been originally larger because it was artificially cut at one end. In transmitted light, it is distinctly darker than the host and contains many brownish translucent to transparent elliptical objects (50-500 μm in long axis) embedded in almost opaque matrix. The elliptical objects probably correspond to the "augen" described by Zolensky et al. [8]. Relatively small augen (5-100 μm in long dimension) are generally angular in shape and appear to be fragments of larger ones.

The augen consist basically of three minerals, olivine (Fo₆₂₋₈₃), Ca-pyroxene

(En₅₂₋₆₀ Wo₁₇₋₃₂) and Na-rich feldspathic glass (7-11 wt.% Na₂O), and their volume proportions and textures differ considerably between augen. Most of them consist largely of parallel intergrowths of fine laths (<1 μm in width, <1-10 μm in length) of olivine, pyroxene and glass. The augen commonly contain relatively coarse olivine grains (5-80 μm in diameter), some with Fe-Mg zoning (Fo₇₆₋₈₃ in cores to Fo₆₂₋₆₃ in rims). The olivine grains show shock features, i. e. undulatory extinction, mosaicism and parallel sets of planar fractures, indicating that MNC-1 was also affected by shock. Some augen are aggregates of such coarse olivine grains and exhibit an appearance similar to porphyritic olivine chondrules.

Matrix of MNC-1 consists predominantly of interlocking granular grains (<1-10 μm in diameter) of Fe-rich olivine coexisting with anhedral Ca-pyroxene; the olivine and pyroxene are compositionally identical to those in the augen. Na-rich feldspathic glass also occurs in minor amounts in interstices between the olivine grains. Fe-Ni metal grains of various sizes (<1-80 μm in diameter) are abundantly dispersed throughout the matrix; they appear to have melted and intruded into interstices between olivine grains, and occasionally form tiny globules similar to those in the melts in the host. Troilite is extremely rare in matrix of MNC-1, while it commonly coexists with Fe-Ni metal in the host.

A bulk major element composition of MNC-1 was determined using a defocused electron beam technique. MNC-1 contains as much as 27.1 wt.% FeO, which is much higher than the reported FeO content of the Manych host (14.6 wt.% [10]); when recalculated to atomic Fe, the value (21.0 wt.%) is close to the total Fe content of Manych (20.8 wt.%, [10]). Another notable compositional feature is a large depletion in S (<0.1 wt.%). Contents of other major elements are generally within the range for most LL chondrites.

Discussion

From our results, it is evident that MNC-1 is distinct from most DIs in CV3 chondrites [e. g., 5, 6]. The texture and mineralogy of matrix of MNC-1, i. e., interlocking granular olivine with interstitial Ca-pyroxene and Na-rich feldspathic glass, suggest that MNC-1 experienced an igneous process. Because the Manych host shows abundant evidence indicating strong shock metamorphism, it is plausible that the igneous process occurred during a shock process. MNC-1 is closely similar in texture and composition to an igneous-textured inclusion from the Julesberg L3 chondrite that was recently described by Ruzicka et al. [11]; the inclusion is composed of angular-to-rounded clasts set in a fine-grained groundmass rich in olivine and feldspathic glass, and is interpreted to have been formed as a clast-laden shock melt.

Shock-induced heat in porous petrologic type 3 chondrites is expected to be larger than that in less porous chondrites of higher petrologic types. Thus, petrologic type 3 chondrites would generate melts at lower shock pressures than chondrites of higher petrologic types [9]. In fact, considerably large volumes of shock-induced melt have been reported from chondrites of relatively low petrologic types (type 3-4) [11, 12]. Therefore, it is probable that shock metamorphism of stage S3 or S4 could

produce melt veins as large as MNC-1 in Manych. The augen in MNC-1 may be partly melted and ablated clasts like those in the inclusion in Julesberg [11]; some of them may be broken porphyritic chondrules. The large depletion of S in MNC-1 appears to be consistent with that MNC-1 experienced high temperature. We also note that MNC-1 is similar in appearance to some pseudotachylites, i. e. veins of fine grains of crystalline to glassy materials that commonly occur in terrestrial fault rocks [e. g., 13, 14] as well as impact craters [15], which are generally regarded to result from comminution and frictional melting of materials in shear zones.

From the bulk major element composition, MNC-1 appears to have originated from LL chondritic material but have been affected by considerable oxidization. The augen in MNC-1 exhibit a texture composed of parallel intergrowth of fine laths that is not observed in the host Manych meteorite. The augen may have experienced some alteration processes which did not affect the host; oxidization of MNC-1 may be related to the processes. However, we cannot exclude the possibility that MNC-1 is a xenolith which solidified elsewhere and was later incorporated to the host meteorite. The present study suggests that MNC-1 represents a chondritic material that experienced a complex sequence of alteration and metamorphism probably on the meteorite parent body, including strong shock and consequent melting.

Acknowledgments

We thank Dr. M. E. Zolensky for providing the Manych sample, and Dr. A. Lin for valuable discussion and information.

References

- [1] Fruland R. M., King E. A. and McKay D. S. (1978) Proc. Lunar Planet. Sci. Conf. 9th, 1305-1329. [2] Johnson C. A., Prinz M., Weisberg M. K., Clayton R. N. and Mayeda T. K. (1990) GCA 54, 819-830. [3] Kojima T., Tomeoka K. and Takeda H. (1993) Meteoritics 28, 649-658. [4] Kojima T. and Tomeoka K. (1996) GCA 60, 2651-2666. [5] Buchanan P. C., Zolensky M. E. and Reid A. M. (1997) GCA 61, 1733-1743. [6] Krot A., Scott E. R. D. and Zolensky M. E. (1997) MAPS 32, 31-49. [7] Fodor R. V. and Keil K. (1975) GCA 40, 177-189. [8] Zolensky M. E., Weisberg M. K., Barret R. A. and Prinz M. (1993) LPSC XXIV, 1583-1584. [9] Stöffler D., Keil K. and Scott E. R. D. (1991) GCA 55, 3845-3867. [10] Jarosewich E. (1990) Meteoritics 25, 323-337. [11] Ruzicka A. Snyder G. A. and Taylor L. A. (1998) GCA 62, 1419-1442. [12] Yamaguchi A., Scott E. R. D. and Keil K. (1999) MAPS 34, 49-59. [13] Magloughlin J. F. (1992) Tectonophysics 204, 243-260. [14] Lin A. (1996) Engineering Geology 43, 213-224. [15] Stöffler D., Bischoff A. Oskierski W. and Wiest B. (1988) In Deep Drilling in Crystalline Bedrock, 277-297.

Behavior of minor elements in olivine and orthopyroxene during metamorphism in LL chondrites

M. Komatsu and M. Miyamoto

Mineralogical Institute, Graduate School of Science, University of Tokyo.

mutsumi@min.s.u-tokyo.ac.jp, miyamoto@min.s.u-tokyo.ac.jp

INTRODUCTION

It is well known that in ordinary chondrite, the abundances of siderophile elements decrease and the degree of oxidation increases in going from H to L to LL chondrites. [1] The proportion of oxidized Fe increases at the expense of metallic Fe. Because Fe is more readily oxidized than Ni or Co, bulk metal becomes increasingly rich in Ni and Co. Moreover, it has been proposed by several authors[2-6] that subtle but systematic changes in the compositions and relative abundances of olivine, pyroxene, and metal with increasing metamorphic grade in equilibrated ordinary chondrites. However relatively little attention has been devoted to the relationship between minor elements and metamorphic grade. In this study we have examined the behavior of minor elements in LL chondrites during the progressive oxidation.

ANALYTICAL METHODS

Thin sections of 46 Antarctic LL chondrites were examined and classified. Petrologic types were assigned according to the petrographic criteria of Van Schumus and Wood[7]. Mineral compositions were measured using the Cameca SX 100 electron microprobe at the Johnson Space Center and the JEOL Superprobe 733 electron microprobe at Geological Institute, University of Tokyo. All mineral composition were made under identical operating conditions.

RESULTS AND DISCUSSION

The systematic increase of FeO content of olivine and orthopyroxene reflects progressive oxidation during metamorphism. The behavior of minor elements vs. FeO content of olivine and pyroxene in LL chondrites are shown in Fig. 1 and Fig. 2.

Fig. 1 summarizes the average contents of minor elements in olivine for each petrologic type of LL chondrites. Each content is too small to be statically meaningful but is included for completeness. We could not find obvious tendency in Al_2O_3 , Cr_2O_3 and MnO in olivine with increasing metamorphic grade, because of their small quantity. Even so we can see the tendency that TiO_2 decreases with increasing metamorphic grade. MnO content is slightly larger than other elements. MnO decreases from type 4 to type 5, then increases type 5 to type 7.

Fig. 2 summarizes the average contents of minor elements in orthopyroxene. We can see

the tendency that Al_2O_3 and Cr_2O_3 decreases with increasing metamorphic degree. TiO_2 increase with increasing metamorphic degree. This tendency is likely to reflect that Ti are easy to be taken into orthopyroxene. MnO decreases from type 4 to type 5, then increases type 5 to type 7. It should be noted that the MnO content in both olivine and orthopyroxene increases from type 5 to type 7.

Taking the normal oxidation process into consideration, the Mn content in olivine and orthopyroxene is likely to decrease with progressive oxidation. The content of minor elements is too small to be meaningful, however, our results are not consistent with the expected idea. Otherwise, if the increase of the MnO content in olivine is caused by only oxidation of orthopyroxene during metamorphism, the results that MnO contents in both olivine and pyroxene increase with metamorphic grade are hard to explain. Because Kellemeyn et al. [8] indicated that there are no significant differences in bulk abundance among petrologic types, the increase of the Mn content implies that some reactions took place during metamorphism. On the assumption that the small amount of Mn came from minerals, the probable explanation is the presence of Mn-containing minerals around silicates. One of possible minerals could be ZnS, but we could not find any ZnS grains nor Mn-containing minerals. In any reactions which provided Mn to silicates, oxygen fugacity must have played an important role in the distribution of Mn. From these points we might go on to an even more examination of the distribution of Mn and behavior of olivine/pyroxene abundance during metamorphism.

L CHONDRITES

We also have attempted to investigate whether these relationships can be applied to L chondrites. Some 10 Antarctic L4-L6 chondrites are studied to date. Significant variations of mineral composition accompanied by metamorphism has not been found at present. It may be partly because the range of mineral composition within each group is smaller than LL chondrites. Further investigation will have to be done.

REFERENCES

- Prior G. T. (1916) *Mineral. Mag.* 17, 33-38. [2] Frederiksson K., Nelen J and Frederiksson B.J (L.H Ahrens, ed.) pp.457-466. [3] Heyse J.V. (1978) *Eath Planet. Sci. Lett* 40, 365-381. [4] Mcsween H.Y. and Patchen A.D. (1989) *Meteoritics* 24, 219-226 [5] Mcsween J.Y and Labotka T.C. (1993) *Geochim. Cosmochim. Acta* 57, 1105 -1114. [6] Komatsu M. and Reid A.M. (1998) *Lunar and Planet. Sci.* XXIX. [7] Van Schumus W.R. and Wood J.A. (1967) *Geochim.Cosmochim. Acta* 31,747-765. [8] Kallemeyn G.W., Rubin. A.M., Wang D., and Wasson J.T. (1989) *Geochim.Cosmochim. Acta* 53, 2747-2767.

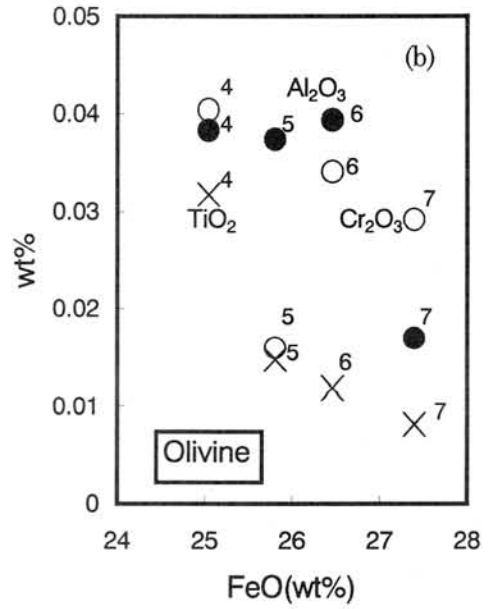
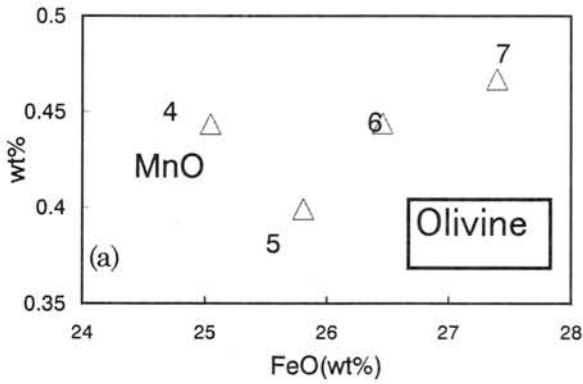


Fig.1 (a) Average MnO content and (b) average Al₂O₃, TiO₂, Cr₂O₃ and TiO₂ contents in olivine for each group of LL chondrites. Δ : MnO, \bullet : Al₂O₃, \circ : Cr₂O₃, \times : TiO₂. Average fayalite contents increase progressively with petrologic type (metamorphic grade).

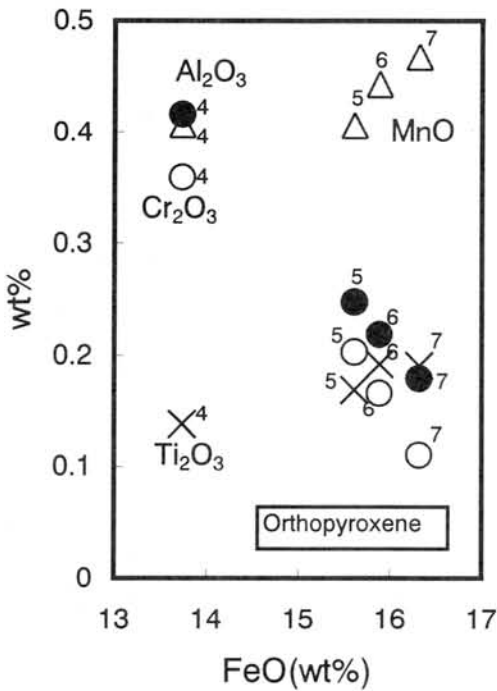


Fig. 2 Average MnO, Al₂O₃, TiO₂, Cr₂O₃ and TiO₂ contents in orthopyroxene for each group of LL chondrites. Δ : MnO, \bullet : Al₂O₃, \circ : Cr₂O₃, \times : TiO₂. Average ferrosilite contents increase progressively with petrologic type (metamorphic grade).

TRACE ELEMENT STUDIES OF LEACHATES AND RESIDUES FROM THE LHERZOLITIC SHERGOTTITE Y-793605

Gabor Kondorosi¹, Yusuke Hirota², Kuniko Hori¹, Noboru Nakamura^{1,2},
Noritoshi Morikawa² and Keiji Misawa³

¹Graduate School of Science and Technology, Kobe University; ²Department
of Earth & Planetary Sciences, Faculty of Science, Kobe University;

³Department of Antarctic Meteorites, National Institute of Polar Research

Y-793605 is a lherzolitic shergottite which has close petrological, chemical and age characteristics to other lherzolitic shergottites (typically ALHA 77005). As part of the consortium study organized by the NIPR [1], we have undertaken U-Th-Pb, Rb-Sr and Sm-Nd isotopic and trace element analyses. Parts of our results have been reported at previous symposiums [2,3]. During our U-Th-Pb study, we found that significant amounts (up to 85 to 95%) of U and Th in mineral separates and the whole rock were leachable in 0.01M HBr, 0.1M HBr and 1M HNO₃. It was found that in an ⁸⁷Rb-⁸⁷Sr evolution diagram, data points of residues show a linear trend which corresponds to an age of 170 ± 13 Ma and an initial ⁸⁷Sr/⁸⁶Sr of 0.71042 ± 0.00007 , while all the 1st leachate data points deviate to the left side of the 180 Ma isochron (indicating a "pseudo" isochron; a mixing line?), and data points of 2nd and 3rd leachates are scattered around the 180 Ma isochron. The leachates have low ²³²Th/²³⁸U and ⁸⁷Rb/⁸⁶Sr ratios which are systematically different from those of the residues. In order to examine acid-leached components and to search their chemical and chronological significance, we have carried out isotope dilution analysis of REE for leachates and residues from the Y-793605 meteorite.

Results for whole rock residue and a leachate are shown in Fig. 1, along with that of bulk whole rock sample. It should be noted that, compared to the bulk sample, the residue indicates more than several times lower absolute abundances and is more depleted in L-REE but has a similarly flat H-REE pattern. A minor positive Eu anomaly is recognizable in the residue. The Sm and Nd abundances (calculated relative to the original weight) are even higher than those of residue, indicating selective leaching of lighter REEs in this fraction. Mass balance considerations suggest that the 2nd and 3rd leachates contain components which are more L-REE enriched and have

higher abundances, relative to the 1st leachates. A role of melt components (impact melts or metasomatic fluids ?) seems to be important for understanding such trace element features.

References:[1]Kojima et al. (1997) Antarctic Meteorite Research 10, 3-10;
 [2]Misawa et al. (1997) Antarctic Meteorite Research 10, 95-108;
 [3]Morikawa et al. (1998) Antarctic Meteorites XXIII 91-92;

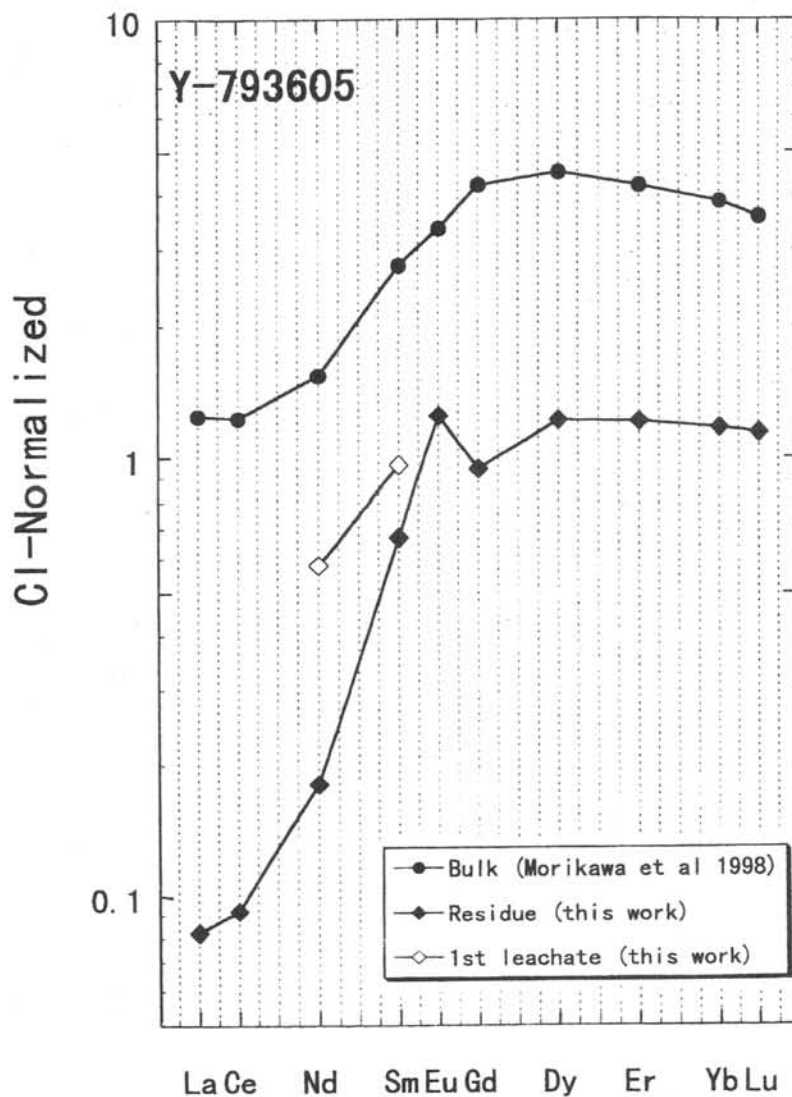


Fig.1 REE patterns for the bulk sample, an acid residue and the 1st leachate from whole rock sample of the lherzolitic Shergottite Y-793605

LUNAR AND MARTIAN METEORITES: SUITES, PAIRING, AND IMPLICATIONS. Marilyn M. Lindstrom, SN2, NASA, Johnson Space Center, Houston TX 77058, USA.

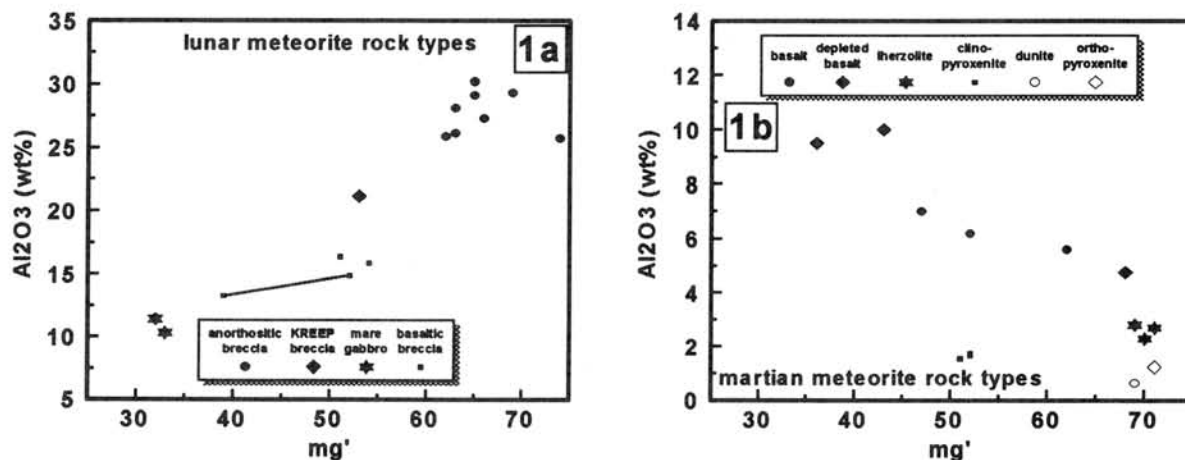
Introduction. The systematic collection of tens of thousands of meteorites from Antarctica and thousands of meteorites from hot deserts has allowed us to recognize meteorites from the Moon and Mars and has contributed most of their known samples. Lunar and martian meteorites are very rare, making up only about 1/1000 of the nearly 20,000 classified Antarctic meteorites. Of the 13 (18 numbered samples) lunar meteorites, 10 (15) are from Antarctica and the remaining 3 are from hot deserts. Of the 13 (14) martian meteorites, 6 are from Antarctica, 1 (2) are from hot deserts, and 6 are from other locations (4 of them being observed falls). Paired meteorites are common, particularly among the lunar meteorites.

Here I summarize the two suites of samples in terms of petrology, geochemistry, and exposure history, and evaluate relationships among samples, particularly with respect to launch pairing. I then consider their significance in interpreting the natures and evolutions of the crusts of the Moon and Mars. More emphasis is put on lunar meteorites because of the extensive database on Apollo and Luna samples with which to compare the meteorites and the global mineralogical and geochemical mapping provided by the Clementine and Prospector missions. This context is nearly absent for martian meteorites which provide the only detailed geochemical information on Mars. [1-4] Viking and Pathfinder robotic soil and rock analyses are much less precise than any sample analyses (see below).

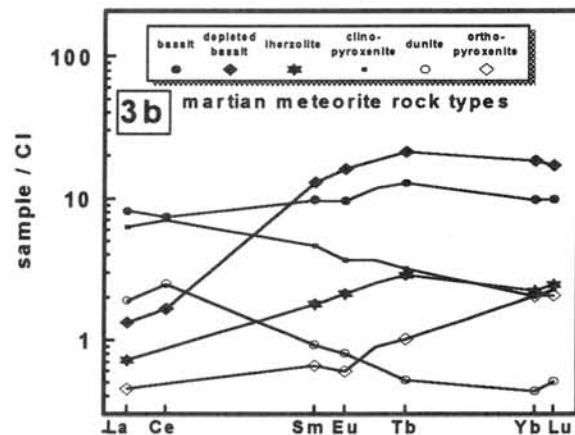
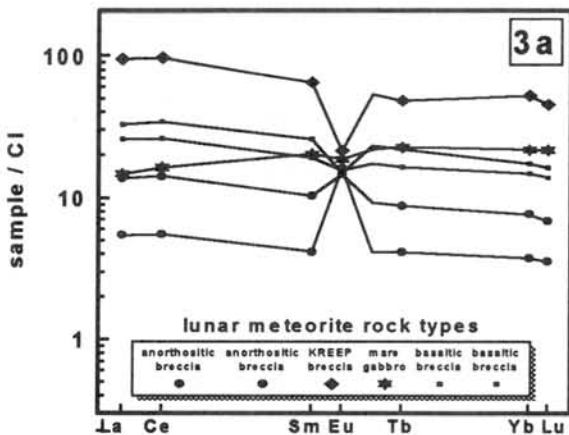
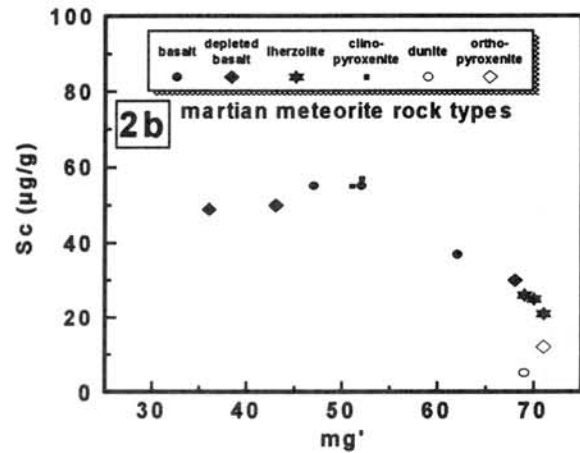
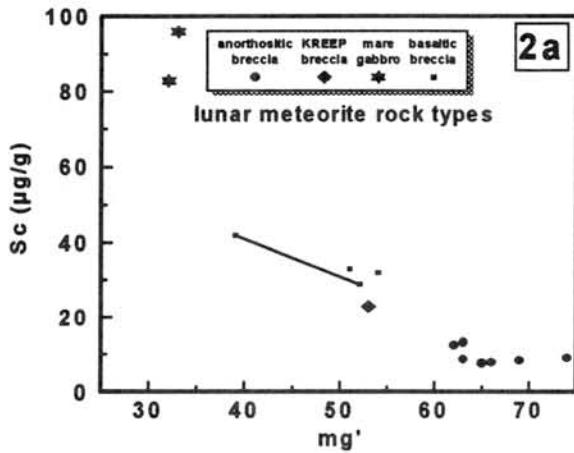
Lunar Meteorites. The 18 individual samples of lunar meteorites represent 13 distinct meteorite falls, based on similarities in find location, petrology, geochemistry, and exposure history. The identical samples are called paired meteorites. The lunar meteorites are generally classified as anorthositic or basaltic. All of the 7 (10) anorthositic lunar meteorites are breccias rich in feldspathic components ranging from igneous cumulates to granulitic breccias and impact melts. The basaltic meteorites include 2 mare basaltic gabbros (Y-793169, A-881757) and 3 (4) breccias dominated by mare basalt components. One sample, Calalong Creek, is a lunar highland breccia with a KREEP-rich composition [5].

Variations within the anorthositic and basaltic groups are relatively small. Although the breccias in each group range from fragmental through mature regolith samples, they often contain similar clast assemblages in slightly different proportions. Variations in clast populations between anorthositic and basaltic breccias show only minimal overlap. However, some anorthositic breccias contain rare basaltic clasts and some basaltic breccias contain feldspathic clasts.

Ranges of bulk compositions within anorthositic and basaltic groups are also relatively small, while the range of compositional variation of the entire lunar meteorite suite is quite large (Fig 1a, 2a, 3a). Anorthositic breccias cluster at the high Al₂O₃ and mg' (molar Mg/(Mg+Fe) x 100), low Sc and REE end of the range, while basaltic meteorites scatter widely at lower Al₂O₃ and mg', and higher Sc and REE. The basaltic gabbros are distinct from the basaltic breccias and represent a different type of basaltic rock [6]. Among the basaltic breccias, a single sample (EET87521) shows much of the total variation (see tie-lines in Figs 2a, 3a), having a range in mg' and Sc suggestive of magmatic differentiation [7]. KREEP-breccia Calalong Creek has the highest REE, but otherwise intermediate composition. Calalong Creek may represent the mixing of an anorthositic highland component with mare basalt, with the addition of 20% KREEP component.



Ejection ages of the lunar meteorites, based on studies of exposure histories [8], are shown versus Al₂O₃ in Fig 4a. The ages for most lunar meteorites are quite young, well under 1 Ma, but the Y82/86 trio is distinctly older (8 Ma). The similar ages, petrology, and composition of the two mare gabbros confirm launch pairing for the two meteorites. Calalong Creek is distinct in all parameters. The remaining meteorites have three different ejection ages, at 0.3, 0.16, and 0.05 Ma. The older two ages belong to anorthositic breccias which are either paired or launch-paired. The youngest age group is extremely diverse, including 2 anorthositic breccias having a very wide range in mg' and all 4 basaltic breccias. This launch pairing is debatable, but I tend to favor it (see below). Together the 18 individual lunar meteorites represent 13 paired meteorites and 6-7 distinct ejection events from the Moon.



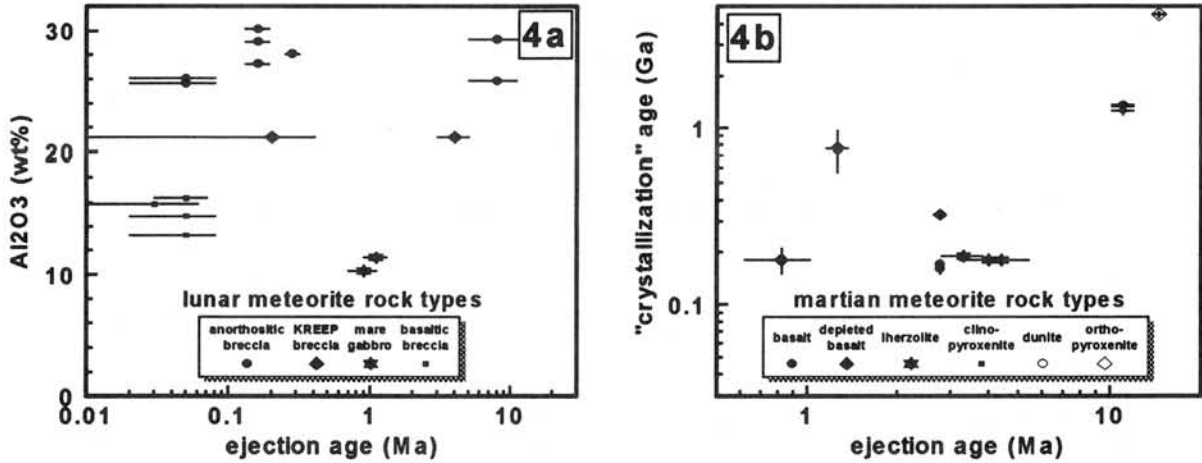
Martian Meteorites. The 14 martian meteorites include few paired samples. Only the Dar al Gani samples appear to be paired meteorites, reducing the number of distinct martian meteorites from 14 to 13. All of the martian meteorites are igneous rocks; basalts or ultramafic cumulates. They include 5 distinct petrologic rock types which are 6 distinct geochemical rock types: 2 basalts, 3 (4) depleted basalts, 3 lherzolites (all shergottites); 3 clinopyroxenites (nakhilites); 1 dunite (Chassigny); and 1 orthopyroxenite (ALH84001). A relationship exists among the basalts and lherzolites in the shergottite clan. EETA79001 is a bi-lithologic depleted basalt in which lithology A includes xenocrysts similar to the minerals in the lherzolites. Although the nature of the relationship is debated, we have argued that it formed by impact mixing of related igneous units [9].

Ranges of bulk compositions in the martian meteorites ([10]: Fig 1b, 2b, 3b) are as wide as those of the lunar meteorites, but at different concentrations. Values of mg' overlap for the two suites, but the maximum values of Al₂O₃ and Sc differ by a factor of two based on the domination of the lunar suite by feldspar accumulation to form the early anorthositic crust compared with pyroxene and olivine accumulation in the martian suite to form young mafic cumulates. Variations within the martian suite are not due to simple accumulation of olivine and/or pyroxene from a single parent basaltic magma, based both on the compatible and incompatible elements [3]. The REE plot shows that there are both "normal" and depleted basalts, while the clinopyroxenites and dunite come from an enriched parent magma [3,9].

The crystallization and ejection ages of martian meteorites are shown in Fig 4b [11,12]. The ejection ages of martian meteorites are significantly longer than for lunar meteorites, as would be expected from astronomical constraints. Two main clusters in martian meteorite ages are apparent; many of the basaltic with all of the lherzolitic shergottites, and all of the clinopyroxenites (nakhilites) with dunite Chassigny. ALH84001 is distinct at the high end of the age spectrum, while EETA79001 is at the low end of the age range. The depleted basalts scatter between. The 6 "points" on Fig 4b could be interpreted as 6 distinct impacts ejecting material from Mars, some of the overlap in crystallization age or ejection age among the shergottites may imply fewer events.

Lunar Meteorites in the Context of the Lunar Database. Numerous authors have compared the lunar meteorites to Apollo and Luna samples. Their textures and clast populations overlap significantly, as do their bulk compositions. The anorthositic breccias are most similar to granulitic and fragmental breccias from North Ray Crater, Apollo 16. These are the most feldspathic and lowest in REE of all polymict lunar samples. These lunar samples would plot with the anorthositic meteorites in Fig 1a, 2a, 3a, while the soils from the same stations have slightly higher REE. The basaltic breccia meteorites are most similar to very-low-Ti basalts from the Apollo 17 and Luna 24 sites, which also show a range in mg'. The basaltic

breccia meteorites, however, have higher REE concentrations than the pure mare basalts. The mare gabbro meteorites represent a new type of 3.9 Ga low-Ti mare basalt. It is notable that the range of variation in breccias from each Apollo site is much greater than the range of variation within either the anorthositic or basaltic meteorite groups. Some sites at interfaces between mare and highland units show very wide ranges in composition and clast populations. The variation is due in part to the admixture of a mafic KREEP component (which is minimal in most meteorites), however, variation in non-KREEP mare and highland components is significant. It is easy to distinguish polymict samples from one lunar site from those of another.



The recent Clementine and Prospector missions give our best global mineralogical and geochemical maps of the Moon [13,14]. They show a relatively uniform highland feldspathic composition interrupted by mafic mare on the nearside with a large Procellarum "hot spot" in Th abundance. Most of the Apollo samples were collected in or near the hot spot, accounting for their high KREEP affinities. Does the limited variation among anorthositic lunar meteorites, in contrast with Apollo samples mean that the highlands crust is uniform everywhere except in the Procellarum region? The comparison of magnesian ALHA81005 with ferroan Y-791197 shows that a range of materials may exist in potentially launch-paired meteorites. Despite their differences, they exhibit some unusual shared clasts, including some similar to those in the basaltic breccias. I propose that this diverse suite represents a site near a mare-highland boundary. I conclude that most of the lunar highlands consists of highly ferroan and feldspathic rocks, but that some more magnesian feldspathic, as well as KREEP-rich, and mare components are available for mixing into polymict breccias and soils. All of this variation is consistent with Apollo sample diversity and the realization that the Moon is a complex planetary body more like the Earth than asteroids. This implies that the numbers of distinct targets represented by the lunar meteorite suite is probably at the lowest end of range allowed by their exposure histories, so that launch pairing is maximized. I estimate the number of impacts which produced the lunar meteorites to be as low as 5-6, depending on the assumptions involved in interpreting exposure data. This implies that they represent about the same number of sites as the Apollo samples, although they are more "typical" in bulk composition.

Martian Meteorites in Context of Martian Geology. There is no database of returned sample analyses or global geochemical mapping for Mars. These await missions planned for the next 10 years. The less accurate Viking robotic analyses of rocks were interpreted to represent weathered basalts, while Pathfinder rock analyses were interpreted to represent andesites [15,16]. There is, however, global geologic mapping which shows a very diverse geologic history including ancient cratered terrain, young volcanic plains, and regions of rivers or floods. Numerous authors have emphasized the point that all but one of the martian meteorites are young igneous rocks, showing that they do not represent the Mars' geologic diversity [2-4]. Mars is a very complex planet, more like Earth than the Moon is, so we should expect more diversity in its meteorite population. This issue was addressed [4,17] in evaluating mechanisms of ejection, but I feel that the planet's diversity also pushes the launch pairing of its known meteorites to the maximum (grouping all shergottites together) even if this requires different assumptions in modeling exposure histories. Thus I estimate the number of distinct impact events for martian meteorites to be as low as 4-5 based on petrologic, geochemical and geologic constraints. The sampling bias toward young igneous rocks is thus more easily interpreted [4,17].

References: [1] Lindstrom et al (1994) *LPSC XXV*, 797-798. [2] Lindstrom (1994) *Meteor.* 29, 491. [3] McSween (1994) *Meteor.* 29, 757-779. [4] Warren (1994) *Icarus* 111, 338-363. [5] Hill et al (1991) *Nature* 352, 614-617. [6] Warren & Kallemeyn (1993) *NIPR* 6, 35-57. [7] Lindstrom et al (1991) *LPSC XXII*, 817-818. [8] Arai & Warren (1999) *MPS* 34, 209-234. [9] Mittlefehldt et al (1999) *MPS*, in press. [10] Meyer (1998) *Mars Meteor. Compend.*, JSC 27672, 237pp. [11] Scherer & Schultz (1996) *LPSC XXX*, 1144. [12] Nyquist et al (1998) *JGR* 103, 31,445-31,455. [13] Laurence et al (1998) *Science* 281, 1484-1489. [14]. Korotev (1999) *LPSC XXX*, 1302. [15] Clark et al (1982) *JGR* 87 B12, 10059-10067. [16] McSween et al, (1998) *JGR*, in press. [17] Gladman et al (1996) *Science* 271, 1387-1392.

Mg-CHONDRULES, Al-CHONDRULES, AND CAI: CONNECTIONS.

MacPherson, G.J., Dept. of Mineral Sciences, National Museum of Natural History, Smithsonian Inst., Washington DC 20560-0119, USA (glenn@glenm.si.edu)

Introduction.

Highly refractory objects in chondritic meteorites – including calcium-aluminum-rich inclusions (CAIs), Al-rich chondrules, and Mg-rich chondrules – are among the most ancient materials formed in our Solar System 4 ½ billion years ago. They are probes into the processes and conditions that existed in the solar nebula. Yet despite 30 + years of intensive studies, the origins of these primitive objects and their relationships to one another are poorly understood. This paper highlights some recent studies of the bulk compositions, magnesium isotopic, and oxygen isotopic compositions of all three groups of objects, and which have begun to shed some light on their origins and relations.

Of particular interest is the relationship between CAIs and ferromagnesian chondrules: did they form by similar or different processes, and at different times or contemporaneously? One clue to understanding this relationship lies in aluminum-rich chondrules, which share some mineralogical and chemical properties with both CAIs and ferromagnesian chondrules.

Bulk Composition Studies.

Aluminum-rich chondrules were postulated [*e.g.* 1] to be intermediate in composition between CAIs and normal chondrules and therefore a petrogenetic link. However, sufficient data now exist to clearly show that the bulk compositions of Al-rich chondrules, CAIs, and ferromagnesian chondrules do not collectively define a smooth linear trend in CMAS (CaO-MgO-Al₂O₃-SiO₂) space. In this sense Al-rich chondrules are not “intermediate” between CAIs and ferromagnesian chondrules and therefore are not simply melted mixtures of CAI material with ferromagnesian chondrules. But the three trends do connect, to form a continuous if complex nonlinear path through CMAS space (Fig. 1). This combined trend curiously mimics – but does not coincide with – that expected from a volatility relationship (condensation or evaporation). Interestingly, a major deviation from equilibrium condensation calculations [*e.g.* 2] is that the trends of Al-rich chondrules and CAIs intersect approximately at the composition of the mineral anorthite rather than at the composition of pyroxene. Therefore CAIs and Mg- and Al-rich chondrules all have volatility-controlled compositions [*see also* 3], probably involving both condensation and evaporation.

Oxygen Isotope Studies.

Ion microprobe studies [4] of oxygen isotopic compositions confirm that Al-chondrules are not the product of mixing known CAI material with ferromagnesian chondrules. This conclusion is based particularly on data from CAIs and chondrules in unequilibrated ordinary chondrites (UOCs), specifically: (a) CAIs in unequilibrated ordinary chondrites (UOCs) have oxygen isotopic compositions that are indistinguishable from those of CAIs in carbonaceous chondrites; and (b) the Al-rich chondrules in UOCs are enriched in ¹⁶O but define a mixing line that greatly extends the line defined by ferromagnesian chondrules from UOCs. This UOC chondrule line does not intersect the combined carbonaceous chondrite/ordinary chondrite CAI field, i.e. the Al-rich chondrules in UOCs do not lie on a mixing line between any known CAIs and UOC ferromagnesian chondrules and therefore cannot represent isotopic mixtures of the two.

If they are isotopic mixtures, the ^{16}O -rich end member is as yet unidentified and multiple ^{16}O -rich carriers were present in the early Solar Nebula. Alternatively, the multiple ^{16}O -rich signatures are not the result of diverse presolar carrier grains but resulted rather from a local nebular process [e.g. 5].

The observation that UOC and carbonaceous chondrite CAIs all have similar oxygen isotopic compositions is significant. One possible interpretation of this result is that CAIs did not form nebula-wide. Instead, CAIs might all have formed locally in a restricted region of the nebula and then were distributed throughout many chondrite accretion regions. If the more diverse oxygen isotopic compositions of carbonaceous and UOC chondrules mean that chondrule formation was a more widespread process than that which formed CAIs, then even though chondrules and CAIs have volatility-controlled compositions they must nevertheless represent fundamentally-different nebular events.

Magnesium Isotope Studies.

The time of formation of Mg-rich chondrules relative to CAIs is not known with certainty, because absolute age-dates of the chondrules are not yet sufficiently precise. But comparative measurements of the decay products of extinct short-lived radionuclides (^{26}Al , ^{129}I , ^{53}Mn) in CAIs and chondrules suggest that the chondrules formed perhaps 2-3 million years later than the CAIs [e.g. 6]. This interpretation is widely criticized, especially in the case of ^{26}Al , for several reasons. First, normal ferromagnesian chondrules do not contain phases with sufficiently high Al/Mg ratios to permit ion probe resolution of excess ^{26}Mg (the decay product of the ^{26}Al), therefore all existing measurements have been made on Al-rich chondrules, whose relation to “normal” chondrules is considered uncertain. Second, the presence of isotopically-anomalous (“FUN”) and non-FUN CAIs side-by-side in chondrites seems to indicate nebular isotopic heterogeneity on a grain-to-grain scale, in materials otherwise believed to be contemporaneous. Therefore, any isotopic differences between CAIs and chondrules might be due to formation of the two kinds of objects contemporaneously but in different isotopic reservoirs. Third, the implied difference in age of formation (>2-3 ma) requires the CAIs to be somehow protected against nebular gas drag and falling into the Sun during this prolonged period. But none of the stated objections to a chronologic interpretation of the Al-Mg isotopic data is fatal: (a) Al-rich chondrules have now been shown on the basis of oxygen isotope evidence [4] to be related genetically to ferromagnesian chondrules rather than to CAIs; (b) data from the short-lived nuclides ^{129}I and ^{53}Mn corroborate the long CAI-chondrule time differences inferred from initial ^{26}Al compositions [6]; and (c) there are nebular processes such as outflow that will tend to counteract the effects of gas drag. Finally, it must be remembered that the implied long 2-3 million year nebular lifetime is not based only on chondrule-CAI comparisons: individual CAIs show clear isotopic evidence for nebular reprocessing (melting) that occurred 2-3 million years after initial CAI formation. Until and unless absolute age data demonstrate the contrary, a possible 2-3 million year age gap between chondrules and CAIs cannot be lightly dismissed.

Conclusions.

CAIs, Mg-rich chondrules, and Al-rich chondrules have bulk compositions that appear to be related to one another by volatility-controlled processes such as condensation and evaporation. However, the CAIs may have been formed in one restricted region of the nebula while chondrule

formation was more widespread. And, despite widespread skepticism, there is good isotopic evidence that chondrule and CAI formation were separated in time by as much as 2 million years.

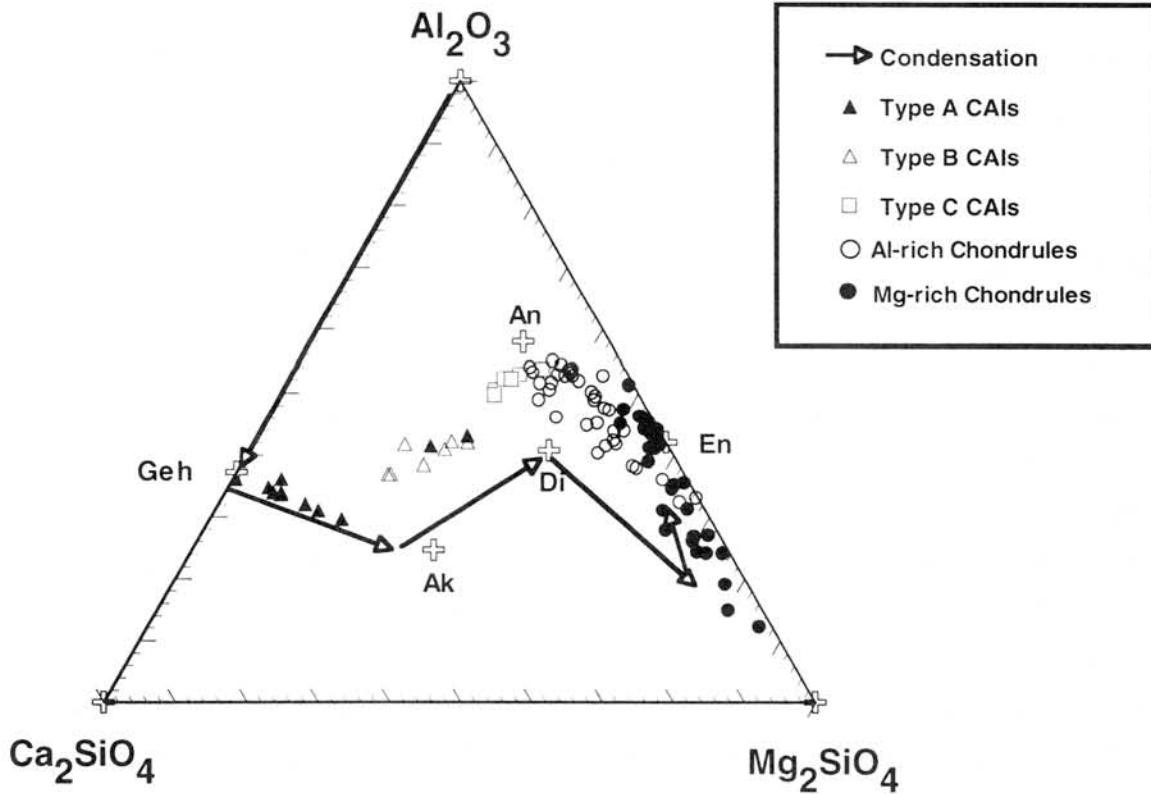


Fig. 1

Compositions of CAIs, Mg-rich chondrules, and Al-rich chondrules projected (from $MgAl_2O_4$) onto the plane Ca_2SiO_4 - Mg_2SiO_4 - Al_2O_3 . Shown for comparison is the trend of bulk condensed solids during equilibrium condensation [2], which parallels but does not coincide with the combined composition trend of the natural objects. The trend of evaporation (not shown) is similar to that of condensation. Type A CAIs plot in the plane of the diagram, but Types B and C CAIs plot progressively farther below the plane (negative spinel), approaching the composition of anorthite. Similarly, the progression from the most forsterite-normative chondrules through Al-rich chondrules trends down below the plane of the diagram towards anorthite

References: [1] Bischoff, A. and Keil, K. 1984. *Geochim. Cosmochim. Acta* **48**, 693-709; [2] Grossman, L. 1972. *Geochim. Cosmochim. Acta* **36**, 597-619; [3] Hashimoto A., *Geochem. Jour.* **17**, 111-145; [4] McKeegan K. D., et al. (1998) *Science* **280**, 414-418; [5] Theimens M. H. and Heidenreich J. E. III (1983) *Science* **219**, 1073-1075; [6] Swindle T. D., et al. (1996) In: *Chondrules and the Protoplanetary Disk* (R. H. Hewins, R. H. Jones, and E. R. D. Scott, eds.), p. 77-86. Cambridge Univ. Press. 346 pp.

ANTARCTIC CHONDRITES IN THE OXYGEN ISOTOPIC SYSTEM

A.A.Marakushev*, A.V.Bobrov**, O.V.Chaplygin**

**Institute of Experimental Mineralogy, Russian Academy of Sciences, Chernogolovka, Moscow District, 142432 Russia; **Chair of Petrology, Geological Department, Moscow State University, Vorob'evy Gory, 119899 Moscow, Russia*

A.A.Marakushev (1997) showed that groups of ordinary (H-L) and carbonaceous (C3) chondrites are connected by an abruptly anomalous trend of oxygen isotopic variation which is observed for the barred chondrules of the Allende meteorite. The evolution of that trend was explained by the hydrogen influence on chondritic melts inside their parental planets (Marakushev, 1994) which was accompanied by the reduction of iron up to the native state and the formation of water, extracting heavy oxygen isotopes according to the reaction in terms of conventional symbols of normative minerals: $2\text{Mg}_{1.5}\text{Fe}_{0.5}\text{SiO}_4$ (initial oxygen) + $\text{H}_2 = \text{Fe} + \text{Mg}_2\text{SiO}_4$ (anomalous light oxygen) + MgSiO_3 (anomalous light oxygen) + H_2O (anomalous heavy oxygen). Anomal distribution of oxygen isotopes in the row of carbonaceous chondrites C3-C2-C1 with successive enrichment in H_2O was also explained by water extraction.

Antarctic chondrites regularly place in the system of oxygen isotopes obtained (*see figure*). Isotopic trend which connects H and C3 chondrites is observed for the barred chondrules and igneous inclusions in Antarctic ordinary chondrites Y-794046, Y-793241, and Y-75097 (Nakamura et al., 1994). ALH84001, in our opinion (Marakushev, Bobrov, 1998), also belongs to the group of these inclusions. This trend is well represented by the barred chondrules of Allende which together with chondrules and igneous inclusions in the ordinary Antarctic chondrites form a full row of oxygen isotopic composition between the ordinary and carbonaceous C3 chondrites. Matrix of the Allende chondrite ($\delta^{17}\text{O} = -1.00\text{‰}$ and $\delta^{18}\text{O} = 3.60\text{‰}$) is significant because it is close to its bulk composition ($\delta^{17}\text{O} = -2.56\text{‰}$ and $\delta^{18}\text{O} = 1.64\text{‰}$). According to the scheme (*see figure*) it may be considered as a product of differentiation of H chondrite melt caused by the separation of barred chondrules under the hydrogen pressure of fluid envelope of the parental chondritic protoplanet. This type of differentiation of chondritic melts (H→C3) results from the extraction of water phase similar to water of ordinary chondrites by the oxygen isotopic composition ($\delta^{17}\text{O} = 5.40\text{‰}$ and $\delta^{18}\text{O} = 4.20\text{‰}$). This water differs from water of carbonaceous chondrites on principle ($\delta^{17}\text{O} = 7.30\text{‰}$ and $\delta^{18}\text{O} = 13.00\text{‰}$). The formation and extraction of water of carbonaceous chondrites result in the different trend of isotopic variation typical for carbonaceous chondrites. It is seen from the porphyric chondrules of Allende, on the one hand, which differ from bulk composition of meteorite by a light isotopic composition of oxygen, and from its dark

inclusions enriched in heavy oxygen isotopes, on the other hand. Variations of isotopic composition of Antarctic carbonaceous chondrites ideally follow two opposite isotopic trends, as it is shown on the diagram (see figure).

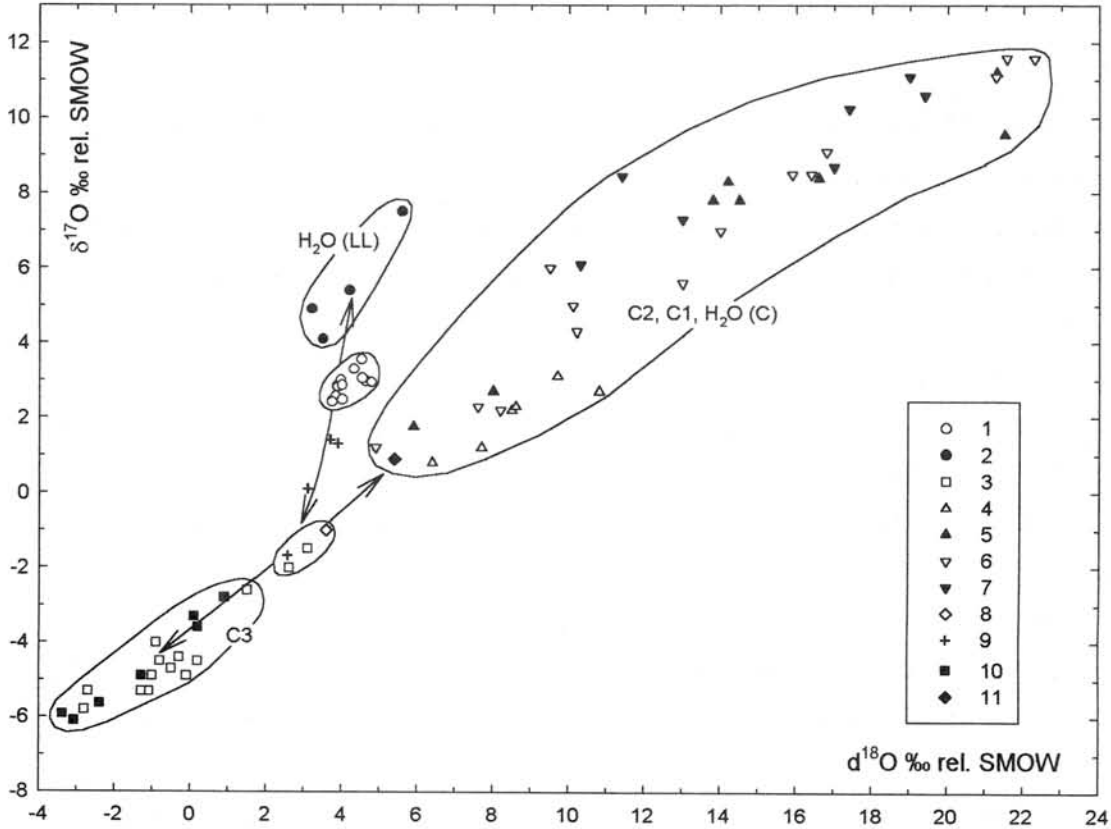


Figure. Antarctic chondrites in the system of oxygen isotope variations: 1 - ordinary chondrites and their igneous inclusions (Jabeen et al., 1998; Nakamura et al., 1994); 2 - water of ordinary chondrites (Clayton et al., 1976; 1977); 3 - C3 chondrites (Kurat et al., 1990); 4 - C2 chondrites (Kurat et al., 1990); 5 - water of C2 chondrites (Clayton et al., 1976; 1977); 6 - C1 chondrites (Kurat et al., 1990; Hou Wei, 1995); 7 - water of C1 chondrites (Clayton et al., 1976; 1977); Composition of Allende matrix (8), its barred (9), porphyric (10) chondrules, and dark inclusion (11) are plotted for comparison (Ikeda, Kimura, 1995; Jabeen et al., 1998)

Variations of isotopic composition of C3 Antarctic meteorites impoverished with water phase and heavy oxygen isotopes are similar to those of porphyric chondrules. By contrast dark inclusions in Allende and C1, C2 carbonaceous chondrites enriched in water contain anomalous concentrations of heavy oxygen isotopes. The role of water phase as a concentrator of heavy oxygen isotopes is clearly seen from these correlations. Its formation under the hydrogen influence on the carbonaceous chondrite melts is accompanied by the development of

liquid immiscibility, splitting them into C3, C2, and C1 chondritic melts which strongly differs by the concentration of water and heavy oxygen isotopes.

It is necessary to mention that dark inclusions in carbonaceous chondrites and ureilites enriched in heavy oxygen isotopes in the development of meteorite magmatism are complementary to light inclusions in carbonaceous chondrites in which oxygen is represented by light isotopes.

References:

- Clayton, R.N., Onuma, N., and Mayeda, T. K.** A classification of meteorites based on oxygen isotopes. – *Earth Planet. Sci. Lett.* 1976. Vol. 30. P. 10–18
- Clayton, R.N., Onuma, N., Grossman, L., and Mayeda, T.K.** Distribution of the presolar component in Allende and other carbonaceous chondrites. – *Earth Planet. Sci. Lett.* 1977. Vol. 34. P. 209–224.
- Hou Wei.** A discussion on the origin of Antarctic Quasi-C1 chondrites and their cosmochemistry signification. – Pap. presented to the 20th symp. on Antarctic meteorites. Tokyo. 1995. P. 80–83.
- Ikeda, Y., Kimura, M.** Anhydrous alteration of Allende chondrules in the solar nebula I: description and alteration chondrules with known oxygen-isotopic compositions. – *Proc. NIPR Symp. Antarct. Meteorites.* 1995. No. 8. P. 97–122.
- Jabeen, I., Kusakabe, M., Nagao, K., Nakamura, T.** Oxygen isotope study of Tsukuba chondrite, some HED meteorites and Allende chondrules. *Antarctic meteorite res.* 1998. No 11. P. 122–135.
- Kurat, G., Brandstatter, F., Koeberl, C.** Lunar meteorite Yamato-793274: a Lunar highland sample possibly rich in mare minerals. – Pap. presented to the 15th symp. on Antarctic meteorites. Tokyo. 1990. P. 193–197.
- Marakushev, A.A.** Two stage evolution of the terrestrial planet recorded in diamond-bearing chondrites. – Pap. presented to the 19th symp. on Antarctic meteorites. Tokyo. 1994. P. 200–202.
- Marakushev, A.A.** Genetic meaning of oxygen isotopic variations of chondrules in chondrites. – Pap. presented to the 22nd symp. on Antarctic meteorites. Tokyo. 1997. P. 97–99.
- Marakushev, A.A. and Bobrov, A.V.** Origin of ALH84001 antarctic meteorite. – Pap. presented to the 23rd symp. on Antarctic meteorites. Tokyo. 1998. P. 66–68.
- Nakamura, N., Morikawa, N., Hutchison, R., et al.** Trace element and isotopic characteristics of inclusions in the Yamato ordinary chondrites Y-75097, Y-793241 and Y-794046. – *Proc. NIPR Symp. Antarct. Meteorites.* 1994. No. 7. P. 125–143.

On the primordial composition of the noble gases in Canyon Diablo

Jun-ichi Matsuda¹⁾, Miwa Namba¹⁾, Teruyuki Maruoka¹⁾ and Gero Kurat²⁾

1) Department of Earth and Space Science, Graduate School of Science, Osaka University, Toyonaka, Osaka 560-0043, Japan.

2) Naturhistorisches Museum, Postfach 417, A-1014 Vienna, Austria.

To examine the primordial components in iron meteorites, we have measured the elemental abundances and isotopic compositions of noble gases in a large graphite nodule in the Canyon Diablo IAB iron meteorite. As the graphite nodule contained metal as a vein, we broke it into small pierces and treated with HCl to remove the metal portion completely. We put the sample in 6M HCl overnight at room temperature six times, then heated it with 12M HCl at 65°C three times, then boiled it with 12M HCl for one hour three times. We washed the graphite sample repeatedly until the supernatant fluid had neutral pH. The sample was named as "CG1". The noble gas elemental abundances and isotopic compositions have been measured by the mass spectrometer VG5400 installed in Osaka University.

The Ne isotopic data are plotted in a three-isotope diagram (Fig. 1). The data points of 600-1200°C fractions of CG-1 are located on the mixing line between the atmosphere and Ne-S (spallogenic component), and those of 1400 and 1600°C lie on the mixing line of the Ne-HL (Ne-A2) and Ne-S. Spallogenic Ne is produced by cosmic-ray reaction from the element of which mass number is larger than that of Ne. Thus Ne is not produced by spallation from carbon. However, some trace elements with high mass may be contained in graphite or other minor phase like cohenite in the graphite nodule could be the target. Here, it should be emphasized that the linear array of data points of 1400 and 1600°C fractions strongly implies that the primordial component of Ne is Ne-HL rather than the solar Ne or Ne-Q of which $^{20}\text{Ne}/^{22}\text{Ne}$ ratios are larger than that of air. This suggests that pre-solar diamonds (the host phase of Ne-HL) was also incorporated in iron meteorite just like the chondrite. It is very curious that there is no solar component in graphite nodule because the solar component should be very common in the solar system.

The Ar data are shown in Fig. 2. The $^{40}\text{Ar}/^{36}\text{Ar}$ ratios of all the fractions were lower than that of the atmosphere, and there was no excess of ^{40}Ar . The interesting feature is the $^{38}\text{Ar}/^{36}\text{Ar}$ ratio which is

higher than that of the terrestrial atmosphere. This is due to the spallation effect and/or the contribution of Ar-HL. The Ar data points are lower than the mixing line between air and Ar-HL (and also than that between air and the spallation component), and seem to be situated inside the triangle area of air, Ar-HL and Ar-Q. Thus the Ar data can not be explained only by the mixing of air and Ar-HL, and indicate the presence of Q. As the Ne concentration in Q is very low, the presence of Ne-Q could not be identified from Ne-data.

The Xe data are plotted in $^{134}\text{Xe}/^{130}\text{Xe}$ and $^{136}\text{Xe}/^{130}\text{Xe}$ diagram (Fig. 3). All the data points beautifully lie on the mixing line between air and Xe-Q, and there seems no contribution from Xe-HL. This is not inconsistent with Ne data which show only the contribution from the HL component. As the Xe content in Q is very high and the Xe/Ne ratio in Q is much higher than that in presolar diamonds (host phase of Xe-HL), only the contribution of Q is observed in Xe data. The $^{129}\text{Xe}/^{130}\text{Xe}$ ratios higher than the atmospheric ratio have been observed in all temperature fractions. The large excess of ^{129}Xe observed in Canyon Diablo graphite nodule indicates that carbonaceous material was taken in iron meteorite during that ^{129}I was still present.

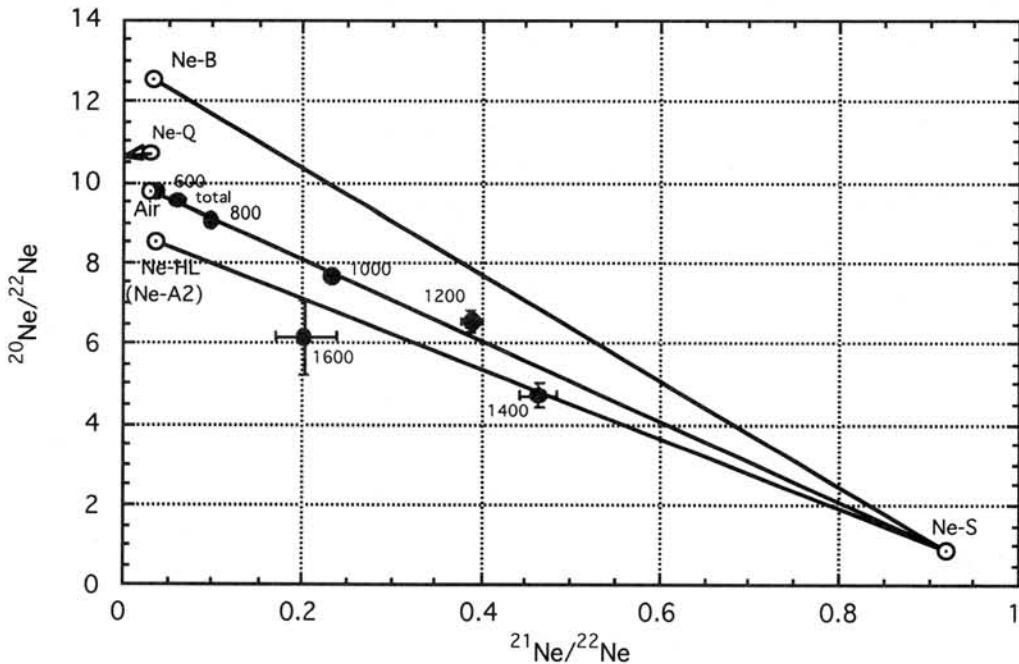


Fig. 1. Ne three-isotope plot.

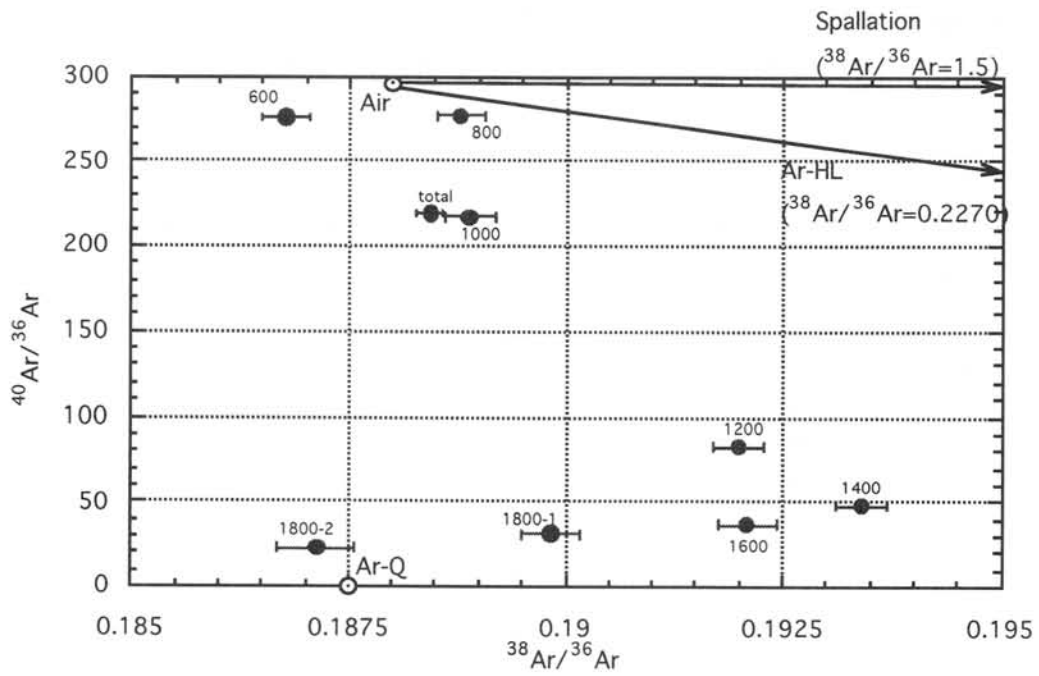


Fig. 2. Ar three isotope plot.

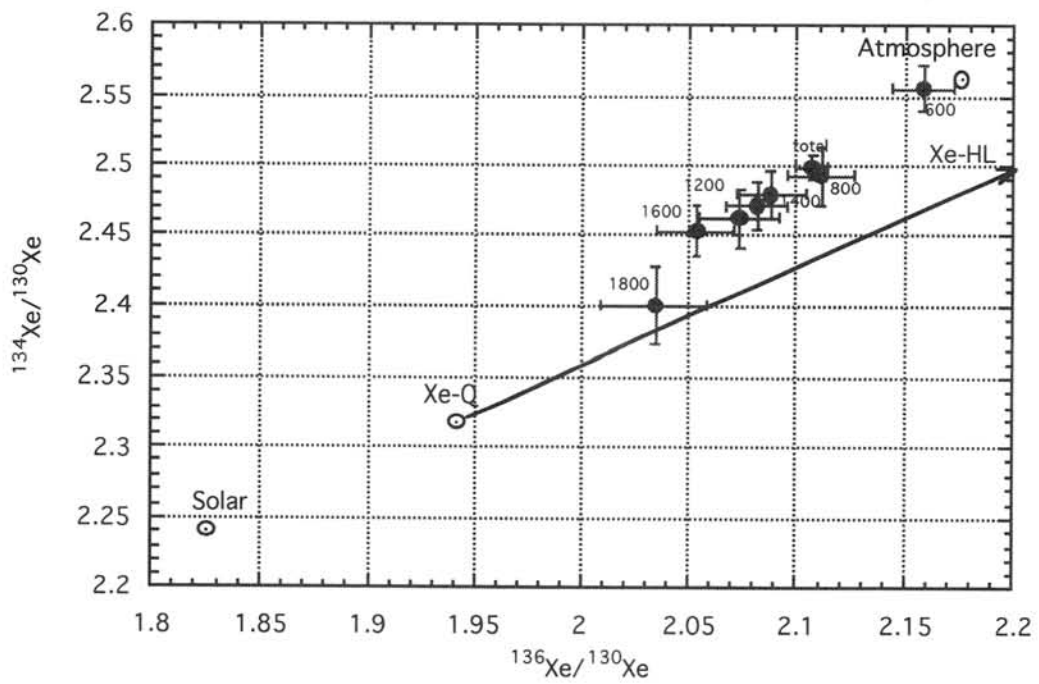


Fig. 3. $^{134}\text{Xe}/^{130}\text{Xe}$ vs. $^{136}\text{Xe}/^{130}\text{Xe}$ diagram.

Olivine megacrysts in the basaltic Martian meteorites Dar al Gani 476 and EETA79001: Cooling rates deduced from Fe-Mg zoning of olivine

Takashi Mikouchi^{1,2}, Masamichi Miyamoto², and Gordon A. McKay¹

¹Mail Code SN2, Planetary Science Branch, NASA Johnson Space Center, Houston, TX77058, USA
(E-mail: TMikochi@ems.jsc.nasa.gov)

²Mineralogical Institute, University of Tokyo, 7-3-1 Hongo, Bunkyo-ku, Tokyo 113-0033, Japan

1. Introduction

Recent recovery of many meteorite samples from the Sahara desert brought about discovery of two new Martian meteorites (Dar al Gani 476 and Dar al Gani 489) and the total number of Martian meteorites now reaches 14. The new meteorite, Dar al Gani 476, is classified as a basaltic shergottite showing close mineralogical and petrological similarities to the lithology A of EETA79001 (Zipfel *et al.*, 1999; Mikouchi, 1999). Dar al Gani 476 is a greenish-brown rock weighing about 2 kg. One of the most characteristic features is the presence of olivine megacrysts reaching several millimeters long. Mikouchi (1999) reported that olivine megacrysts have a preferred orientation for their longer dimensions. Olivine grains are set in a fine-grained groundmass of pyroxene and plagioclase glass (maskelynite) (Fig. 1). Olivine megacrysts are present as single or compound crystals. They are usually subhedral, but large near-euhedral crystals are sometimes observed. Small anhedral grains are also present. Large olivine grains are interpreted as xenocrysts due to their extremely large sizes and magnesian compositions relative to the surrounding groundmass (Mikouchi, 1999) although their euhedral to subhedral forms hint of a phenocrystic origin. In this study we estimated cooling rates of olivine megacrysts by using Mg-Fe zoning profiles observed in both Dar al Gani 476 and lithology A of EETA79001 in order to compare their cooling histories. We employed the calculation methods similar to Miyamoto and Takeda (1994) and Miyamoto *et al.* (1999). Although several data were reported for the diffusion coefficient of Fe-Mg in olivine, we used that of Misener (1974) because it shows the best match with the observed profile (Miyamoto and Mikouchi, 1998).

2. Samples and Analytical Methods

We analyzed polished thin sections of Dar al Gani 476 and lithology A of EETA79001. The sample of Dar al Gani 476 and lithology A of EETA79001 were supplied by University Museum, University of Tokyo and The Meteorite Working Group, NASA Johnson Space Center, respectively. Chemical zoning of olivine was measured by electron microprobes (JEOL Superprobe 733 at Ocean Research Institute, University of Tokyo and JEOL JXA 733 mkII at Geological Institute, University of Tokyo). The accelerating voltage was 15 kV and the beam current was 12 nA on a Faraday cage. Counting times at peak wavelengths were 20-30 s. The background intensity of each element was counted on both sides of the peak wavelength.

3. Results

Olivine megacrysts in Dar al Gani 476 are chemically zoned from the Fo₇₆ core to the Fo₆₂ rim. MnO is correlated with FeO and is zoned from 0.4 to 0.7 wt%. CaO is fairly constant (0.2-0.3 wt%). Smaller anhedral olivine is chemically homogenous (Fo₆₂₋₅₈). Nevertheless, there is no distinct difference in abundance between large euhedral grains and small anhedral grains. Intermediate grains showing slight zoning are also present. These observations suggest that all olivine grains share the same origin and smaller grains are produced by the effect of off-

center cuts of large grains. Olivine megacrysts in the lithology A of EETA79001 show similar petrographic and mineralogical characteristics and they are also interpreted to be xenocrysts (Steele and Smith, 1982; McSween and Jarosewich, 1983). Their compositional range is wider than that of Dar al Gani 476 and is Fo₈₁₋₅₅. Minor elements are as abundant as those are in Dar al Gani 476.

Assuming that $D^{\text{Atomic Mg/Fe}}_{\text{olivine/melt}}$ is 0.35 (Stolper, 1977), a melt having the bulk composition of Dar al Gani 476 (Atomic Mg/(Mg+Fe) = 0.68 from Zipfel *et al.* (1999)) would be in equilibrium with olivine of Fo₆₁. We also calculated the olivine composition in equilibrium with the groundmass (average composition of several microprobe line analyses of groundmass). The obtained composition is Fo₅₈. These compositions generally agree with the rim composition of the Dar al Gani 476 olivine and also with smaller homogeneous olivine. It is therefore likely that olivine grains in Dar al Gani 476 are xenocrysts. Probably, small homogeneous olivine grains are also xenocrysts, but homogenized by contact with the magma. The presence of fragment-like olivine grains having Mg-rich composition at the edge show evidence that the zoning pattern is of primary igneous origin (Fig. 1). Thus, we believe that original igneous zoning is almost preserved.

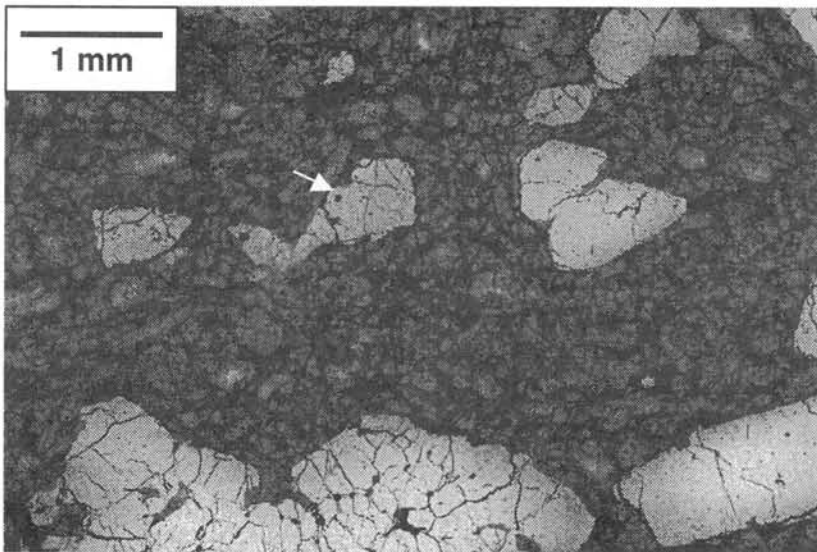


Fig. 1. Mg X-ray map of the Dar al Gani 476 Martian meteorite. The brighter area shows concentration of higher Mg content. The brightest phases are olivine grains. Note that they are embedded in a fine-grained groundmass of pyroxene and plagioclase. Olivine shows clear chemical zoning. In many cases they are zoned from core to rim, but Mg-enriched area is also observed at the grain edge (arrow), suggesting that olivine preserves original igneous zoning.

By assuming these assumptions, we estimated a cooling rate of the Dar al Gani 476 olivine by employing a method similar to Miyamoto and Takeda (1994). We assumed that original chemical zoning of olivine megacrysts was produced by fractional crystallization, then it was slightly modified by atomic diffusion due to contact with the melt. The profile produced by fractional crystallization broadly agrees with the observed profile (Fig. 2). However, slight disturbance near the edge may suggest diffusive modification by the contact with the magma. The cooling rate that preserves the chemical zoning of olivine megacrysts is about 2 °C/hour for the temperature range from 1300 °C to 1100 °C. The termination temperature of cooling (1100 °C) was deduced from equilibration temperature for groundmass pyroxenes (pigeonite and augite) (Mikouchi, 1999). The cooling rate from 1200 down to 1100 °C that prevents modification of primary zoning is 0.5 °C/hour. Therefore, these results mean that the Dar al Gani 476 olivine cooled faster than these cooling rates. The cooling rates of 0.5-2 °C/hour are slightly faster than that of olivine xenocrysts in lithology A of EETA79001 (0.07-0.6 °C/hour) (Kaiden *et al.*, 1998). We re-calculated the cooling rate of olivine xenocrysts in lithology A of EETA79001 by assuming the effect of both fractional crystallization and atomic diffusion (Miyamoto *et al.*, 1999). The obtained cooling rate is 0.1-1 °C/hour (1300-700 °C), which almost agrees with

that of Dar al Gani 476. Hence, we suggest that Dar al Gani 476 and lithology A of EETA79001 experienced similar cooling histories. The burial depth that corresponds to the calculated cooling rates of both Dar al Gani 476 and lithology A of EETA79001 is less than 1 m from the surface if we assume covered by rock-like material.

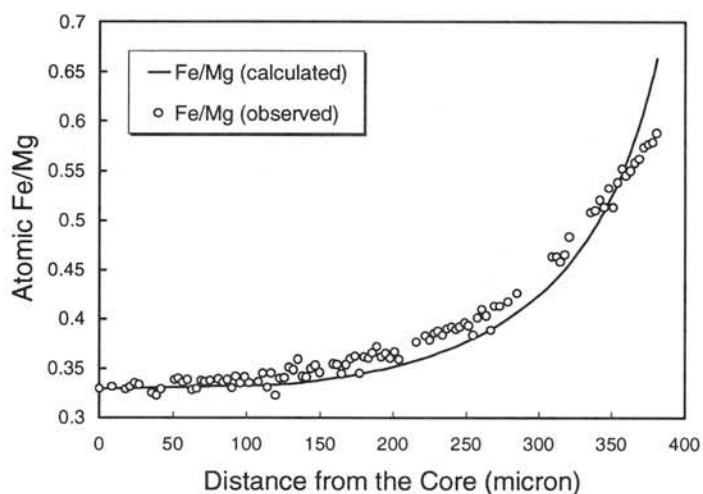


Fig. 2. Observed (open circles) and calculated (solid line) Fe/Mg zoning profiles of the olivine megacryst in Dar al Gani 476. The calculation is based upon assumption that it is produced by closed-system fractional crystallization (Rayleigh equation). In this case, the about 35 vol.% liquid remained. Both profiles show agreement with each other in general. However, slight difference is clear especially at the edge parts. This can be interpreted by diffusive modification of the primary igneous zoning profile by contact with the magma.

4. Discussion

The most appropriate geological settings for the formation at such burial depth as shallow as 1 m from the surface would be within the lava flows near the surface. Probably, the partial foliated texture of aligned olivine megacrysts (Mikouchi, 1999) and pyroxene prisms in Dar al Gani 476 was attributed to flow alignment in the extruded lava. Mikouchi (1999) reported that pigeonite and augite are present as separate grains in Dar al Gani 476 and discussed its related cooling history to Shergotty and Zagami. However, this study shows that Dar al Gani 476 experienced rapid cooling history similar to EETA79001 (Mikouchi *et al.*, 1998).

Unlike EETA79001, the absence of the olivine-orthopyroxene-chromite xenolith is also observed in our section of Dar al Gani 476 (Zipfel *et al.*, 1999). Further study is required to discuss petrogenetic relationship between Dar al Gani 476 and EETA79001, especially by considering this difference.

Acknowledgement

We thank University Museum, University of Tokyo and The Meteorite Working Group, NASA Johnson Space Center for the samples.

References

- Kaiden H. *et al.* (1998) *Antarct. Meteorite Res.*, **11**, 94-104.
- McSween H. Y. Jr. and Jarosewich E. (1983) *Geochim. Cosmochim. Acta*, **47**, 1501-1513.
- Mikouchi T. *et al.* (1998) *Meteoritics and Planet. Sci.*, **33**, 181-189.
- Mikouchi T. (1999) *Lunar Planet. Sci.*, **XXX**, Abst. #1557, Lunar and Planet. Inst., Houston.
- Misener D. J. (1974) In *Geochemical Transport and Kinetics*, (A. W. Hofmann *et al.*, eds.) pp. 117-129, Carnegie Inst., Washington, Publ. 634.
- Miyamoto M. and Takeda H. (1994) *Jour. Geophys. Res.*, **99**, 5669-5677.
- Miyamoto M. and Mikouchi T. (1998) *Mineral. Jour.*, **20**, 9-18.
- Miyamoto M. *et al.* (1999) *Lunar Planet. Sci.*, **XXX**, Abst. #1323, Lunar and Planet. Inst., Houston.
- Steele I. M. and Smith J. V. (1982) *Proc. Lunar Planet. Sci. Conf.*, **13th**, *Jour. Geophys. Res.*, **87**, A375-A384.
- Stolper E. (1977) *Geochim. Cosmochim. Acta*, **41**, 587-611.
- Zipfel J. *et al.* (1999) *Lunar Planet. Sci.*, **XXX**, Abst. #1206, Lunar and Planet. Inst., Houston.

DIFFERENTIATION OF THE MATRIX MATERIAL IN THE KAINSAZ (CO) CARBONACEOUS CHONDRITE

Mitreikina O.B. and Zinovieva N.G.

Department of Petrology, Faculty of Geology, Moscow State University, Moscow 119899, RUSSIA

The matrix of the Kainsaz (CO) carbonaceous chondrite accounts for a significant part of its volume. The fabric of the meteorite resembles the sideronitic textures of some mafic terrestrial rocks, whose silicate material is submerged in a iron-ore matrix. The part of silicate material is played in the chondrite by magnesian olivine-pyroxene and aluminous chondrules and their fragments. The iron-rich matrix is heterogeneous in texture and composition. We examined portions of the matrix that are least contaminated with fragments. In terms of crystallinity, the matrix material is clearly classified into two types: M1 is a highly crystalline matrix material with typical magmatic textures, it composes well defined separated patches; and M2 is a cryptocrystalline or fine-grained variety of matrix, which occurs around crystalline matrix portions, fills all interstices between magnesian chondrules, and intrudes and disintegrates them. Figures 1 - 4 demonstrate the main varieties of the matrix material.

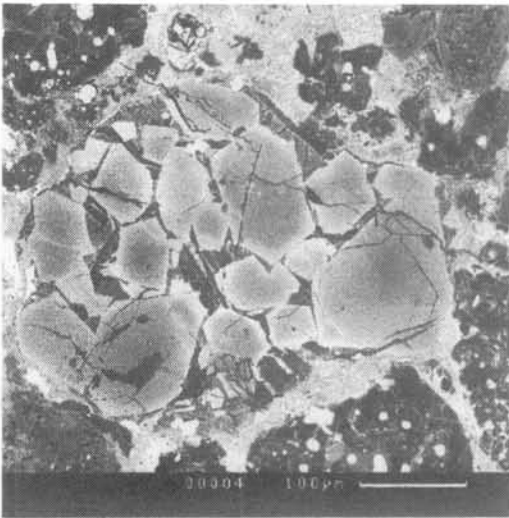


Fig. 1

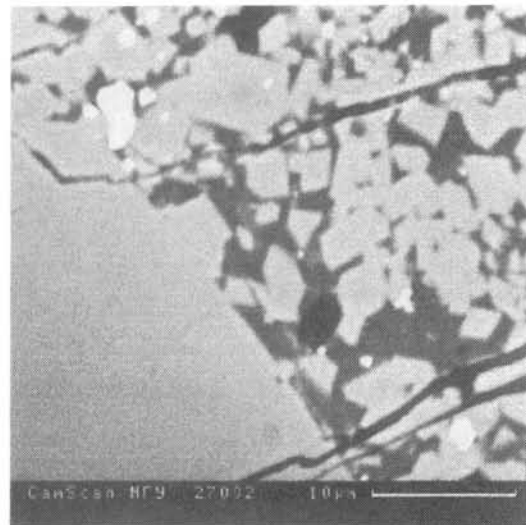


Fig. 2

The matrix of the type M1-a (Fig. 1) consists of chondrule-shaped porphyritic patches of zoned olivine phenocrysts and partly crystallized interstitial pyroxene-plagioclase glass. The boundaries between these segregation and the M2 matrix are sharp at contacts with the interstitial material but can hardly be discerned at contacts with olivine, whose composition in the outermost zones (Fa = 58-60) approaches the composition of the M2 matrix. The cores of zoned olivine grains compositionally approximate the olivine of magnesian chondrules of the meteorite: Fa = 10 - 12 and lower. The interstitial material of M1-a matrix segregations is high in alumina, alkalis, and phosphorus. The plagioclase quantitatively dominates over pyroxene, and the thin plagioclase laths are much more acid (An = 46-50) than the plagioclase in the magnesian chondrules (An = 80-85). Sometimes, the M1 matrix composes zone around a single large zoned olivine grain. In this case, a fine porphyritic texture develops, in which fine (2-3 mm) euhedral olivine crystals (Fa = 62-64) are equally distributed in glass of pyroxene-plagioclase composition (Fig. 2). The contents of the plagioclase component decreases towards the boundaries of the zones, and the rock grades into a cryptocrystalline M2 matrix. The bulk composition of these zones resembles

the composition of chondrule-shaped segregations and is practically the same as the bulk composition of the meteorite itself (analyses were taken by microprobe scanning over the surface of a thin section; Table 1, analyses 3, 4; Fig. 5).

The M1-b matrix is also porphyritic but differs by its very low contents of alumina and alkalis and, consequently, the predominantly olivine-pyroxene composition of the groundmass. Figure 3 demonstrates that the crystallization center was an irregularly shaped fragment of magnesian olivine (Fa = 12 in the core of the grain), which is overgrown by more ferrous olivine (Fa increases to 56 in the grain margin), which acquired an euhedral short-prismatic habit. The process of crystallization ended with an eutectoid olivine-pyroxene assemblage, whose olivine is slightly more ferrous (Fa = 58-60) and the pyroxene is augite. The boundaries between areas of the cryptocrystalline material and the matrix are almost indiscernible.

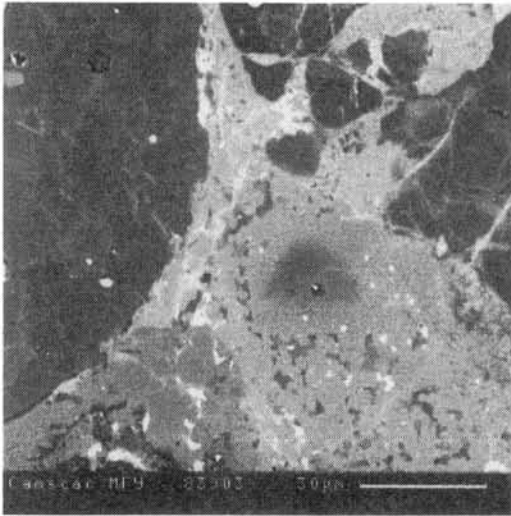


Fig. 3

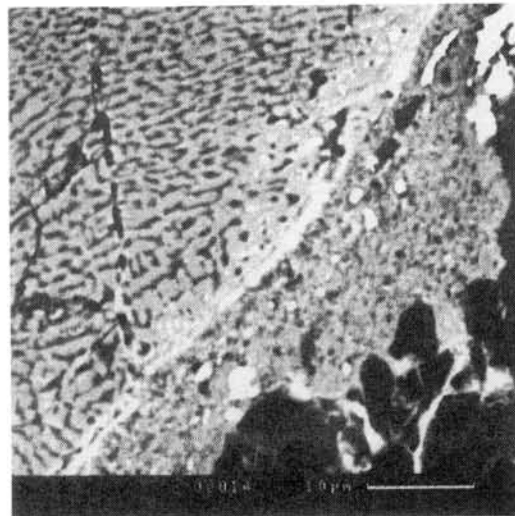


Fig. 4

In places, the M1-b matrix contains no xenoliths of magnesian chondrules and forms clearly separated chondrule-like eutectoid zones, whose texture strikingly differs from the cryptocrystalline matrix (Fig. 4). The olivine of these zones has the same composition as in the M2 matrix, although the bulk chemistry of the eutectoid zones differs from the composition of the cryptocrystalline matrix by somewhat elevated concentrations of Si and Mg (Table 1, analyses 5, 6). As can be seen from the diagram of Fig. 5, the composition of these zones is practically identical to that of the lower part of the compositional field of the M2 matrix.

The M2 matrix has a very fine-grained, nearly cryptic texture. The minerals that can be fairly reliably identified in it are fayalite (Fa = 75-77) and thin microlites of a metal, which are oriented in the direction of matrix movement. The matrix is generally highly permeable, a fact testifying to its high mobility.

Comparison between the average compositions of chondrules and the matrix (Table 1, Fig. 5) indicates that separation of the silicate mineral assemblages of the crystalline zones from the matrix resulted the strong depletion of the latter in Si, Mg, Al, alkalis and strong enrichment in Fe at the nearly unchanging contents of Ca in all varieties of the matrix material. The bulk composition of the residual matrix (M2: Table 1, no. 6), its low crystallinity and high permeability led us to conclude that the matrix was produced by the consolidation of a saturated iron-ore solution, which was in equilibrium with the M1

crystallization products but displayed strong chemical aggressiveness with respect to the magnesian chondrules of the reduced stage of meteorite differentiation. The alterations of the matrix composition apparently occurred in a series of discontinuous-continuous stages, during all of which stable silicate parageneses were separated from the iron-silicate melt, causing its differentiation with a systematic compositional evolution and the enrichment of the residual matter in the iron-ore component. Hence, the matrix provides evidence of the principal tendency in the differentiation of the meteoritic material into silicate and metallic constituents, a process that proceeded under highly oxidized conditions.

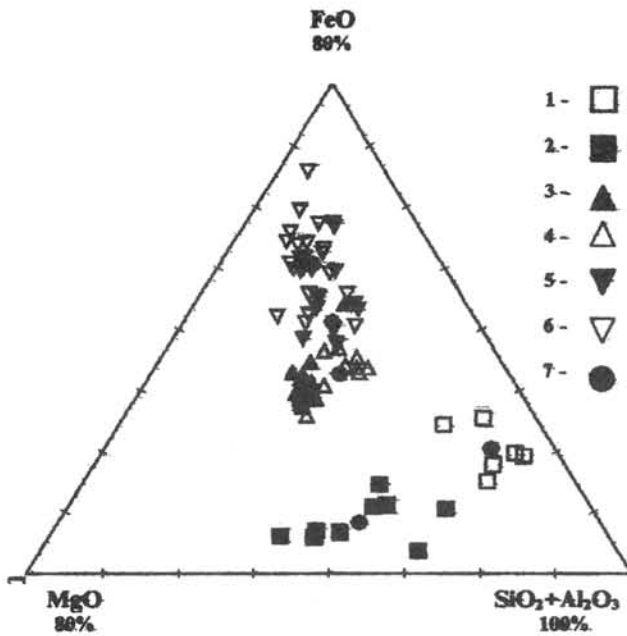


Fig. 5. Major-element plot showing the composition of the Kainsaz (CO) chondrite.
 1 - 2 - Chondrules: 1 - aluminous-alcic, 2 - magnesian;
 3 - bulk composition of the meteorite;
 4 - M1-a matrix;
 5 - M1-b matrix;
 6 - M2 matrix;
 7 - averaged compositions of chondrules and the matrix (Table 1).

Table 1.

Averaged composition of the chondrule and matrix material of the Kainsaz meteorite

	1	2	3	4	5	6
SiO ₂	27.05	50.84	35.54	37.48	35.72	28.12
TiO ₂	1.05	.26	-	-	-	-
Al ₂ O ₃	31.04	4.48	3.11	4.47	1.86	2.15
Cr ₂ O ₃	-	.58	.49	.35	.47	.33
FeO	16.64	7.78	28.93	30.6	39.03	47.74
MnO	-	.23	.17	.21	.39	.22
MgO	6.91	29.39	26.08	20.86	18.15	16.09
CaO	5.39	4.74	2.19	2.3	2.29	2.14
Na ₂ O	7.83	.69	.77	2.28	.87	.34
K ₂ O	1.36	-	-	-	-	-
P ₂ O ₅	-	-	.35	.42	.41	.3
S	1.13	.25	.82	.24	.23	.22
Ni	.47	.19	1.19	.45	.5	1.77

Note. Numbers 1-6 are the same as in Fig. 5

This study was financially supported by the Russian Universities - Basic Res. Foundation, Grant 5014.

Noble gases in five aubrites, Cumberland Falls, Mayo Belwa, Mt. Egerton, Norton County and Peña Blanca Spring

Yayoi N. Miura¹⁾, Keisuke Nagao²⁾ and Ryuji Okazaki^{2),3)}

¹⁾ Earthquake Research Institute, University of Tokyo, Yayoi, Bunkyo-ku, Tokyo 113-0032, Japan.

²⁾ Laboratory for Earthquake Chemistry, Graduate School of Science, University of Tokyo, Hongo, Bunkyo-ku, Tokyo 113-0033, Japan.

³⁾ Department of Earth and Planetary Sciences, Faculty of Science, Kyushu University, Hakozaki, Fukuoka 812-8581, Japan

Introduction Aubrites (enstatite achondrites) are composed of nearly Fe-O free enstatite with rare minerals formed under highly reducing conditions [1-3]. Aubrites would have been formed on parent body(ies) with highly reducing condition like enstatite chondrites via igneous processes. Relationship of aubrites to enstatite chondrites was suggested according to oxygen isotopic signatures, that is, enstatite chondrites and achondrites have been produced from a reservoir having the same oxygen isotopic compositions [4]. However, it is not clear so far whether the precursor of aubrites is known enstatite chondrites (*e.g.* [1]) or not (*e.g.* [3]). Here we measure noble gases in five aubrites, Cumberland Falls, Mayo Belwa, Mt. Egerton, Norton County and Peña Blanca Spring, in order to investigate cosmic-ray irradiation histories, trapped noble gas components and nucleogenic isotope signatures, which must be helpful to clarify relation between aubrites and enstatite chondrites. Light noble gases were reported previously for several aubrites (three aubrites among the five in this study except for Mayo Belwa and Mt. Egerton; *e.g.* [5]), whereas heavy noble gas data are limited for Norton County [6] and another aubrite Pesyanoe [7].

Samples and experiments Whole rock samples consisting of several small fragments with 0.1 - 0.2 g in total weights have been wrapped with Al foil, and set into a gas extraction/purification system connected to a modified VG5400 mass spectrometer. Noble gases were extracted at two temperatures of 700 °C and 1800 °C (only at 1800 °C for Mt. Egerton). The system and analytical procedures are essentially similar to those given in [8].

Results and discussion Isotopic compositions of He and Ne show that Ne is entirely cosmogenic for all the measured aubrites and He is also dominant in cosmogenic. Although it has been reported that some aubrites contain large amounts of solar type noble gases [5, 7], the measured five aubrites do not contain. Mayo Belwa and Cumberland Falls have lower $^3\text{He}/^4\text{He}$ ratios (~ 0.1) than the typical pure cosmogenic one (~ 0.2), which is likely due to addition of radiogenic ^4He or possibly small contribution of solar He. Measured Ar is a mixture of cosmogenic, trapped and radiogenic ^{40}Ar . Table 1 summaries cosmogenic light noble gases and the cosmic-ray exposure ages obtained based on cosmogenic ^3He and ^{21}Ne (T_3 and T_{21}). Because of uncertainty for the target element abundances and dependence of P_{38} on them, T_{38}

could not be determined. Internal discrepancies between T_3 and T_{21} are observed except for Mayo Belwa. The reason may be that the production rates adopted in the present study are not suitable for these aubrites or they have complex irradiation histories. Shorter ages of T_3 for Cumberland Falls and Mt. Egerton might have been caused by loss of cosmogenic ^3He .

Cosmogenic ^{81}Kr (a half life = 2.1×10^5 years) has been detected for Cumberland Falls and Mayo Belwa. The concentration of ^{81}Kr is less than the detection limit, $\sim 6 \times 10^{-16}$ cm^3STP for ^{81}Kr , for the other measured aubrites, for which the concentrations are $< (3 - 5) \times 10^{-15}$ $\text{cm}^3\text{STP/g}$. On the basis of ^{81}Kr and other cosmogenic Kr, ^{81}Kr -Kr exposure ages are obtained (Table 1). Mayo Belwa gives an accurate T_{81} of 113 ± 17 Ma, which agrees with T_3 and T_{21} . Mayo Belwa and Norton County have characteristically long cosmic-ray exposure ages among stony meteorites. Any enstatite chondrite with such long exposure age was not found; the fact may imply that parent body(ies) for aubrites is different from those of enstatite chondrites as suggested by [3].

Trapped Ar, Kr and Xe for four aubrites (excepting Cumberland Falls) indicate the terrestrial atmosphere - like elemental compositions. After subtracting cosmogenic components (for this, a two component mixing between the terrestrial atmosphere and cosmogenic is assumed), elemental compositions of trapped Ar, Kr and Xe plot near that of the terrestrial atmosphere with slight fractionation favoring heavier noble gases on the diagram of $^{36}\text{Ar}/^{132}\text{Xe}$ versus $^{84}\text{Kr}/^{132}\text{Xe}$. Contribution of adsorbed terrestrial atmosphere may account for the trapped noble gases in the four aubrites. On the other hand, one aubrite, Cumberland Falls, plots between Ar rich (sub-solar) and planetary type components. Isotopic compositions of trapped Kr and Xe of this aubrite is, however, not clear at present, because contribution of cosmogenic and fissionogenic Xe is significant. Figure 1 shows the three-isotope-plot of $^{134}\text{Xe}/^{132}\text{Xe}$ versus $^{136}\text{Xe}/^{132}\text{Xe}$. Although two fractions (1800 °C of Mayo Belwa and 1800 °C of Peña Blanca Spring) are plotted below the terrestrial atmospheric Xe, these can be explained by addition of cosmogenic ^{132}Xe . Four aubrites except Cumberland Falls have trapped Xe similar to the terrestrial atmosphere in isotopic compositions. Xenon released at 1800 °C of Cumberland Falls shows notable amounts of excess ^{134}Xe and ^{136}Xe ; the data plot near the direction of ^{238}U -derived fission Xe on Fig. 1. However, if we consider possible contribution of cosmogenic ^{132}Xe based on other cosmogenic Xe isotopes (e.g. ^{126}Xe), the Xe data point shifts to the circular area between ^{244}Pu -derived and ^{238}U -derived fission Xe lines. Though the concentration of excess ^{136}Xe is slightly variable depending on the trapped Xe component, the lower limit is calculated to be 3.2×10^{-13} $\text{cm}^3\text{STP/g}$. This concentration corresponds to 93 ppb of ^{238}U (at present) assuming the 4.5 Ga retention age. This calculated U abundance is several times higher than the U content in the bulk Cumberland Fall reported in [9].

References

- [1] Watters T.R. and Prinz M. (1979) *Proc. Lunar Planet. Sci. Conf. 10th*, 1073-1093. [2] Okada A. *et al.* (1989) *Meteoritics* **23**, 59-74. [3] Keil K. (1989) *Meteoritics* **23**, 195-208. [4] Clayton R.N. (1993) *GCA* **69**, 1999-2017. [5] Eberhardt P. *et al.* (1965) *JGR* **79**, 4427-4434; Zähringer J. (1968) *GCA* **32**, 209-237. [6] Munk M.N. (1967) *EPSL* **3**, 457-465. [7] Marti K. (1969) *Science* **166**, 1263-1265; Kim and Marti (1992) *Lunar Planet. Sci.* **XXIII**, 689. [8] Miura Y.N. *et al.* (1998) *GCA* **62**, 2369-2387. [9] Shimaoka T. *et al.* (1995) *Lunar Planet. Sci.* **XXVI**, 1291-1292. [10] Eugster (1988) *GCA* **52**, 1649-1662. [11] Swindle (1988) *Meteorites and the Early Solar System*, pp. 535-564, Univ. of Arizona Press; Huss *et al.* (1996) *GCA* **56**, 3311-3340.

Table 1. Concentrations of cosmogenic noble gases, cosmic-ray exposure ages and concentration of trapped ^{132}Xe in the measured aubrites.

	^3He	^{21}Ne	^{38}Ar	T_3	T_{21}	T_{81}	$[\text{Xe}]_t$
	$10^{-9}\text{cm}^3\text{STP/g}$			Ma			$10^{-12}\text{cm}^3\text{STP/g}$
Cumberland Falls	272	253	4.48	16	56	40 ± 18	3.2
Mayo Belwa	1800	490	18.7	104	119	113 ± 17	9.4
Mt. Egerton	163	104	1.58	9.3	23	n.d.	33
Norton County	2650	615	24.8	150	110	n.d.	5.2
Peña Blanca Spring	712	77.4	3.01	41	20	n.d.	4.2

The production rates of cosmogenic ^3He and ^{21}Ne were calculated based on the formula presented in [10]. Correction about chemical compositions was applied for Mayo Belwa, Norton County and Peña Blanca Spring using literature data, and shielding correction using $(^{22}\text{Ne}/^{21}\text{Ne})_c$ was applied for the five aubrites.

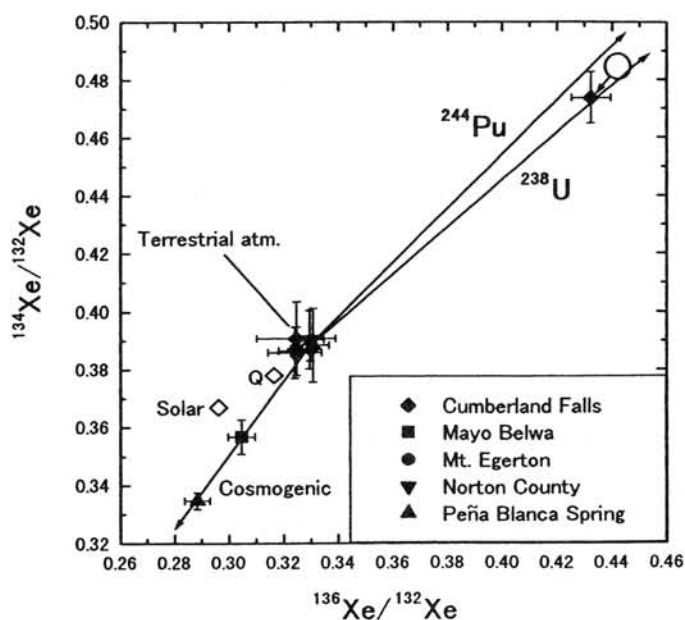


Fig. 1. Plot of $^{134}\text{Xe}/^{132}\text{Xe}$ vs. $^{136}\text{Xe}/^{132}\text{Xe}$ for the measured aubrites with the meteoritic and terrestrial Xe as references [11]. The directions of ^{238}U -derived and ^{244}Pu -derived fission Xe and cosmogenic Xe are also shown. The circle near Cumberland Falls (at right upper side) shows an estimated area excluding cosmogenic ^{132}Xe .

A short period of chondrule formation: The ^{26}Al - ^{26}Mg evidence from two type II chondrules in a highly unequilibrated ordinary chondrite

Smail Mostefaoui*, Noriko T. Kita*, Hiroko Nagahara[†],
Shigeo Togashi*, and Yuichi Morishita*

**Geological survey of Japan, 1-1-3 Higashi, Tsukuba 305-8567, Japan*

[†]*Geological Institute, University of Tokyo, Hongo, Tokyo 113-0033, Japan.*

Introduction: One of the mostly debated subjects in meteoritics is the origin of chondrules, their heating mechanisms, and the timing scales of their formation. Relative chronometer based on the decay of the extinct radionuclide ^{26}Al (half life = 0.73 My) applied to individual chondrules from different chondrites will determine the period of chondrule formation. In our previous work, [1-2], five ferromagnesian chondrules from the least equilibrated chondrite Semarkona (LL3.0) showed a narrow range of the initial $^{26}\text{Al}/^{27}\text{Al}$ ratios = $(4-9) \times 10^{-6}$, indicating that these chondrules formed within a period of 1 My. Their formation time was nearly 2 My later than CAIs ($^{26}\text{Al}/^{27}\text{Al} = 4.5 \times 10^{-6}$, [3]) if the $^{26}\text{Al}/^{27}\text{Al}$ ratio in the solar system was homogeneous in the beginning. Compared to the Semarkona chondrules, many Al-rich chondrules from Chainpur (LL3.4) showed significantly lower initial $^{26}\text{Al}/^{27}\text{Al}$ ratio of $< 10^{-6}$ [4-5], implying that the Al-Mg system in chondrules was easily disturbed by the thermal metamorphism in the parent body, even for the unequilibrated chondrites of type 3.4 [1-2].

In this work we continue studying the Al-Mg system in ferromagnesian chondrules containing mesostasis with high Al/Mg ratios in other chondrites. In order to avoid the problem of the disturbance of the isotopic systematics in the parent body, we looked for the less metamorphosed chondrite members. We chose Bishunpur (LL3.1), which is one of the most primitive ordinary chondrites. Although much work has been performed for this meteorite in order to understand the early evolution of the solar system [e.g. 6], no ^{26}Al - ^{26}Mg data were available for their chondrules.

Samples and experiments: Two type II chondrules (C4, 1.0×1.2 mm; and C18, 0.8×1.1 mm) were examined in a polished thin section of Bishunpur (M3816, Natural History Museum, Vienna). Both chondrules show a porphyritic structure. C4 is a porphyritic-pyroxene (PP) chondrule, and C18 a porphyritic-olivine-pyroxene (POP). Pyroxene in C4 has a coarse structure. C18 shows a coarse, barred texture consisting of elongated laths of pyroxene intergrown with olivine. Quantitative analyses of major elements in minerals and glasses were performed using an electron microprobe (JEOL JXA-8800R). Pyroxene composition in C4 is (Wo₃En₈₂Fs₁₅) and in

C18 is (Wo15En66Fs19- Wo6En75Fs19). Olivine in C18 is FeO-rich (Fo=76-78). Mesostasis surfaces in both chondrules are relatively small, but in C4 are larger and more abundant than that in C18. Electron microprobe analysis of the mesostasis in both chondrules indicated the presence of plagioclase (An91Ab9 in C18 and An90Ab10 in C4). They contain a significant amount of fine-grained inclusions having Ca-pyroxene composition. For SIMS measurements we selected plagioclase which have high Al/Mg ratios (~50) in order to detect the ^{26}Mg excess. We used the Cameca IMS 1270 at the Geological Survey of Japan for SIMS analysis [1-2]. The primary ion of O_2^- was shaped to a diameter of ~5 μm . The generally presence of the Ca-pyroxene inclusions in plagioclase makes it difficult to avoid the high Mg ion intensity from the inclusions. We carefully selected the areas that are free of the Ca-pyroxene inclusions by observing the Al and Mg ion images before each analysis. The mass resolution was set to 3500 in order to separate MgH^+ and Ca^{++} interferences from Mg isotopes. The measured $^{26}\text{Mg}/^{24}\text{Mg}$ ratios were corrected for mass fractionation, and terrestrial standards were analyzed in order to evaluate the accuracy of Mg isotopic ratios and matrix effect on measured $^{27}\text{Al}/^{24}\text{Mg}$.

Results and discussion: The measured $^{27}\text{Al}/^{24}\text{Mg}$ ratios vary from 30 to 60 with ^{26}Mg excess up to 6 ‰. The initial $^{26}\text{Al}/^{27}\text{Al}$ ratios for the two chondrules were estimated from the slope of the isochron with assuming that the initial Mg isotopic ratios in chondrules were the same as in terrestrial standards. The initial $^{26}\text{Al}/^{27}\text{Al}$ ratios are estimated to be $(9.7 \pm 4.9) \times 10^{-6}$ in C4, and $(5.4 \pm 5.2) \times 10^{-6}$ in C18. The formation ages relative to CAIs were calculated to be 1.6 (+0.7/-0.4) My for C4, and 2.2 (+3.5/-0.7) My for C18. This is the first evidence for live- ^{26}Al from chondrules in Bishunpur. Because of the relatively large errors, the age difference between these two chondrules can not be distinguished within the analytical error (2σ). These data are in the same range of ferromagnesian chondrules in Semarkona. This indicates that ferromagnesian chondrules in both LL chondrites (Semarkona and Bishunpur) formed contemporary within a short period (~1 My). More data from a variety of chondrule types are necessary for understanding the relationship between the formation times of chondrules and their properties, such as petrology, bulk chemistry, and oxygen isotopes. The Al-Mg isotopic systematic of chondrules of different types are now in progress, and further results will probably clarify such a relationship to be more conclusive.

References: [1] Kita N. T. et al. (1998) *Meteoritic & planet. Sci.* A83. [2] Kita N. T. et al. (1999) in preparation. [3] McPherson et al. (1995) *Meteoritics* 30, 365-386. [4] Russell S. S et al. (1996) *Science* 273, 757-762. [5] Russell S. S et al. (1997) *Lunar Planet. Sci.* XXVIII, 1209-1210. [6] Rambaldi E. R. and Wasson J. T. (1981) *GCA* 45, 1001-1015.

CHONDRULE FORMATION BY CONDENSATION OF MAJOR ELEMENTS. H. Nagahara¹, N. T. Kita², K. Ozawa³, and Y. Morishita⁴, ¹Geol. Inst., Univ. Tokyo, Hongo, Tokyo 113-0033, Japan (hiroko@geol.s.u-tokyo.ac.jp), ²Geol. Surv. Japan, Tsukuba, Ibaraki, 305-8567, Japan (noriko@gsj.go.jp), ³Inst. Study Earth's Inter., Okayama U., Misasa, Tottori 682-0193, Japan, ⁴Geol. Surv. Japan.

Introduction: Formation of chondrules in an open system has been now widely accepted, but the knowledge has been limited to volatile elements, such as volatile loss in type IA or A1 chondrules and volatile addition during or after cooling [1-4]. In the present study, we found evidence for major element condensation that is directly related to chondrule formation. We further estimated the conditions of crystallization and cooling.

Observation: Chondrules studied are CH5 and CH13 from Semarkona (USMN 1805-9), which are characterized by highly refractory compositions, anomalous porphyritic texture, and perfectly rounded shape. CH5 is about 800 μ m and CH13 500 μ m in diameter, and both consist of forsterite and glass. Forsterite is euhedral to partly hopper suggesting fairly rapid cooling, and are rimming the inner surface of the chondrule. The modal abundance of forsterite is much less in the center.

Both CH5 and CH13 are highly refractory in bulk composition; forsterite is poor in FeO (<1.0 wt%), and glass is rich in CaO and Al₂O₃. The concentration of trace elements (FeO, CaO, and Al₂O₃) in forsterite is similar to those in other type IA or group A1 chondrules [5,6]. Forsterite is zoned regarding trace elements: Al₂O₃ and CaO decrease and FeO increases from the core to the rim. This represents either crystallization in lowering temperature or the change of melt composition from highly to less refractory during crystallization.

The glass is also zoned, where Al₂O₃, CaO, MgO and TiO₂ decrease and SiO₂, Na₂O, K₂O and FeO increase from the center to the surface. Strong depletion of MgO and enrichment of Al₂O₃ are observed around forsterite, but the distribution of SiO₂, CaO and Na₂O appears to be unaffected by the presence of forsterite. SiO₂ decreases monotonously from the surface to the center, whereas Na₂O and K₂O are enriched only near the surface. Na₂O is specifically enriched along perlitic cracks that resemble those in rhyolite glass formed by cooling contraction or expansion due to hydration. Two different compositional correlation among elements are recognized for the glass. One is a trend for the entire chondrules: Al₂O₃ and MgO decrease with increasing SiO₂ from ~48 wt. to 57 wt. The other is a trend for the surrounding area of forsterite crystals: Al₂O₃ decreases and MgO increases rapidly with small increase of SiO₂ (47-48 wt%).

Mg isotopic compositions were obtained with Cameca IMS-1270 SIMS at Geological Survey, Japan, with reference of ²⁵Mg/²⁴Mg of 0.12663 [7] and ²⁶Mg/²⁴Mg of 0.139354, the mean value of mass fractionation corrected from the terrestrial standards. The measured Mg isotopic ratios of forsterite and glass are between -3 and -4 permil/amu and +0.5 and +2 permil/amu, respectively, which are in the similar ranges for the instrumental mass fractionation of the terrestrial olivine and glass standards. Therefore, Mg isotopes of forsterite and glass are assumed to be unfractionated. Mg isotopic ratio of glass in CH5 and CH13 are constant regardless of location within the chondrules and the difference in chemical compositions. The Mg isotopic composition of forsterite is related to the Al₂O₃ concentration, which is heavier in the Al₂O₃-rich portion and lighter in the poor region. The

higher Al_2O_3 content are located in the center of forsterite crystals, suggesting that Mg isotopic composition changed during crystallization of forsterites.

Discussion: Crystallization of forsterite in a closed system does not explain the observed elemental distribution. The two compositional trends within a chondrule requires two different mechanisms. The Al_2O_3 enrichment and MgO depletion around forsterite are due to forsterite crystallization, but the significant SiO_2 enrichment toward outside is not. A simple evaporation process does not explain the observation, because SiO_2 , the most volatile element among four major elements, is enriched at the rim. Therefore, the chondrules should have undergone a condensation process during cooling. Isotopically heavier Mg remains in the core of forsterite crystals, but in forsterite rim and in the glass, it is diluted by isotopically lighter Mg that condensed in the later stage. SiO_2 condensation continued after forsterite crystallization, because SiO_2 concentration is higher in the portion where glass is directly facing the chondrule wall than the portion where forsterite directly grows from. Highly homogeneous distribution of CaO is due to rapid diffusion of CaO in silicate melt [8]. Na_2O and K_2O condensation took place at lower temperatures than SiO_2 , because their diffusion penetration distance is smaller than that of SiO_2 in spite of much larger diffusion coefficients of those elements than Si in silicate melt [9].

Formation condition of CH5 and CH13 is examined from equilibrium and kinetic points of view. The crystallization temperature was estimated by equilibrium calculation with thermochemical data by Berman [10]. The liquidus temperature of forsterite for the present glass composition is about 1290°C for the central portion of the chondrule and 1100°C for the rim portion. The chondrules are thought to have been heated at temperature $\sim 1300^\circ\text{C}$, and if the effect of supercooling in a kinetic condition is taken into consideration, crystallization of forsterite should have taken place below this temperature. Crystallization of forsterite continued to temperatures below 1100°C . The liquidus temperature of protoenstatite is above that of forsterite at the rim. Protoenstatite, however, is not present in CH5 and CH13, suggesting that cooling of the chondrules was rapid enough to suppress the reaction of forsterite and melt to form protoenstatite. The cooling condition was estimated by using the SiO_2 zoning profile in the glass portion. Assuming a constant surface SiO_2 composition, binary effective diffusion coefficient of Si by Zhang [11], linear cooling, and initial temperature of 1300°C that is inferred from the maximum liquidus temperature, the time required for SiO_2 coming from outside to reach the center of the sphere was obtained. The cooling rate obtained is $0.02^\circ/\text{sec}$ ($72^\circ/\text{hour}$) from 1300°C to 1000°C . At 1000°C , elemental diffusion becomes very slow and therefore the SiO_2 zoning profile was frozen. Because the minimum time for SiO_2 to reach the sphere center was estimated, this is the maximum rate estimation. The cooling rate could be smaller if the SiO_2 concentration of the chondrule center was lower than the present value when SiO_2 diffusion just reached there. The obtained cooling rate is consistent with the timescale of “flash melting” at higher temperatures.

Conclusions: Evidence for direct condensation of SiO_2 and MgO that is directly responsible for chondrule formation is found in Semarkona chondrules. Although the history below crystallization of forsterite is roughly estimated, the earlier history of the chondrules has been still unclear. Relationship to the origin of other common chondrules is a serious problem. For quantitative understanding of the chondrule formation and ambient nebular conditions as a temperature and time sequence, isotopic data for other elements, particularly for Si and O, and age information will be necessary.

References: [1] Alexander, C.M.O'D. (1996) in Chondrules and the protoplanetary disk, 233-241, [2] Sears, D.W.G. et al. (1996), *ibid.*, 221-231, [3] Noguchi, T. (1989) Proc. NIPR Symp. Antarct. Met. 2, 169-199, [4] Matsunami, S. et al. (1993) GCA 57, 2101-2110, [5] Jones, R.H. and Scott, E.R.D. (1989) Proc. 19th LPSC 523-536, [6] DeHart, J.M. et al. (1992) GCA 56, 3791-3807, [7] Catanzaro, E.J. et al. (1966) J. Res. Nat. Bur. Standards 70a, 453, [8] Liang, Y., et al. (1996) GCA 60, 4353-4367, [9] Henderson, P. et al. (1985) CMP 89, 263-272, [10] Berman, R. G. (1983) Ph. D. thesis, Univ. Chicago, [11] Zhang, Y. et al. (1989) CMP 102, 492-513.

Cosmogenic ^{10}Be and ^{26}Al in Iron Meteorites and the Inclusions.

H. Nagai, M. Kokubo, T. Kobayashi, and M. Honda

Nihon University, Department of Chemistry, Sakura-josui, Setagaya, Tokyo 156-8550

Introduction:

^{10}Be ($T_{1/2}$: 1.5my) and ^{26}Al (0.7my) are popular members of long-lived cosmogenic radio-activities in meteorites. Many iron meteorites have been irradiated continuously in space by galactic cosmic rays for longer than 100 million years. There are groups of large size objects, which have been recovered with more than ten thousand kilogram. After the long irradiation, these nuclides reached to their saturation levels, and the local samples have been shielded at various extents depending on the depth inside the meteoroid. In general, shielding effects are functions of depth and size of the objects. In an extremely large meteorite, however, the function can simply be approximated to that of 2π geometry, and the products can be compared directly as the functions of depth only. On the other hand, the contents of the products are getting very low with depths. By a recently developed highly sensitive detection method, accelerator mass-spectrometry (AMS), the lowest level activities can be determined even at deeper than 1000 g/cm² where the production rates may be estimated to about 1/1000 relative to those at near surface or those of smaller meteorites.

Besides Fe-Ni alloy, some iron meteorites are known to contain inclusions composing carbon, phosphorus, sulfur, chromium, and silicates. For productions of smaller mass nuclides these inclusions are important targets because the mass differences between target and the products are small and the production rates are much higher in the high energy nuclear reactions. It is well known that in stony meteorites, especially chondrites, productions of ^{26}Al and also ^{10}Be are 20 and 5 times higher respectively than in the Fe-Ni of irons. Extremely high production of ^{10}Be in carbon, about 30 times, has already been reported (Nagai et al.1993). The presence of Si and Al is responsible to an enhancement of ^{26}Al production, and oxygen is important to ^{14}C and ^{10}Be . A higher ^{26}Al in Mundrabilla troilite relative to Fe-Ni has been pointed out (Aylmer et al. 1988).

It has been known that the productions of ^{26}Al relative to those of ^{10}Be in iron meteorites are always close to 1 but slightly lower (Microvich et al.1994, Xue et al.1995). Fig.1 is illustrating the situation with several examples of iron meteorites. Some of them are smaller meteorites such as Grant IIIB, Henbury IIIA, Nativitas IIIA, Treysa IIIB, and Warburton Range, Ni rich ataxite. Others are popular large irons such as Campo del Cielo IA, Canyon Diablo IA, Cape York IIIA, Gibeon IVA, Odessa IA, and Sikhote Alin IIB. Throughout these irons, especially with various fragments of Gibeon, we realize that the ratios of $^{26}\text{Al}/^{10}\text{Be}$ are fairly constant at 0.75 ± 0.13 (1σ), $n=27$, or including metal phases in stony irons, 0.71 ± 0.13 , $n=55$. (More than 30 metallic samples separated from chondrites gave the similar results.) A linear relation between contents in logarithmic scales is drawn covering a range from 6 (small irons) to 0.0004 (Gibeon) $\text{dpm}^{10}\text{Be}/\text{kg}$ (Nagai et al. 1993, Nishiizumi et al. 1995) even for examples of the heaviest shielding.

High ^{26}Al productions in the inclusions.

Some non-magnetic dark sulfide inclusions have been taken mechanically from the sliced pieces of large irons, Odessa, Canyon Diablo, Cape York, and Toluca. The chemical compositions were examined non-destructively by neutron activation method. The S content was determined with ^{37}S , $t_{1/2}$: 5.0min, 3104keV γ . Some spherical sulfide samples of three Odessa fragments contain 0.9-1.1 %Cr, 500-800 ppmMn, and lower levels of Ni and Co(200-290ppm), whereas Fe and sulfur are at 49-63 and 42-31 % respectively. Cape York and Toluca samples gave lower than 27%S indicating their impurities. Some preliminary samplings for meteoritic phosphides (Buchwald,1975, Jochum et al.1980) were also made for Odessa and Toluca. 5 gram size metallic pieces were dissolved in dilute acids and insoluble fine grains were collected. Thus 0.25g magnetic fraction, composing Ni/Fe = 0.2 but low Cr and Mn, was recovered from Odessa, which was dissolved in aqua regia, and treated as the schreibersite.

Table 1 shows that the ratios of $^{26}\text{Al}/^{10}\text{Be}$ are substantially higher in the inclusions than those in the Fe-Ni. On the other hand, ^{10}Be in Fe-Ni of Odessa 98 seem to be similar in both inclusions. When the sulfides contain some carbon, such as in Landes IA, the situation can be different. More data with better sample characterizations are necessary to systematize relations between targets and shielding effects.

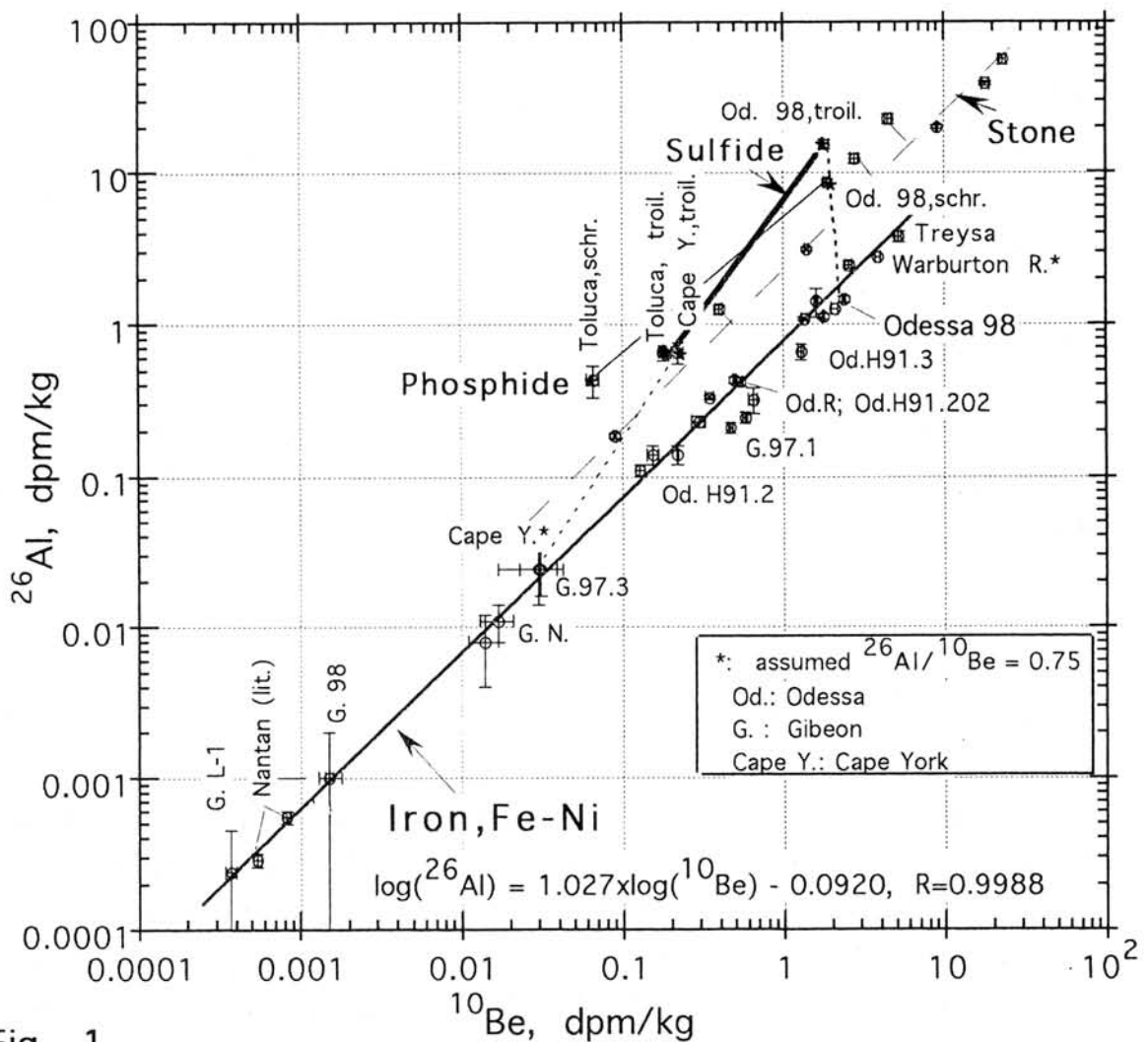


Fig. 1

Table 1. Productions found in Inclusions Relative to Fe-Ni

Sample, ID	Inclusion	^{26}Al dpm/kg	^{10}Be dpm/kg	Inclusion / Fe-Ni* $^{26}\text{Al}/^{10}\text{Be}$
Odessa, 98	sulfide,41%S	15.4±1.1	1.81±0.11	11
Odessa, 98	phosphide	8.6±0.7	2.1±0.1	5.5
Cape York, 97	sulfide,27%S	0.66±0.09	0.18±0.01	4.9
Toluca, 98	sulfide,crude	0.65±0.10	0.22±0.02	3.9
Toluca, 98	phosphide	0.41±0.08	0.074±0.013	7.4

*: 0.75 is assumed in Fe-Ni.

References: Aylmer et al. (1988) *EPSL* **88** 107, Buchwald (1975) *Handbook of Iron Meteorites*, Jochum et al. (1980) *Z. Naturf.* **35a** 57, Michlovich et al. (1994) *J. Geophys. R.* **99**, 187, Nagai et al. (1993) *Geochim.* **57**, 3705, Nishiizumi et al. (1995) *Meteoritics* **30** 556, Xue et al. (1995) *Meteoritics* **30** 303

Characterization of cosmic dust samples by Synchrotron Radiation X-ray fluorescence analysis

○ Izumi Nakai¹ • Nahoko Kondo¹ • Miho Sasaki¹ • Yasuko Terada¹ • Kentaro Terada² • Takaaki Noguchi³ and Tomoki Nakamura⁴

1) Dept. of Applied Chemistry, Sci. Univ. of Tokyo, Kagurazaka, Shinjyuku, Tokyo 162-0825, Japan

2) Dept. of Earth and Planet. System Sci., Hiroshima Univ., 1-3-1 Kagamiyama, Higashihiroshima 739-8526, Japan

3) Dept. of Materials and Biological Sci., Ibaraki Univ., Bunkyo 2-1-1, Mito 310-8512, Ibaraki, Japan

4) Earth and Planetary Sci., Kyushu Univ., Hakozaki Fukuoka 812-8581, Japan

This study has been made as a consortium study for the Antarctic micrometeorites (AMMs) (Nakamura et al, 1999). There are two purposes on this research. One is to carry out an initial characterization of the AMMs, which were collected at the Dome Fuji Station. The AMM working group is conducting a joint examination on the AMMs by various analytical methods such as EPMA, SIMS, INAA, etc., among which our XRF analysis comes to the first because of the nondestructive nature of this method. Another purpose is to try to classify the cosmic dusts by their trace element compositions. Because of the extremely small sizes of the samples, it is difficult to classify the cosmic dust by mineral identification through microscopic observation and XMA technique. Therefore, it is useful if one can classify the sample based on the nondestructive chemical analysis. This classification also helps to study the origin of the cosmic dusts. We have utilized the synchrotron radiation (SR) as an excitation source of the XRF analysis because of the high sensitivity of the technique.

Samples include unmelted AMM collected at the Dome Fuji Station in 1996. The cosmic spherules from Antarctica and deep sea sediments are also examined. Based on the S/Si intensity ratios measured by SEM-EDS, the unmelted AMMs were divided into three groups; "group 1" (most important, least heated): AMMs with the S/Si ratios (r) similar to those of CM chondrites ($r = 0.1 \sim 0.2$); "group 2" (moderately heated): those with $r = 0.05 \sim 0.1$ and > 0.2 ; "group 3" (heavily heated) : those with $r < 0.05$. SR-XRF measurements were made at BL-4A of Photon Factory, Tsukuba using monochromatized radiation (X-ray energy: 10, 19 or 20.55keV) with Si(111) double crystals. XRF spectra were measured with Si(Li)-SSD for 600 to 1000 sec. The net intensities of the XRF spectrum of each element were calculated.

Figure 1 shows some examples of the spectra of the I-type(a), S-type (b) and unmelted AMM of the group 1(c). The compositions of the trace elements for the I-type spherules are characterized by the presence of Mo and Rb and the absence of Ca, Mn, Cu, Se, Sr, Y, and Zr, while those of the S-type spherules are characterized by the abundance of Ca and Mn and the lack of Mo, Rb with minor Sr, Y, and Zr. On the other hand, unmelted AMMs contain

significant amounts of Cu and Se, which exhibit positive correlation with the S/Si ratio. They also contain minor Pb and Y, while Rb and Mo are almost absent. Table 1 shows a summary of this tendency. SR-XRF is particularly sensitive to the trace heavy elements such as Rb, Sr, Y, Zr, Mo, which have large ionic radii or high ionic charges and exhibit characteristic behavior during cosmochemical processes. Therefore, these elements could become fingerprints for classification of the cosmic dusts and for estimation of their origin. The present analysis indicates that these elements exhibit characteristic distribution to each group and that this approach is hopeful. A further study including statistical analysis is now underway.

References Nakamura et al. (1999) Antarctic Meteorite Res., 12, in press.

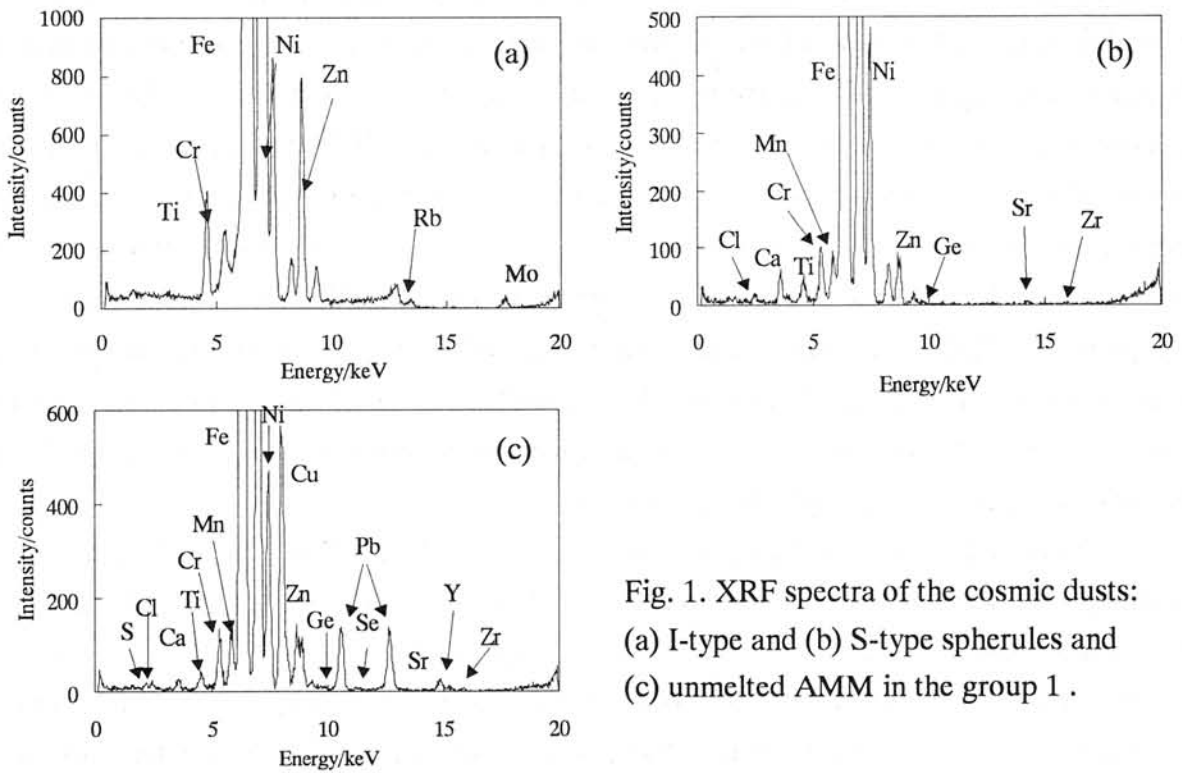


Fig. 1. XRF spectra of the cosmic dusts: (a) I-type and (b) S-type spherules and (c) unmelted AMM in the group 1 .

Table 1. Summary of the characteristic of the trace element chemistry for the cosmic dust samples.

		S	Cu•Se	Pb•Y	Mn•Sr•Zr	Zn	Rb•Mo
Spherules	S-Type	-	Deficient		Concentrate	Concentrate	Deficient
	I-Type	-	Deficient		Deficient	Concentrate	Concentrate
AMMs	S/Si	Group 1: 10-20 %	▼	Present	No Tendency		Deficient
		Group 2: 5-10 %					
		Group 3: under 5 %					

CONSORTIUM STUDIES OF FIVE ANTARCTIC RUMURUTI-GROUP CHONDRITES: A PROGRESS REPORT

Noboru Nakamura (1,2), Shinobu Sawada(2), Minako Tamaki(1), Gabor Kondorosi(2),
Naoya Imae(3), Hideyasu Kojima(3), Robert N. Clayton(4,5) and Toshiko K. Mayeda(4)

(1) Department of Earth & Planetary Sciences, Faculty of Science, Kobe University (2) Graduate School of Science and Technology, Kobe University; (3) Department of Antarctic Meteorites, National Institute of Polar Research; (4) Enrico Fermi Institute, University of Chicago; (5) Also at Department of Chemistry and Department of the Geophysical Sciences, University of Chicago

In order to obtain better understanding of the origin and evolution of Rumuruti (R)-group chondrites, (mini) consortium studies have been undertaken on five Antarctic R-chondrites (Y-791827, Y-793575, Y-82002, A-881988, Y-75302). Preliminary results of petrography and major element chemical compositions have been reported in [1]. In addition, results of rare gas analyses and K-Ar age determinations and those of INAA and ICP-MS were also reported at the last symposium [2,3]. We have been continuously making efforts to clarify the trace element chemical features and Rb-Sr isotopic characteristics, and here we report preliminary results and, also, revisited oxygen isotopic compositions.

The oxygen isotopic analyses were carried out at the University of Chicago and the preliminary results were reported at the last symposium. Because of peculiar result for the specimen Y-793575 (chip 106), a new analysis of Y-793575 (chip 105) was carried out, as well as a re-analysis of the earlier sample. The new results together with those of other four meteorites are shown in Fig.1. We now confirm that all five meteorites under investigation have R-chondrite composition.

For trace element and Rb-Sr isotopic analyses, about 20 mg-sized aliquots of the powder samples (125-200mg of sizes) were acid-decomposed and subjected to isotope dilution analyses of REE, alkalis and alkaline earths and Rb-Sr isotopic analyses. Results are shown in Fig. 2. Four R-chondrites have generally flat REE-patterns and absolute lithophile-abundances are mostly within the range of ordinary chondrites [4]. However, a careful inspection indicates that they are more or less fractionated compared to each other. Somewhat L-REE depleted features are clearly recognizable, which is the first case reported for R-chondrites.

Alkali- (typically Rb-) abundances are variable and generally parallel with absolute REE-abundances and Al-contents [1]. On the other hand, two trace alkaline earths (Sr and Ba) are rather uniform in abundance and generally consistent with Mg [1].

References: [1] H. Kojima et al. (1998) *Antarctic Meteorites XXIII* 54-57. [2] K. Nagao et al. (1998) *Antarctic Meteorites XXIII* 101-103. [3] H. Ozaki et al. (1998) *Antarctic Meteorites XXIII* 123-125. [4] G. Kallemeyn et al. (1996) *Geochim. Cosmochim. Acta* 60, 2243-2256.

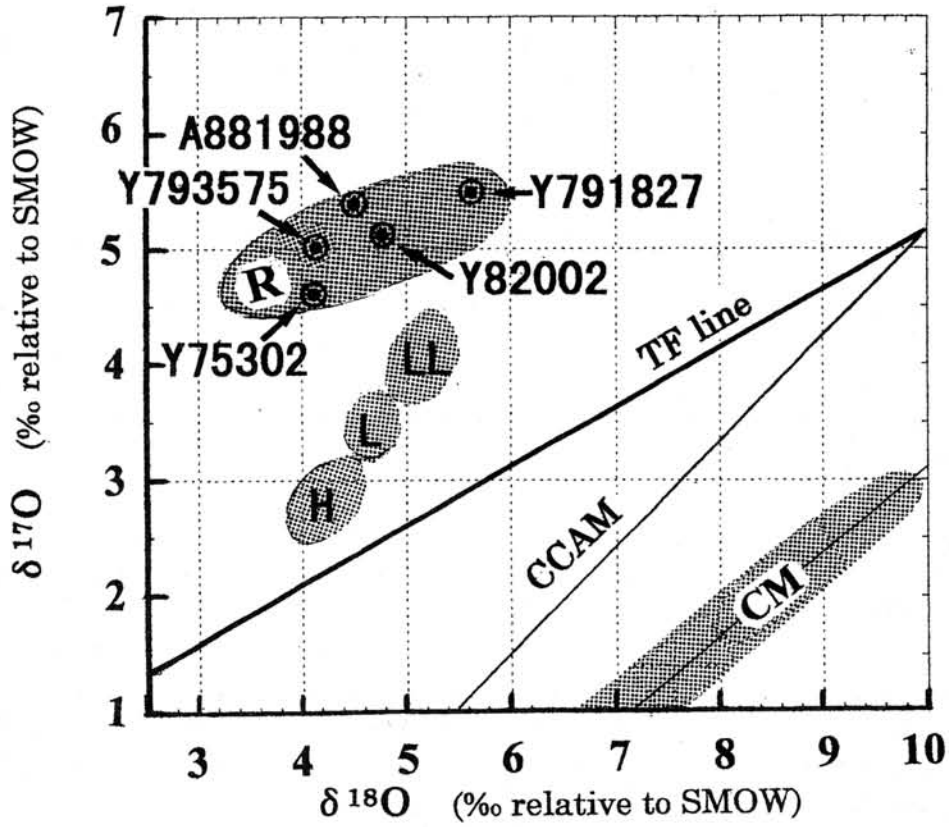


Fig. 1 Oxygen isotopic compositions of five Antarctic R-chondrites

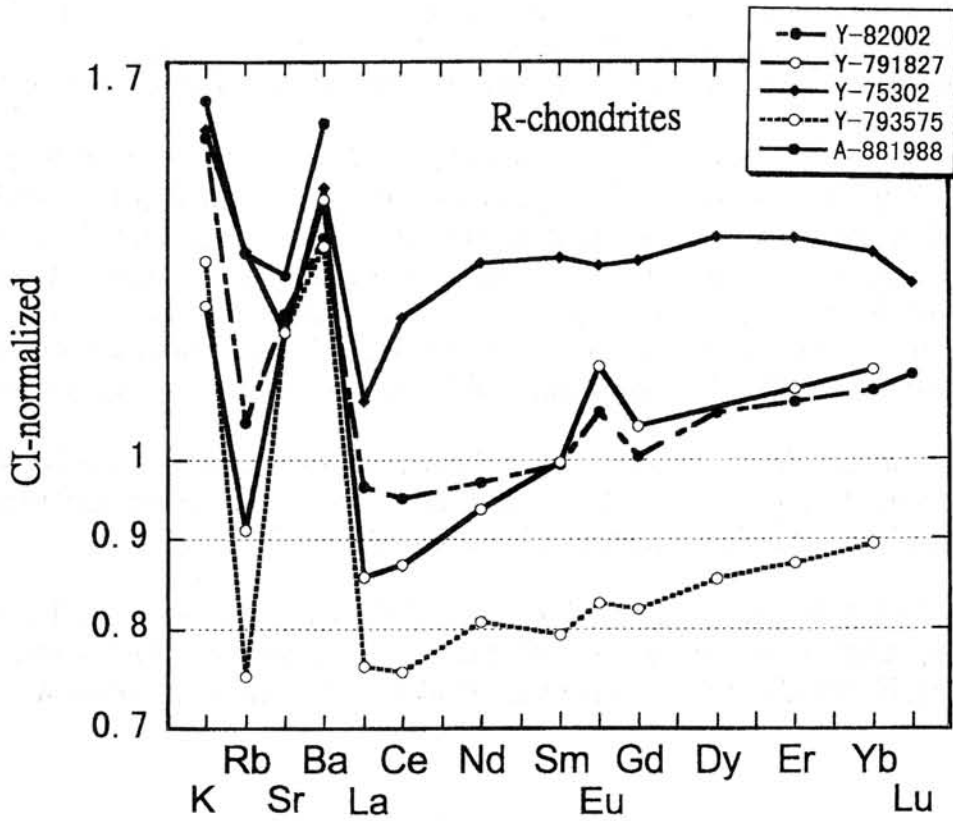


Fig. 2 Trace element abundance patterns for five Antarctic R-chondrites

SOLAR WIND IN MICROMETEORITES: CHARACTERIZATION BY STEPPED PYROLYSIS

Tomoki Nakamura and Nobuo Takaoka

Earth and Planetary Sciences, Faculty of Science, Kyushu University 33,
Hakozaki, Fukuoka 812-8581, Japan

Antarctic micrometeorites were identified in the precipitated material of a water tank in the Dome Fuji Station (Nakamura *et al.*, 1999a). They show major and trace element compositions similar to those of chondrites (Imae *et al.*, 1999; Nakai *et al.*, 1999) and a variety of mineralogy (Noguchi and Nakamura, 1999; Imae *et al.*, 1999; Nakamura *et al.*, 1999b). As a part of the consortium study, noble gas signatures of micrometeorites were investigated by a noble-gas mass spectrometer at Kyushu University.

Samples are a set of magnetic fine particles less than 300 μm in size with high sedimentation rates in the water, having been separated from F960901 precipitated material (Nakamura *et al.*, 1999a). Based on the terrestrial accretion rates of micrometeorites (Taylor *et al.*, 1998) and snow-fall rates around the Dome Fuji Station, 100 mg of the sample particles should contain 1236.5 μg micrometeorites (Nakamura *et al.*, 1999a). Constituents other than micrometeorites are dominated by iron or iron oxides that are artificial contaminants probably welding evaporate generated by some activities around the station. In the present investigation we further separated the sample particles into three fractions: particles ranging in size less than 70 μm , those from 70 to 200 μm , and those from 200 to 300 μm . Noble gas analyses were done for the following two sets of particles: 20.0 mg of 70-200 μm particles, which are expected to contain 0.247 mg micrometeorites, and 16.1 mg of < 70 μm particles, which would contain 0.199 mg micrometeorites. Noble gases in the former were extracted by total melting at 1700 $^{\circ}\text{C}$ and those in the latter by stepped pyrolysis at 400, 700, 1000, 1300, and 1700 $^{\circ}\text{C}$. Heating duration at each temperature is 25 minutes that include temperature rising periods of a furnace, thus real heating duration is shorter. Detailed examination of heating profiles using thermocouples indicates that the real heating duration at the designated temperatures is approximately 15 minutes.

Ne isotopic ratios and release patterns of solar-wind derived ^4He , ^{20}Ne , and ^{36}Ar are shown in Figures 1 and 2. Gas concentrations in Fig. 2 were determined by dividing extracted gas amounts by expected weights of micrometeorites being contained in the samples. Large amounts of He and Ne with solar-gas isotopic ratios were extracted, while Ar appears to be a mixture of atmospheric and solar Ar, because $^{40}\text{Ar}/^{36}\text{Ar}$ ratios in the step-heating analysis were variable from 80 to 286. Concentrations of the solar-wind derived ^{36}Ar (Fig. 2) were obtained by separating the concentrations of measured ^{36}Ar into those of $(^{36}\text{Ar})_{\text{air}}$ and $(^{36}\text{Ar})_{\text{solar}}$ using $^{40}\text{Ar}/^{36}\text{Ar}$ ratios.

Light noble gases in micrometeorites are dominated by solar-wind derived noble gases, because cosmogenic and trapped components can not be separated even by the stepped pyrolysis. Ne three isotope diagram (Fig. 1) shows that in the stepped pyrolysis Ne isotopic ratios are plotted almost on the tie line connecting SEP-Ne and SW-Ne, except for that of 1700 $^{\circ}\text{C}$ fraction. This suggests that a major part of Ne in micrometeorites is solar-wind Ne with energy higher than 1 MeV, although small amounts of low-energy solar wind is contained as is observed in 700 $^{\circ}\text{C}$ fraction. Presence of abundant solar gases and scarcity of cosmogenic gases strongly indicate that

micrometeorites had been small particles in the interplanetary space to be exposed to solar wind efficiently. This also points against the idea that micrometeorites are products of explosions of volatile-rich carbonaceous chondrite-like objects in the upper atmosphere.

The $^{20}\text{Ne}/^{22}\text{Ne}$ ratios generally correlate with extracted ^{20}Ne concentrations in the stepped pyrolysis: 700 and 1000 °C fractions show high $^{20}\text{Ne}/^{22}\text{Ne}$ ratio (Fig. 1) and high ^{20}Ne concentrations (Fig. 2). This tendency is also observed in lunar soils (e. g., Srinivasan *et al.*, 1972) and is ascribed to spatial heterogeneity of solar Ne distribution within minerals (Benkert *et al.*, 1993), i. e., surface layers contain abundant solar Ne with high $^{20}\text{Ne}/^{22}\text{Ne}$ ratio and towards inner layers the concentrations and the isotopic ratios steeply decrease. This heterogeneity might also exist in micrometeorites, but apparent differences are observed between micrometeorites and lunar soils: micrometeorites lack Ne with very high $^{20}\text{Ne}/^{22}\text{Ne}$ ratio over 13 in the low temperature fractions unlike lunar soils (cf., Srinivasan *et al.*, 1972). This suggests that micrometeorites have lost solar gases located at the uppermost surfaces that would be directly exposed to solar winds and contain most solar gases in the case of lunar soils, most likely due to frictional heating upon atmospheric entry. The degrees of gas loss can be estimated from elemental ratios: $^4\text{He}/^{20}\text{Ne}$ and $^{20}\text{Ne}/^{36}\text{Ar}$ ratios of micrometeorites are 65 and 6, which are far below compared with those of contemporary solar winds, 570 and 28, recorded in Al-foils of satellites (Geiss, 1973). Based on these elemental ratios it is estimated that at least 79 % of ^{20}Ne and 98 % of ^4He have been lost from micrometeorites.

References: Benkert *et al.* (1993) *J. Geophys. Res.*, **98**, 13147-13162; Geiss (1973) *13th Intl. Cosmic Ray Conf.*, **5**, 3375-3398; Imae *et al.* (1999) in this volume; Nakai *et al.* (1999) in this volume; Nakamura *et al.* (1999a) *Antarctic Meteorite Research*, **12**, 187-198; Nakamura *et al.* (1999b) in this volume; Noguchi and Nakamura (1999) in this volume; Srinivasan *et al.*, (1972) *Proc. Third Lunar Planet. Conf.*, **2**, 1927-2945.

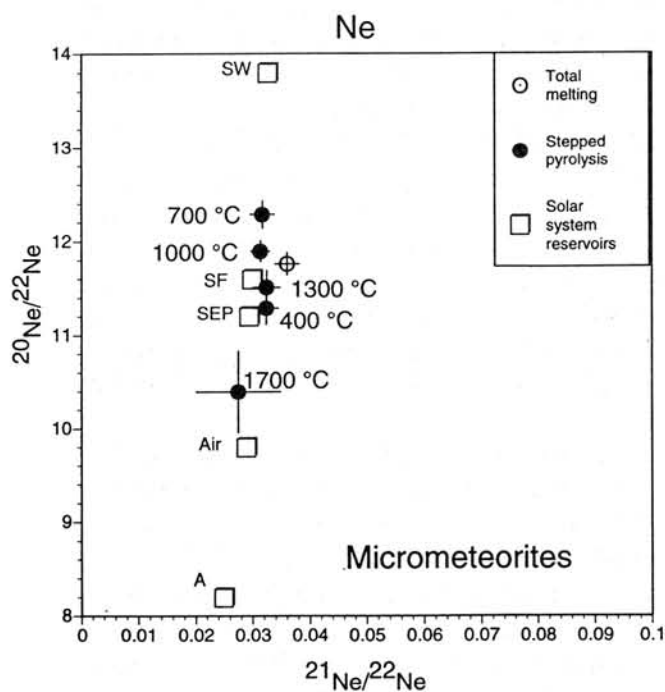


Figure 1

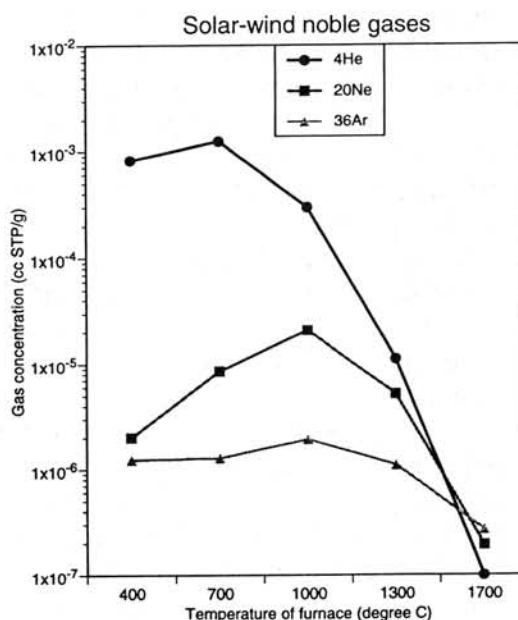


Figure 2

RELATIVE MINERAL ABUNDANCE OF INDIVIDUAL MICROMETEORITES COLLECTED AT THE DOME FUJI STATION

Tomoki Nakamura¹, Takaaki Noguchi², and Yoshihiro Nakamuta¹

¹*Earth and planetary Sci., Fac. of Sci., Kyushu Univ., Hakozaki, Fukuoka 812-8581, Japan,* ²*Dept. of Materials and Biological Science, Ibaraki Univ., Bunkyo 2-1-1, Mito 310, Ibaraki, Japan.*

We have X-rayed individual micrometeorites for diffraction analysis using a Gandolfi camera, which enables us to determine relative abundances of minerals comprising micrometeorites without any destructive process (e. g., Nakamura and Nakamuta, 1996). Relative mineral abundance of micrometeorites reflects mineralogy of precursor objects and thermal effects upon transition from space to earth. Out of 230 micrometeorites recovered from the Dome Fuji Station (Nakamura et al., 1999a), 34 particles that consist of 26 particles (hereafter Group 1; Noguchi et al., 1999) rich in volatile element S with S/Si ratios from 0.1 to 0.2 similar to those of CM chondrite Murchison, 5 particles (Group 2) with S/Si ratios from 0.05 to 0.1 and more than 0.2, and 3 particles (Group 3) poor in S with S/Si ratio less than 0.05 were chosen for the present analysis. S-rich micrometeorites are likely to preserve mineralogy and chemistry of precursors of micrometeorites in interplanetary space, because they have experienced lower degrees of heating during atmospheric entry relative to S-poor micrometeorites.

Individual micrometeorites were glued to the top of 3- μ m glass fibers and exposed to Cr-K α X-ray for 12 to 60 hours in a Gandolfi camera to obtain powder diffraction photographs. 3 particles with approximately 100 μ m in diameter that contain equal weights of forsterite, orthoenstatite, troilite, and magnetite are prepared as a standard sample for calibration of relative abundance of the four minerals. Reflection line profiles of micrometeorites are variable from very sharp to broad depending on crystallinity, chemical composition, and grain size of minerals, thus integrated intensities of reflections are calculated using the profile fitting technique (Nakamuta and Motomura, 1999) and were used for determination of relative mineral abundance.

Diffraction patterns of individual micrometeorites are essentially similar between particles especially within the Group 1. Most Group 1 particles contain following four kinds of minerals as major phases: olivine and orthopyroxene with various compositions, sulfides that are mostly pyrrhotite or troilite and occasionally pentlandite, and iron oxides that are mostly magnetite and rarely maghemite. Abundance ratios of olivine and orthopyroxene (pyroxene / olivine + pyroxene) in Group-1 particles show a wide range of diversity from 0 to 1, but they peak at approximately equal proportion of olivine and pyroxene. It is evident that, compared with fine-grained matrix material of anhydrous carbonaceous chondrites like Allende, micrometeorites of the Group 1 are remarkably rich in orthopyroxene. A possible explanation for the enrichment of orthopyroxene is that micrometeorites had been contained abundant phyllosilicates when they were in space, but atmospheric heating decomposed hydrous phases into olivine and orthopyroxene (Greshake et al., 1996; Yano and Noguchi, 1998). Bulk and mineral compositions of most micrometeorites are closely resemble to matrix material of CM chondrites, although some are similar to those of CI and CR chondrites (Steel, 1992; Genge et al., 1997; Engrand and Maurette, 1998). If micrometeorites have had CM-like mineralogy, then the major phase was

cronstedtite that is dehydrated and decomposed at temperature above 470 °C (Caillere and Henin, 1957).

Based on the relative mineral abundances of micrometeorites collected at Cap Prudhomme (Maurette et al., 1991), Nakamura et al. (1999b) categorized fine-grained micrometeorites into 5 classes with increasing heating effects. Phase I: most phyllosilicates are converted to olivine with low crystallinity, but small amounts of phyllosilicates such as tochilinite and cronstedtite are still present. Phase II: phyllosilicates are absent. Instead broad reflection of olivine is dominant. Sulfides are present, but small amounts of magnetite are generated. Internal texture of this phase of micrometeorites shows characteristic fibrous texture as a results of pseudomorphic dehydration of phyllosilicates as is observed in thermally metamorphosed CM chondrites (Matsuoka et al., 1996). Phase III: Broad reflections of orthopyroxene and those of olivine are major silicate reflections. Sulfides are still remained, but the amounts are smaller than those in Phase I and II. Presence of orthopyroxene indicates decomposition of phyllosilicates at high temperatures (e. g., Shirozu, 1962). Phase IV: Olivine and small amounts of orthopyroxene are present, but their reflections are sharper than those in Phase III. Sulfides are almost absent due to evaporation loss. Instead, magnetite is abundant. Micrometeorites of this phase begin to partially melt, because small bubbles are generated in the interior. Phase V: Sharp reflections of olivine and magnetite are dominant. Orthopyroxene and sulfide are absent. The melting degrees are higher than phase IV.

Based on the obtained X-ray diffraction patterns and relative mineral abundances, most micrometeorites collected at the Dome Fuji Station were classified into above five categories. Group 1 particles are mostly belonging to phase III, some are phase II and IV, and only one particle is phase I that appears to contain saponite, not cronstedtite. Group 2 belongs to phase III and IV. Group 3 belongs to phase III, IV, and V. There are some particles that do not belong to any category. These results indicate that most micrometeorites have experienced heating to varying degrees to change their initial mineralogy, provided that precursor material of micrometeorites had hydrous chondrite-like mineralogy.

Acknowledgments: We thank Dr. Tachibana, Osaka University, for kindly giving us orthoenstatite powder used for standard samples.

References: Caillere and Henin (1957) In “*The differential thermal investigation of clays.*” pp207-230; England and Maurette (1998) *Meteoritics Planet. Sci.*, **33**, 565-580; Genji et al. (1997) *GCA*, **23**, 5149-5162; Greshake et al. (1996) In “*The Cosmic Dust Connection*” pp. 303-310; Maurette et al. (1991) *Nature*, **351**, 44-46; Matsuoka et al. (1996) *Proc. NIPR Symp. Antarct. Meteorites*, **9**, 20-36; Nakamura and Nakamuta (1996) *Proc. NIPR Symp. Antarct. Meteorites*, **9**, 37-50; Nakamura et al. (1999a) *Antarctic Meteorite Research*, **12**, 187-198; Nakamura et al. (1999b) *Meteoritics and Planet. Sci.*, submitted; Nakamuta and Motomura (1999) *Meteoritics and Planet. Sci.*, submitted; Noguchi et al. (1999) in this volume; Shirozu (1962) *Clay Science*, **1**, 108-113; Steel (1992) *GCA*, **56**, 2923-2929; Yano and Noguchi (1998) *Antarct. Meteorite Res.*, **11**, 136-154.

Carbon minerals in ureilites: Implications for the genesis of diamond

Y. Nakamuta and Y. Aoki

Dept. Earth and Planetary Sciences, Faculty of Science, Kyushu University,
Fukuoka, 812-8581 Japan.

1. Introduction

Ureilite is a group of achondrite and the meteorites of this group are unique in containing relatively large amounts of carbon which takes the forms of diamond, graphite and lonsdaleite (Vdovykin, 1970). Urey (1956) considered that diamonds in ureilites were formed under fairly high temperatures and high pressures as those of the earth in the parent body or bodies of lunar mass or greater. Lipschutz (1964) showed that diamond in two of the three ureilites investigated by him showed a pronounced crystallographic orientation and argued for that the diamonds were produced by shock-conversion of graphite during breakup of the meteorite's parent body or bodies rather than high gravitational pressure. In addition to the two hypotheses for the origin of diamonds in the ureilites, Arrhenius and Alfvén (1971) suggested that the ureilitic diamonds might be a disequilibrium condensate directly formed from a low-pressure vapor phase in the solar nebula. This hypothesis was supported by Fukunaga et al. (1987) on the basis of noble-gas contents of diamond and graphite in the ureilites. The origin of diamonds in the ureilites has been controversial until now (Goodrich, 1992).

In this study, we obtained clear x-ray powder diffraction patterns from 50-100 μm grains of carbon minerals selected from crashed Antarctic ureilites, ALH-78019, Y-82100, Y-791538 and ALH-77257, and the Kenna ureilite by using a Gandolfi camera. Occurrence of carbon minerals in polished thin sections preserved in NIPR were also observed with a reflected light by a optical microscope.

2. Occurrence of carbon minerals

Reflected light views of carbon minerals in polished thin sections were shown in Fig. 1. Carbon minerals in ALH-78019 and Y-82100 show tan-gray color and metallic luster and occur in olivine crystals with the euhedral shape of graphite or interstitially with an anhedral shape. Carbon minerals in Y-791538 and ALH-77257 are very similar to those of ALH-78019 and Y-82100 in the modes of occurrence except that they are black in color and do not show metallic luster. Until now, many workers have repeatedly suggested that carbon minerals occur mostly along the grain boundaries of olivine and pyroxene as a matrix. However, the reflected light views in Fig. 1 clearly show that carbon minerals occur as blades in olivine and pigeonite crystals or as anhedral crystals interstitial to them and not as a matrix at grain boundaries. The reduction rims of the olivine are observed around carbon minerals and along the grain boundaries and cracks of olivine crystals. The rims are relatively narrow in ALH-78019 and Y-82100 and develop widely in Y-791538 and ALH-77257.

3. X-ray results

The x-ray powder diffraction patterns of the carbon grains from each samples are shown in Fig. 2.

The patterns suggest that ALH-78019 and Y-82100 contain only graphite, being a mixture of 2H- and 3R-polytypes, and Y-791538, Kenna and ALH-77257 contain both graphite and diamond. Lonsdaleite has been reported from ureilites (Vdovykin, 1970 etc.), however, it is not contained in any samples of this study. The relative intensities of diamond to graphite are variable among ureilites of this study. ALH-77257 shows the strongest intensity of diamond and is followed in order of the intensity by Kenna and Y-791538. The 002 reflection of graphite, appearing at around 40° (2θ) in the x-ray pattern, tails toward the higher angle side when graphite and diamond coexist in a sample. The tailing of the basal reflection reveals the presence of distorted graphite of which basal spacing is collapsed a little compared to the normal one.

4. Discussion and Conclusions

In ALH-78019 and Y-82100, graphites occur as blades in olivine or pigeonite crystals or as blades or anhedral crystals interstitial to olivine and pigeonite crystals. The modes of occurrence suggest that the graphite in these meteorites has crystallized together with olivine and pigeonite during igneous processes as suggested by Berkley and Jones (1982). The sharp x-ray diffraction lines of the graphite support the igneous origin of it in these meteorites. Carbon minerals in Y-791538 and ALH-77257 are composed of graphite and diamond, however, the modes of occurrence are very similar to those of graphite in ALH-78019 and Y-82100 except that they are black in color and do not show metallic luster. The modes of occurrence suggest that graphite crystals, having crystallized during the same processes as those of ALH-78019 and Y-82100, may have converted to diamonds in Y-791538 and ALH-77257.

The presence of collapsed graphite is noticeable in ureilites which contain both graphite and diamond. Endo et al. (1994) found in their experiments that the basal spacing of graphite collapsed when natural graphite was compressed at high pressures and temperatures of diamond formation and the collapsed graphite was recovered. Then, the collapsed graphite in ureilites is thought to give a certain evidence for the high pressure genesis of diamonds.

The modes of occurrence of carbon minerals and the properties of graphite reveal that diamonds have been produced by shock-conversion of the graphite which crystallized together with olivine and pigeonite during igneous processes. The relative x-ray intensities of diamond to graphite are variable among ureilites. Then, the intensity ratio between diamond and graphite can be used as a quantitative indicator of shock-effects on ureilites. The ratio of diamond to graphite becomes larger in the order, ALH-79019 and Y-82100, Y-791538, Kenna, and ALH-77257.

References

Arrhenius G. and Alfvén H. (1971) *Earth Planet. Sci. Letters* **10**, 253-267.

Berkley J. L. and Jones J. H. (1982) *J. Geophys. Res.* **87**, A353-A364.

Endo S. et al. (1994) *Phys. Rev.* **B49**, 22-27.

Fukunaga K. et al. (1987) *Nature* **328**, 141-143.

Goodrich C. A. (1992) *Meteoritics* **27**, 327-352.

Lipschutz M. E. (1964) *Science* **143**, 1431-1434.

Urey H. C. (1956) *Astrophys. J.* **124**, 623-637.

Vdovykin G. P. (1970) *Space Sci. Rev.* **10**, 483-510.

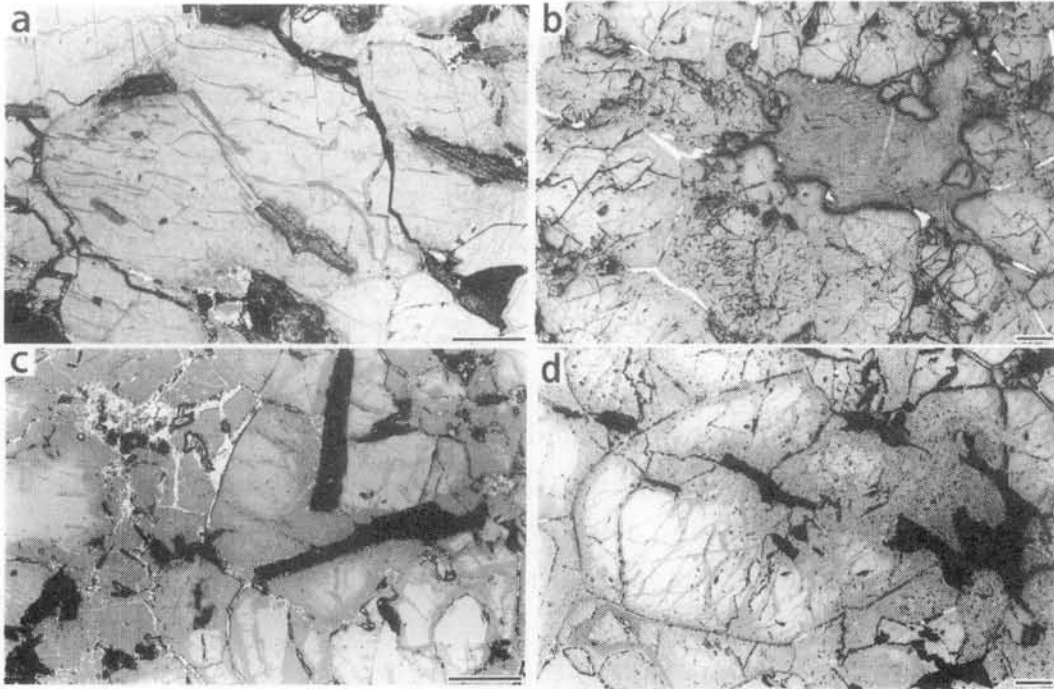


Fig. 1. Reflected light views of carbon minerals in polished thin sections. a: ALH-78019, b: Y-82100, c: Y-791538, d: ALH-77257. Bars in each photographs show 0.2 mm in length.

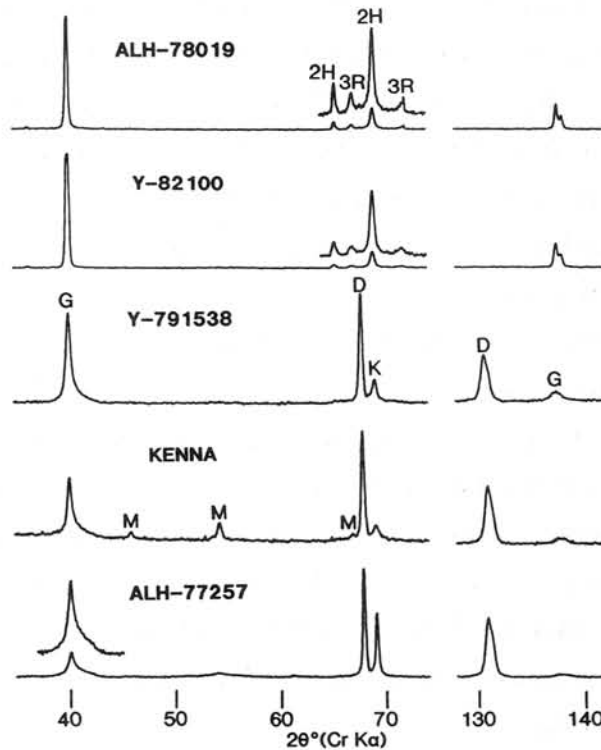


Fig. 2. X-ray powder diffraction patterns of the carbon grains from each samples. 2H and 3R: reflections from 2H- and 3R-graphites, respectively. G, D, K, and M: reflections from graphite, diamond, kamacite, and maghemite, respectively.

The influence of hot water alteration on noble gas composition in the Allende meteorite

Eiji Nakasyo, Teruyuki Maruoka, Jun-ichi Matsuda

Department of Earth and Space Science, Graduate School of Science, Osaka University,
Toyonaka, Osaka 560-0043, Japan

Introduction

Noble gases trapped in chondrites are located mainly in a small carbonaceous residue named “phase Q”. Phase Q remains during chemical treatment in HF and HCl, and dissolves by oxidization. The phase Q has not been isolated yet although many authors attempt to isolate and identify it [1,2].

One of hypothesis is that Q might originate from a surface layer of pre-solar diamond which was altered by the ionized noble gases, based on the observation that the elemental abundance of noble gases in Q resembles that of ionized noble gases by plasma process. To confirm our model Yoshida [3] carried out an experiment to reproduce the phase Q in synthetic diamonds by implanting noble gases in a plasma process. The implanted diamonds released noble gases by oxidation of HNO₃ which also affected the real phase Q. However, they released noble gases even after boiling in a hot water. To examine the effects of hot water on the phase Q and other phases of noble gas, we have carried out the laboratory experiment.

Sample and Experiment

We prepared two samples to compare noble gas compositions before and after artificial thermal alteration. The sample (AC-1) is the original matrix material of the Allende meteorite which was separated by the freeze-thaw disaggregation method. The AC-1 was heated at 200°C in a pressure vessel under 15 atmosphere water-vapor pressure for a week and designated as HM-1. Noble gases in these two samples were extracted by stepped pyrolysis (800°C, 1000°C, 1200°C, 1400°C, 1600°C) and measured with a sector-type mass spectrometer, VG5400, at Osaka University.

Result and Discussion

The concentrations of all noble gases in HM-1 are lower than that in AC-1. Here, we show the Xe data as an example (Fig.1). In ¹³⁰Xe/¹³²Xe vs.

$^{131}\text{Xe}/^{132}\text{Xe}$ diagrams (Fig.2), the data points are located near of Q-Xe (Wieler et al. [3]) except for 800°C which is largely affected by air. This diagram shows that the atmospheric component did not affect the treated sample at high temperatures. However, the combination of these isotopic ratios can hide the effect of HL component due to the small difference of data positions in this diagram. In $^{134}\text{Xe}/^{136}\text{Xe}$ vs. $^{130}\text{Xe}/^{132}\text{Xe}$ diagrams (Fig.3), the data points of HM-1 are closer to Q-Xe than those of the AC-1. Therefore, the HL component is easier to be lost by the hot water treatment. Huss et al [4] reports that the phase Q is more resistant to thermal metamorphism than the diamond which is the HL component carrier with increasing petrologic sub-type. Present results are consistent with their report.

Our sample was prepared by heating it at 200°C for one week. Experiments on different conditions for temperatures and heating time will reveal the thermal history of each chondrite.

References

- [1] Lewis R.S., Srinivasan B., and Anders E. (1975) *Science* 190, 1251-1262.
- [2] Tang M. and Anders E.(1988) *Geochim. Cosmochim. Acta* 52, 1245-1254.
- [3] Yoshida T.(1997) Ms. Thesis for Osaka University.
- [4] Huss G.R., Lewis R.S., Hemkin S. (1996) *Geochimica et Cosmochimica Acta* 17, 3311-3340.
- [5] Huss G.R., Lewis R.S.(1994) *Meteoritics*29, 791-810.
- [6] Nier A.O.(1950) *Phys. Rev.* 79,789-793.

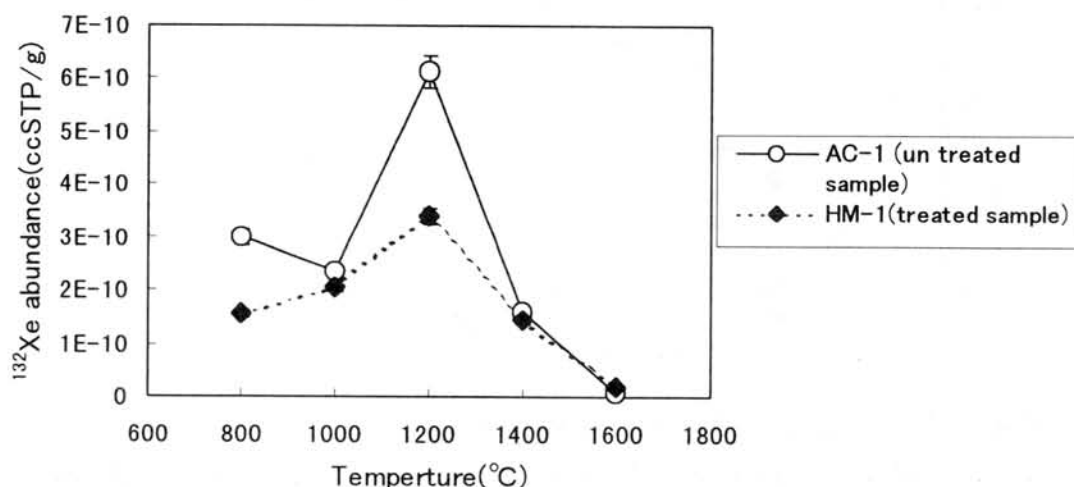


Fig.1. Thermal release pattern of ^{132}Xe in AC-1 and HM-1

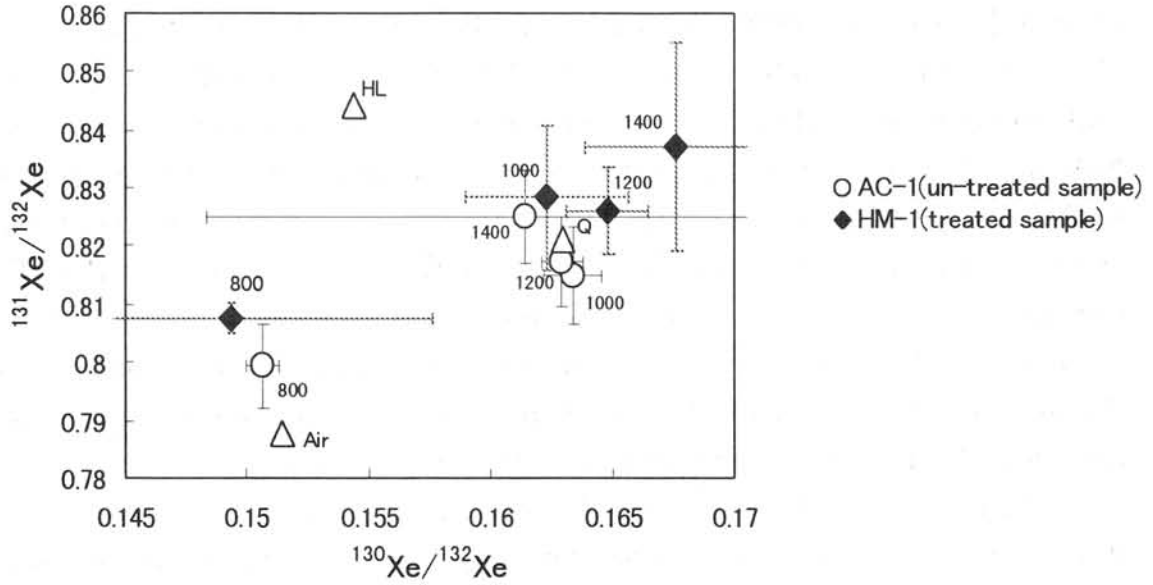


Fig.2. $^{130}\text{Xe}/^{132}\text{Xe}$ vs. $^{131}\text{Xe}/^{132}\text{Xe}$ diagram.

HM-1 is the sample that is altered by hot water treatment, and AC-1 is the sample that is not altered. The data of 1600°C are excluded because of the large uncertainty.

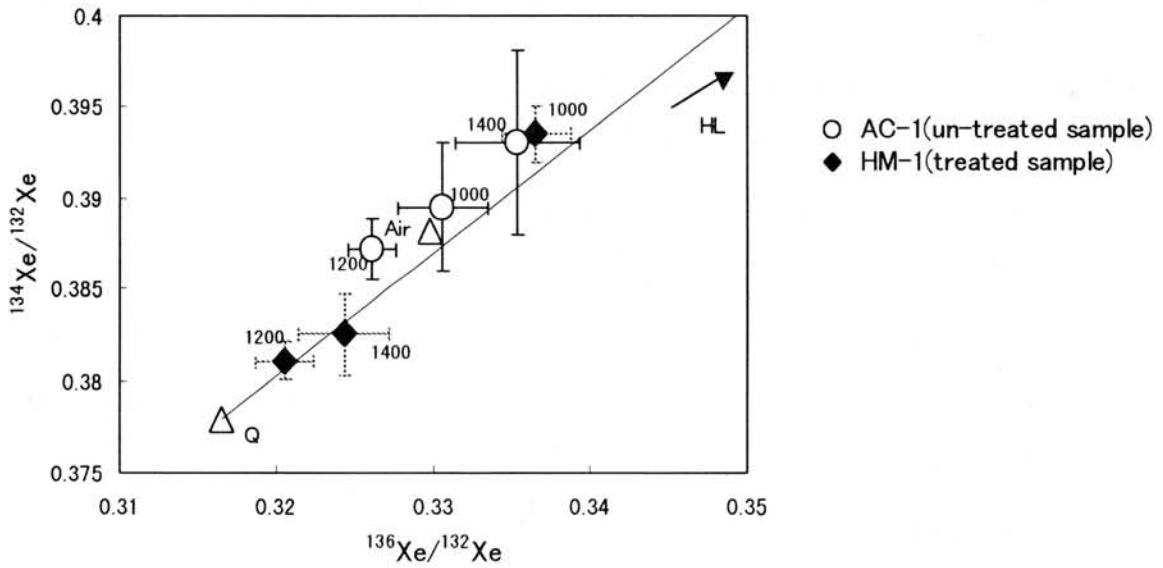


Fig.3. $^{130}\text{Xe}/^{132}\text{Xe}$ vs. $^{134}\text{Xe}/^{132}\text{Xe}$ diagram.

The data of 800°C are excluded because of air contamination. The data of 1600°C are also excluded because of the large uncertainty.

The data source of Q is from [4], HL is from [5], Air is from [6]

Molecular and isotopic distributions of polyaromatic hydrocarbons (PAHs) in three Asuka carbonaceous chondrites (CM2) from Antarctica

Hiroshi Naraoka

Department of Chemistry, Tokyo Metropolitan University, Hachioji, Tokyo 192-0397.

Introduction

Polyaromatic hydrocarbons (PAHs) have been reported from carbonaceous chondrites (Pering and Ponnampertuma, 1971; Naraoka et al., 1988), a martian meteorite (McKay et al., 1996), and interstellar environment (Allamandola et al., 1987). PAHs should be important compounds to study organic cosmochemistry and origins of life in the universe. Although extraterrestrial organic matters have been extensively studied on the Murchison (CM2) (e.g. Cronin et al., 1988), Antarctic meteorites give us new opportunities to examine the occurrence of organic compounds. In this study, PAHs were examined in three Antarctic carbonaceous chondrites, including carbon isotopic compositions of individual compounds.

Samples and experimental

Three Asuka (A-) CM2 chondrites, A-881280, A-881334 and A-881458, were recovered from Nansen Plateau (~73°S; ~24°E), Queen Maud Land, Antarctica in 1989 by the 29th JARE. Bulk carbon concentrations ranged from 1.5 to 2.5 wt% (Naraoka et al., 1997). Powdered samples of the interior parts of chondrites (~0.5g) were extracted with benzene/CH₃OH and subjected to silica gel column chromatography to obtain a PAH fraction. Molecular identification was carried out using gas chromatography/mass spectrometry. Carbon isotopic compositions of individual PAHs were determined using gas chromatography/combustion/mass spectrometry by coinjected *n*-alkanes as isotopic internal standards. Isotope values are reported in the usual δ notation relative to PDB (Peedee Belemnite).

Results and discussion

More than 20 PAHs were identified in the extract of A-881458 from naphthalene to benzo[ghi]perylene (Fig. 1), being fluoranthene and pyrene abundant (~3.5 $\mu\text{g/g}$). Such a molecular abundance is similar to PAHs in Murchison (Pering and Ponnampertuma, 1971) and Y-791198 (Naraoka et al., 1988). Carbon isotopic compositions of naphthalene and biphenyl (~-26‰) are similar to those of terrestrial PAHs, but different from phenanthrene (-14.0‰), fluoranthene (-8.3‰) and pyrene (-15.8‰) which are more ¹³C-enriched (Fig. 2). In particular,

fluoranthene and pyrene have the same chemical formula ($C_{16}H_{10}$) and may have a similar thermodynamic characteristics isotopically. Therefore, the isotopic difference is attributable to a kinetically-controlled formation mechanism for the PAHs. The molar H/C ratios of individual PAHs may be used as a "cyclization index". A H/C- $\delta^{13}C$ plot (Fig. 2) indicates that the PAHs are more depleted in ^{13}C with decreasing the H/C ratios. The isotope distribution is consistent with the kinetically-controlled formation mechanism. A similar isotope trend was reported by Gilmour and Pillinger (1992). However, this study suggests two series of isotopic trend shown as "pyrene series" and "fluoranthene series" in Fig. 2. Such isotopically different series may indicate a distinctive reaction pathway for the formation of PAHs.

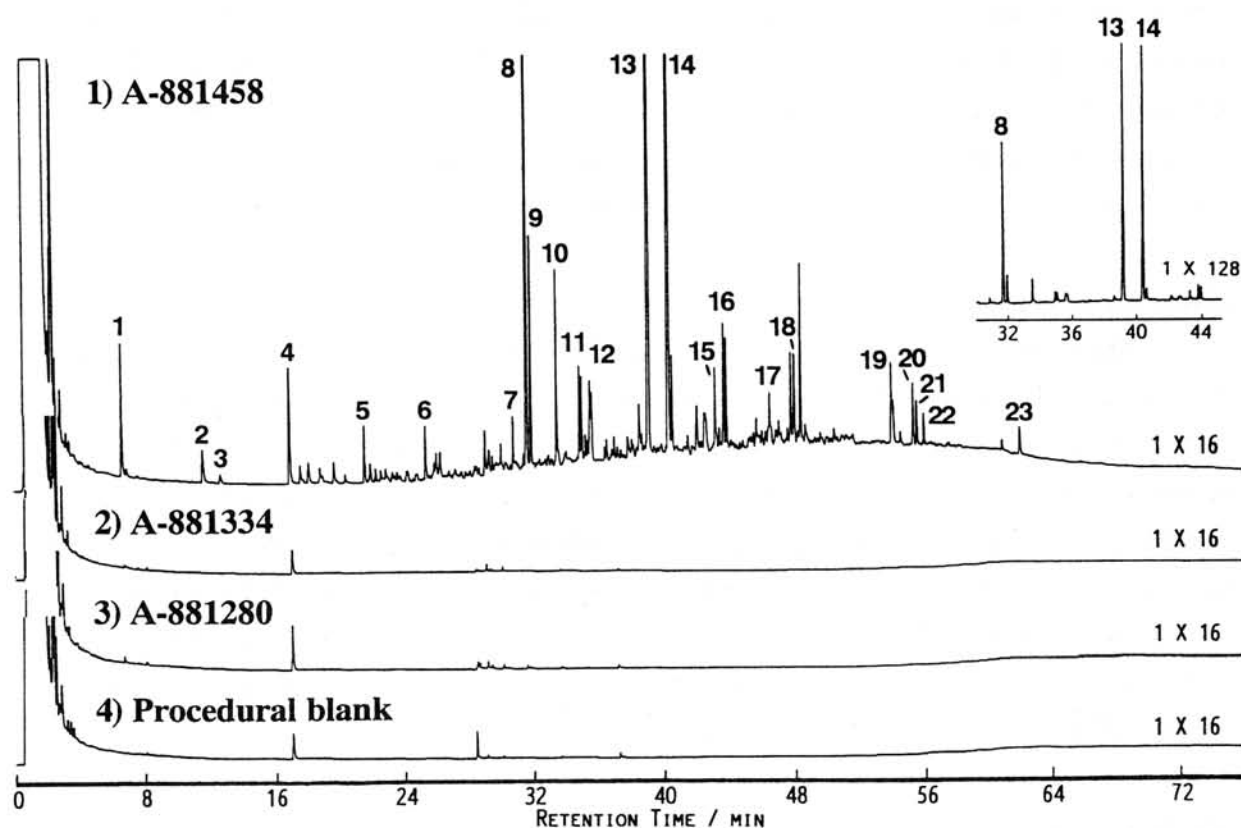


Fig. 1. Gas chromatograms of PAHs from three Asuka carbonaceous chondrites. 1) A-881458, 2) A-881334, 3) A-881280 and 4) procedural blank. Peak numbers denote: 1, naphthalene; 2, 2-methylnaphthalene; 3, 1-methylnaphthalene; 4, diphenyl; 5, acenaphthene; 6, fluorene; 7, dibenzothiophene; 8, phenanthrene; 9, anthracene; 10, carbazole; 11, 3- and 2-methylphenanthrenes; 12, 9- and 1-methylphenanthrenes; 13, fluoranthene; 14, pyrene; 15, 2,3-benzofluorene; 16, methylfluoranthene or methylpyrene; 17, benzo[ghi]fluoranthene; 18, crysene and/or triphenylene; 19, benzofluoranthenes; 20, benzo[e]pyrene; 21, benzo[a]-pyrene; 22, perylene; 23. benzo[ghi]perylene.

On the other hand, A-881280 and A-881334 are depleted in PAHs in spite of a comparable bulk carbon content to A-881458. The molecular distribution of PAHs is consistent with that of monocarboxylic acids (Naraoka et al, 1999). The depletion is not due to weathering on ice, because the degrees of weathering are small and similar among the three chondrites. Probably the latter two chondrites may have been subjected to aqueous alteration or metamorphism on their meteorite parent bodies.

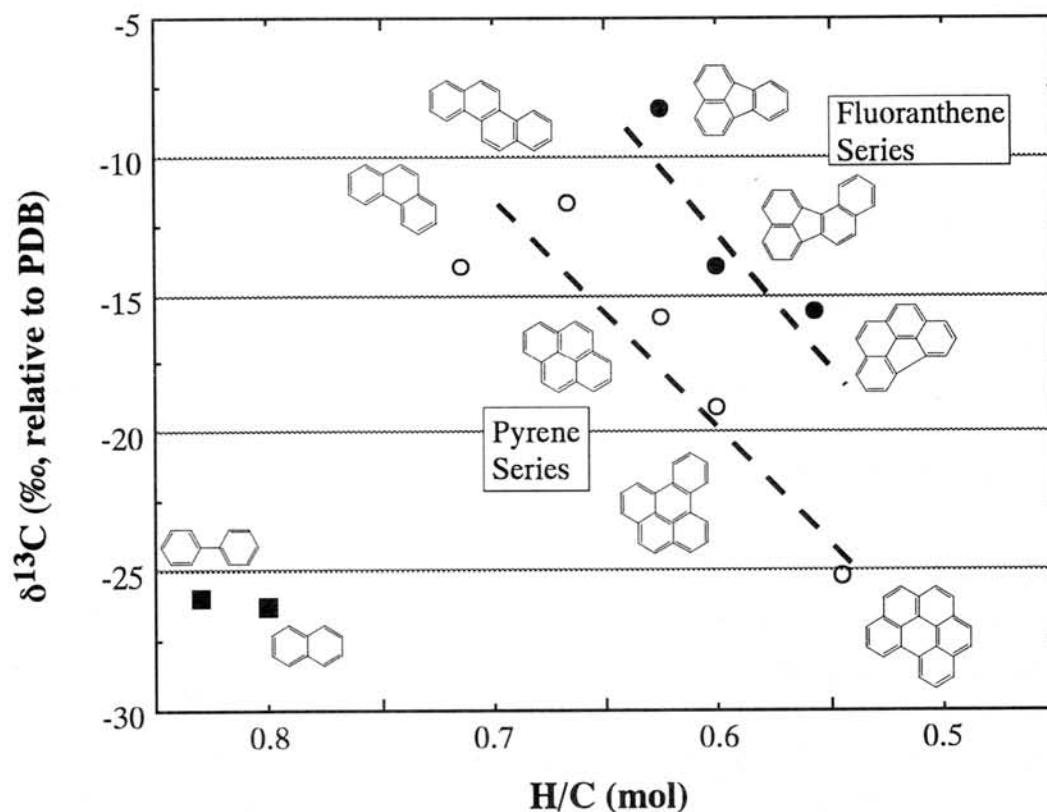


Fig. 2. Carbon isotopic compositions of individual PAHs depending on their H/C molar ratios from A-881458 carbonaceous chondrite.

References Allamandola, L. J. et al. *Science* **237**, 56-59 (1987); Cronin, J. R. et al. *Meteorites and the Early Solar System*, pp. 819-857 (1988); Gilmour, I and Pillinger, C. *Meteoritics*, **27**, 224-225 (1992); McKay, D. S. et al. *Science* **273**, 924-930 (1996); Naraoka, H. et al. *Chem. Lett.*, **1988**, 831-834 (1988); Naraoka, H. et al. *Geochem. J.*, **31**, 155-168 (1997); Naraoka, H. et al. *Origins of Life Evol. Biosphere*, **29**, 187-201 (1999); Perring, K. L. and Ponnamperna, C. *Science*, **173**, 237-239 (1971)

An Oxygen Isotope Study of Enstatite Meteorites

J. NEWTON^{1,2*}, I.A. FRANCHI¹ and C.T. PILLINGER¹

¹Planetary Sciences Research Institute, The Open University, Walton Hall, Milton Keynes, MK7 6AA, U.K.

²Department of Earth and Planetary Physics, University of Tokyo, Hongo 7-3-1, Bunkyo-ku, Tokyo 113, Japan

*Correspondence authors address: newton@gpsun01.geoph.s.u-tokyo.ac.jp

Introduction

Four discrete parent bodies of reduced mineralogy (1) are represented by two unmelted groups of meteorites (the EH and EL chondrites) and two melted groups (aubrites and the Shallowater meteorite). Meteorites from these four bodies are notable in that they fall on a line on a plot of $\delta^{17}\text{O}$ against $\delta^{18}\text{O}$ which coincides with that of the terrestrial fractionation line (TFL); that is, the deviation in $\delta^{17}\text{O}$ from the TFL, defined as $\Delta^{17}\text{O}$, is 0 ‰ (2). Here we present oxygen isotope measurements of 53 enstatite meteorites, including 16 EH chondrites and 21 EL chondrites of a variety of petrologic types, two anomalous E3 chondrites, 13 aubrites and a specimen of the Shallowater body.

Analytical

Oxygen was extracted from the powdered samples by a laser fluorination technique, using an improved but analogous system to that of (3). In this method, samples are heated using a 25W CO₂ laser, with BrF₅ as the fluorinating agent.

In order to be sure that oxygen isotope measurements were indicative of extraterrestrial processes, possible weathering products in meteorite finds, such as carbonates and rust, were removed by treating powdered sample with 1M HCl.

Results

The oxygen isotope data have been grouped according to chemical type and illustrated on a plot of $\Delta^{17}\text{O}$ against $\delta^{18}\text{O}$ (Fig. 1). On this type of diagram, mass dependant fractionations form horizontal trends, with the TFL following $\Delta^{17}\text{O} = 0$ ‰. It is evident that, with a few exceptions (Cumberland Falls, LEW 87223, Galim (b), PCA 91461 and South Oman), the $\Delta^{17}\text{O}$ values are such that they lie close to the TFL as expected (2).

The compositions of two of these three outlier samples are readily explained by interactions with other meteoritic material. The Cumberland Falls aubrite ($\Delta^{17}\text{O} = 0.531$ ‰) is a breccia which is known to contain altered LL chondrite clasts (4), with $\Delta^{17}\text{O}$ values of 0.93‰ (5). The Galim (b) chondrite is a heavily shocked representative from a shower of stones which yielded two chondritic types, the other, Galim (a), being LL6 (6,7). The $\Delta^{17}\text{O}$ value (0.211‰) is consistent with shock-induced interaction between the two lithologies (8).

LEW 87223 ($\Delta^{17}\text{O} = 0.353\text{‰}$) is an anomalous chondrite, with some suggestions that it is an EL3 which has gained metal and lost sulphide by shock (9) or that it represents a new group with possible links to H chondrites (10). The last suggestion is interesting given its oxygen isotope composition. Both PCA 91461 and South Oman lie almost 0.3‰ below the TFL. There is no known information about clasts in these meteorites. Given that they both lie about 1‰ above that section of the CR line (11,12), and close to ureilitic compositions (13), these are the favoured candidates for any clasts these might contain.

Ignoring the five outlying samples discussed above, and those finds which are tainted by terrestrial contamination, there is an increase in homogeneity in the oxygen isotope compositions from EH to EL to aubrite (Table 1), consistent with increased equilibration; our sample set is biased by EL's of mainly high petrologic type and EH's of lower petrologic type. Overall, though, the chemical groups are indistinguishable in terms of oxygen isotopes.

A comparison of enstatite chondrites of different petrologic types (Table 2) produces an interesting correlation: those of lower petrologic type are more enriched in ^{16}O . The fact that the more equilibrated chondrites are fractionated toward higher $\delta^{18}\text{O}$ values has been documented before (2), but the reason is not immediately clear, as the correlation is opposite in sign to that of the ordinary chondrites (14), so cannot be explained by a reduction process involving carbon, or aqueous alteration. Shock appears to hold the key: it has been speculated that loss of a plagioclase-rich melt produced by shock (15) could explain the differences between unequilibrated and equilibrated enstatite chondrites, since loss of such a liquid would produce a residue enriched in lighter isotopes, as heavy oxygen tends to partition itself into plagioclase (16).

Acknowledgements

ANSMET, the Natural History Museum London and EUROMET provided the majority of the samples in this study. Galim (b) was provided by the Muséum National d'Histoire Naturelle, Paris.

		$\delta^{17}\text{O} \text{‰}$	$\delta^{18}\text{O} \text{‰}$	$\Delta^{17}\text{O} \text{‰}$
EH	n=12	2.762 ± 0.442	5.292 ± 0.652	0.010 ± 0.118
EL	n=19	2.911 ± 0.178	5.559 ± 0.326	0.020 ± 0.063
AUB	n=8	2.660 ± 0.152	5.158 ± 0.258	-0.022 ± 0.048

Table 1: mean oxygen isotope compositions of the chemical groups

		$\delta^{17}\text{O} \text{‰}$	$\delta^{18}\text{O} \text{‰}$	$\Delta^{17}\text{O} \text{‰}$
E3	n=6	2.574 ± 0.214	5.049 ± 0.375	-0.051 ± 0.051
E4-5	n=8	2.848 ± 0.402	5.393 ± 0.574	0.044 ± 0.113
E6	n=13	2.972 ± 0.161	5.682 ± 0.305	0.017 ± 0.060

Table 2: mean oxygen isotope compositions of the different petrologic types

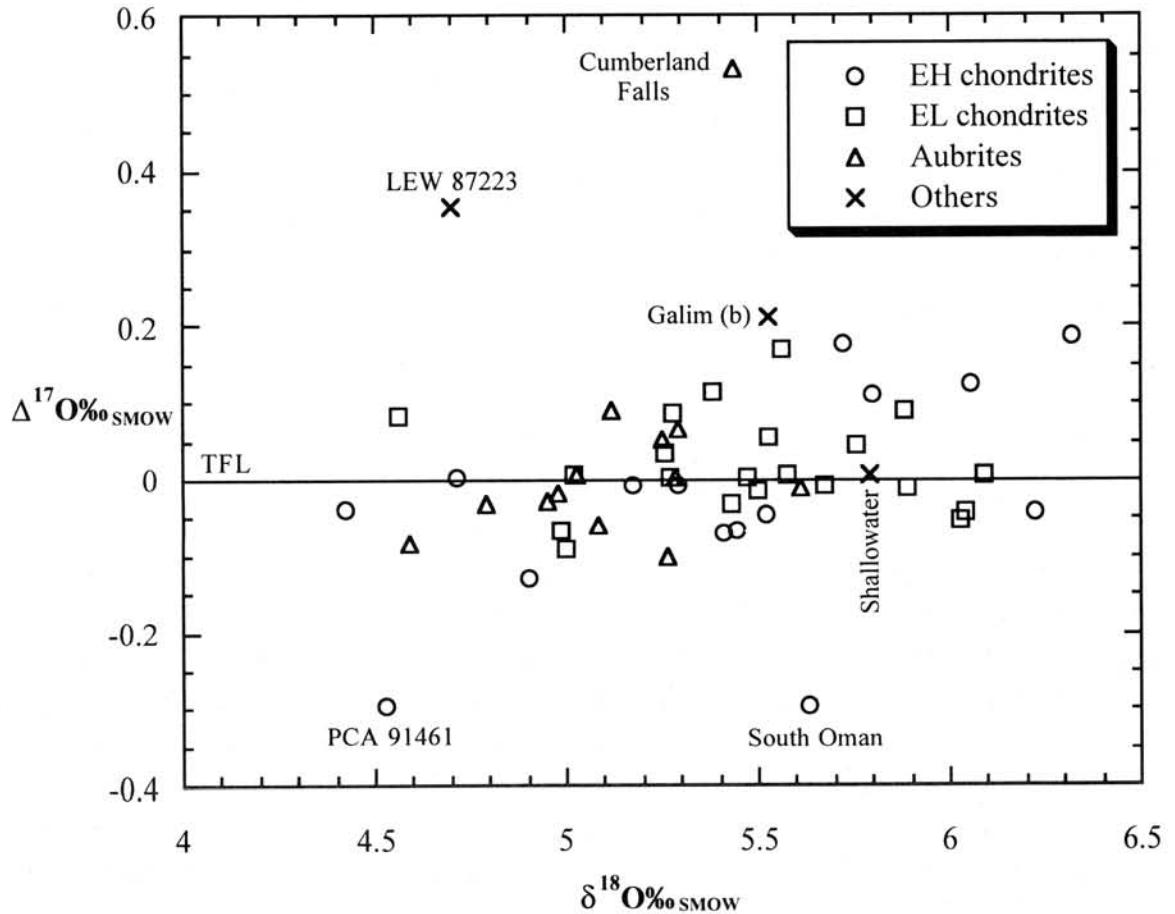


Fig. 1. Oxygen isotope plot of enstatite chondrites and aubrites

References

- (1) Keil K. (1989). *Meteoritics* 24, 195-208.
- (2) Clayton R.N. *et al.* (1984). *J. Geophys. Res.* 89 Suppl., C245-C249.
- (3) Franchi I.A. *et al.* (1992). *Meteoritics* 27, 222.
- (4) Kallemeyn G.W. and Wasson J.T. (1985). *Geochim. Cosmochim. Acta* 49, 261-270.
- (5) Verkouteren R.M. and Lipschutz M.E. (1983). *Geochim. Cosmochim. Acta* 47, 1625-1633.
- (6) Christophe-Michel-Lévy M. and Bourot-Denise M. (1983). *Lunar Planet. Sci.* 14, 113-114.
- (7) Christophe-Michel-Lévy M. and Bourot-Denise M. (1988). *Mineral. Mag.* 52, 519-525.
- (8) Rubin A.E. (1997). *Meteoritics and Planetary Science* 32, 489-492.
- (9) Zhang Y. *et al.* (1995). *J. Geophys. Res.* 100, 9417-9438.
- (10) Grossman J.N. *et al.* (1993). *Meteoritics* 28, 358.
- (11) Bischoff A. *et al.* (1993). *Geochim. Cosmochim. Acta* 57, 1587-1603.
- (12) Weisberg M.K. *et al.* (1993). *Geochim. Cosmochim. Acta* 57, 1567-1586.
- (13) Franchi I.A. *et al.* (1992). *Meteoritics and Planetary Science* 32, A44.
- (14) Clayton R.N. *et al.* (1991). *Geochim. Cosmochim. Acta* 55, 2317-2337.
- (15) Weeks K.S. and Sears D.W.G. (1985). *Geochim. Cosmochim. Acta* 49, 1525-1536.
- (16) Clayton R.N. *et al.* (1976). *Earth Planet. Sci. Lett.* 30, 10-18.

THERMOLUMINESCENCE OF JAPANESE ANTARCTIC METEORITES III

K. Ninagawa¹, S. Toyoda¹, N. Imae², and Kojima²

¹ Department of Applied Physics, Okayama University of Science, 1-1, Ridai-cho, Okayama 700, Japan

² National Institute of Polar Research, 9-10, Kaga 1-chome, Itabashi-ku, Tokyo 173, Japan

Natural TL (thermoluminescence), the luminescence of a sample that has received no irradiation in the laboratory, reflects the thermal history of the meteorite in space and on Earth. Natural TL data thus provide insights into such topics as the orbits of meteoroids, the effects of shock heating, and the terrestrial history of meteorites. Induced TL, the response of a luminescent phosphor to a laboratory dose of radiation, reflects the mineralogy and structure of the phosphor, and provides valuable information on the metamorphic and thermal history of meteorites. The sensitivity of the induced TL is used to determine petrologic type of type 3 ordinary chondrites.

Then the natural TL of meteorites, along with induced TL data and cosmogenic radionuclide (*e.g.*, ²⁶Al) and noble gas abundance data, have been used to identify potentially paired fragments of Antarctic ordinary chondrites. As reliable pairing approach, TL properties within large chondrites have been analyzed, taking advantage of the fact that serial samples from these meteorites are known to be paired [1]. Then new set of TL pairing criteria: 1) the natural TL peak height ratios, LT/HT, should be within 20%; 2) that ratios of raw natural TL signal to induced TL signal should be within 1.5; 3) the TL peak temperatures should be within 20°C and peak widths within 10°C was proposed. This set of TL pairing criteria are less restrictive than previously used [1].

Last year we have applied these new TL pairing criteria to TL data of fifteen Japanese Antarctic unequilibrated chondrites, measured under Okayama TL instrument and measuring conditions [2]. This time we measured TL of more fifteen Japanese Antarctic unequilibrated chondrites. The data of them were listed in Table 1. Ratio of natural TL signal (raw data as number of counts) to Dhajala-normalized TL sensitivity vs. natural TL peak height ratio is plotted in Fig.1. Y-793573 and Y-8014, and Y-793370 and Y-793325 are potentially paired, respectively.

The petrographic subtype of these unequilibrated ordinary chondrites were also determined from their TL sensitivity and Y-75029 (H3) and Y-791856 (H3) was found to have petrographic types under 3.3.

References: [1] Ninagawa *et al.* (1998): *Antarctic Meteorite Res.*, **11**, 1-17. [2] Ninagawa *et al.* (1998): *papers presented in the 23th Symposium on Antarctic Meteorites.*, 110-111.

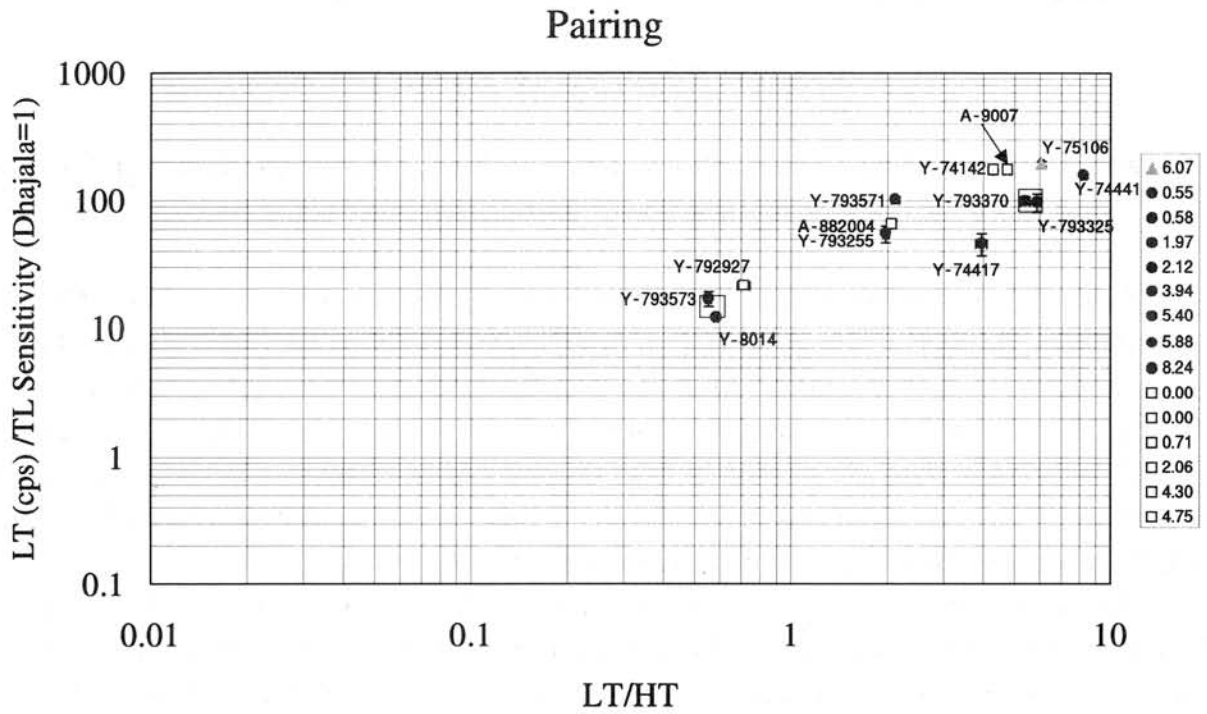


Fig. 1 Ratio of natural TL signal to Dhajala-normalized TL sensitivity vs. natural TL peak height ratio.

Table Thermoluminescence data of Okayama for fifteen unequibrated Japanese ordinary chondrites

Meteorite Class	Natural TL		Induced TL				LT /TL Sens. (x10 ³)	Pairing
	LT/HT	LT (10 ³ counts)	TL Sensitivity (Dhajala=1)	Peak Temp. (°C)	Width (°C)	TL Subtype		
Y-75106 LL3	6.07±0.09	171.9±5.1	0.89±0.02	163±1	123±1	3.7	194±7	
Y-793573 L3	0.55±0.01	19.6±2.5	1.17±0.01	159±2	125±0	3.8	17±2	○
Y-8014 L3	0.58±0.01	4.7±0.0	0.39±0.01	159±6	135±2	3.6	12±0	○
Y-793255 L3	1.97±0.04	25.0±2.1	0.45±0.06	156±2	128±1	3.6-3.7	55±8	
Y-793571 L3	2.12±0.05	25.3±1.3	0.25±0.00	165±3	121±1	3.6	103±5	
Y-74417 L3	3.94±0.16	7.2±0.3	0.16±0.03	92±12	87±3	3.4-3.6	46±9	
Y-793370 L3	5.40±0.18	89.4±0.5	0.90±0.06	133±1	119±1	3.7-3.8	100±7	○
Y-793325 L3	5.88±0.01	27.1±2.5	0.28±0.04	144±4	126±1	3.5-3.6	97±15	○
Y-74441 L3	8.24±0.15	19.8±0.2	0.12±0.01	120±3	144±2	3.5	158±8	
Y-75029 H3		0.1±0.0	0.009±0.002	194±9	311±7	3.1-3.2	14±2	
Y-791856 H3		0.8±0.1	0.031±0.002	94±15	113±7	3.3	26±2	
Y-792927 H3	0.71±0.03	5.5±0.2	0.26±0.00	151±1	128±2	3.6	21±1	
A-882004 H3	2.06±0.01	36.4±0.9	0.56±0.03	150±4	113±5	3.7	65±4	
Y-74142 H3	4.30±0.04	221.1±11.1	1.27±0.04	153±1	130±2	3.8	174±10	
A-9007 H3	4.75±0.09	63.7±1.1	0.37±0.02	150±5	115±1	3.6	174±8	

Mineralogy of Antarctic micrometeorites recovered from the Dome Fuji Station

○Takaaki Noguchi¹ and Tomoki Nakamura²

1) Dept. of Materials and Biological Sciences, Ibaraki Univ., Bunkyo 2-1-1, Mito 310-8512, Japan

2) Dept. of Earth and Planet. Sci., Kyushu Univ., Hakozaki, Fukuoka 812-8581, Japan

Introduction Many micrometeorites (MMs) have experienced heating during atmospheric entry. Some of them were partially to totally melted (“scoriaceous” MMs). Others were not melted although affected thermally (unmelted MMs). There are unmelted MMs that contain phyllosilicates (e. g. Kurat et al., 1994; Klöck and Stadermann, 1994). Chemical compositions of phyllosilicate-bearing unmelted MMs have the lithophile trace element abundances similar to CM and CR chondrites (e. g. Jessberger et al., 1999). From the mineralogical point of view, there are two types among such MMs: serpentine-bearing MMs, which sometimes contain tochilinite-like mineral, and saponite-bearing MMs, which do not contain serpentine. In this consortium study, unmelted Antarctic MMs (AMMs) recovered from the Dome Fuji Station were divided into three groups, on the basis of S/Si intensity ratios measured by SEM-EDS (Noguchi et al., 1999), in order to estimate heating during atmospheric entry. We assumed that unmelted AMMs with S/Si ratios similar to those of CM chondrites (called “group 1” AMMs in this consortium study) are most probable to contain phyllosilicates, although phyllosilicate-rich MMs tend to be depleted in S (e. g. Jessberger et al., 1999). We investigated the “group 1” AMMs by Gandolfi camera and TEM to check our assumption and to investigate the relationship between bulk mineralogy and microstructure of the same grains.

Samples and Methods Each unmelted AMM was exposed to Cr-K α X-ray for 12 to 60 hours in a Gandolfi camera to obtain a powder diffraction pattern, in order to investigate bulk mineralogy of each AMM. After investigation by Gandolfi X-ray camera, each AMM was embedded in epoxy resin and microtomed by Leitz-Reichert Super Nova ultramicrotome for TEM observation. Microstructure and mineralogy of each AMMs were obtained by JEOL JEM-2000FX II. Remainders of each embedded AMM were observed by LV-SEM, JEOL JSM-5300LV with Oxford ISIS EDS in order to observe texture and analyze qualitatively of each AMM.

Results The authors investigated six AMMs for this study. Among them, here we report mineralogy of two AMMs: F96CI024 and F96CI025.

(1) *Bulk mineralogy* F96CI024 has a strong diffraction peak at about 0.97 nm. This diffraction peak is attributed to 001 reflection of saponite. A diffraction peak at 0.45 nm is attributed to 02l prizm reflection due to stacking disorder of saponite. Diffraction peaks that are attributed to pyrrhotite and magnetite are strong. Diffraction peaks attributed to olivine and low-Ca pyroxene are very weak. X-ray diffraction data suggest that F96CI024 is composed mainly of saponite, pyrrhotite, and magnetite and that olivine and low-Ca pyroxene are minor components in this AMM.

F96CI025 has diffraction peaks attributed to pyrrhotite, olivine, and low-Ca pyroxene. Diffraction peaks attributed to magnetite are weak. Shapes of diffraction peaks of olivine and low-Ca pyroxene indicate that crystallinity (or grain size) of them is low. X-ray diffraction data suggest that F96CI025 is composed mainly of pyrrhotite and very fine-grained olivine and low-Ca pyroxene and that does not contain phyllosilicates.

(2) *TEM observation* Low magnification bright-field images of F96CI024 show that the matrix of this AMM is composed of sub- μm sized phyllosilicate with sub- μm sized magnetite and pyrrhotite. Subhedral to euhedral magnetite and pyrrhotite grains with more than 2 μm across are embedded in the

matrix. High-resolution bright-field images of the phyllosilicate reveal that it has about 1.0 nm lattice fringes. The lattice fringes are curved and contain many stacking disorders. The spacing of the phyllosilicate suggests that it is saponite. Serpentine, which has 0.7 nm lattice fringes, were not observed.

Low magnification bright-field images of F96CI025 show that this AMM is very porous. Selected area electron diffraction (SAD) pattern of relatively coarse-grained areas of the matrix ($< 1 \mu\text{m}$ across) suggests that they are composed mainly of olivine, pyrrhotite, and magnetite. SAD pattern of fine-grained areas of the matrix ($< 200 \text{ nm}$ across) suggests that they contain low-Ca pyroxene in addition to minerals found in coarse grained areas.

As shown above, crystallographic data obtained by a Gandolfi camera correspond well to major minerals observed by TEM.

(3) *SEM observation* F96CI024 has compact matrix, in which encloses Fe-sulfide and magnetite grains. Their grain sizes range from more than $10 \mu\text{m}$ across to less than $1 \mu\text{m}$. One euhedral Fe-Ni-sulfide grain was observed. Plaquette magnetite was observed but framboidal magnetite was not observed in this AMM. F96CI025 has very porous fine-grained matrix. The AMM contains fragments of magnesian olivine and Fe-sulfide with more than $10 \mu\text{m}$ across.

Discussion

F96CI024 has a totally hydrated mineral assemblage. Saponite was observed but serpentine was not observed in F96CI024. Relict anhydrous minerals are rare. Although framboidal magnetite that was found in BI91/3-108 was not found in F96CI024 during SEM observation, aggregates of magnetite (each grain is less than 100 nm across) were found during TEM observation. Texture and mineralogy of this AMM are very similar to those of a phyllosilicate-rich AMM, BI91/3-108 (Kurat et al., 1994; Klöck and Stadermann, 1994). It is suggested that both AMMs were formed under similar physico-chemical conditions. Phyllosilicate mineralogy of them is different from that of CI and CM chondrites. Parent bodies of these AMMs are probably different from CI and CM parent bodies.

Summary We investigated AMMs that experienced weak heating during atmospheric entry by Gandolfi X-ray camera and TEM. Major mineral phases estimated by using a Gandolfi camera correspond well to mineralogical data obtained by TEM. We found a phyllosilicate-rich MM, F96CI024, which has very similar texture and mineralogy of an AMM reported by Kurat et al. (1992). Phyllosilicate in this MM is 1.0 nm-phyllosilicate (saponite), and serpentine was not observed. The phyllosilicate-rich AMM has more compact and finer-grained matrix than an AMM without phyllosilicate.

Acknowledgement SEM observation of two AMM samples was performed at Tokyo Institute of Technology. We thank Dr. H. Yurimoto for his permission to use LV-SEM.

References Jessberger et al. (1999) in press; Klöck and Stadermann (1994) In: Analysis of interplanetary dust, 51-87; Kurat et al. (1992) LPSC XXIII, 747-748; Kurat et al. (1994) GCA, 58, 3879-3904; Nakamura et al. (1999) in this volume; Noguchi et al. (1999) in this volume

Antarctic micrometeorites recovered from the Dome Fuji Station: a combined study of mineralogy, bulk chemistry, and isotopic compositions.

○Takaaki Noguchi¹, Naoya Imae², Tomoki Nakamura³, Wataru Nozaki³, Kentaro Terada⁴, Takeshi Mori⁴, Izumi Nakai⁵, Nahoko Kondo⁵, Miho Sasaki⁵, Toshio Murakami⁶, Takaaki Fukuoka⁷, Ken-ichi Nogami⁸, Rie Oomori⁸, Hideo Ohashi⁹

1) Dept. of Materials and Biological Sci., Ibaraki Univ., Bunkyo 2-1-1, Mito 310-8512, Ibaraki, Japan

2) Earth and Planetary Sci., Kyushu Univ., Hakozaki Fukuoka 812-8581, Japan

3) Nat. Inst. of Polar Res., 1-9-10 Kaga, Itabashi, Tokyo 173-8515, Japan

4) Dept. of Earth and Planet. System Sci., Hiroshima Univ., 1-3-1 Kagamiyama, Higashihiroshima 739-8526, Japan

5) Dept. of Applied Chemistry, Sci. Univ. of Tokyo, Kagurazaka, Shinjyuku, Tokyo 162-0825, Japan

6) Computer Center, Gakushuin Univ., 1-5-1 Mejiro, Toshima, 171-8588, Japan

7) Dept. of Environmental Systems, Fac. of Geo-environmental Sci., Rissho Univ., 1700 Magechi, Kumagaya, Saitama 360-0914, Japan

8) Dept. of Physics, Dokkyo Univ., School of Medicine, Mibu, Tochigi 321-0293, Japan

9) Dept. of Ocean Sci., Tokyo Univ. of Fisheries, Kounan, Minato, Tokyo 108-8477, Japan

Initial examination and curation of Antarctic micrometeorites (AMMs) which were recovered from the Dome Fuji Station have started from last year (Nakamura et al., 1999). As well as initial examination and curation, a digital catalog of identified AMMs has been open on the web site at Gakushuin University (Nakamura et al., 1999). At the end of last year, the authors of this abstract (AMM working group) found more than 200 AMMs in the unprocessed samples collected at the Dome Fuji Station in 1996. A consortium study for these AMMs has started at the end of last year. The AMM working group is investigating the identified AMMs by various methods.

Mechanisms of accretion onto the Earth are different between MMs and meteorites. Because of the accretion mechanism of MMs, MMs must represent more unbiased collection of asteroidal samples. This means that MMs contain samples of asteroids that were not found among meteorite samples. However, MMs are very small (most of them are $< 100 \mu\text{m}$ across) and they show various mineralogy and chemistry. Therefore, significance of this consortium study would be lessened if different MMs were used for different kinds of study. The AMM working group investigates the same MMs by various methods. Figure 1 shows the flow chart of this consortium study. In this consortium study, AMM samples were first investigated by non-destructive methods such as XRF, then investigated by destructive methods such as mass spectrometry of rare gases. Due to the deficiency of machine times, not all the identified AMMs could be characterized by non-destructive methods such as synchrotron-XRF and Gandolfi X-ray camera. Therefore, the order of priority was decided for the identified AMMs, to choose AMMs that preserve pristine mineralogy and chemistry. One of the volatile element, sulfur, was used for the parameter of the order. Based on the S/Si intensity ratios measured by SEM-EDS, the AMMs were divided into three groups. AMMs with the ratios similar to those of CM chondrites (S/Si ratios: 0.1 ~ 0.2) were classified as "group 1" (most important, least heated), because most of AMMs have chemical compositions similar to CM and CR chondrites (e. g. Jessberger, 1999). AMMs which have the ratios 0.05 ~ 0.1 and > 0.2 were classified as "group 2" (moderately heated). AMMs which have the ratios < 0.05 were classified "group 3" (heavily heated).

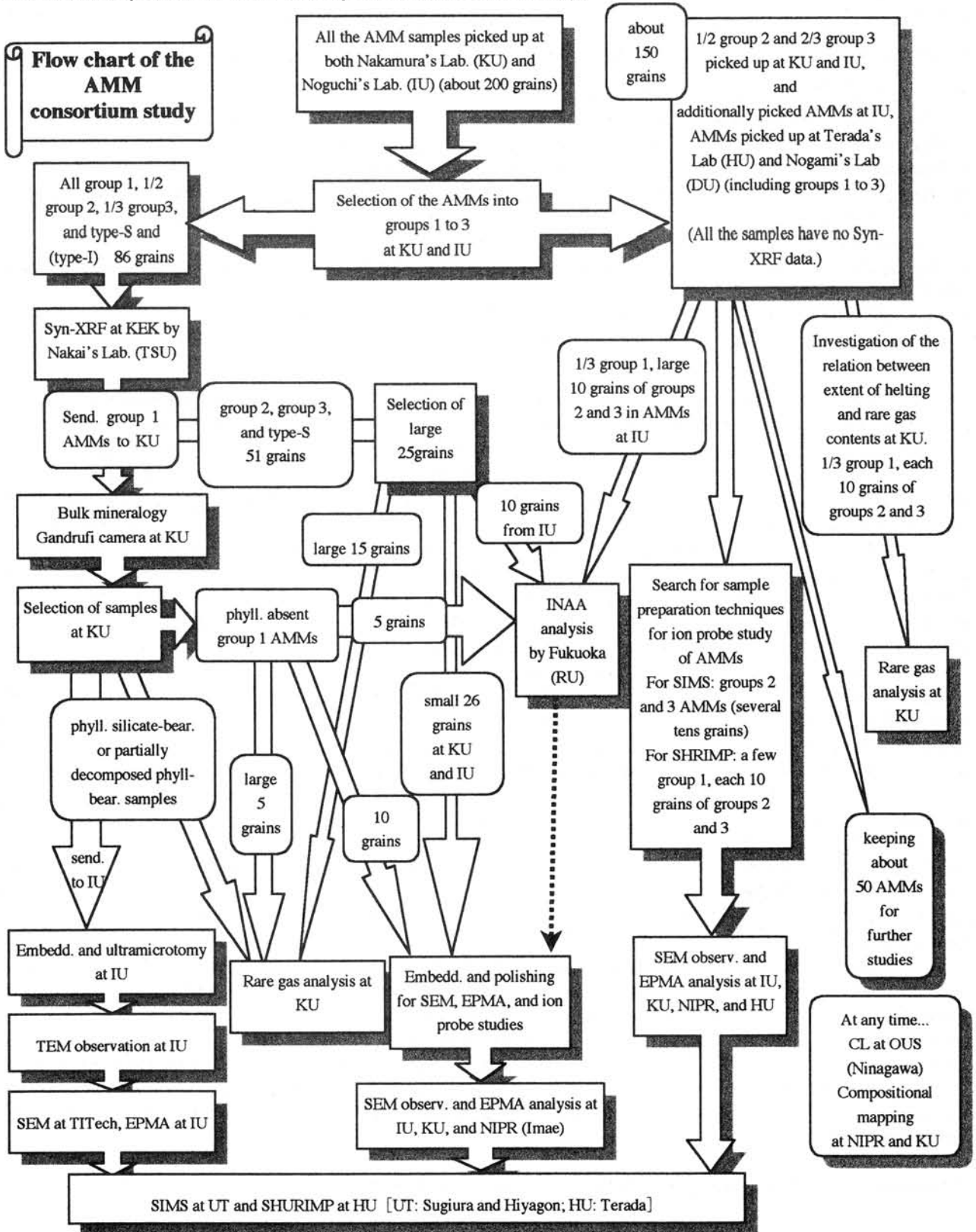
All the group 1 AMMs, 1/2 of all the group 2 AMMs, 1/3 of all the group 3 AMMs, all S-type spherules (very rare among the identified AMMs) were investigated by synchrotron-XRF at KEK. Major and trace element compositions of the AMMs were characterized by synchrotron-XRF. Then, all the group 1 AMMs were investigated by Gandolfi X-ray camera to find phyllosilicate-bearing AMMs. Phyllosilicate-bearing AMMs are investigated by TEM, SEM, EPMA, secondary ion mass spectrometry (SIMS and SHRIMP), mass spectrometry of rare gases, and INAA. Group 1 AMMs without phyllosilicates and all the groups 2 and 3 AMMs are also investigated by SEM, EPMA, secondary ion mass spectrometry (SIMS and SHRIMP), mass spectrometry of rare gases, and INAA.

References

Nakamura et al. (1999) Antarctic Meteorite Res., 12, in press.

Figure 1 Flow chart of this consortium study.

Abbreviations KU: Kyushu Univ., IU: Ibaraki Univ., HU: Hiroshima Univ., DU: Dokkyo Univ., TSU: Tokyo Sci. Univ., NIPR: National Institute of Polar Res., OUS: Okayama Univ. of Sci., TITech: Tokyo Inst. of Tech., UT: Univ. of Tokyo



DARK INCLUSIONS IN THE MOKOIA CV3 CHONDRITE: RECORD OF AQUEOUS ALTERATION, THERMAL METAMORPHISM AND SHOCK METAMORPHISM

Ichiro Ohnishi and Kazushige Tomeoka

Department of Earth and Planetary Sciences, Faculty of Science, Kobe University, Nada, Kobe 657-8501, Japan

INTRODUCTION

Dark inclusions (DIs) are common in CV3 chondrites, particularly in Allende, and have been described mainly from this meteorite [e.g., 1]. DIs are lithic clasts that range in size from 1 mm to several cm and consist mainly of fine grains of Mg-Fe silicates. Although previous workers favored that DIs are aggregates of primitive nebular condensates [e.g., 2, 3], recent studies of DIs [e.g., 4-7] suggested that they were affected by various degrees of aqueous alteration and subsequent dehydration on the meteorite parent body. Kojima and Tomeoka [5] suggested that fine fibrous grains of Fe-rich olivine common in DIs were formed by dehydration of phyllosilicate. However, most of DIs and their host CV3 chondrites consist almost exclusively of anhydrous minerals and contain little hydrous mineral such as phyllosilicate, which hinders our understanding of the previous aqueous alteration process that DIs may have experienced.

Mokoia is a unique member of the CV3 group, because it contains abundant hydrous phyllosilicates in matrix, chondrules and Ca-Al-rich inclusions (CAIs). Tomeoka and Buseck [8] showed evidence that the phyllosilicates in Mokoia were produced by aqueous alteration of anhydrous silicates probably on the meteorite parent body. Therefore, it is expected that a DI in Mokoia, if found, would provide more direct information regarding the secondary processes that most DIs in CV3 chondrites may have experienced. Previously, one DI has been reported from Mokoia by Cohen et al. [9], but no mineralogical and petrographic details were described. We performed an extensive survey of Mokoia thin sections and found a total of six relatively large ($>500\ \mu\text{m}$) inclusions (clasts) that appear brownish translucent in transmitted light, and here present the results of detailed mineralogical and petrographic study of these DIs. Our study revealed much evidence that the DIs were affected by not only thermal metamorphism but also shock metamorphism after aqueous alteration.

RESULTS

The host meteorite: Mokoia is a breccia composed of millimeter to submillimeter clasts that consist of chondrules and CAIs embedded in a fine-grained matrix. The matrix of Mokoia consists largely of fine grains ($<1\text{-}10\ \mu\text{m}$ in diameter) of Fe-rich olivine that occur in subhedral to euhedral plates or in anhedral grains. The olivine grains show a wide range of Fe/Mg ratios (Fa0-Fa90) compared to those in other CV3 chondrite matrices [10]. Minor minerals in matrix are magnetite, saponite, Fe-Ni sulfide, enstatite, Ca-rich clinopyroxene, nepheline and sodalite. Ca-rich clinopyroxene occurs as porous, commonly ring-shaped aggregates ($5\text{-}30\ \mu\text{m}$ in diameter). In places, magnetite occurs as aggregates of spherical, equant grains ($1\text{-}10\ \mu\text{m}$ in diameter), analogous to framboidal magnetite. Saponite occurs widely in interstices between the olivine grains in matrix and also in discrete clusters ($10\text{-}50\ \mu\text{m}$ in size). The Mokoia matrix shows a high proportion of pores, mostly interstitial spaces between matrix grains, exhibiting a loosely compacted appearance. The porosity of the matrix, measured by image processing of backscattered electron images, is in the range between 16 and 28%, which is considerably higher than the matrices of most other CV3 chondrites [11]. Chondrules and CAIs in Mokoia also contain phyllosilicates, saponite and high-Al phyllosilicates (HAP); HAP have been identified as a unit cell-scale intergrowth of Na-rich phlogopite and serpentine [8].

Dark inclusions: The DIs range in size from 0.5 to 2.5 mm and, in BSE images, they are distinctly bright, thus are easily distinguishable from the host meteorite. The DIs are composed mostly of chondrules and chondrule fragments embedded in a fine-grained matrix. The matrix of the DIs consists largely of fine grains of Fe-rich olivine and minor magnetite, Fe-Ni sulfide, Ca-rich clinopyroxene, andradite, sodalite and saponite; these constituent

minerals are common with those in the matrix of the host meteorite. However, the olivine grains in the DI matrix are distinctly more Fe-rich and more homogeneous in composition (Fa45-65) than those in the host meteorite matrix. The matrix grains in the DIs are much more compacted than those in the host meteorite; the measured porosity (1-5 %) is much lower than that of the host meteorite matrix (16-28 %). The Fe enrichment of olivine and the denser packing of the grains are probably the main causes of the bright contrast when imaged using backscattered electrons. Fine grains (1-10 μm in diameter) of magnetite and Fe-Ni sulfide are dispersed in high densities; in places, magnetite occurs as framboidal aggregates. Phyllosilicates in matrix and chondrules are much lower in amount than in the host meteorite; in the matrix, the occurrence of saponite is mostly limited to the areas in which olivine grains are relatively loosely compacted and show low Fe/Mg ratios. The olivine grains located close to large magnetite and Fe-Ni sulfide grains tend to be highly enriched in Fe, which suggests that Fe diffused from these Fe-rich phases to surrounding olivines.

Another notable characteristic common to most of the DIs is the occurrence of high densities of fractures in the matrix that range in width from 2 to 10 μm and in length from 100 to 1000 μm . They are mostly randomly oriented and form networks. Fractures terminate at the boundaries between the DIs and the host meteorite, indicating that they formed prior to incorporation to the present location. The fracture density is higher in the areas where matrix grains are more strongly compacted. In one of the DIs showing the highest fracture densities, fractures extend radially from a chondrule (~800 μm in diameter). In some chondrules, olivine crystals show planar fractures in transmitted light. Planar fractures in olivine are known to be characteristic of shock metamorphism and indicative of shock stages S3-S4. Previous petrographic study of Scott et al. [12] indicated that Mokoia is shock stage S1, virtually unshocked. Our observations of the host meteorite also support their classification. Thus these features in the DIs strongly suggest that they suffered impact-induced shock metamorphism of stage S3-S4 before final lithification.

One of the clasts has a wide, long vein (~70 μm wide and ~1 mm long) filled with dense aggregates of submicrometer-size granular silicates (probably olivine and pyroxene) and Fe-Ni sulfide. The vein contains small, angular to irregularly shaped fragments (1-10 μm in diameter) of forsterite, enstatite, Ca-rich clinopyroxene, plagioclase and spinel. The vein also contains numerous tiny vesicles (<1 μm in diameter). From texture and mineralogy, we believe that this vein is a shock-induced melt. Our broad-beam analysis and X-ray chemical mapping revealed that the vein is similar in composition to the matrix of the host meteorite but is relatively enriched in Fe, Ca and S. In addition to this large vein, we also found numerous narrow veins (~2 μm in width and 100-500 μm in length) composed mainly of tiny grains (<1 μm) of magnetite and Fe-Ni sulfide. They commonly extend from large magnetite and sulfide grains and form interconnected networks. In some areas, veins form along straight, shear plane-like fractures that run in parallel.

DISCUSSION

The DIs in Mokoia contain chondrules and chondrule fragments in a fine-grained olivine-rich matrix. The major mineral constituents are common with those in the host meteorite. They also contain the same phyllosilicates (saponite and HAP) as in the host meteorite in both matrix and chondrules. These features suggest that the DIs are probably clasts that are genetically related to the host meteorite, and they have been once involved in the aqueous alteration process similar to that experienced by the host meteorite. However, the DIs show a variety of mineralogical and textural characteristics different from the host meteorite. The more homogeneous, Fe-rich composition of olivine and the scarcity of phyllosilicates in the matrix of DIs suggest that they experienced thermal metamorphism and dehydration. These characteristics are consistent with the contention previously proposed for the dark inclusions in other CV3 chondrites (e.g., Allende, Vigarano) [4-6], i.e., they have experienced aqueous alteration and subsequent thermal dehydration.

Of particular interest is that these DIs in Mokoia show characteristics indicative of additional metamorphism, i.e., shock metamorphism. The matrix of the DIs in Mokoia show highly compacted texture, bearing a close resemblance to those observed in Leoville, Efremovka, Bali and Grosnaja CV3 chondrites [6, 13], which were classified to shock stages S3-S4 [12]. The porosity of the matrix in the Mokoia DIs (1-5 %) is close to those of these meteorites; the porosities of the Efremovka and Bali matrices are reportedly 1 % and 2 %, respectively.

respectively [11]; the porosities of the Leoville and Grosnaja matrices are currently unavailable. From the shock classification proposed for ordinary chondrites [14], the occurrence of such a large melt vein as observed in the Mokoia DI indicates shock stage S4 or higher. The occurrence of planar fractures in olivine is consistent with shock stage S3 or higher. Recently Tomeoka et al. [15] conducted shock experiments of the Murchison CM chondrite and revealed that local melting such as melt veins and pockets were formed at peak pressures from 20 to 30 GPa. The melts produced in Murchison contain numerous globules of Fe-Ni metal and sulfide and vesicles as well as small fragments of olivine and pyroxene in a silicate-rich matrix, exhibiting an appearance similar to the melt vein in the Mokoia DI. Tomeoka et al. [15] found that local melts were mostly produced from Murchison matrix but they are consistently enriched in Fe and S and sometimes in Ca relative to the matrix. This compositional feature also resembles that in the melt vein in the Mokoia DI.

From these observations and evidence, we conclude that the DIs in Mokoia are clasts from the Mokoia parent body and they experienced not only thermal metamorphism but also shock metamorphism after aqueous alteration. They were probably shocked to stages S3-S4. This implies that strong impact events occurred locally on the Mokoia parent body. It is not clear whether the heat source for the thermal metamorphism can be mainly ascribed to shock events but is possible. Our results suggest that the Mokoia meteorite is a breccia composed of clasts from different locations in the parent body, between which the extents of aqueous alteration, thermal metamorphism and shock metamorphism differ considerably. This implies that the Mokoia parent body was not a homogeneous, dry, quiet body, but rather was a heterogeneous, dynamically processing body in which aqueous alteration, thermal metamorphism and shock metamorphism occurred actively.

Acknowledgment— We thank Dr. J.A. Wood for providing us the Mokoia samples.

References

- [1] Johnson C. A., Prinz M., Weisberg M. K., Clayton R. N. and Mayeda T. K. (1990) *Geochim. Cosmochim. Acta* 54, 819-830.
- [2] Kurat G., Palme H., Brandstätter F. and Huth J. (1989) *Z. Naturforsch.* 44a, 988-1004.
- [3] Palme H., Kurat G., Spettel B and Burghelle A. (1989) *Z. Naturforsch.* 44a, 1005-1014.
- [4] Kojima T., Tomeoka K. and Takeda H. (1993) *Meteoritics* 28, 649-658.
- [5] Kojima T. and Tomeoka K. (1996) *Geochim. Cosmochim. Acta* 60, 2651-2666.
- [6] Krot A. N., Scott E. R. D. and Zolensky M. E. (1995) *Meteoritics* 30, 748-775.
- [7] Krot A. N., Petaev M. I., Scott E. R. D., Choi B-G., Zolensky M. E. and Keil K. (1998) *Meteorit. Planet. Sci.* 33, 1065-1085.
- [8] Tomeoka K. and Buseck P. R. (1990) *Geochim. Cosmochim. Acta* 54, 1745-1754.
- [9] Cohen R. E., Kornacki A. S. and Wood J. A. (1983) *Geochim. Cosmochim. Acta* 47, 1739-1757.
- [10] Scott E. R. D., Barber D. J., Alexander C. M., Hutchison R. and Peck J. A. (1988) In *Meteorites and the Early Solar System* (eds. J. F. Kerridge and M. S. Mathews) Univ. Arizona Press, Tucson, pp. 718-745.
- [11] Corrigan C. M., Zolensky M. E., Dahl J., Long M., Weir J., Sapp C. and Burkett P. J. (1997) *Meteorit. Planet. Sci.* 32, 509-515.
- [12] Scott E. R. D., Keil K. and Stöffler D. (1992) *Geochim. Cosmochim. Acta* 56, 4281-4293.
- [13] Nakamura T., Tomeoka K. and Takeda H. (1992) *Earth Planet. Sci. Lett.* 114, 159-170.
- [14] Stöffler D., Keil K. and Scott E. R. D. (1991) *Geochim. Cosmochim. Acta* 55, 3845-3867.
- [15] Tomeoka K., Yamahana Y. and Sekine T. (1999) *Geochim. Cosmochim. Acta*, in press.

Crush-released noble gases from ureilites

R. Okazaki^{1, 2)}, T. Nakamura¹⁾, N. Takaoka¹⁾ and K. Nagao²⁾

1) Department of Earth and Planetary Sciences, Faculty of Science, Kyushu University 33, Hakozaki, Fukuoka 812-8581, Japan

2) Laboratory for Earthquake Chemistry, Graduate School of Science, University of Tokyo, Hongo, Bunkyo-ku, Tokyo 113-0033, Japan

Introduction

Ureilites are achondrites which have well developed plutonic textures with chemical compositions typical of igneous rocks. They also have primitive characteristics, e.g., high abundance of siderophile elements and "planetary-type" noble gases, and the oxygen isotopic signature of unequilibrated solar system materials. Ureilites are enriched in carbonaceous materials which occurs between and within olivine and pigeonite grains. Although ureilitic olivines have relatively uniform chemical compositions, their outer rims are reduced and contain Ni-poor metallic iron. It is generally accepted that the reduction rims were produced by solid-state reactions between olivine and interstitial carbonaceous materials. During the reduction processes, noble gases might have been released from carbonaceous carrier phases and accumulated in the rims and grain boundaries.

Samples studied in this work are ALH-78019 and Kenna which are classified as a very low- and medium-shocked ureilites, respectively. Slices of ~800 μm in thickness were prepared from the two ureilites. Noble gases were extracted by step-crushing consisting of four and six steps for each sample in order to investigate the variation of concentration and isotopic compositions. Each crushing step consisted of 300-600 strokes. Released gases were measured using a modified VG5400 mass spectrometer.

Results and discussion

Large amounts of noble gases were released by crushing from both samples. The crush-released noble gases are almost free of cosmogenic and radiogenic components. Isotopic ratios of Ar, Kr and Xe are not atmospheric but similar to those of a typical trapped component in ureilites. As shown in Fig. 1, isotopic ratios of Ne released by crushing ALH-78019 are almost identical to those of the HF/HCl acid residue which contains planetary-type gases [Wacker, 1986]. On the other hand, crush-released Ne from Kenna is close to the bulk sample [Wilkening and Marti, 1976] which is typically cosmogenic. Fig. 2 shows the release patterns of noble gases obtained by crushing together with cumulative amounts of each isotope released in all the crushing steps relative to bulk samples. ALH-78019 shows a steep decrease with increasing crushing steps except for cosmogenic ^{21}Ne , whereas Kenna shows a gentle decrease. Total amounts of the gases from Kenna are more abundant relative to those from ALH-78019. Microscopic observations show that olivine grains in Kenna are more reduced than ALH-78019 [Berkley *et al.*, 1976; Berkley and Jones, 1982]. Thus, it is reasonable to postulate that gases obtained by crushing the two meteorites are trapped components located in the reduction rims that are fragile to crushing. The crush-released Ne from Kenna can be explained by contamination from a cosmogenic component emitted from newly formed surfaces of silicates. This interpretation is consistent with a longer exposure age

(33 Ma) of Kenna [Wilkening and Marti, 1976; Goodrich *et al*, 1987] compared to that of ALH-78019 (0.1 Ma) [Wacker, 1986].

Elemental ratios of the crush-released heavy noble gases from the ALH-78019 and Kenna are plotted in Fig. 3 along with reported elemental ratios in bulk samples of the meteorites. It can be seen from the figure that noble gases released by crushing are fractionated relative to those in the bulk meteorites which are enriched in Ar and Kr. This fractionation effect is more pronounced in Kenna than in ALH-78019. If the formation of reduction rims resulted from shock heating, we speculate that shock effects were responsible for the fractionation of gases released by crushing. The shock effects will produce increases in pressure and temperature, and changes in structures of carbonaceous materials. Although Wacker (1986) reported no correlation between shock *pressure* and the $^{36}\text{Ar}/^{132}\text{Xe}$ ratios in *bulk* samples, increased temperature and structural changes could produce the inferred fractionation in noble gases.

As a test for this hypothesis of shock effects on noble-gas compositions, further crushing experiments, together with petrographic studies must be carried out on other shock-affected ureilites. Also, it is necessary to investigate the relationship between elemental ratios (e.g. $^{36}\text{Ar}/^{132}\text{Xe}$) and shock-related temperature and structural changes in the meteorites.

References

- Wacker J. (1986) *G.C.A.* **50**, 633-642.
 Wilkening L. L. and Marti K. (1976) *G.C.A.* **40**, 1465-1473.
 Goodrich C. A. *et al.* (1987) *Meteoritics* **22**, 191-218.
 Berkley J. L. *et al.* (1976) *G.C.A.* **40**, 1429-1437.
 Berkley J. L. and Jones J. H. (1982) *Proc. L.P.S.C.* **13th**, *J.G.R.* **87**, A353-A364.
 Goodrich C. A. *et al.* (1987) *G.C.A.* **51**, 2255-2273.

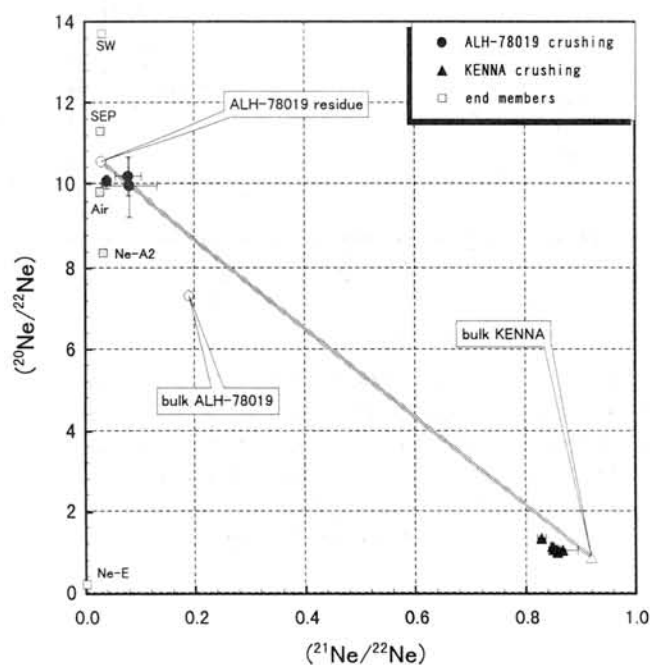


Fig. 1: Neon isotopic correlation plot for ALH-78019 and Kenna ureilites. Isotopic ratios of Ne by crushing ALH-78019 is close to those of the acid residue.

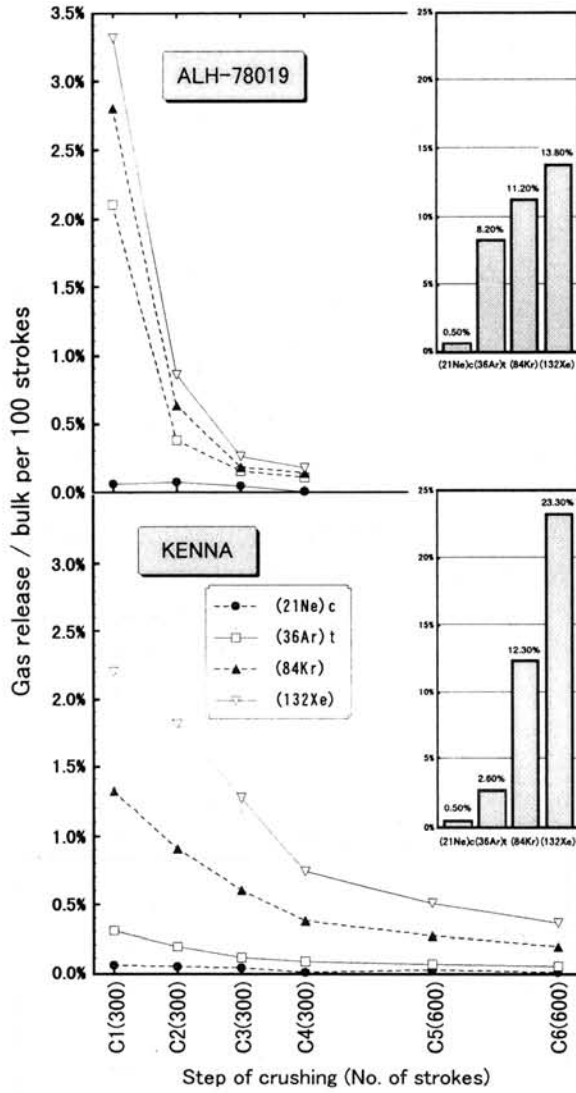


Fig. 2: Fractions of crush-released gases relative to bulk concentration per 100 strokes. A release pattern for ALH-78019 show a very steep decrease whereas that for Kenna are gentle. Cumulative amounts of each isotope released in all the crushing steps are also shown at the upper-right of the diagram.

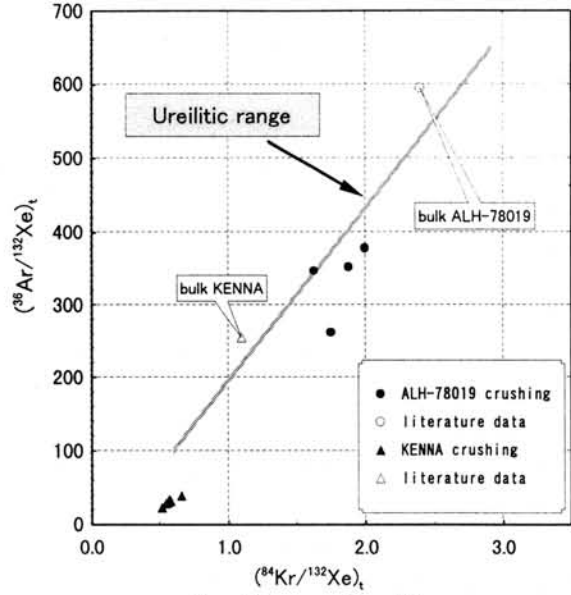


Fig. 3: Trapped $^{36}\text{Ar}/^{132}\text{Xe}$ vs. $^{84}\text{Kr}/^{132}\text{Xe}$. Elemental ratios of crush-released gases are enriched in heavier gases relative to those in bulk samples.

Noble Gas Measurement in Individual Micrometeorites Using Laser Gas-extraction System

T. OSAWA¹⁾, K. NAGAO¹⁾, T. NAKAMURA²⁾ and N. TAKAOKA²⁾

1) Laboratory for Earthquake Chemistry, Graduate School of Science, University of Tokyo, Hongo, Tokyo 113-0033, Japan

2) Department of Earth and Planetary Sciences, Faculty of Science, Kyushu University, 33, Hakozaki, Fukuoka 812-8581, Japan

Introduction

Antarctic micrometeorites, series F96C and F96D, recovered from water tank at Dome Fuji station [1] have been characterized as extraterrestrial material by members of Antarctic micrometeorite working group. Noble gas isotopic compositions are expected to serve as a key indicator for the identification of material of extraterrestrial origin. In the present work, samples with diameters ranging from 100-200 micrometer were selected to try to measure all noble gases in individual particles.

Experimental procedures

Single micrometeorites were carefully picked and dropped each into a platinum crucible with a diameter of 2 millimeter and settled in a sample holder made of stainless steel. Thirty-seven platinum crucibles can be set in the sample holder. For noble gas extraction, individual samples were heated using a slightly defocused Nd-YAG CW laser beam by increasing output power. Extracted gases were purified by two Ti-Zr getters and noble gases except for He were collected on a cryogenically cooled trap at 15K. Ne, Ar, Kr and Xe were released successively at 45, 100, 135 and 250K and the isotopic composition of each gas analyzed on a modified VG5400 mass spectrometer (MS-III).

Results and discussion

Measured amounts and isotopic ratios of all noble gases (not corrected for blank) in 12 micrometeorites are presented in Table 1. The sample weights are 0.4 - 7.1 μ g, except for spherule CK005 (21.5 μ g). Measured amounts of noble gases are very small and variable among the samples. Blank levels are comparable for some samples. Based on the released amounts of He and Ne, the samples may be separated into two groups, gas-rich and gas-poor. The highest concentration of ⁴He for DK026 (3×10^{-3} cm³STP/g) is, however, lower than in single IDPs [2]. In Fig.1 ³He/⁴He ratios are plotted against measured ⁴He amounts. The gas-rich samples show ³He/⁴He ratios similar to SEP-He, suggesting implantation of solar energetic particles (SEP), while the gas-poor samples have lower ³He/⁴He. The SEP-like ³He/⁴He ratios are similar to the data by Kehm et al. [3], but the trend in Fig. 1 is quite different from that of previous work on IDPs by Nier and Schlutter [4] and Kehm et al.[3]. Ne isotope data may be separated into two groups; SEP-like Ne and Ne with atmospheric or lower

$^{20}\text{Ne}/^{22}\text{Ne}$ ratios, which corresponds to the gas-rich and the gas-poor samples, respectively. The latter data are not presented in Fig. 2 because of an ambiguity in correction for doubly charged ^{40}Ar and CO_2 for the small amounts of Ne. Cosmogenic Ne component is negligible in all the samples, which may indicate very short cosmic-ray exposure age. Ar-3 isotope plot is shown in Fig. 3. The $^{40}\text{Ar}/^{36}\text{Ar}$ ratios are separated into two groups, too. The plots with lower $^{40}\text{Ar}/^{36}\text{Ar}$ correspond to those with higher $^{20}\text{Ne}/^{22}\text{Ne}$, which obviously demonstrates the solar origin. The $^{38}\text{Ar}/^{36}\text{Ar}$ ratios for these samples are between the ratios for solar wind and SEP. Noble gas abundance patterns for typical micrometeorites, normalized to ^{36}Ar are plotted in Fig.4. Compared to lunar soil or planetary gas, micrometeorites have a large diversity. From the plot patterns, however, we can hardly distinguish samples with solar or planetary noble gas components. $^{129}\text{Xe}/^{132}\text{Xe}$ ratios do not show large excesses in ^{129}Xe , and are similar to those of carbonaceous chondrites though the experimental errors are still large due to extremely small amounts of Xe ($<3 \times 10^{-14} \text{ cm}^3 \text{STP}$).

The noble gas data obtained in the present work clearly indicates that the gas-rich micrometeorites are small objects in space, of extraterrestrial origin, and not fragments produced from break up of meteorites fell in Antarctica.

References

- [1] Nakamura T. et al., *Antarctic Meteorites X X III* (1998) 104-106
- [2] Nier A.O. and Schlutter D.J., *Meteoritics*,25 (1990) 263-267
- [3] Kehm K. et al., *LPSC X X X* (1999) 1398.
- [4] Nier A.O. and Schlutter D.J., *Meteoritics*,28 (1993) 675-681

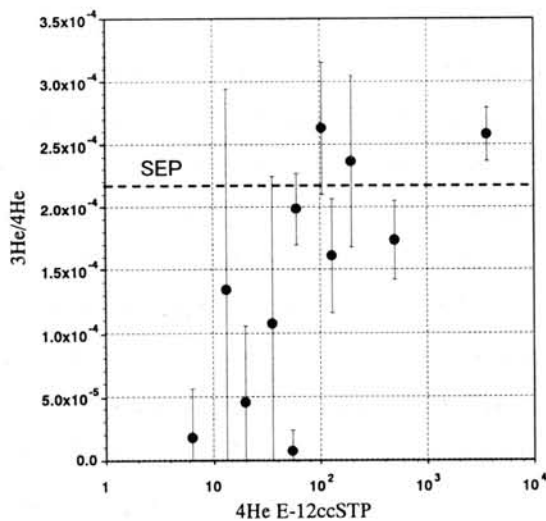


Fig.1 $^3\text{He}/^4\text{He}$ isotopic ratios plotted against ^4He content.

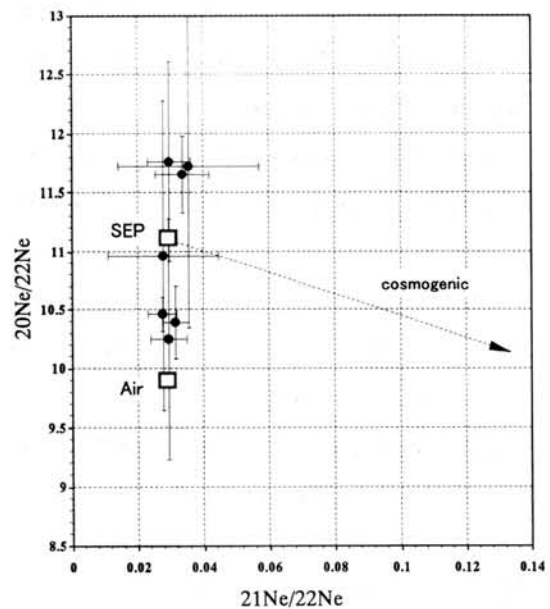


Fig.2 Ne isotopic ratios in Micrometeorites

Table 1 Isotopic ratios and amounts of noble gases released from individual micrometeorites (preliminary results)

sample	weight (μg)	type	^4He $10^{-12}\text{cm}^3\text{STP}$	$^3\text{He}/^4\text{He}$ 10^{-4}	^{20}Ne $10^{-12}\text{cm}^3\text{STP}$	$^{20}\text{Ne}/^{22}\text{Ne}$	$^{21}\text{Ne}/^{22}\text{Ne}$	^{40}Ar $10^{-9}\text{cm}^3\text{STP}$	$^{38}\text{Ar}/^{36}\text{Ar}$	$^{40}\text{Ar}/^{36}\text{Ar}$	^{84}Kr $10^{-15}\text{cm}^3\text{STP}$	^{132}Xe $10^{-15}\text{cm}^3\text{STP}$	$^{129}\text{Xe}/^{132}\text{Xe}$
F96CK005	21.5	Sp	29.4	nd	1.56	6.5 ± 1.4	0.032 ± 0.021	0.11	0.200 ± 0.006	320.4 ± 5.9	5.9	5.3	1.14 ± 0.29
F96DK002	7.1	Mm	60.2	1.98 ± 0.03	40.4	11.72 ± 0.14	0.036 ± 0.004	0.14	0.191 ± 0.003	34.0 ± 0.2	45.7	35.2	1.02 ± 0.10
F96DK014	3.0	Mm	104.0	2.63 ± 0.53	5.22	10.5 ± 0.8	0.028 ± 0.007	0.11	0.195 ± 0.004	137.0 ± 2.6	3.6	20.7	0.98 ± 0.12
F96DK016	1.0	Mm	54.7	0.07 ± 0.17	0.65	7.6 ± 1.3	0.024 ± 0.017	0.13	0.186 ± 0.024	306.3 ± 6.7	9.2	11.4	1.01 ± 0.17
F96DK019	2.7	Mm	35.7	1.1 ± 1.2	21.21	11.8 ± 0.3	0.030 ± 0.004	0.08	0.198 ± 0.004	54.9 ± 1.1	4.6	5.8	1.18 ± 0.17
F96DK026	1.1	Mm	3659.0	2.58 ± 0.21	14.48	11.00 ± 0.32	0.028 ± 0.008	0.16	0.195 ± 0.003	65.1 ± 1.0	5.9	11.4	0.96 ± 0.19
F96DK029	1.0	Mm	494.3	1.73 ± 0.32	5.81	10.4 ± 1.0	0.032 ± 0.006	0.20	0.184 ± 0.006	62.8 ± 0.8	2.8	5.3	1.06 ± 0.08
F96DK036	0.9	Mm	196.0	2.36 ± 0.68	7.25	11.65 ± 0.57	0.034 ± 0.008	0.16	0.189 ± 0.003	43.4 ± 0.3	15.7	14.3	0.99 ± 0.16
F96DK044	1.1	Mm	6.4	0.17 ± 0.39	2.02	8.2 ± 2.1	0.045 ± 0.030	0.08	0.180 ± 0.012	275.4 ± 6.2	1.4	0.2	nd
F96DK051	0.4	Mm	19.9	0.45 ± 0.60	0.52	8.0 ± 1.0	0.054 ± 0.030	0.07	0.188 ± 0.011	248.60 ± 4.3	2.5	3.6	nd
F96DK052	1.4	Mm	128.7	1.61 ± 0.45	3.55	10.3 ± 1.0	0.030 ± 0.010	0.18	0.191 ± 0.005	121.8 ± 2.2	14.9	12.4	0.91 ± 0.27
F96DK060	1.0	Mm	13.4	1.3 ± 1.6	0.6	7.3 ± 1.5	0.049 ± 0.025	0.09	0.187 ± 0.014	247.7 ± 4.1	3.8	13.1	1.08 ± 0.21
blank1			3.1	nd	1.79	7.9 ± 1.7	0.083 ± 0.038	0.08	0.189 ± 0.041	299.3 ± 7.2	4.8	1.1	nd
blank2			6.3	nd	0.37	7.8 ± 0.9	0.068 ± 0.034	0.07	0.189 ± 0.010	296.5 ± 5.8	0.2	nd	nd

'Sp' and 'Mm' stand for spherule and micrometeorite respectively

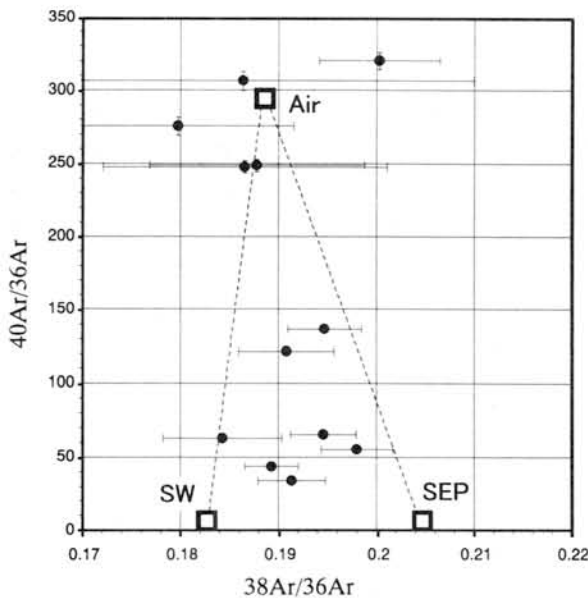


Fig.3 Ar isotopic ratio in Micrometeorites

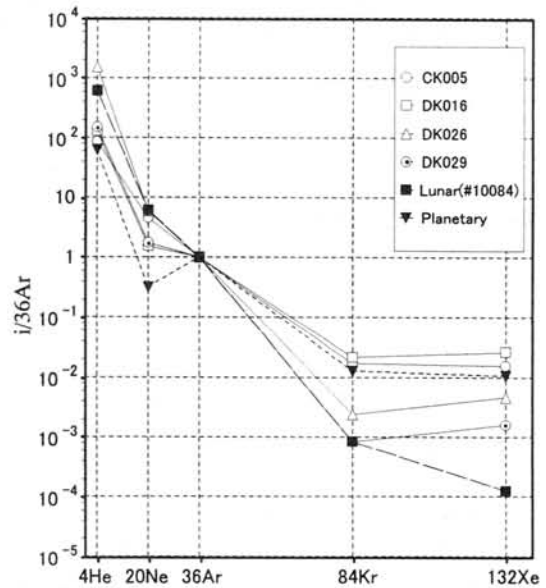


Fig.4 Noble gas abundance pattern normalized to ^{36}Ar

Weathering effects on the chemical composition of Antarctic UOCs

Hiromasa Ozaki, Gregory W. Kallemeyn and Mitsuru Ebihara
Graduate School of Science, Tokyo Metropolitan University
Hachioji, Tokyo 192-0397, Japan

Introduction

The Antarctic continent is mostly covered with a thick layer of ice, deposited over a long period of time. Being trapped in this ice, fallen meteorites have been preserved over thousands of years. Antarctic meteorites are most susceptible to weathering processes related to water while on the surface of the ice, just after they fall or upon re-emerging to the surface in a "blue ice" region. Antarctic meteorites apparently experienced some petrologic alteration processes in Antarctica after falling. It is important to evaluate the influence of terrestrial weathering on the chemical compositions of the Antarctic meteorite specimens. Although weathering processes caused some changes in mineralogy (e.g., Velbel, 1988; Gooding et al., 1986) and/or redistributions of elements (e.g., Shimizu et al., 1983; Laugenour et al., 1993a,b; Shinonaga et al., 1994), the particular mechanisms have not been clearly identified. Based on an INAA study of the composition of Antarctic chondrites, the weathering effects on chemical compositions will be discussed.

Major element concentrations and their ratios are used for the compositional classification of chondrites. Chemical classification also includes the determination of mineral phase compositions: Fa in olivine and pyroxene, the abundance of metallic phases, and the Co content of kamacite. Van-Schmus and Wood (1967) pointed out that their classification scheme was not always effective for type 3 ordinary chondrites because of their heterogeneous nature. Type 3 chondrites are often called unequilibrated ordinary chondrites (UOC). Based on an INAA study of UOCs, Sears and Weeks (1986) proposed some compositional parameters for classifying UOCs, but these parameters are not well-defined. Among non-Antarctic meteorites, the number of UOCs is small, while there is a relatively large number of UOCs among the Antarctic collection.

Experimental

About 30 - 50 mg of each powdered meteorite sample was weighed and doubly sealed in clean polyethylene bags. Neutron irradiations were carried out in the TRIGA II reactor at the Institute for Atomic Energy, Rikkyo University. For the analysis of elements with short-lived nuclides, samples were irradiated for 100 sec. After a 5 - 10 minute cooling period, γ -ray intensities were measured for about 300 seconds. The samples were then irradiated for 6 hours at the same reactor. After irradiation, three consecutive measurements were made for each sample following cooling intervals of one week, 10 days and one month. Elemental concentrations were calculated by comparing γ -ray intensities for the samples with those for reference samples, JB-1 and Allende.

Results and Discussions

The elemental concentrations for the Antarctic meteorites in this study were compared to the mean concentrations of meteorite falls of the corresponding groups (data from Kallemeyn et al., 1989). As is generally understood, alkaline elements are easily leached by water from the solid materials of chondrites (Fulton and Rhodes, 1984; Deninnson and Lipschutz, 1987). For Na, which is only one alkaline element determined in this study, apparent depletions are noted in some specimens. We could not determine a correlation between Na depletion and weathering index. Because weathering indices are based on a visual

estimate of the degree of surface Fe oxidation, they are not always good indicators of the weathering effects for other elements.

The standard deviations of the elemental concentrations for each meteorite group are noticeably larger than those for the Allende replicate analyses. Those for the siderophile elements are especially large. These large standard deviations may reflect either a greater heterogeneity in the sample, or a mobilization of elements caused by a secondary alteration process. The Ni-normalized values have relatively small percent deviations for all the siderophiles, suggesting that selective mobilization of some specific elements did not occur. The siderophile contents in Antarctic meteorites tend to be lower than those in non-Antarctic meteorites. The data would scatter randomly if the fluctuations were caused by heterogeneity of metal in the samples. Therefore, some siderophile element fluctuations are probably caused by mobilization of elements rather than heterogeneity in the samples. The degree of siderophile element depletions relative to non-Antarctic meteorites is variable, but larger than that for Na. Therefore, the siderophile elements appear to be more susceptible to weathering than Na. It is likely that the siderophile element contents in Antarctic chondrites have been lowered to various degrees by terrestrial weathering effects. There are no apparent correlations between the relative abundances of siderophile elements and the weathering index. As mentioned earlier, the weathering indices are visual estimations of the degree of rustiness of the metallic Fe phases in the meteorites. A lack of correlation between the siderophile abundances and the weathering index suggests that the index is poor indicator of siderophile element loss. It is probably only good for estimating the loss of water-soluble minerals. Therefore, the degree of depletion of siderophile element contents can be used as another type of weathering index.

Several classification parameters has been used for the ordinary chondrite groups. Among those parameters, siderophile element contents are a better classificational parameter for UOCs in general (Kallemeyn et al., 1989; Sears and Weeks, 1986). For Antarctic UOCs, however, this is not always true, because some Antarctic meteorites have lost some of their metallic phases during Antarctic weathering, as noted above. In Fig. 1, the relationship between the Ir and Ni contents of the ordinary chondrites are illustrated. There is a clear hiatus between the H and L groups. Between the L and LL groups, there is no clear hiatus, but the situation changes if one reclassifies seven meteorites. There are, however, no definite reasons for their classification. Based on Fig. 1, we suggest that these seven chondrites should be reclassified. After such a reclassification, good correlations within each ordinary chondrite group are found. The slopes of the fitted lines agree well with the Ir/Ni ratios for the metallic phases of the corresponding groups (Rambaldi et al., 1978, 1979; Kong et al., 1995a, 1995b; Kong and Ebihara, 1996). This further supports the reclassification of the seven meteorites.

Although Morgan et al. (1985) suggested that siderophile abundances in H chondrites were depleted in type 3 chondrites relative to other petrologic types, the type 3 samples (Tieschitz and Bremervörde) they used were reclassified into an H/L group (Kallemeyn et al., 1989). Sears and Weeks (1986) suggested that siderophile contents decrease with increasing petrologic type based on their own large data set of UOCs and some data for EOCs from the literature. However, they used many Antarctic meteorites for the UOCs and non-Antarctic meteorites for the EOCs. As mentioned above, most Antarctic meteorites have experienced weathering and likely lost some metallic phases to varying amounts. Therefore, the validity of their conclusion comes into question.

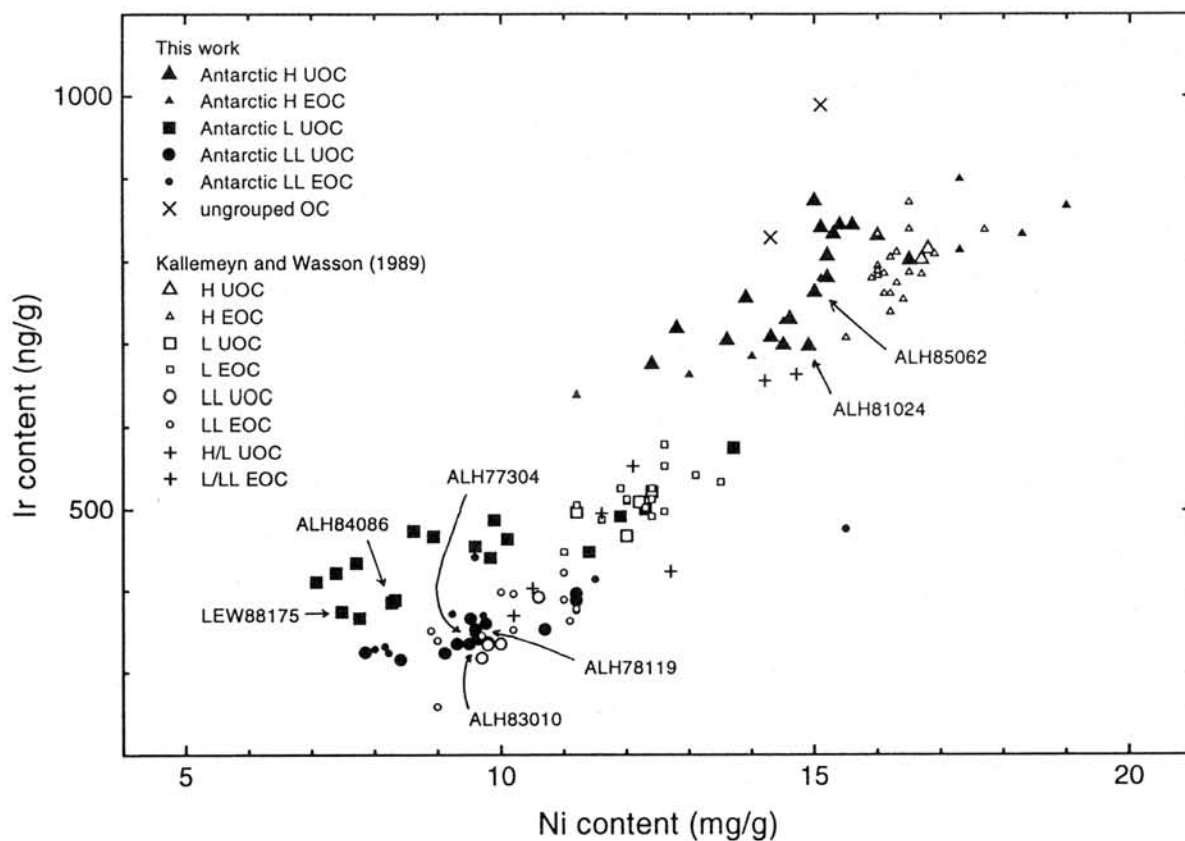


Figure 1 Relationship between Ni and Ir contents in ordinary chondrite groups. The labelled meteorites have been reclassified.

References

- Dennison, J. E. and Lipschutz, M. E. (1987) *Geochim. Cosmochim. Acta* **51**, 741-754.
- Fulton, C. R. and Rhodes, J. M. (1984) *Proc. 14th Lunar Planet. Sci.* B543-B558.
- Gooding, J. L. (1986) *Geochim. Cosmochim. Acta* **50**, 2215-2223.
- Kallemeyn, G. W., Rubin, A. E., Wang, D. and Wasson, J. T. (1989) *Geochim. Cosmochim. Acta* **53**, 2747-2767.
- Kong, P. and Ebihara, M. (1996) *Geochim. Cosmochim. Acta* **60**, 2667-2680.
- Kong, P., Ebihara, M., Endo, K. and Nakahara, H. (1995a) *Proc. 8th NIPR Symp. Antarct. Meteorites* 237-249.
- Kong, P., Ebihara, M., Nakahara, H. and Endo, K. (1995b) *Earth Planet Sci. Lett.* **136**, 407-419.
- Langenauer, M. and Krähenbühl, U. (1993a) *Earth Planet Sci. Lett.* **120**, 431-442.
- Langenauer, M. and Krähenbühl, U. (1993b) *Meteoritics* **28**, 98-104.
- Morgan, J. W., Janssens, M.-J., Takahashi, H., Hertogen, J. and Anders, E. (1985) *Geochim. Cosmochim. Acta* **49**, 247-259.
- Rambaldi, E. R., Cendales, M. and Thacker, R. (1978) *Earth Planet. Sci. Lett.* **40**, 175-186.
- Rambaldi, E. R., Wänke, H. and Larimer, J. W. (1979) *Proc. 10th Lunar Planet. Sci. Conf.* 997-1010.
- Sears, D. W. G. and Weeks, K. S. (1986) *Geochim. Cosmochim. Acta* **50**, 2815-2832.
- Shimizu, H., Masuda, A. and Tanaka, T. (1983) *Mem. Natl. Inst. Polar Res., Spec. Issue* **30**, 341-348.
- Shinonaga, T., Endo, K., Ebihara, M., Heumann, K. G. and Nakahara, H. (1994) *Geochim. Cosmochim. Acta* **58**, 3735-3740.
- Van-Schmus, W. R. and Wood, J. A. (1967) *Geochim. Cosmochim. Acta* **31**, 747-765.
- Velbel, M. A. (1988) *Meteoritics* **23**, 151-159.

PORTALES VALLEY, A METAL-VEINED H6 CHONDRITE WITH EVIDENCE OF INTERNALLY-GENERATED PARTIAL MELTING OF Fe-Ni-S. L. J. Pinault¹ (pinault@pgd.hawaii.edu), E.R.D. Scott¹, D.D. Bogard², and K. Keil¹. ¹Hawai'i Institute of Geophysics and Planetology, SOEST, University of Hawai'i at Manoa, Honolulu, HI 96822. ²NASA Johnson Space Center, Houston, TX 77058, USA.

Introduction: The Portales Valley meteorite fell in June 1998 in New Mexico, producing a strewn field of about 7.5 x 2 km. Some 50 fragments weighing a total of 80 kg have been recovered, with the two largest specimens accounting for about 50% of the total mass retrieved [1,3]. It is classified as an H6 chondrite based on its mineral compositions [1] and oxygen isotopic composition [2]. While some fragments appear to be entirely composed of chondritic material, others contain thick metal veins exceeding a cm in width. We obtained and analyzed a pair of samples of Portales Valley: one featuring a characteristic metal vein, and another sample from inside a 1.45 kg fragment which is entirely composed of chondritic material [3].

We believe Portales Valley's unique structure is singularly important in offering clues to the origins of many other meteorite types. Recent arguments that the H asteroid was subject to extensive impact melting [4-6] were inspired by possible links to IIE irons [6] and studies of the H6 chondrite Y-791093, which is locally enriched in metal-sulfide [5] and appears to have close links to Portales Valley. We argue here that heating by ²⁶Al seems generally more plausible than impact heating to account for Portales Valley's formation. We also argue elsewhere that troilite and minor amounts of Fe,Ni were melted in certain H6 chondrites on the basis of our studies of unshocked, fine-grained H6 chondrites like Portales Valley, Guarena, Kernouve, and Estacado, and comparisons with the acapulcoites and winonaites [8]. Our analyses of Portales Valley focused on three key materials: the metal vein, chondritic material adjacent to the vein, and the chondritic stone with no veins.

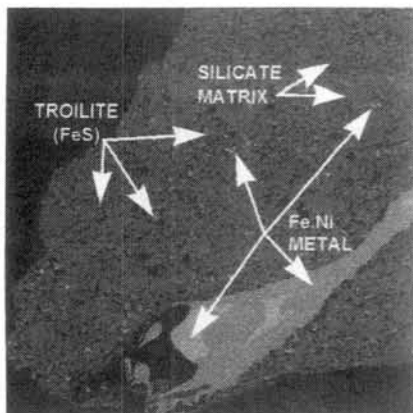


Fig. 1

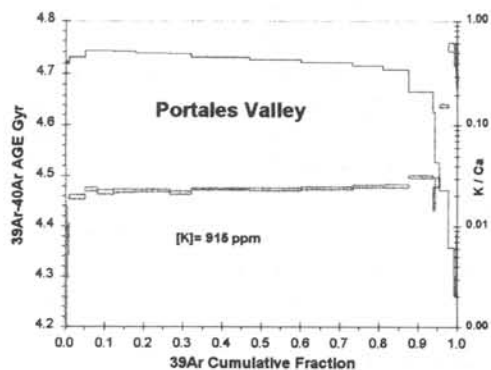


Fig. 2

Metal Vein: The vein examined (Fig. 1) contains some troilite at the edges but otherwise it is 95 to 100 percent Fe,Ni metal in composition (Tab. 1). Etching revealed an octahedral pattern of kamacite bands up to 0.5 mm in width. Continuity of the Widmanstatten pattern shows that parent taenite crystals were at least several cm in dimension, and must have crystallized slowly over periods greater than several weeks [9]. Analyses of the Ni concentrations at the centers of taenite grains give a cooling rate of ~5 K/Myr using cooling curves of Willis and Goldstein [10]. Other workers have estimated a cooling rate of ~10°C/Myr, in the 700°C to 500°C range [11].

Chondritic Material Adjacent to Vein: The chondritic material neighboring the vein (clasts or matrix depending on the sample, but in general matrix) is type 6. However, it is finer grained than many H6 chondrites. Like Kernouve and Guarena, it appears to be deficient in the larger olivine and orthopyroxene crystals; metallic Fe,Ni and troilite grains are also finer grained than in typical type 3-5 chondrites. This chondritic material is enriched in troilite and depleted in Fe,Ni metal relative to H chondrites; taenite to kamacite ratios also appear higher than H values. Point counting confirmed this (Table 1). Phosphates appear to be concentrated at the metal-silicate border of the vein. What appear to be isolated interstitial troilite grains (30-200 μ m in size) in areas as large as a cm or more in size show parallel optical extinction showing that they are part of a single interstitial troilite crystal.

Chondritic Stone with No Veins: The material analyzed from the second sample, which we infer was located at least 5 cm away from any metallic veins also has olivine and orthopyroxene compositions typical of an H chondrite (Tab. 2). However the Fe/(Fe+Mg) values in both olivines and low-Ca pyroxenes are higher than those measured next to the metallic veins. Textures are also fine-grained as in the chondritic material adjacent to the vein but modal abundances of metallic Fe,Ni and troilite appear to be normal for H chondrites.

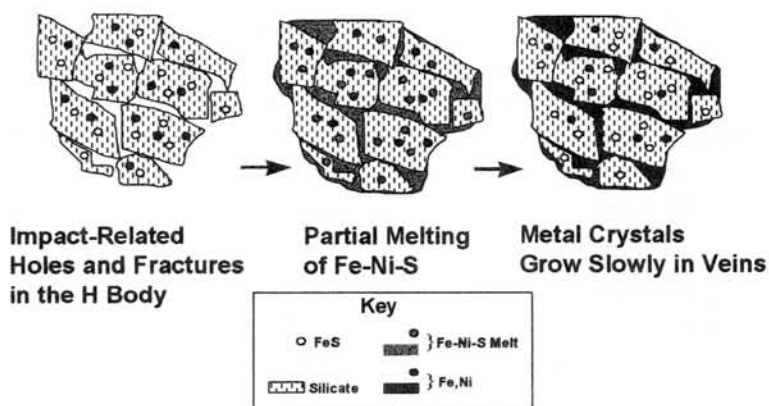
³⁹Ar-⁴⁰Ar Ages for Portales Valley. ³⁹Ar-⁴⁰Ar analyses (Fig. 2) yield a total average age across all extractions of 4.486 Gyr. The first few extractions (<1% ³⁹Ar release) suggest little diffusive loss of ⁴⁰Ar at low temperatures. Portales Valley's ³⁹Ar-⁴⁰Ar age, and the relatively slow cooling rate inferred from Ar diffusion data, are consistent with S1 shock stage and slow cooling. The ³⁹Ar-⁴⁰Ar age shows that Portales Valley and its veins were formed during the ~100 Myr that the ordinary chondrite bodies were believed to have experienced metamorphism.

Nature of the Formation Event: Did the impact that formed Portales Valley's chondritic clasts also heat the rock and make the metal veins by shock melting? Rubín and Ulf-Møller [11] and Kring et al. [7] argue in favor of shock melting and suggest that evidence for shock in the silicates was subsequently erased by recrystallization. But there are many difficulties with shock or impact heating [12] and we believe it is possible that ²⁶Al (or another internal heat source) may be responsible. Larger metal veins in shocked chondrites like Rose City are normally associated with whole-rock melting. It is true that strong shock may melt and redistribute metallic Fe,Ni and troilite into fractures without causing significant melting of silicate [13]. However, such Fe-Ni-S melt veins are typically only a few micrometers in width. Larger veins can be formed in shocked chondrites that experienced significant whole-rock melting, e.g., as in Rose City and Chico. But in these cases we expect to find complementary, large volumes of silicate melt which are free of metallic Fe,Ni and troilite. These are absent in Portales Valley. Recrystallization can conceal the texture of silicate melts, but should not obliterate large volumes of metal-free silicate. Only a young age for the meteorite would require an impact origin.

Could the metal veins in Portales Valley have been derived from a large melt pool, in which metal separated from silicate and was then injected into more distant chondritic material? This seems unlikely because impact melt pools do not fractionate on asteroids. Quick mixing of impact melt with cold clasts, and rapid cooling, prevent fractionation to form the required impact melt [12]. In addition, the enrichment of troilite relative to metal in the vein and surrounding chondritic material seems to favor a local derivation of the metal vein.

An Internal Heating Model for Portales Valley Formation: The distribution of metal and troilite between the vein and adjacent chondritic material is the opposite expected when chondritic material is heated above ~1000°C to form Fe-Ni-S melts. Normally, in these circumstances the resulting melt veins are rich in FeS, and the chondritic residue is poor in FeS. We propose the following model. 1) A major impact created open fractures at depth in the H parent body. 2) When the peak metamorphic temperatures exceeded the Fe-S eutectic temperature, the Fe-S melt permeated through the fractures. 3) The cm-sized troilite crystals show that Fe-Ni-S melts flowed along silicate grain boundaries allowing large FeS excesses to build up in the chondritic portion.

Internal Heating Model for Portales Valley Formation



Conclusions and Implications: We conclude that all of Portales Valley must have been above 1000°C, so that all the FeS melted. Petrologic studies and the 4.49 Gyr ³⁹Ar-⁴⁰Ar age imply formation before this time. Impact melting models fail to satisfy the constraints, e.g. the large metal veins interpenetrating the unmelted chondritic portion of the meteorite, and the distribution of metal and troilite. Slow heating and slow cooling imply formation of Portales Valley during parent body metamorphism, without the need for impact heating.

References: [1] Kring D.A. et al. (1999) *Proc. LPSC XXX*, #1618 [2] Clayton R.N. (1998) personal communication. [3] Farmer M. (1998) website <http://www.concentric.net/~Farmer/PV1.htm>. [4] Gaffey M. J. And Gilbert S. L. (1998) *MAPS* 35, 1281. [5] Ikeda Y. et. al. (1997) *Antarct. Met. Res.* 10, 335. [6] Casanova I. et. al. (1995) *Science* 268, 540. [7] Kring et al. (1999) *MAPS* in press. [8] Scott E.R.D. and Pinault, (1999) *Proc. LPSC XXX*, #1507. [9] Scott E.R.D. (1982) *GCA* 46, 813-823 [10] Willis J. and Goldstein J. I. (1981) *Proc. LPSC* 12, 1135-1143. [11] Rubin A.E. and Ulf-Møller (1999) *Proc. LPSC XXX*, #1125 [12] Keil K. et al. (1997) *MAPS* 32, 349-363. [13] Stoffler D. et al. (1991) *GCA* 55,3845-3867. Special thanks to Drs. Sasha Krot and Anders Meibom for their invaluable assistance.

Table 1 Modal Abundances
Areas of Portales Valley vs. Other H Chondrites

(Volume %)	Metal	FeS	Silicates	Cr ¹
Portales Valley				
Metal Vein	95-100	0-5	0	0
Adjacent to Vein	4	12	81	1
Away from Vein	8	4	88	1
<hr/>				
Kernouve (H6)	8	5	85	1
Guarena (H6)	10	7	83	1

¹Chromite

Table 2 Composition of Olivine and Low-Ca Pyroxene in Chondritic Regions

	Fa mol.%	+/- 1 sigma	Fs mol.%	+/- 1 sigma
Adjacent to Vein	18.8	+/- 0.4	16.8	+/-0.2
Away from Vein	19.7	+/-0.3	17.4	+/-0.2

ORIGINS OF LARGE, IGNEOUS-TEXTURED INCLUSIONS IN ORDINARY CHONDRITES. Alex Ruzicka, Gregory A. Snyder, and Lawrence A. Taylor.

Department Geological Sciences, University of Tennessee, Knoxville, TN, 37996, U.S.A.

Predominantly igneous-textured inclusions within ordinary chondrites have important implications for early solar system processes. The inclusions are larger than typical chondrules and are depleted in FeNi-metal and troilite relative to the host rocks. Various origins for the inclusions have been proposed, including (1) shock-melting of ordinary chondrites with accompanying loss of metal and sulfide [e.g., 1,2], (2) chondrule-formation involving unusually large volumes of melt production [e.g., 3,4], and (3) igneous differentiation processes occurring within ordinary chondrite parent bodies [e.g., 5,6,7]. Ruzicka et al. [8] subdivided large inclusions in ordinary chondrites into two chemical types (Na-rich and -poor). More recently, we compiled geochemical data for all inclusions in ordinary chondrites >0.3 cm across that have been studied to date. Based on this expanded database, we reassessed the origin of the inclusions. The available data support our previous conclusion [8] that such inclusions can be subdivided into two types which may have originated differently.

Na-rich inclusions. Na-rich inclusions have generally chondritic or superchondritic abundances of volatile elements (Mn, Na, K), and have Na/Al values ≥ 0.35 (atomic). Most inclusions belong to this group. Those analyzed for trace-elements primarily have relatively unfractionated compositions similar to ordinary chondrite silicate, although two inclusions (AC-1 and Bar-1) are LREE-enriched and have small positive Eu anomalies [5,9]. All of the inclusions are depleted in siderophile and chalcophile elements relative to the hosts. Uncommon clast-bearing inclusions, which on textural grounds appear to be clast-laden impact melts [8,10], belong to the Na-rich type, as do "troctolitic" inclusions found in some metamorphosed chondrites [5,11,12,13]. One of the troctolitic inclusions (Bar-1) [5] has an intermediate Na/Al ratio (0.32) and an uncertain classification.

The major-element compositions of Na-rich inclusions significantly overlap that of melt-pocket glasses in ordinary chondrites [8]. They appear to fall on a mixing line defined by bulk ordinary chondrite silicate and (albitic) plagioclase (Fig. 1). Such inclusions apparently formed by the addition or (less commonly) removal of albitic plagioclase from an ordinary chondrite composition.

As melt-pocket glasses were produced by hypervelocity impacts on chondrite parent bodies [e.g., 14,15], the close chemical similarity between the melt-pockets and Na-rich inclusions suggests that the latter formed by shock-melting of chondritic material. Enrichment of a feldspar component can arise by the preferential melting and accumulation of melted feldspar during impact processes [e.g., 16,17]. Feldspar-enrichment can explain those inclusions that have modest LREE-enrichments and positive Eu anomalies. Other Na-rich inclusions, which have nearly unfractionated trace-element abundances, could have formed by whole-rock melting of ordinary chondrites. All of the inclusions lost metallic melts or solids. Analyzed splits of two troctolitic inclusions in Y-794046 and Y-75097 have distinctive fractionations among REEs [e.g., 11,13], which can be explained by the sequestering of the REE into phosphate in unanalyzed portions of the inclusions during metamorphic equilibration [e.g., 13,18].

Na-poor inclusions. Compared to Na-rich inclusions, Na-poor inclusions have lower abundances of volatile elements such as Mn, Na, and K, lower Na/Al values, and different chemical trends on variation diagrams (Fig. 2). Only four Na-poor inclusions, Bo-1 [6,19], Bo-2

[20], CB8 [7], and LEW-1 [19], all from type 3 chondrites, have been analyzed for trace-elements. All four show volatility-correlated depletions of elements more volatile than Mn, suggestive of vapor-fractionation processes.

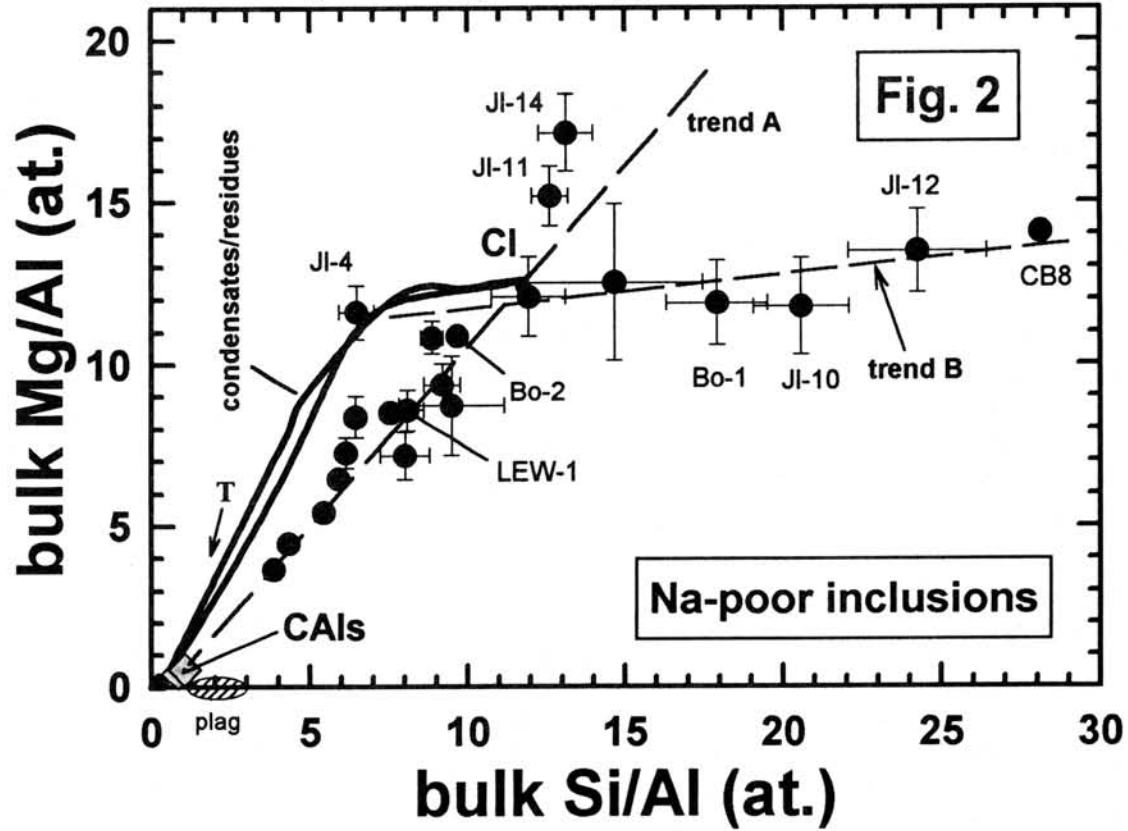
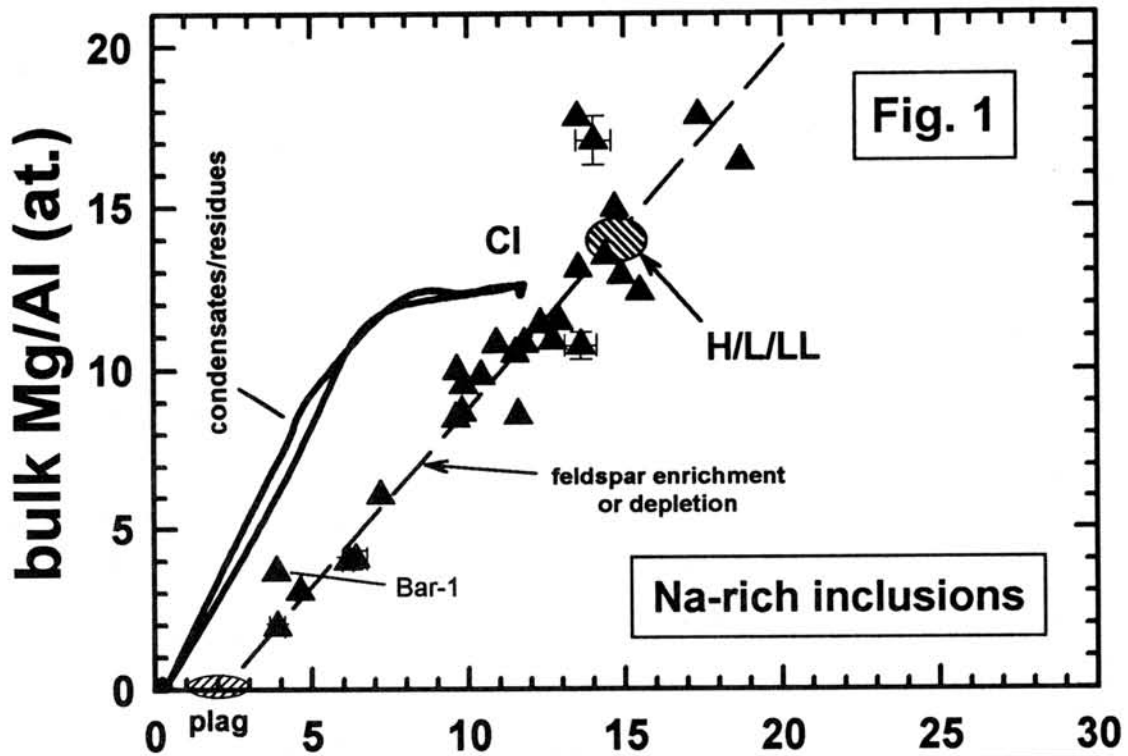
Based on Si/Al and Mg/Al ratios, Na-poor inclusions appear to define two trends (A and B) that appear to be systematically related to condensate/residue curves (Fig. 2), the latter calculated using the PHEQ program [21]. The two trends intersect near the CI-chondrite ("solar") composition (Fig. 2).

Trend A is a mixing line connecting CI-chondrites and Ca-Al-rich inclusions (CAIs); it is offset to lower Si/Al values compared to the feldspar-variation trend described by Na-rich inclusions. Inclusions lying on Trend A have CI-like proportions of normative olivine and pyroxene, but vary in their Al abundances. Those with Al abundances > CI-chondrites can be explained as having formed by the melting of CAI + CI-chondrite mixtures; those with lower Al abundances (Jl-11 and Jl-14) can be explained as having formed by the melting of CI-like material with a deficit of CAIs. The CI-normalized, major- and trace-element abundances of Al-rich inclusions LEW-1 and Bo-2 are relatively uniform and high for elements more refractory than Si, and are progressively depleted for elements that are increasingly volatile. This is consistent with these inclusions having formed by the melting of CAI-like and CI-chondrite-like mixtures.

Trend B parallels the low-temperature portion of the vapor-fractionation curve and extends from olivine-rich inclusions, such as represented by Jl-4, to silica-rich inclusions such as Bo-1, Jl-10, Jl-12, and CB8 (Fig. 2). The silica-rich inclusions on Trend B can be explained as having formed by the melting of material that originated by the removal of an olivine-rich condensate or residue from a system of CI-like composition, either by fractional condensation or by fractional vaporization. The CI-normalized major- and trace-element abundances of Bo-1 and CB8 reach maximum values for elements of intermediate volatility such as Si, suggesting that both high-temperature (olivine- and refractory-rich) and low-temperature components were removed.

Summary. Geochemical data suggest that Na-rich inclusions formed by shock-melting and that the precursors to Na-poor inclusions formed by vapor-fractionation processes. However, this conclusion may be oversimplified. Metasomatism, involving an enrichment of volatile elements, is known to have affected the margins of both Na-poor inclusions [8] and Na-rich inclusions [e.g., 5,8], raising the possibility that some Na-rich inclusions (e.g., Bar-1?) are chemically-modified Na-poor inclusions. Moreover, Na-poor inclusions show chemical anomalies that indicate they experienced mineral-specific fractionations in addition to volatility-related fractionations [19]. Finally, the textures and shapes of the inclusions are variable and do not obviously correlate with their chemistry [8]. Evidently, the physical, thermal, and chemical histories of inclusions in ordinary chondrites were varied and complex.

References: [1] Dodd R.T. and Jarosewich E. (1976) *Meteoritics* 11, 1-20. [2] Keil K. et al. (1980) *EPSL* 51, 235-247. [3] Binns R.A. (1967) *Min. Mag.* 36, 319-324. [4] Weisberg M.K. et al. (1988) *Meteoritics* 23, 309-310. [5] Hutchison R. et al. (1988) *EPSL* 90, 105-118. [6] Ruzicka A. et al. (1995) *Meteoritics* 30, 57-70. [7] Bridges J.C. et al. (1995) *Meteoritics* 30, 715-727. [8] Ruzicka A. et al. (1998) *GCA* 62, 1419-1442. [9] Fodor R.V. et al. (1974) *Meteoritics* 7, 495-507. [10] Fodor R.V. et al. (1980) *Meteoritics* 15, 41-62. [11] Yanai K. et al. (1983) *Mem. NIPR Sp. Issue* 30, 29-35. [12] Sack R.O. et al. (1994) *JGR* 99, 26029-26044. [13] Nakamura N. et al. (1994) *Proc. NIPR* 7, 125-143. [14] Dodd R.T. and Jarosewich E. (1982) *EPSL* 59, 355-363. [15] Stöffler D. et al. (1991) *GCA* 55, 3845-3867. [16] Schaal R.B. and Hörz F. (1977) *PLSC* 8th, 1697-1729. [17] Hörz F. and Cintala M. (1997) *MAPS* 32, 179-209. [18] Torigoye N. et al. (1993) *Proc. NIPR* 6, 100-119. [19] Ruzicka A. et al. (1999) *LPS XXX*, #1516. [20] Rubin A.E. et al. (1981) *GCA* 45, 2213-2228. [21] Wood J.A. and Hashimoto A. (1993) *GCA* 57, 2377-2388.



Oxygen isotope microanalysis of a zoned orthopyroxene megacryst in A-881526 diogenite

Hisao Satoh

Institute of Mineralogy, Petrology and Economic Geology, Tohoku University, Aoba, Sendai 982-8578, Japan
Present address: Geological Survey of Japan, Higashi, Tsukuba 305-8567, Japan; E-mail: hsatoh@gsj.go.jp

1. Introduction

Diogenites along with howardites and eucrites (HED) provide important information about planetary magmatism. In general, HED-members are believed to be igneous cumulate rocks and to be genetically related. Orthopyroxenes (Opx) of diogenites have been extensively studied using incompatible trace elements, to find the HED's parental body such as asteroid 4 Vesta [1,2,3]. According to oxygen isotopic analyses on a number of whole-rock achondrites by Clayton and Mayeda [4], most HED, mesosiderites, pallasites, and IIIAB iron meteorites fall in a single mass-dependent fractionation trend with a slope of 0.52 and a slight shift of -0.25‰ in $\Delta^{17}\text{O}$ value [5] in the three isotope diagram ($\delta^{18}\text{O} = 1.8\text{--}4.0\text{‰}$; $\delta^{17}\text{O} = 0.8\text{--}1.8\text{‰}$), suggesting derivation from a common parental body. Among these achondrites, HED have higher $\delta^{18}\text{O}$ and $\delta^{17}\text{O}$ values ($3.0\text{--}4.0\text{‰}$ and $1.2\text{--}1.8\text{‰}$, respectively), probably due to minerals enriched in heavier O-isotopes such as plagioclase and orthopyroxene [4].

Analysis of oxygen isotopes of the Earth's crust-mantle rocks provides important information about (1) magmatic conditions and processes during cumulate formation (igneous processes), and (2) metamorphism with or without fluid and deformation (metamorphic processes), especially for study of petrogenesis. Large Opx crystals in diogenites may preserve petrogenetic information as successive growth zones. This information can be obtained by O-isotopic microanalysis.

2. Sample and Analytical Procedures

A diogenite in the Asuka-88 collection (A-881526) [6] was selected as especially suitable for microanalysis. This diogenite clast is composed of very coarse-grained Opx ($>95\%$), with large Opx clasts (~ 5 mm, greenish) in a fine pyroxene matrix (<0.5 mm, white), with trace amounts of troilite, clinopyroxene, chromite, and silica phase, representing a typical monomict breccia.

A laser-fluorination (LF) oxygen isotope analysis was employed on Opx microchips separated from this diogenite specimen. The LF system comprises a CW-mode CO_2 laser (JLC-200, $\lambda=10.6\mu\text{m}$), a BrF_5 -reaction chamber, and cryogenic purification line. Extracted O_2 was converted to CO_2 by hot CVD-diamond plates at 1000°C . Obtained CO_2 was measured with a Finnigan MAT-252 mass spectrometer and recalculated against VSMOW-SLAP mass-scale. Obtained $\delta^{18}\text{O}$ data were internally compared with working standards: NBS 28 ($= 9.64\text{‰}$), NBS 30 ($= 5.10\text{‰}$), IOLV, and IOPX (Ichinomegata olivine and Opx). Especially, the replicate

analysis on IOLV (n = 12) and IOPX (n = 5) showed that the $\delta^{18}\text{O}$ data and reproducibilities were 5.85 ± 0.07 and $6.41 \pm 0.06\text{‰}$ (1σ), respectively [7].

A diogenite clast including Opx megacryst was cemented with soluble-glue and sliced into halves by a paper-thin cut-off saw. One part was sliced again (0.5 mm thick) and mounted on adhesive tape for microchip sampling. Fragmented chips, each 0.3-1.3 mg more than the sample-size limit of 0.2 mg for Opx, were separated and used for LF analysis. The other part was prepared for electron microprobe analysis using a JEOL JXA-8800. This preparation makes a pair of face-sharing slices, and enhances the comparison between O-isotopic and chemical analyses.

3. Results and Discussion

The resultant $\delta^{18}\text{O}$ analysis of A-881526 diogenite showed a range from 3.60 to 4.21‰. Compared to the whole-rock $\delta^{18}\text{O}$ data of HED [4], the $\delta^{18}\text{O}$ values of A-881526 Opx are slightly higher and its $\delta^{18}\text{O}$ range exceeds the analytical reproducibility ($1\sigma = \pm 0.06\text{‰}$). In an O-isotopic profile of a large Opx, $\delta^{18}\text{O}$ values display a weak but steady decrease from center (4.1‰) to margin (3.9‰) (Fig. 1). This may indicate O-isotope zoning. In contrast, white Opx matrix was only slightly higher (4.15-4.21 ‰) than cores of greenish coarse Opx grain (3.9‰). Before the LF microanalysis, Opx grains were assumed to be more isotopically homogeneous than terrestrial mantle rocks, probably due to the absence of fluid-rock interaction. Indeed, similar analysis on an Opx megacryst in a terrestrial mantle peridotite (spinel lherzolite from Horoman, Japan) showed a wider variation of $\delta^{18}\text{O} = 4.89\text{-}6.11\text{‰}$ [8] than this diogenite. This observed weak $\delta^{18}\text{O}$ heterogeneity could not be produced by weathering in ice sheets because the fine-grained Opx matrix should always be lower in $\delta^{18}\text{O}$ than coarse Opx (e.g., $\delta^{18}\text{O}$ value of SLAP is -55.5‰).

Chemically, Opx grains show Mg-rich major elemental compositions with a narrow variation ($\text{Wo}_{4.8}\text{En}_{73.71}\text{Fs}_{23.21}$) as previously reported on this specimen [6] and summarized by Mittlefehldt et al. [9]. Only Al_2O_3 and Cr_2O_3 clearly displayed core to rim zoning from 0.8-1.2 and 0.8-0.5, respectively (Fig. 1). Applying the pyroxene geothermometer [10] for host Opx and minor Cpx inclusions ($\text{Wo}_{41}\text{En}_{48}\text{Fs}_{11}$), the formation temperature of this diogenite can be estimated as ~ 1100 °C. If Opx ($\delta^{18}\text{O} \approx 4\text{‰}$) and also Cpx crystallized at this temperature, the oxygen isotopic composition of the host magma can be calculated as 4.5‰ based on the oxygen isotopic fractionation factor between basaltic melt and pyroxene ($\Delta_{\text{melt-px}} = +0.5\text{‰}$ at 1100 °C) [11]. The O-isotopic evolution from 3.0-4.0‰ previously reported in HED-members [4] may be explained by the followed process. In the magmatic system, the $\delta^{18}\text{O}$ value of Opx phenocryst is lower than host basaltic magma. Residual magma can be enriched in $\delta^{18}\text{O}$ value by fractional crystallization of Opx as cumulate (orthopyroxenite). Thus, the rim of Opx megacryst and fine-grained matrix evolved to heavier $\delta^{18}\text{O}$ as crystallization progressed. However, the $\delta^{18}\text{O}$ profile of Opx megacryst cannot be explained by this simple crystallization differentiation.

A remarkable feature of this diogenite Opx is occurrence of numerous silica phases that frequently appear with chromite grains (50-200 μm) as veinlets and myrmekitic intergrowths along cracks in strongly deformed crystal domains. Chemical composition of these chromites is around $\text{Mg}_{0.2}\text{Fe}_{0.8}\text{Cr}_{1.6}\text{Al}_{0.4}\text{O}_4$, which is typical in diogenite [9]. Although the silica phases were not identified mineralogically, their Al_2O_3 and Na_2O concentrations are unusually high (0.3-0.9 and 0.1-0.3 wt%, respectively) and clearly exhibit a coupled substitution of $\text{Si}^{4+} + = \text{Na}^+ + \text{Al}^{3+}$. This may suggest that these silica phases could be exsolution products of initially Si and Cr-rich pyroxene. Such a Si-rich pyroxene is restricted in ultrahigh-pressure metamorphic rocks and products of high-P experiments over 4.0 GPa [12]. Therefore, the occurrence and chemical features of silica exsolutions may suggest high-pressures. Extensive exsolution and high-Al zones in Opx probably could have been produced during decompression by shock deformation. It is not clear if such extreme conditions may also have destabilized high-P Opx and induced slight redistribution of oxygen isotopes as well as cations. More detailed microanalysis using an ion microprobe may reveal the relation between exsolution and formation of chemical and isotopic zonation.

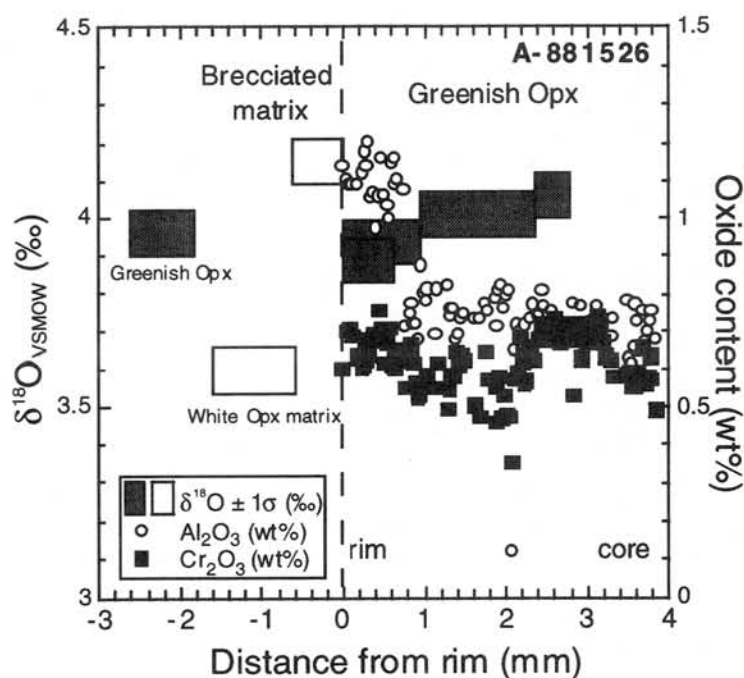


Fig. 1 $\delta^{18}\text{O}$ and chemical profiles from a zoned Opx megacryst to matrix in A-881526 diogenite clast.

References: [1] Consolmagno and Drake (1977) *G.C.A.*, 41, 1271-1282. [2] Fowler et al. (1995) *G.C.A.*, 59, 3071-3084. [3] Papike (1996) *Ame.Min.*, 81, 525-544. [4] Clayton and Mayeda (1996) *G.C.A.*, 60, 1999-2017. [5] $\Delta^{17}\text{O} = \delta^{17}\text{O} - 0.52\delta^{18}\text{O}$ [6] Yanai (1993) *Proc. NIPR Symp. Antarct. Meteorites*, 6, 148-170. [7] Satoh and Ohmoto in prep. [8] Satoh unpublished [9] Mittlefehldt et al. (1998) *Rev.Min.*, 36, 4-2-195. [10] Lindsley (1983) *Ame.Min.*, 68, 477-493. [11] Kyser et al. (1981) *C.M.P.*, 77, 11-23. [12] Liou et al. (1998) *Rev.Min.*, 37, 33-96. This research was funded by JSPS Postdoctoral Research Fellowship.

MAGNESIUM ISOTOPE ABUNDANCES IN STONY ANTARCTIC MICROMETEORITES

C. Schnabel¹, G.F. Herzog¹, S. Taylor², M.P. Field³, and R.M. Sherrell³

¹Department of Chemistry, Rutgers University, Piscataway, NJ 08854-8087

²Cold Regions Research and Engineering Laboratory, 72 Lyme Road, Hanover, N.H. 03755-1290

³Institute of Marine and Coastal Sciences, Rutgers University, New Brunswick, NJ, 08901-8521

Introduction - To first order, stony micrometeorites contain chondritic proportions of the elements [1]. For certain elements such as Cr, Mn, Fe, and Ni [1] and Rb [2], however, large depletions often occur. Possible explanations for the depletions include evaporation, phase segregation and loss, and both terrestrial and extraterrestrial weathering (e.g., [3, 4]). With evaporative loss of an element comes the possibility of mass-dependent fractionation of the isotopes. Mass-dependent fractionation is well established for Cr, Fe, and Ni in metallic micrometeorites [5, 6] and for oxygen in both metallic and siliceous micrometeorites [7, 8]. While magnesium is often fractionated in CAIs (e.g., [9, 10]) evidence concerning micrometeorites is inconsistent. Nagahara and Ozawa [11] suggest that Mg fractionation should be possible in the forsterite of submillimeter grains but Nagahara et al. [12] report no large enrichments of heavy Mg isotopes in either of two chondrules. Esat et al. [13] analyzed thirteen small (10-20 μm) extraterrestrial particles of various types and found significant mass-dependent fractionation of Mg ($\Phi_{\text{Mg}} = 11 \pm 1 \text{‰/AMU}$) in only one of them. Ion microprobe analyses of seven type-S spherules gave measured values of Φ_{Mg} from 2 to 7‰/AMU [5], which correspond to Mg losses of 10-30%, assuming open system evaporation. Those authors [5] cautioned, however, that the samples have unfractionated Si isotopes and no enrichment of refractory elements, both of which might be expected if Mg evaporated to a significant degree [14]. In high-precision analyses of five silicate spherules, Misawa et al. [15] observed no detectable mass-dependent fractionation of Mg. We set out to measure the isotopic composition of Mg in additional stony micrometeorites in order to check the possible influence of evaporation. In particular, we anticipated that it might be possible to use the extent of mass-dependent fractionation to improve estimates of average pre-entry composition.

Experimental methods - Taylor et al. [16] collected the samples analyzed here from the bottom of the South Pole water well. Each micrometeorite was weighed to within $\pm 5 \mu\text{g}$ and dissolved in 49% HF. After a first evaporation, one drop of 70% HClO_4 was added to the residue and evaporated to drive off fluorides. The residue was taken up in enough 2% aqueous solution of high-purity HNO_3 to give a solution with a concentration of $\sim 1 \text{ ppm Mg}$. To make the isotopic measurements we used a Finnigan MAT high-resolution, inductively coupled plasma mass spectrometer (HR-ICP-MS) operated in low resolution ($M/\Delta M=300$) mode. Potential polyatomic interferences (water based) were both reduced and overwhelmed by microconcentric desolvation, which decreased oxide formation ~ 100 -fold and increased sensitivity ~ 10 -fold relative to conventional methods of sample introduction. A self-aspirating micro-concentric nebulizer enhanced stability by eliminating the periodic surges in sample flow associated with peristaltic pumps. Extended (5-minute) rinses of the instrument with 10% HNO_3 helped to control an increase in blank that reflected instrument memory. Corrections for blanks ($< 1\%$ of signal) and instrumental fractionation (1 to 3% per AMU depending on day) were made by running appropriate blanks at regular intervals and one standard for every sample. Precision ($1-\sigma$) estimated from run-to-run variability ranged from ± 0.6 to $\pm 4.3\%$, with $\pm 1.5\%$ typical. To check the accuracy of the procedures we analyzed fractionated Mg samples kindly provided by Drs. D.A. Papanastassiou and A.M. Davis (Table 1).

Table 1. Mg and $\delta^x\text{Mg} \pm 1\sigma^*$ (‰) in fractionated samples

Sample	$\delta^{25}\text{Mg}$	$\delta^{26}\text{Mg}$
BG82HB1		
This work (N=4)	14.7±2.3	27.1±4.3
Ref. [9]	15.0	28.5
EK25-S2-TE		
This work (N=3)	13.5±0.4	27.8±0.6
Ref. [17]	13.6	26.4
SC16		
This work (N=4)	10.4±1.3	20.3±1.1
A. Davis	8.8	17.5

* $\sigma = \sqrt{\sum \delta_i^2 / (N - 1)}$

Results - The Mg contents average 15%, a value that may be compared with 18% for other stony Antarctic micrometeorites, 13% for deep-sea micrometeorites (probably because of etching), and 15% for stratospheric dust [1]. Mg contents and isotopic abundances of the micrometeorites are consistent with no mass-dependent fractionation, although in one micrometeorite, T-3, Φ_{Mg} could be as high as 2 ‰/AMU (Table 2). In general, our results agree better with those of [15] than with those of [5].

Discussion - Both laboratory and theoretical studies of forsterite suggest that open-system evaporation

results in measurable isotopic fractionation [11, 18]. As the siliceous micrometeorites melted, it follows that they must have frozen before much evaporation could occur. Love and Brownlee [19] estimate that micrometeorites spend 1-2 s at peak temperatures that rarely exceed 1973 K. In their laboratory experiments, Davis et al. [18] allowed forsterite to evaporate for no less than 240 s. Our results for T-3 limit the extent of open-system evaporation of Mg to ~10% and, with appropriate modeling, could be used to constrain the bulk time temperature histories of the particles.

Table 2. Masses (μg), Mg contents (wt %) and $\delta^x\text{Mg}$ (‰) of siliceous micrometeorites.

Sample	Mass	Mg	$\delta^{25}\text{Mg}$	$\delta^{26}\text{Mg}$
T-2	53.0	16.1	0.8±1.5	1.2±2.4
T-3	34.8	15.4±0.4	1.2±0.9	2.4±0.6
T-4	38.0	15.0±1.5	0.5±1.0	-0.5±1.9
T-5	40.1	12.0±1.0	0.4±2.9	-0.5±2.8
T-6	32.7	19.9		
T-7	21.3	21.7±3.0	-0.1±2.3	-0.4±2.2
T-8	32.2	14.3±1.1	-0.1±1.2	1.2±1.2
T-10	66.5	21.3		
T-11	23.5	11.9		
T-12	23.7	15.0		
T-13	20.6	16.9		

Several lines of evidence suggest that further searches for isotopic effects in siliceous micrometeorites may prove productive. Engrand et al. [8] have demonstrated that the oxygen isotope abundances of type-S spheres are fractionated with respect to the field defined by unmelted cosmic spherules. Love and Brownlee [19] note that peak atmospheric temperatures depend on incoming velocities, which presumably vary. Nyquist et al. [20] reported orally on small but significant fractionation of Cr and Fe isotopes in siliceous deep-sea spheres. Finally, Taylor (pers. comm.) has described

large, melted Antarctic micrometeorites, having no Fe, high Mg/Si ratios, and increased Al, Ca, and Ti contents, attributes that are consistent with loss of mass by vaporization.

References - [1] Brownlee D.E. et al. (1997) *Meteoritics Planet. Sci.* 32, 157-175. [2] Papanastassiou D.A. et al. (1983) *Earth Planet. Sci. Lett.* 64, 341-355. [3] Engrand C. et al. (1995) *Lunar Planet. Sci. XXVI*, 375-376. [4] Genge M.J. et al. (1996) *Geochim. Cosmochim. Acta* 61, 5149-5162. [5] Davis A.M. et al. (1991) *Lunar Planet. Sci. XXII*, 281-282. [6] Herzog G.F. et al. (1999) *Geochim. Cosmochim. Acta*, in press. [7] Clayton R.N. et al. (1986) *Earth Planet. Sci. Lett.* 79, 235-240. [8] Engrand C. et al. (1998) *Lunar Planet. Sci. XXIX*, CD-ROM, 1473.pdf. [9] Papanastassiou D.A. and Wasserburg G.J. (1983) *Meteoritics* 18, 370-371. [10] Brigham C.A. et al. (1987) *Lunar Planet. Sci. XVIII*, 129-130. [11] Nagahara H. and Ozawa K. (1997) *Lunar Planet. Sci. XXVIII*, 997-998. [12] Nagahara H. et al. (1999) *Lunar Planet. Sci. XXX*, CD-ROM, 1342.pdf. [13] Esat T.M. et al. (1979) *Science* 206, 190-197. [14] Hashimoto A. (1983) *Geochem J.* 17, 111-145. [15] Misawa K. et al. (1992) *Geochem. J.* 26, 29-36. [16] Taylor S. et al. (1998) *Nature* 392, 899-903. [17] Papanastassiou D.A. and Brigham C.A. (1989) *Astrophys. J.* 338, L37-L40. [18] Davis A.M. et al. (1990) *Nature* 347, 655-658. [19] Love S.G. and Brownlee D.E. (1991) *Icarus* 89, 26-41. [20] Nyquist L.E. et al. (1995) *Meteoritics* 30, 558-559.

H isotopic compositions in ALH84001

N.Sugiura and H.Hoshino

Department of Earth and Planetary Physics, Univ. of Tokyo
sugiura@geoph.s.u-tokyo.ac.jp

H isotopic compositions in the martian meteorite ALH84001 have been studied to elucidate the evolution the martian atmosphere. A pioneer study [1] was made by stepped heating and $\delta D = 783$ permil was obtained. This was considerably lower than those observed in other martian meteorites and H isotopic fractionation over the past a couple of billion years was suggested as a possible explanation. First measurements of H isotopic compositions of ALH84001 by SIMS were made by [2]. The measurements were made using Cs primary beam. They reported an average $\delta D = 221$ permil for three carbonates. Similar values were also reported for whitlockites. In a follow-up study, they [3] measured H isotopic compositions using oxygen primary beam. The δD values for carbonate remained unchanged from the previous study but higher values ($\delta D \sim 500$ permil) were reported for whitlockite.

At the LPS conference this year, we [4] reported our results of H isotopic measurements by SIMS using Cs primary beam. The δD values ranged from 293 to 1344 permil for carbonates. It was suggested that the variation in the isotopic compositions is mainly caused by terrestrial contamination. The lower δD values previously reported by Boctor et al.[2,3] could be consistent with our results if their sample had higher terrestrial contamination. There remains a possibility that even the highest value we obtained for carbonate may still be significantly affected by some amounts of terrestrial contamination. In fact, at the same LPS conference, Boctor et al.[5] reported higher values (up to 1748 permil) of δD for feldspathic glass in ALH84001. They also observed inverse correlation between the δD values and the water concentration. Therefore, it is our opinion that the true δD value in ALH84001 is probably higher than the highest value ever obtained by SIMS analyses so far.

At the antactic meteorite symposium, we will report up to date results of our H isotope measurements of carbonate and other minerals in ALH84001.

references

- [1] L.A. Leshin et al. (1996) GCA 60, 2635-2650.
- [2] N.Z. Boctor et al. (1998) LPS, XXIX.
- [3] N.Z. Boctor et al. (1998) Meteoritics & Planet. Sci. 33, A18.
- [4] N. Sugiura and H.Hoshino (1999) LPS, XXX, #1324.
- [5] N.Z. Boctor et al. (1999) LPS, XXX, #1397.

The possibility of Mg/Si fractionation by incongruent evaporation of enstatite

Shogo TACHIBANA and Akira TSUCHIYAMA

Dept. Earth and Space Sci., Osaka Univ., 1-1 Machikaneyama, Toyonaka, Osaka 560-0043, JAPAN

e-mail: tachi@ess.sci.osaka-u.ac.jp

Abstract: Numerical calculations were made in order to evaluate the evaporation behavior of enstatite at 1400°C in a closed system, which consisted of enstatite and nebular gas, based on our experimental results. The timescales for evaporation and the possibility of the Mg/Si fractionation in the primitive solar nebula were discussed. The incongruent evaporation of enstatite in a closed system can be divided into CE (complete evaporation), PE/F (partial evaporation with forsterite residue) and PE/EF (partial evaporation with enstatite and forsterite residue) depending on the dust enrichment factor, η ($=([\text{Si}]/[\text{H}])/([\text{Si}]/[\text{H}]_{\text{solar}})$). The evaporation of enstatite in the case of PE/F or PE/EF is a potential mechanism for Mg/Si fractionation in the nebula.

Introduction: Variations of Mg/Si ratios have been known among chondritic meteorites. Enstatite (MgSiO_3) evaporates incongruently to form forsterite (Mg_2SiO_4) as an evaporation residue. Hence, the evaporation of enstatite might have played an important role for Mg/Si fractionation in the early solar nebula.

We have done evaporation experiments on enstatite both in vacuum and in hydrogen gas with continuous evacuation [1], and found that enstatite evaporated incongruently to form a thin forsterite layer on the surface of enstatite. Especially, the forsterite layer was quite thin in hydrogen gas. Hence, we concluded that evaporation of enstatite could not cause the Mg/Si fractionation in the solar nebula if the evaporation took place in a fully open system, where evaporated gases were taken away immediately like experimental conditions.

However, evaporation in the solar nebula would not necessarily occur in a fully open system. In the present study, we made numerical calculations to evaluate the evaporation behavior of enstatite in a closed system, which consisted of enstatite and nebular gas. In the calculations, we used our experimental results [1] and a quasi-equilibrium evaporation model [2]. We discussed both timescales for evaporation of enstatite and the possibility of the Mg/Si fractionation in the nebula.

Experiments and Evaporation Kinetics of Enstatite: The evaporation experiments showed that enstatite evaporated incongruently to form a polycrystalline forsterite layer on the enstatite surface as an evaporation residue. In vacuum experiments, its thickness increased with time at the beginning, and then became constant.

When a forsterite layer is not porous, the formation of the forsterite layer should be controlled by diffusion of ions through the layer (diffusion-controlled evaporation of enstatite). Forsterite, which is formed by evaporation of enstatite, should also evaporate from the surface. Hence, the formation rate of the forsterite layer is expressed by

$$dX_{\text{Fo}}/dt = k_{\text{En}}/2X_{\text{Fo}} - k_{\text{Fo}}, \quad (1)$$

where X_{Fo} is the thickness of the forsterite layer, t is time, k_{En} [L^2t^{-1}] is the diffusion-controlled evaporation rate constant of enstatite, and k_{Fo} [Lt^{-1}] is the surface reaction-controlled evaporation rate constant of forsterite. Eq.(1) shows that X_{Fo} increases with time and it becomes constant when X_{Fo} reaches X_{Fo}^* ($= k_{\text{En}}/2k_{\text{Fo}}$). Further evaporation proceeds with a forsterite layer of a constant thickness, X_{Fo}^* (steady state evaporation). This is consistent with experimental results. The evaporation rate of enstatite is equal to k_{Fo} in the steady state. The value of k_{En} at 1400°C, which was obtained from X_{Fo}^* in vacuum experiments, was 6×10^{-13} [$\text{cm}^2 \text{sec}^{-1}$]. The value of k_{Fo} at 1400°C was extrapolated from experimental evaporation rate constants of forsterite [3,4].

Eq.(1) can be used only when the evaporation of enstatite is controlled by diffusion. However, the evaporation of enstatite might be controlled by the surface reaction when X_{Fo} is so small that the diffusion-controlled evaporation rate is larger than the surface reaction-controlled evaporation rate. If this is the case, the formation rate of a forsterite layer is expressed by

$$dX_{\text{Fo}}/dt = k'_{\text{En}} - k_{\text{Fo}}, \quad (2)$$

where k'_{En} [Lt^{-1}] is the surface-reaction-controlled evaporation rate constant of enstatite.

X_{Fo} in hydrogen gas ($p(\text{H}_2)=10^{-3}$ and 10^{-5} bar) is much smaller (sub-micron) than that in vacuum experiments. The diffusion-controlled evaporation rate of enstatite (k_{En}) seems to have little dependence on a surrounding gas atmosphere. On the other hand, k_{Fo} is enhanced by hydrogen [e.g., 5-7]. Hence, a thin forsterite layer in hydrogen gas is also explained by eq.(1) with the same k_{En} as in vacuum and larger k_{Fo} in hydrogen gas.

Calculation:

Assumptions: Several assumptions were made for calculations. (I) The canonical (NVT) ensemble was assumed. (II) The elements in the system were Mg, Si, O, H, C and He. (III) The elemental abundance of O, C,

and He relative to H was given by the solar abundance [8], while Mg/Si ratio was fixed at 1 (*c.f.*, the solar Mg/Si ratio is 1.074). (IV) Gas species were H, H₂, H₂O, O, O₂, OH, CO, He, SiO, and Mg. (V) Enstatite grains were only the initial solid phase, and their radii were uniform, R₀. (VI) The [Si]/[H] ratio in the system was expressed by a dust enrichment factor, η ([Si]/[H])_{solar}, where ([Si]/[H])_{solar} was the solar elemental ratio.

Evaporation rates: The value of k_{En} at 1400°C in vacuum was used as the diffusion-controlled evaporation rate of enstatite. The surface reaction-controlled evaporation rate of forsterite and enstatite, k_{Fo} and k'_{En}, were estimated from

$$k_{Fo} \text{ or } k'_{En} [L t^{-1}] = \alpha_i \Omega_i (p_i^{eq}(SiO) - p(SiO)) / \sqrt{2\pi m_{SiO} k T} \quad (i = \text{forsterite, enstatite}), \quad (3)$$

where α_i is an evaporation coefficient which shows kinetic constraints for evaporation, Ω_i is a molar volume of i, p^{eq}_i(SiO) is an equilibrium vapor pressure of SiO with i, p(SiO) is a partial pressure of SiO in the system, m_{SiO} is a molecular weight of SiO, k is the Boltzman constant, and T is the absolute temperature.

Calculation procedure: (I) Partial pressures of gases (H, H₂, H₂O, O, O₂, OH, CO, He, SiO, and Mg) in the system were calculated. The equilibrium vapor pressures of enstatite and forsterite, p^{eq}_i(SiO), were also calculated, respectively. (II) Two different evaporation rates of enstatite were calculated (*i.e.*, k_{En} and k'_{En}), and the smaller one was adopted as the actual evaporation rate of enstatite. (III) The amounts of forsterite and enstatite that evaporate for duration, Δt, were evaluated, respectively. The change of X_{Fo} was calculated from eq.(1) or (2) depending on the evaporation mode of enstatite. The change of the grain size, R, was calculated by using k_{Fo}. (IV) The evaporated gases were left in the system. Partial pressures of gases were recalculated.

Results: We have investigated the evaporation behavior of enstatite dust particles with R₀=1 and 10μm at 1400°C and the initial total pressure of 10⁻⁵bar. The value of η ranged from 0.01 to 1x10⁴. The changes of R (R₀=1μm), X_{Fo} and Mg/Si ratios in solid and gas are plotted against time with different η (1[solar], 1000 and 5000), respectively, in Fig.1. The evaporation behavior of enstatite can be divided into three (CE, PE/F and PE/EF, see below) in accordance with η. In Fig.2, the comparison of timescales (τ) for the three different evaporation behaviors is shown. In Fig.3, τ with R, X_{Fo} and Mg/Si [Solid, Gas] at t=τ for R₀=1μm are plotted against η.

Complete evaporation (CE): When η is 0.01-400, enstatite grains evaporate completely within a few hours for R₀=1μm or within a day for R₀=10μm (Fig.1a; τ_{CE} in Fig.2). When η is smaller than 100, X_{Fo} is much smaller (<0.02μm) than the grain size and nearly constant throughout the evaporation except for the final stage of evaporation. This evaporation behavior is similar to that in a fully open system. In the case of η > 100, X_{Fo} becomes larger with η. This is because a partial pressure of SiO(g) increases with evaporation and makes k_{Fo} smaller (see eq.(3)).

Partial evaporation with forsterite residue (PE/F): In the case of 450 < η < 3000, no enstatite is left but residual forsterite is equilibrated with a surrounding gas atmosphere within a few hours for R₀=1μm (Fig.1b; τ_{PE/F} in Fig.2). For grains of R₀=10μm with η=1000, it takes about 10days for equilibration (τ_{PE/F} in Fig.2). X_{Fo} increases with time and then evaporation ceases when the grain turns completely into forsterite. The final size of the forsterite grain becomes larger with larger η (Fig.3).

Partial evaporation with enstatite and forsterite residue (PE/EF): Both enstatite and forsterite achieve the equilibrium state after some degree of evaporation (η > 3100) (Fig.1c). It takes less than a few hours (τ_{PE/EF}) for R₀=1μm or within a day for R₀=10μm for equilibration (τ_{PE/EF} in Fig.2). R and X_{Fo} at the equilibrium state become larger and smaller, respectively, with increasing η. The Mg/Si ratio in a gas phase at the equilibrium state is constant (~0.053) irrespective of η. This constant gaseous Mg/Si ratio is explained by the equilibrium of the reaction;



The equilibrium constant of the reaction (4) (K=p^{eq}(Mg)/p^{eq}(SiO)) at 1400°C is 0.053, and equal to the above constant value of the gaseous Mg/Si ratio.

Possibility of Mg/Si Fractionation:

CE: An enstatite grain evaporates with a thin forsterite layer like evaporation in a fully open system, and the timescale for CE, τ_{CE}, is less than a day. Hence, it is difficult to cause a large degree of Mg/Si fractionation.

PE/F: At the equilibrium state, the Mg/Si ratio in solid becomes 2 regardless of η because forsterite alone is left in the system, while the Mg/Si ratio in gas ranges widely from 1 to 0.053 depending on η. Thus, Mg/Si fractionation is expected if gas-solid separation takes place. Moreover, if the timescale for gas-solid separation was shorter than τ_{PE/F}, variations of Mg/Si ratios both in solid and gas could be expected.

PE/EF: Unlike PE/F, the Mg/Si ratio in solid ranges from 2 to 1 at the equilibrium state depending on η, and

the Mg/Si ratio in gas is always constant (0.053). If the timescale for gas-solid separation was shorter than $\tau_{PE/F}$, variations of Mg/Si ratios both in solid and gas could be expected like PE/F. Thus, Mg/Si fractionation is expected in the case of PE/EF as well.

Conclusion: Our calculations indicate that incongruent evaporation of enstatite in a closed system is a potential mechanism for Mg/Si fractionation in the solar nebula as long as the dust/gas ratio in the system is much higher ($\eta > 400$) than the canonical solar nebula. If evaporation of enstatite occurred under the dust-enrichment conditions in the solar nebula, Mg/Si variations among chondrites would have been made by recondensation of Si-rich gas that evaporated from enstatite since Mg/Si ratios of chondrites are mostly less than that of the solar abundance.

Acknowledgement: The authors thank Dr. H. Nagahara for her kind help in the experiments and valuable discussion on evaporation kinetics. This work was supported by JSPS Research Fellowship for Young Scientists (J.C.).

References: [1] Tachibana S. *et al.* (1998) *LPS*, **XXIX**, 1539. [2] Tsuchiyama A. and Tachibana S. (1998) *LPS*, **XXIX**, 1538. [3] Hashimoto, A. (1990) *Nature*, **347**, 53-55. [4] Wang J. *et al.* (1993) *LPS*, **XXIV**, 1480. [5] Nagahara H. and Ozawa K. (1996) *GCA*, **60**, 1445-1459. [6] Tsuchiyama A. *et al.* (1998) *Mineral. J.*, **20**, 113-126. [7] Hashimoto A. (1998) *Meteoritics & Planet. Sci.*, **33**, A65. [8] Anders E. and Grevesse N. (1989) *GCA*, **53**, 197-214.

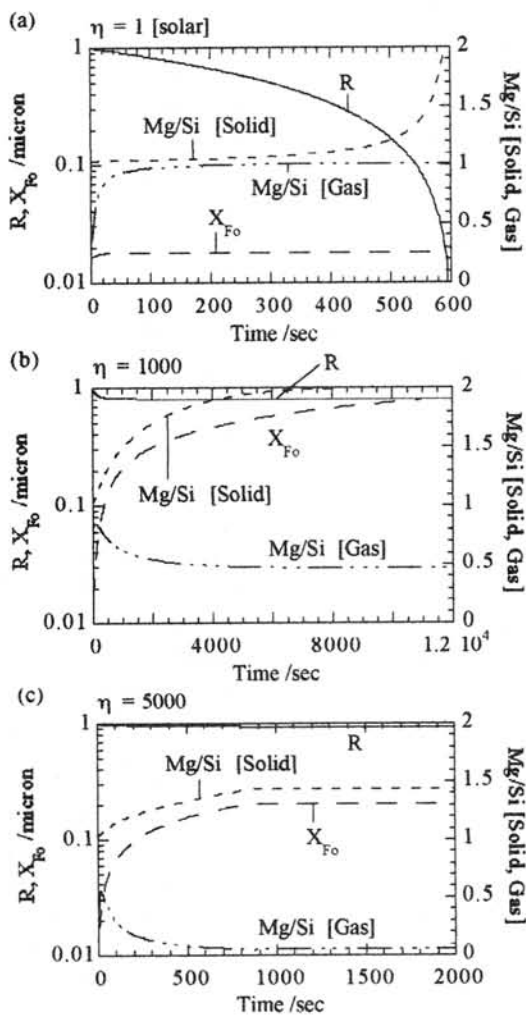


Fig.1 R, X_{Fo} and Mg/Si ratios in solid and gas vs. time. (a) $\eta=1$ (solar abundance), (b) $\eta=1000$ and (c) $\eta=5000$

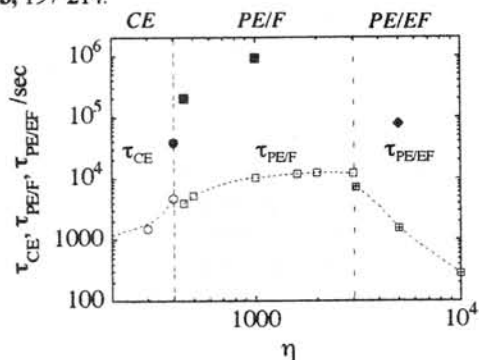


Fig.2 Timescales for CE, PE/F and PE/EF (τ_{CE} , $\tau_{PE/F}$ and $\tau_{PE/EF}$) vs. η . $\tau_{PE/F}$ and $\tau_{PE/EF}$ are the timescales for 99.99% equilibration. Open symbols: $R_0=1\mu\text{m}$; Filled symbols: $R_0=10\mu\text{m}$.

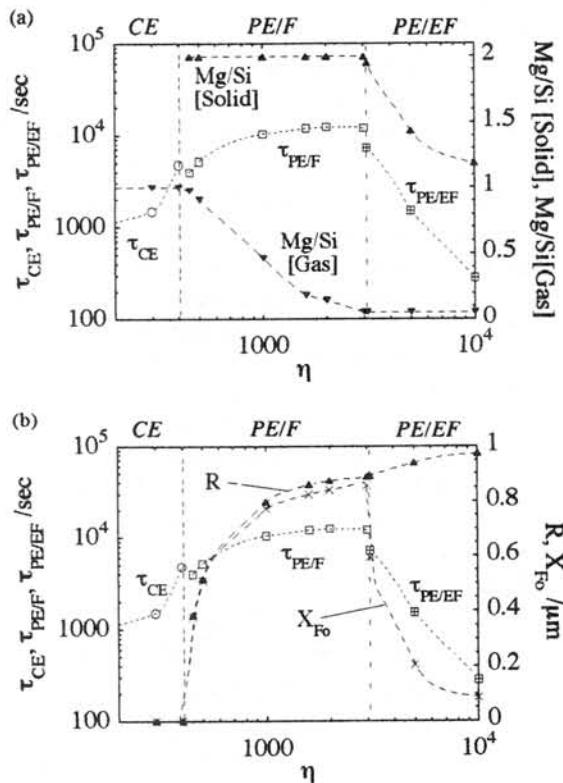


Fig.3 τ for $R_0=1\mu\text{m}$ vs. η . (a) τ with Mg/Si [Solid, Gas] at $t = \tau$, (b) τ with R and X_{Fo} at $t = \tau$.

MINERALOGY OF Y791192, HED BRECCIA AND ITS CRATERING HISTORY ON A VESTA-LIKE BODY.

Hiroshi Takeda¹, Kazuto Saiki² and Teruaki Ishii³.

¹Research Inst., Chiba Inst. of Technology, 2-17-1 Tsudanuma, Narashino City, Chiba 275-0016 and, Dept. of Phys. & Earth Sci., Faculty of Sci., Univ. of Ryukyus, Nishihara, Okinawa 903-0213.

²Res. Inst. of Materials and Resources, Fac. of Eng. and Resource Sci., Akita Univ., Akita 010-8502,

³Ocean Res. Inst., Univ. of Tokyo, 1-15-1 Minamidai, Nakano-ku, Tokyo 164-0014, Japan.

Introduction

Difficulty in classification of achondrites with mineralogical features intermediate between diogenites and eucrites, promoted a group of meteoriticists to use an acronym, HED (Howardites, Eucrites, Diogenite) achondrites [1]. Occurrence of such breccias can be understood by astronomical evidence linking Vesta and the HED achondrites [2] and by the presence of large impact craters on Vesta observed by the Hubble Space Telescope [3]. In order to clarify this problem on the formation of such breccias as an event taken place on a Vesta-like body, we investigated Y791192 by mineralogical techniques.

Y791192 has been previously classified as a polymict eucrite [4], but we proposed last year that this HED achondrite may have affinity to Type B diogenites known in the Yamato meteorite collection [5]. They are also called Y75032-type achondrite, because Y75032 is the largest and representative specimen. Takeda and Mori [6] demonstrated that they are link materials between diogenites and eucrites. Y75032-type achondrites have a common characteristic texture with shocked pyroxene fragments and glassy veins and contain pyroxene fragments with chemical compositions slightly more Fe-rich than common diogenites and variable amounts of cumulate eucrites. Based on a possible geological setting of various types of HED breccias, postulated by Metzler et al. [7], we interpreted a formation mechanism of the Y75032-type HED breccias by a cratering event on a Vesta-like body.

Samples and Experimental Techniques

Polished thin section (PTS), Y791192.91-3, supplied by the National Institute of Polar Research (NIPR) was used for this study. The PTS was studied by an optical microscope, and the chemical compositions of the minerals were obtained by electron probe microanalyzer (EPMA) JEOL 733 at Ocean Research Inst. (ORI) of Univ. of Tokyo. The data were compared with those of other Y75032-type pyroxenes [4-6].

Results

Mineralogy of Y791192

Small angular to subangular fragments less than 1 mm in diameter, of pyroxene and minor plagioclase, are set in dark glassy matrix. Sizes of the fragments are fairly uniform except for one large eucritic lithic clast (Fig. 1). The largest pyroxene fragment is 0.8×0.9 mm in size and that of plagioclase 0.3×0.6 mm. One brown eucritic pyroxene fragment (0.3×0.45 mm) shows fine exsolution lamellae. A few subrounded plagioclase crystals are 0.25×0.18 in size. The large eucritic clast 2.5×1.2 mm in size shows variolitic texture of acicular, brown pyroxene (up to 0.1×0.6 mm) and white plagioclase (up to 0.1×0.8 mm). A small fragment of this type measures 0.55×0.45 mm in size. This meteorite is different from major Y75032-type achondrites, but are similar to Y791439 in that it contains an more eucritic and less diogenitic components as in Y75032. Y791439 contains abundant fragments of cumulate eucrites with a fragment of ordinary eucrite pyroxene.

Chemical compositions of pyroxene in Y791192 distribute in the same regions as those of the Y75032-type achondrites, but the diogenitic components are small and ordinary eucrite pyroxenes are more abundant than those of previously described members (Fig. 2). Saiki and Takeda [8] recognized six types of pyroxenes in another PTS (.91-2). The plagioclase compositions show characteristics of the Y75032 plagioclase with some high Na-rich compositions (Fig. 3). The acicular pyroxene crystals show uniform mg# with variations along the tie line of the exsolved pair (Fig. 2). The plagioclase also shows chemical zoning within the crystal. The glass compositions are the same as those of the Y75032-type.

Discussion

Y791192 has been classified as a polymict breccia, but this study support the reclassification as an unusual howardite or polymict cumulate eucrite with affinity to Y75032 [4]. Seventeen Y75032-type achondrites have been described in Catalog of the Antarctic Meteorites [4] with their pyroxene quadrilaterals. Takeda et al. [6] showed more diversity of pyroxene chemistry than those we studied previously [5]. They pointed out three subclasses of the Y75032-type breccias as summarized below: *Diogenitic members*: Y75032Y791000, Y791072, Y791187, Y791188, Y791189, Y791199, Y791202, Y791204, Y791422, Y791466, Y791467, and Y791603. Pyroxene compositions are nearly uniform and cluster around $mg\# = Mg \times 100 / (Mg + Fe)$ 67 mole % [4,5].

Diogenites with Cumulate Eucrites: Y791073, Y791200, and Y791201. Pyroxenes with *mg#* down to 50. The *mg#*s of pyroxene range from 70 to 50 and cover the entire range between Fe-rich diogenites and cumulate eucrites.

Cumulate Eucrites with Diogenites and Rare Eucrites: Y791439 and Y791192. More abundant clasts of cumulate eucrite than those of Y75032, with minor ordinary eucrite.

Saiki and Takeda [8] divided pyroxene chemical compositions of Y791439 into six types: diogenite-type (D1 and D2), Binda-type, Moore-County-type (MC1 and MC2), and rare Juvinas(JV)-type. The diogenite-type pyroxenes are the most magnesian in the meteorite, and are similar to Fe-rich diogenites. The chemical compositions of Binda-type pyroxenes are slightly more Fe-rich than Binda, but many of them have blebs typical of the Binda cumulate eucrite. Minor plagioclase grains are present in the matrix. The pyroxene fragments of Y791192 are similar to those of Y791439 ($\text{Ca}_{15}\text{Mg}_{35}\text{Fe}_{50}$), but Y791192 contains an ordinary eucrite clast with variolitic texture. The eucritic clast shows dark fine-grained variolitic texture of brown pyroxene and white lathes of plagioclase, but their pyroxenes are homogenized.

The pairing of Y75032-type achondrites are mostly based on their unique shock melt veins and clustered pyroxene compositions around *mg#* 67. Other members with abundant cumulate eucrites share the above common features with the diogenite-rich members. Since it is difficult to identify fragments of diogenitic pyroxene from the Binda-type pyroxene in cumulate eucrites, we can classify Y791192 as an unusual howardite. If the amounts of ordinary eucrite are small (<10%), Y791192 can be a polymict cumulate eucrite. Another key item, which links these meteorites as a paired sample, is the presence of pyroxene with thin blebby, wavy, augite inclusions aligned along one orientation. The exsolution mechanism of these pyroxenes has been explained in our previous work [6]. Because this kind of pyroxene can be produced only for a special chemistry and cooling rates [9], the presence of such pyroxene can be used as a key to identify the pairing and deduce cooling history.

Combined textural and chemical studies of Y75032-type pyroxene revealed that these achondrites experienced shock event in the history of the crustal evolution before they finally ejected from the Vesta-like body by the last large impact. The presence of ordinary eucrite clast in Y791439 and Y791192 suggests that the excavation took place after the global crustal metamorphism as suggested by Yamaguchi et al. [10]. The preservation of partly maskelynitized plagioclase and impact melt glass implies that thermal annealing did not take place after the last impact event. Metzler et al. [7] postulated a possible geological setting of various types of HED breccias. They considered a crater formation on the possible structure of the HED parent body crust with the rock sequence basalts-gabbro-pyroxenite with increasing depth after Takeda [11,12]. Then, they constructed the figure, which represents a cross section through an impact crater that modified the primary rock sequence and led to the formation of various kinds of breccias, dikes and shock veins. The origin of the Y75032-type breccias should take into account the fact that they were not formed by deposition of impact ejecta or fall out. Such deposits may include all components of a layered crust as in howardites and polymict eucrites [12]. Close association of Fe-rich diogenites and cumulate eucrites with rare ordinary eucrites suggests that formation mechanism of these breccias are different from that of howardite, which might have been formed by one of the large impact crater with diogenite at the crater floor of Vesta. If we accept a picture of an impact crater of Metzler et al. [7], the Y75032-type breccias might be formed near the crater floor where the boundaries of diogenites and cumulate eucrites were disturbed by impact and mixed with impact melts in local scale.

In conclusions, characteristic textures with impact melt glass and pyroxene textures and chemistry suggest that Y791192 is rather similar to Y791493 and belongs to a subclass of the 75032-type HED achondrites, which contains more eucritic component. Formation of such complex breccias can be best explained by a geological setting with a cratering event proposed for the layered crust model of the Vesta-like body [12].

Acknowledgments: We acknowledge the NIPR for supplying us with the sample. This work was supported by a grant of the ORI and by a Grant-in-Aid for Scientific Research from the Japanese Ministry of Education, Science and Culture and Japan Scientific Foundation. We are indebted to Dr. N. Imae for his assistance in classification of the Yamato meteorites, to Mrs. M. Hatano and Mrs. M.

Okamoto for their technical assistance and to Drs. A. Yamaguchi, L. E. Nyquist, D. D. Bogard, Y. Ikeda, D. Mittlefehldt, for discussion and Prof. M. Miyamoto for discussion and supports.

References:

[1] TAKEDA H., MORI H., DELANEY J.S., PRINZ M., HARLOW G.E., and ISHII T. (1983) *Mem. Natl. Inst. Polar Res., Spec. Issue* **30**, 181-205. [2] BINZEL R. P. and XU S. (1993) *Science* **260**, 186-191. [3] THOMAS P. C., BINZEL R. P., GAFFEY M. J., STORRS A. D., WELLS E. N. and ZELLNER B. H. (1997) *Science* **277**, 1492-1495. [4] YANAI K. and KOJIMA H. (1995) *Catalog of the Antarct. Meteorites*. 230 pp. NIPR, Tokyo. [5] TAKEDA H., SAIKI K. and ISHII T (1998) *Antarctic Meteorites* **23**, 148-150. [6] TAKEDA H. and MORI H. (1985) *Proc. Lunar Planet. Sci. Conf.* **15th**, *J. Geophys. Res.* **90**, C636-C648. [7] METZLER K., BOBE K. D., PALME H., SPETTEL B. and STOFFLER D. (1995) *Planet. Space Sci.* **43**, 499-525. [8] SAIKI K. and TAKEDA H. (1999) *Meteoritics Planet. Sci.* in press. [9] ISHII T. and TAKEDA H. (1974) *Mem. Geol. Soc. Japan* **11**, 19-36. [10] YAMAGUCHI A., TAYLOR G. J., and KEIL K. (1996) *Icarus* **124**, 97-112. [11] TAKEDA H. (1982) LPI Technical Report No. 82-02. [12] TAKEDA H. (1997) *Meteoritics & Planet. Sci.* **32**, 841-853.

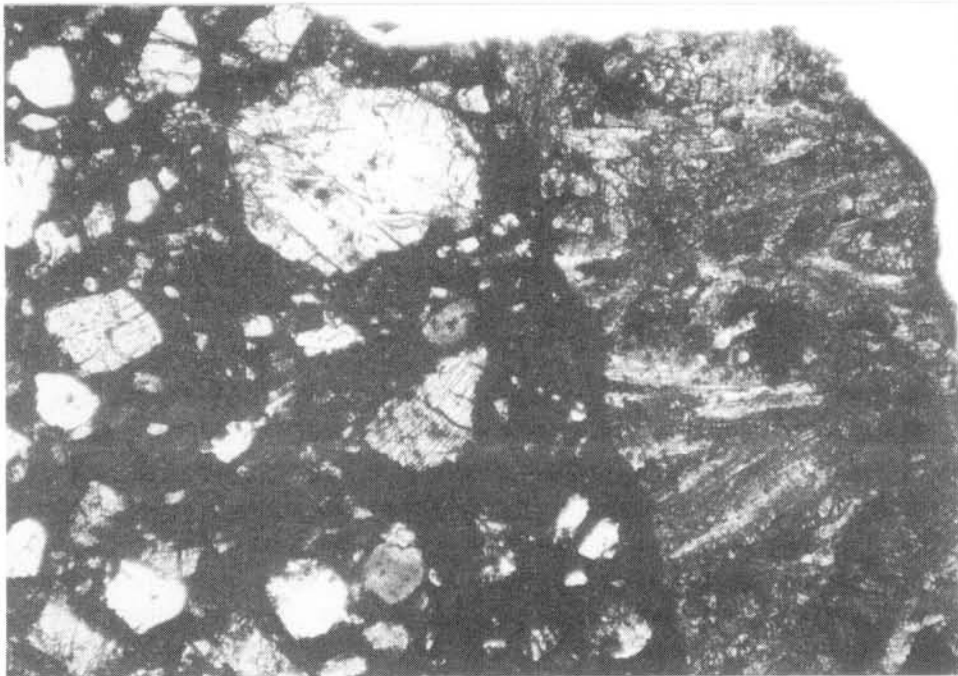


Fig. 1. Photomicrograph of a eucritic clast (right side) in Y791192,91-3. Light colored fragments set in the dark glassy matrix are mostly from cumulate eucrites. Width is 3.3 mm.

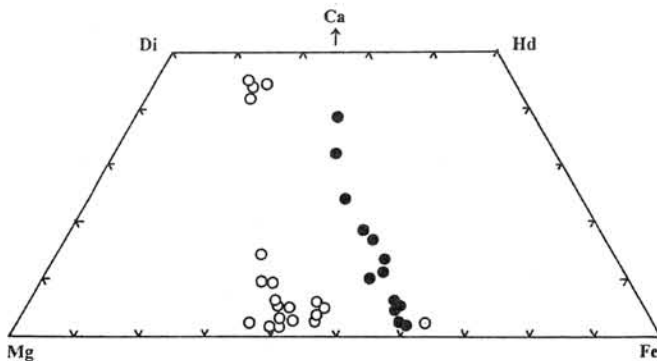


Fig. 2. Pyroxene quadrilateral of Y791192,91-3. Solid circles: Eucritic clast; open circles: pyroxene fragments in the matrix, mostly cumulate eucrites.

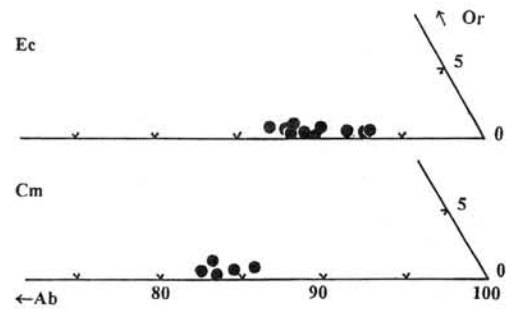


Fig. 3. Plagioclase compositions plotted in the Or-Ab-An diagram. Ec: Eucritic clast; Cm: fragments in the matrix.

Isotopic studies on Antarctic micrometeorites collected at the Dome Fuji station in 1996 using SHRIMP

Kentaro Terada¹, Yuji Sano¹, Takeshi Mori¹, Tomoki Nakamura², Wataru Nozaki², Takaaki Noguchi³, Naoya Imae⁴, Takaaki Fukuoka⁵ and Japan AMM working group

¹Earth and Planetary Sciences, Hiroshima University

²Earth and Planetary Sciences, Kyushu University

³Materials and Biological Sciences, Ibaraki University

⁴National Institute of Polar Research

⁵Environmental Systems, Rissho University

Introduction

More than 200 Antarctic micrometeorites (AMMs) of which sizes are typically 50~100 μm , were found among the precipitated fine particles recovered from a water tank in the Dome Fuji station in 1996 (Nakamura et al. 1999). According to back scattered images and so on, it is found that they consist of sub-minerals and have suffered from partial melting more or less. Secondary ion mass spectrometry (SIMS) has great importance for chemical and isotopic analysis of AMMs in some ways. That is, (1) spatial resolution of analysis is 5~30 μm , (2) handling samples is relatively easy and one can avoid surface contamination by rastering, (3) it is a quasi-undestructive analysis although the "pits" of which depth are a few μm are made.

Sensitive High Resolution Ion MicroProbe (SHRIMP) was installed at Hiroshima university in 1996. Since then, the remarkable geochemical results concerning in-situ U/Pb dating and REE analysis of various zircons and apatites has been reported (Sano et al, 1999a,b,c). Very recently, the technique of REE analysis in basalt glass has been established (Sano et al, 1999d). So, we tentatively, applied the techniques and U/Pb dating for the glassy particles (not chondritic AMMs), which were also collected at the Dome Fuji station. Preliminary results are reported in this abstract. More detail results including the chondritic AMMs will be presented at the symposium.

Sample preparations

About twenty glassy-particles were cast into epoxy resin with standard glass "NIST610". They were polished until they were exposed through their mid-sections to provide a flat surface for sputtering of secondary ions. After the surface was finished using 0.25 μm diamond paste, major components were analyzed using electron probe microanalyser (EPMA). The chemical compositions of almost these particles except for one spherule (GS-01) are almost same ($\text{SiO}_2=40\%$, $\text{Al}_2\text{O}_3=13\%$, $\text{MgO}=6\%$, $\text{CaO}=40\%$, $\text{FeO}=0.1\%$). These are very similar to those of the glassy spheres found in the recent fossil sediments in Hungary (Dosztaly and Don 1997). On the other hands, major components of GS-01 are different ($\text{SiO}_2=53\%$, $\text{Al}_2\text{O}_3=45\%$, $\text{MgO}=0\%$, $\text{CaO}=0\%$, $\text{FeO}=0\%$). These features of two kinds of samples are quite different from those of previous works concerning glassy spherule collected in Antarctica and Greenland ice (Koeberl C et al 1989 and Engrand private communication 1999).

SHRIMP analysis

About 5 nA O_2^- primary beam was focused to sputter a 20- μm -diameter area on the glassy sample and the positive secondary ions were extracted using 10 kV. A

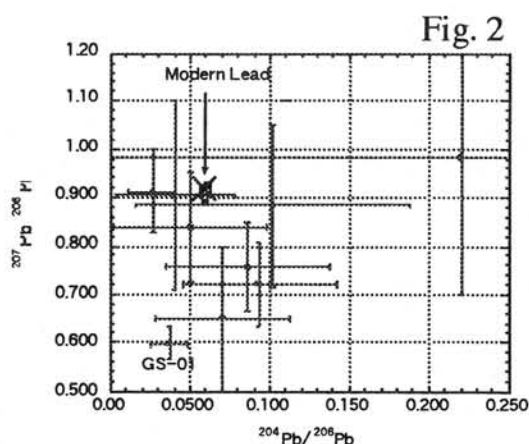
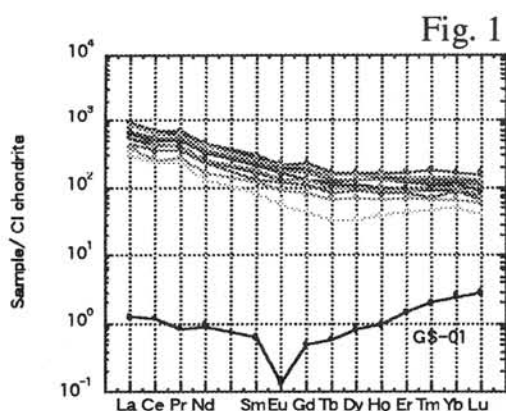
mass resolution $M/\delta M$ of 5600 at 1% peak height was employed for U/Pb analysis. These conditions are same with that of U/Pb dating of zircon and apatite. A mass resolution $M/\delta M$ of 9000 at 1% peak height was employed for REE analysis in order to separate heavy REEs from oxide of light REEs in the standard glass "NIST610" with adequate flat topped peaks. The magnet was cyclically peak-stepped from mass 104 ($^{28}\text{Si}_2^{16}\text{O}_3^+$) to mass 254 ($^{238}\text{U}^{16}\text{O}^+$) for U/Pb dating analysis, and from mass 104 ($^{28}\text{Si}_2^{16}\text{O}_3^+$) to mass 175 ($^{175}\text{Lu}^+$) for REE analysis. No isobaric interferences were found in that mass range. Each concentration was calibrated as follows,

$$X_{\text{sample (ppm)}} = \left(\frac{X^+}{^{28}\text{Si}_2^{16}\text{O}_3^+} \right)_{\text{sample}} \times X_{\text{NIST (ppm)}} \left(\frac{X^+}{^{28}\text{Si}_2^{16}\text{O}_3^+} \right)_{\text{NIST}}$$

where X_{NIST} (ppm) was accurately determined using ICP-MS. The more details of REE analysis and calibration of data will be given somewhere.

Preliminary results

Figure 1 shows REE abundance patterns of glassy spheres normalized to CI chondrite. All spheres except for GS-01 show the almost same concentrations of REEs and progressive depletion of heavy REEs. These data suggested that the origins of these particles are same. They are also similar to those of glass spherule found in Hungary sediments. On the other hands, the pattern of GS-01 is very chondritic with Ce negative anomalies, although small excesses of heavy REE are recognized. U concentrations range from 1 to 10 ppm. Figure 2 shows $^{207}\text{Pb}/^{206}\text{Pb}$ - $^{204}\text{Pb}/^{206}\text{Pb}$ correlation of glassy spheres. Pb/Pb ratios of almost particles are not inconsistent with terrestrial modern lead within the error. On the other hands, the Pb/Pb ratio of GS-01 is radiogenic. The Pb/Pb and U/Pb ratios of this spherule indicate that the crystallization occurred ago 700 ± 413 Ma (1σ) at least, although it depends on the model of initial Pb ratios.



Reference

- Dosztaly L. and Don G 1997
- Koerberl C. and Hagen E. H. (1989) *G. C. A.* **53**, 937-944
- NAKAMURA T. et al (1999) *Antarctic Meteorite Research* **12**
- SANO Y. et al (1999a) *Chemical Geology* **153**, 249-258.
- SANO Y. et al (1999b) *G.C.A.* accepted.
- SANO Y. et al (1999c) *Nature* accepted
- SANO Y. et al (1999d) *Analytical Science* submitted.

Relation between grain size distributions and the petrologic types of ordinary chondrites

T. Tomiyama¹ and M. Kitamura²

¹ *Department of Polar Science, School of Mathematical and Physical Science, Graduate University for Advanced Studies, Itabashi, Tokyo 173-8515, Japan.* ² *Department of Earth and Planetary Sciences, Faculty of Science, Kyoto University, Sakyo-ku, Kyoto 606-0315, Japan.*

Introduction :

The chemical-petrological classification of chondrites proposed by Van Schmus & Wood (1967) has been widely accepted. In this classification system, petrologic types from 3 to 6 are commonly used to express the degree of equilibration of the chondrites. Two kinds of criteria for the classification of petrologic types have been used: the degrees of chemical equilibration and of textural equilibration. The degree of chemical equilibration is determined quantitatively by chemical homogeneity observed within and among grains of constituent minerals. On the other hand, the determination of the degree of textural equilibration has been qualitative such as chondrule/mitrices appearance. In the present study, grain size distributions (GSD) of constituent minerals of ordinary chondrites which is one of the basic parameters expressing the degree of textural equilibration, are measured quantitatively and the relation between GSD and the petrologic types is discussed. The GSD measurement was carried out in back-scattered electron images (BEIs), because GSD in a submicroscopic scale can be expected to be more sensitive for the equilibration than GSD in a macroscopic scale.

Samples and Experimental Method :

37 polished thin-sections of less weathered H3-6 L3-6 LL3-6 chondrites were selected for this study. 20 BEIs were taken in randomly selected areas of each sample, as digital gray-level images. These images were 512 x 400 pixel, 256 gray-level data. The length of the side of each square pixel is 0.45 μm . A computer program was originally written for the measurement of GSD in image analysis. The program calculates the distances from each pixel to grain boundaries in various directions in an image and the area of the mineral grain which includes the pixel. Grain size is defined as the calculated area.

It can be expected that metal/sulfide (metal) grains show different behavior from silicate grains during the equilibration processes. In this study, these two distinct kinds of grains are classified in the images. Identification of these two kinds of grains was rather easy because of their differences in brightness in digital BEIs. More detailed distinction among each kind of minerals was not carried out in the present study because of their little difference in brightness in BEIs.

Results :

Mean grain sizes of constituent minerals in each chondrite are plotted against the petrologic types (Fig.1 a,b). The mean grain sizes of silicate minerals (Fig.1a) in L chondrites show slight positive correlation with the petrologic types, while those in H chondrites show no apparent correlation. In higher petrologic types (5,6) of LL chondrites, the mean grain sizes show negative correlation with the petrologic types. Mean sizes of metal grains in L and H groups increase with the increase of the petrologic types, while such tendency are not observed in LL chondrites (Fig.1b).

Discussion :

The relation between GSD and the petrologic types observed in the present study can not be simply explained by a prograde metamorphism model where chondrites of higher petrologic types were formed from those of lower petrologic types only by a progressive annealing process. If higher types were formed from type 3, additional modification of GSD such as the fragmentation by shock events (Stöffler et al., 1991) is required to explain GSD .

On the other hand, in the auto-metamorphism model, chondrites are considered to have experienced their own cooling history; chondrites of higher petrologic types cooled more slowly than those of lower petrologic types. Textural investigations for unequilibrated chondrites (e.g, Ashworth, 1977; Dodd, 1976) indicate that some pre-accretionary processes influenced GSD. If pre-accretionary processes are responsible for GSD of each chondrite, GSD is not necessarily correlated with the petrologic types.

It is difficult in the present study to decide which model is more suitable for explaining the measured GSD, because of the limited number of studied samples in each chemical group. However, it can be concluded that the prograde metamorphism model with only progressive annealing processes can not explain the measured GSD.

References :

Van Schmus W. R. and Wood J. A. (1967) A chemical-petrological classification for the chondritic meteorites **GCA** **31**, 747-765. Stöffler D., Keil K., Scott E.R.D. (1991) Shock metamorphism of ordinary chondrites **GCA** **55**, 3845-3867. Ashworth J.R. (1977) Matrix textures in unequilibrated ordinary chondrites **EPSL** **35**, 25-34. Dodd R.T. (1976) Accretion of the ordinary chondrites **EPSL** **30**, 281-291.

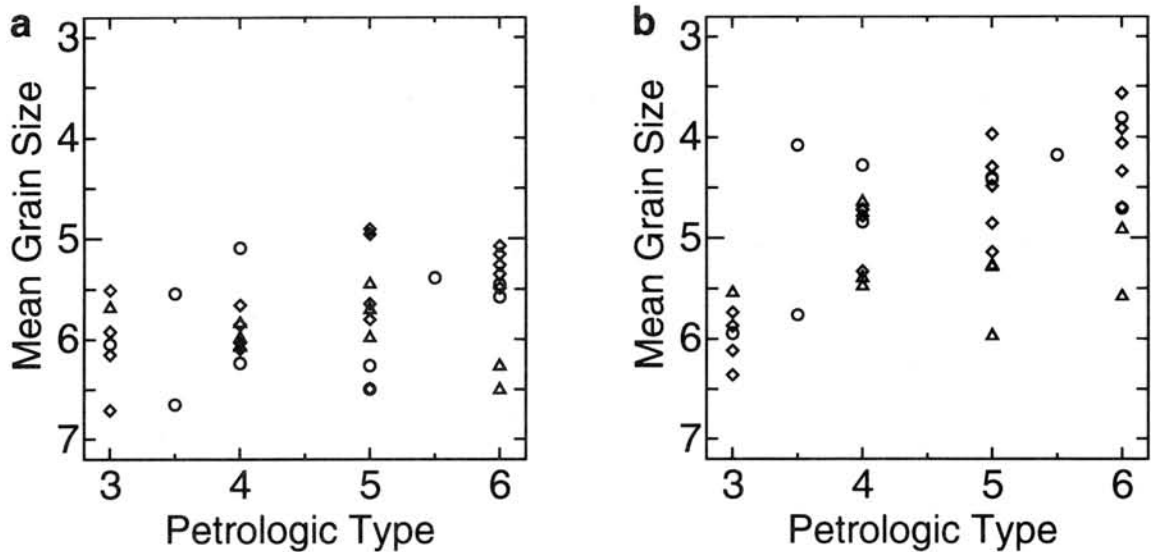


Fig.1 Mean grain size and petrologic type

Mean grain size are plotted against the petrologic types for silicate grains (a) and for metals (b). Open circles, diamonds and triangles represent for the results of H ,L and LL chondrites. Following the usual practice in geological GSD analysis, size parameter is represented by ϕ unit scale. ($\phi = -\log_2 \frac{\text{diameter}}{1mm}$)

A New Approach for The Formation of Olivine-Chondrules by Aero-Acoustic Levitation

K. Tsukamoto, H. Satoh (Faculty of Science, Tohoku University),

Y. Takamura (Dep. Material Science, University of Tokyo),

K. Kuribayashi (ISAS)

A new aero-acoustic levitation method has successfully been employed to realize container-less syntheses of forsterite-chondrules from extremely supercooled ($\sim 1000^\circ\text{C}$) melt. In-situ observation of dynamic crystallization and the temperature change of levitating melts were carried out at every 1/1000s, which reproduced a realistic formation of the rim and the internal texture of chondrules. A new model for the rim formation during recalescence will be presented. Our challenge will gain a new insight into the formation process of the rim-bearing chondrules, which is closely related to the thermal history in the solar nebula.

Introduction

What we have learned from recent microgravity experiments is the considerable reduction of nucleation rate, which indicates the possibility of preparing very large supercooled melt in space. Concerning the reasons of this nucleation reduction in microgravity, one may refer to (1) the suppression of gravitational convection and to (2) the suppression of heterogeneous nucleation rather than homogeneous nucleation. It is also important to refer that crystallization melt is possible without any container if the melt is levitated.

Chondrules have been regarded as the result of spherical crystallization from large supercooled melt. Because of the importance in space science, many attempts have been made to reproduce the texture of these chondrules. Among others the texture of barred-olivine has been believe to be one of the keys to "read" the initial stage of crystallization from the meteorites.

During their synthesis of the chondrules in an electric-furnace, they succeeded to reproduce not only barred-olivine but also porphyritic textures and dendrites. Nevertheless all failed to reproduce the double structure, the rim and the internal texture which is very common in natural chondrules. We paid attention to the formation the rim, which is regarded as the product of initial crystallization from the melt droplet.

Experimental

In order to achieve much larger supercooling we employed aero-acoustic levita-

tion method for the first time, in which using standing wave of 22kHz of acoustic waves a small sphere a few mm in diameter could be levitated. This method has been used to simulate crystal growth in microgravity, though the gravity cannot be reduced but container-less crystallization can be realized.

Forsterite and Fe-bearing forsterite were melted during the levitation using CO_2 laser (1.5KW) and then quenched by stopping the laser heating. The temperature was recorded to a digital an oscillograph by two-color pyrometer with the time interval of $1/1000\text{s}$. The image during the levitation was also recorded with the same time interval *in situ* by ultra-high speed TV camera. The *ex situ* analysis was done in such a way that the external morphology of the synthesized chondrules were observed by *SEM*, followed by cutting the crystal both for polarization microscopy and for elementary analysis.

Results and discussions

A temperature history of the melt sphere is shown in fig.1 as an example, the temperature of which was measured by two-color pyrometer so that the better calibration is possible. Fig. 1 is such an example, in which one can see the drop of the tempera-

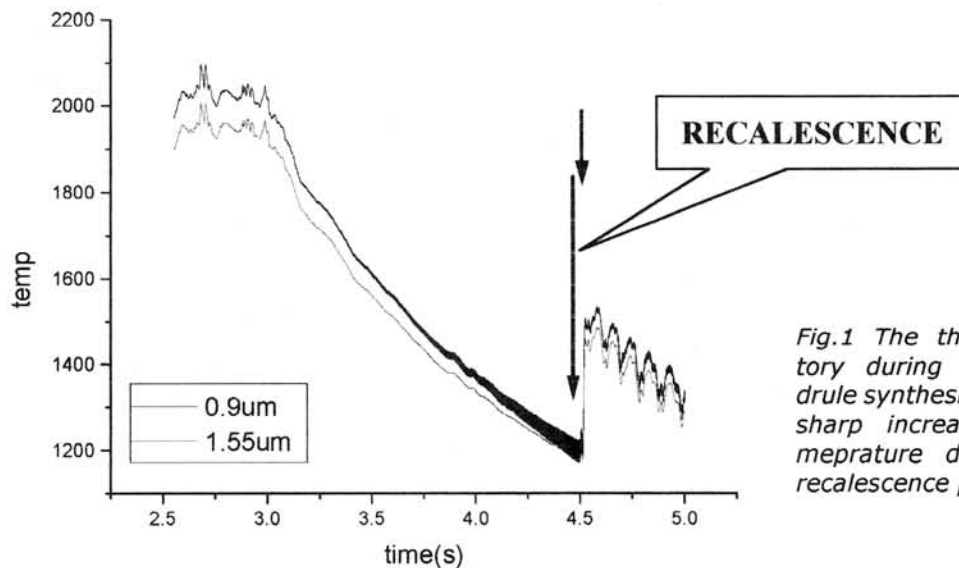


Fig.1 The thermal history during the chondrule synthesis. Note the sharp increase of temperature due to the recalescence process.

ture from $\sim 2000^\circ\text{C}$ to $\sim 1000^\circ\text{C}$, followed by the sharp increase of the temperature approaching to the melting point of the forsterite. This sharp temperature increase is caused by recalescence due to the release of the latent heat during crystallization, which in turn shows that nucleation and crystal growth on the chondrule melt starts during the increasing temperature. The corresponding images of this process are shown in fig.2,

in which the images are shown every 0.01s during the recalescence process of 0.1s.

Several two-dimensional islands in the form of dendrite nucleate on the sphere and spread over the surface, the process of which can be visualized by ultra-high speed TV camera (fig.2). In 0.1s the total surface coverage is completed and the temperature again starts to decrease. The growth rate of the islands reaches a few cm/s. The process

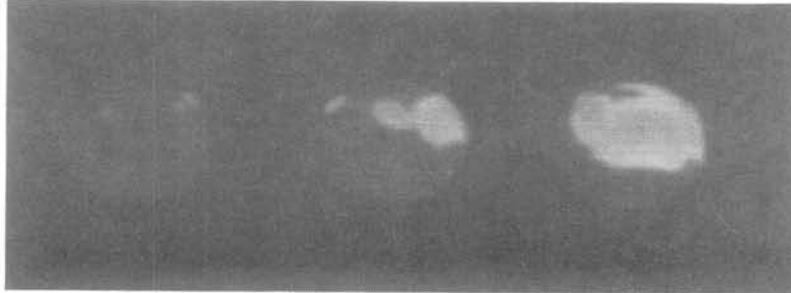


Fig.2 Ultra-high speed TV images from a rotating crystallizing forsterite melt. The time interval is 0.1s. This crystallization process is completed in 0.1s of recalescence process.

can be regarded as the rim formation process. During the cooling after the recalescence process crystallization in the internal body starts, leading the formation of some textures like barred-olivine texture

though the texture depends on the supercooling.

It has to be emphasized here that this short recalescence process plays an important role to form the double structure, the rim and the internal texture and that the total crystallization process could be finished in a single second. Thermal history will be discussed based on the relatively slower thermal diffusivity compared to that of metal melt, which shows few double structures. The dendritic branch space as a function of supercooling will also be discussed together with the true three-dimensional barred-olivine texture.

Mg isotopic anomaly of two types of anorthite in CAIs

T. Ushikubo¹, H. Hiyagon¹, N. Sugiura¹ and A. A. Uf'yanov²

1: Department of Earth and Planetary Physics, University of Tokyo, Tokyo, Japan

2: Department of Geology, Moscow State University, Moscow, Russia

Introduction

²⁶Mg excess which is found in some meteorites is strong evidence for existence of live ²⁶Al (half life: 0.71 Myrs) in the early solar system. Initial ²⁶Al/²⁷Al ratios of CAIs show nearly the same value of 5.0×10^{-5} which is called the canonical value [1]. So, Al-Mg chronology using ²⁶Mg excess is an useful method to investigate time difference of metamorphic events of CAIs because difference in initial ²⁶Al/²⁷Al ratios from the canonical value means difference in time.

Anorthite in CAIs is an important phase to know timing of metamorphic events of CAIs. First, initial ²⁶Al/²⁷Al ratios can be obtained precisely because anorthite have high Al/Mg ratios. And secondly, anorthite in CAIs are classified into two types according to their origin; primary anorthite which formed at CAIs' formation and secondary anorthite which are alteration products.

We measured Mg and O isotopic ratios of two CAIs; CAI1 from Allende (CV3) and E44 from Efremovka (CV3). Using these data (especially anorthite data), we will discuss timing of metamorphic events of CAI.

Results and Discussion

Mg isotopic ratios of the CAI1 and the E44 were measured by SIMS (CAMECA ims-6f) of University of Tokyo. Anorthite in the E44 are large grains (about 500 μ m in diameter) with sharp grain boundary (Fig. 1) and have O isotopic anomaly of -45 ‰. These features suggest that they are primary anorthite. On the other hand, anorthite in the CAI1 are small anhedral grains (about 50 μ m in diameter) and they are found with grossular in interstitial of melilite and fassaite (Fig. 2). So we conclude that anorthite in the CAI1 are secondary anorthite.

Results of Mg isotopic measurements of the E44 are shown in Fig. 3a. Mg isotopic data of anorthite do not form isochron. Initial ²⁶Al/²⁷Al ratios of anorthite show large variation (0.9 to 4.5×10^{-5}) and these variation are related to the position in anorthite grains. Near the grain margin, initial ratios are lower than those of inner part of the grain. This suggests that isotopic exchange of Mg took place between anorthite and surrounding Mg-rich minerals

[2]. Primary anorthite of the E44 originally had initial $^{26}\text{Al}/^{27}\text{Al}$ ratios as high as 4.5×10^{-5} , close to the canonical value, but lost Mg isotopic anomaly near the grain boundary during some heating events. Heating events occurred at least 1.8 Myrs after CAI formation judging from the observed lowest ratio (0.9×10^{-5}).

Anorthite in the CAI1 also show Mg isotopic anomaly (Fig. 3b). This means that metamorphic events which formed secondary anorthite occurred when ^{26}Al was still alive. Assuming that Mg isotopic data of anorthite in the CAI1 consist a single isochron, the initial $^{26}\text{Al}/^{27}\text{Al}$ ratio is about 1.9×10^{-5} , corresponding to 1.0 Myrs after CAI formation. Considering the possibility of a later Mg isotopic exchange like that inferred for the anorthite in the E44, the metamorphic events of may have occurred *within* 1.0 Myrs after CAI formation. This initial $^{26}\text{Al}/^{27}\text{Al}$ ratio is higher than those of chondrules (about 1.0×10^{-5} [3, 4]), so metamorphic events of CAIs occurred before chondrules formation.

References

- [1] MACPHERSON G. J., DAVIS A.M. and ZINNER E. K. (1995) *Meteoritics* 30, 365-386.
- [2] PODOSEK F. A., ZINNER E. K., MACPHERSON G. J., LUNDBERG L. L., BRANNON J. C. and FAHEY A.J. (1991) *Geochim. Cosmochim. Acta* 55, 1083-1110.
- [3] RUSSELL S. S., SRINIVASAN G., HUSS G. R., WASSERBURG G. J. and MACPHERSON G. J. (1996) *Nature* 273, 757-762.
- [4] KITA N. T., NAGAHARA H., TOGASHI S. and MORISHITA Y. (1998) *Meteorit. Planet. Sci.* 33, A83-A84 (abstract).

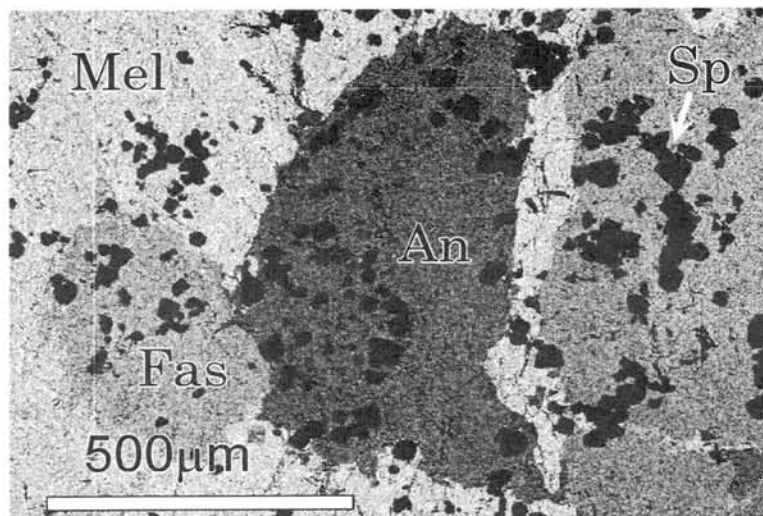


Fig. 1 Back scattered electron image of anorthite of E44. This CAI consists of spinel (Sp), anorthite (An), fassiate (Fas) and melilite (Mel). Anorthite grain is large and has sharp grain boundary.

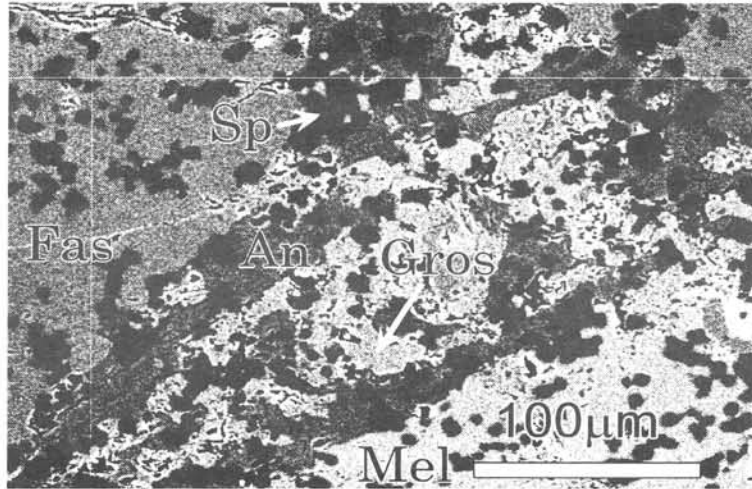


Fig. 2 Back scattered electron image of anorthite of CAI1. Anorthite grains are small and anhedral grain and exist with grossular (Gros).

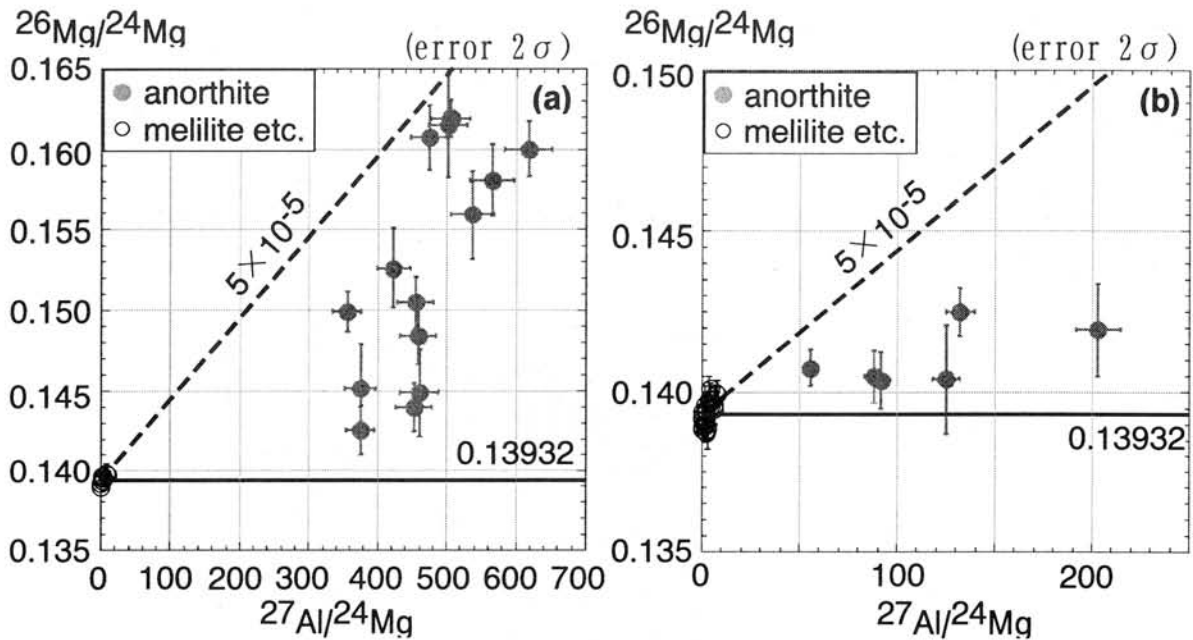


Fig. 3 Results of Mg isotopic measurements.

(a) Mg isotopic ratios of E44. Anorthite data do not form an isochron, This trend can be explained by Mg isotopic exchange between anorthite (large excess ^{26}Mg) and other Mg-rich minerals (small excess ^{26}Mg).

(b) Mg isotopic ratios of CAI1. Secondary anorthite which is an alteration product from primary phases shows larger isotopic anomaly. This means that secondary anorthite formed before all ^{26}Al decayed.

Differentiation of siderophile elements in the Moon and the HED parent asteroid

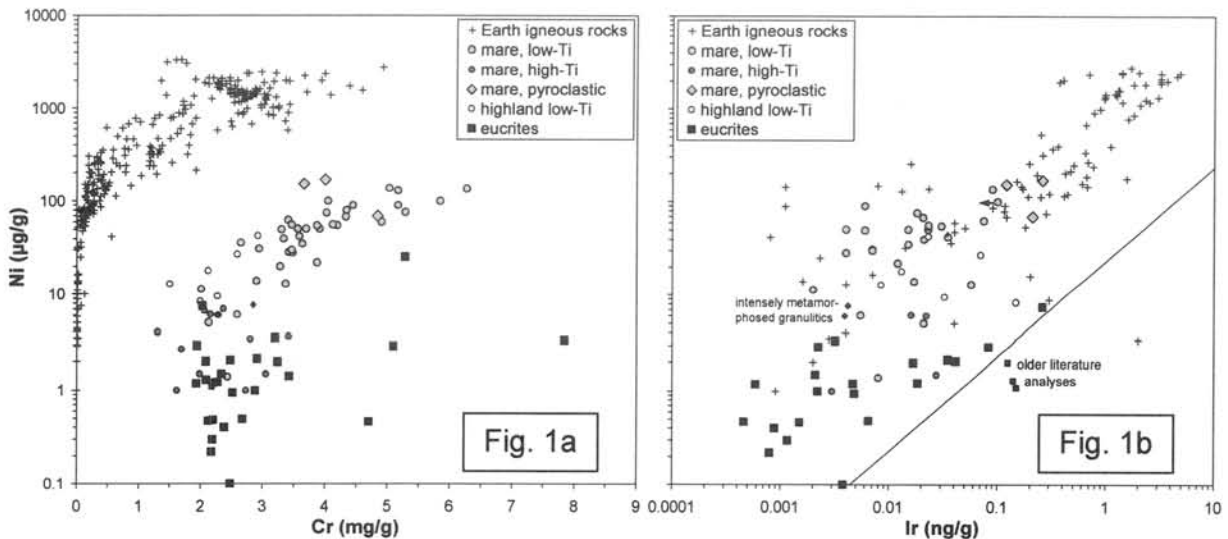
PAUL H. WARREN^{1,2}

¹ Institute of Geophysics, UCLA, Los Angeles, CA 90095-1567, U.S.A. (current address)

² Mineralogical Institute, University of Tokyo, Hongo, Tokyo 113-0033, Japan

With important technical assistance from numerous UCLA colleagues, especially G. W. Kallemeyn and F. T. Kyte, I have used radiochemical neutron activation analysis (RNAA) to determine several highly siderophile elements, including Ni, Re, Os and Ir, in some 40 HED meteorites (Table). These elements have seldom been determined in HEDs, mainly because they occur at extremely low abundances. Most of the scarce previous data for PGE in HEDs come from a few of my own papers [e.g., 1] and Morgan et al. [2].

Although these elements are notoriously siderophile, within the context of a silicate differentiation system they tend to behave much like compatible transition elements. Using a large database of high-quality data for Earth, Moon, Mars and HED basaltic-ultramafic igneous rocks, plots of Ni or Ir vs. elements such as Mg, V and Cr (e.g., Fig. 1a) generally result in very systematic, albeit nonlinear, positive correlation trends (plots involving V among Earth rocks exhibit instead a negative correlation, an effect of the Earth's high $f(O_2)$). The trends are far from linear, because at the "evolved" (e.g., low-Cr) ends, increasing sulfide fractionation profoundly reduces the siderophile concentrations. The concentrations at the "primitive" ends of these trends provide valuable clues



to the bulk-mantle composition for the siderophile elements [3]. For lunar samples, I utilize a database that I recently compiled [4], mainly by extending the compilation of Wolf et al. [5] to add Mg, Cr, V, etc.

Application of this methodology to eucrites is severely hampered by the limited compositional range of these basalts, in terms of Mg, Cr and V. The only Mg-, Cr- and V-rich eucrites are pyroxene-plagioclase accumulates. The diogenites are more Mg-rich, but they are nearly monomineralic orthopyroxene. Assuming that sulfide fractionation has not been vastly more pervasive than on the Moon (where low-Ti mare basalts are not S-saturated [6], i.e., apparently left no sulfide in their source regions), plots such as Fig. 1a suggest that Ni and PGE are even more depleted in the HED mantle than in the lunar mantle, which is depleted by at least a factor of 4 relative to Earth's mantle. For complex and not entirely clear reasons, the Moon/Earth depletion factors look larger vs. Cr than vs. Mg. The major element, Mg, is probably more reliable for this purpose.

In a sense, it is remarkable that the lunar and HED mantle siderophile depletions are not much greater. In the case of the Earth and Mars, siderophiles appear to have been added as a veneer after differentiation of the core [1]. High-pressure dampening of metal/silicate partitioning behavior [e.g., 7] also played some role in the case of the Earth. By many models [e.g., 8], the Moon formed largely from, and thus inherited its bulk composition from, Earth's mantle. The Moon appears to possess a core amounting to 1-2 wt% of its bulk mass [9], and the HED asteroid presumably also has at least a small core [10]. The depletion factor Δ implied by an equilibrium between the silicate portion of the planet and its core can be calculated from the simple mass balance

$$\Delta = 1/(Dc + [1-c])$$

where c is the weight fraction of the core, and D is the core/silicate (metal/silicate?) distribution coefficient.

With a low-pressure metal/silicate D of the order 5×10^5 [11] and perhaps much higher [12], Ir should have been depleted in the lunar mantle to about $0.0002 \times$ the bulk-Moon concentration (which in any event is presumably not chondritic for siderophile elements, given the Moon's gross depletion in Fe-metal). For Ni, the metal/silicate D is roughly $25 \times$ lower [11], so core-mantle equilibration for Ni should have resulted in $\Delta \approx 0.005$ and Ni/Ir $\approx 25 \times$ the bulk-Moon ratio. Ni is also far less chalcophile than PGE [e.g., 13], so sulfide fractionation, too, should have tended to result in fractionation of Ni/Ir. Yet the Ni/Ir ratio is remarkably similar among basaltic rocks from Earth, the Moon, and the HED asteroid (Fig. 1b). The history of core-mantle differentiation on such bodies was evidently very complex, but a disequilibrium veneer is unambiguously implied by the lunar and HED data (albeit these veneers may have been slight in proportion to the less definite Earth veneer), while the relative constancy of Ni/Ir, at about 10-40 times chondritic in each of the bulk mantles, looms as a challenge for any unified, overall model.

Table: Concentrations of siderophile elements, determined by RNAA, in HED meteorites and the angrite Asuka-881371.

sample	mass mg	Ni $\mu\text{g/g}$	Ge ng/g	Re ng/g	Os ng/g	Ir ng/g	Au ng/g
As-881371,105 eucrites	83	112	50	0.031	0.26	0.25	0.167
ALH81001,16b	127	1.01	<30	<0.014	0.256	0.0253 $\pm 8\%$	0.0171
EET87520,10a	297	0.10 $\pm 39\%$	0.70 $\pm 11\%$	<0.0017	0.0026 $\pm 33\%$	0.0038 $\pm 9\%$	0.0048 $\pm 13\%$
EET87542,7a	254	0.34	1630	<0.0023	nd	0.0019	0.052
EET87542,7b	274	0.25 $\pm 17\%$	1390	0.0006 $\pm 34\%$	0.0038 $\pm 20\%$	0.00042 $\pm 35\%$	0.057
LEW86002,10b	335	0.47 $\pm 7\%$	0.75 $\pm 10\%$	0.0011 $\pm 39\%$	0.0036 $\pm 15\%$	0.00046 $\pm 25\%$	0.0097 $\pm 7\%$
LEW88010,5	364	2.06	1.60	<0.014	0.080	0.041	0.0164
Millbillillie CG	123	0.68 $\pm 10\%$	2.1 $\pm 9\%$	0.0023 $\pm 16\%$	<0.006	0.00105 $\pm 20\%$	0.032
Millbillillie FD	201	0.38 $\pm 16\%$	0.78 $\pm 9\%$	<0.004	0.0056 $\pm 15\%$	0.0040	0.037 $\pm 7\%$
Millbillillie FG	144	1.83 $\pm 7\%$	1.76 $\pm 12\%$	0.0064	0.068 $\pm 8\%$	0.050	0.216
PCA91007,4	291	7.5	6.2	0.020	0.29	0.26	0.072
PCA91078,10a	286	0.22 $\pm 14\%$	1.22	<0.0024	0.116	0.00079 $\pm 10\%$	0.0175
PCA91159,5	218	0.46	31.1	0.0089	<0.0049	0.00150	0.032
RKP80204,14 cumulate eucrites	246	0.48	1.5	0.0069	0.0052	0.0065	0.046
A881394,56a	274	7.7	2.9	0.0158	0.007	0.0042	0.028
ALH85001,25b	279	2.9	19.0	0.0044	<0.015	0.0022	0.0077
Y791438,54 diogenites	229	0.95	0.72 $\pm 13\%$	<0.0067	0.119	0.0048	0.0079
ALH77256,96a	348	35.3	63	0.0062	0.098	0.079	0.36
LAP91900,26	512	17.6	<20	0.0052 $\pm 8\%$	0.081	0.055	0.064
Y75032,90	471	27	12.5	0.0102	0.024	0.019	0.039
Y791200,86 polymict eucrites	249	14.7	16.4	0.0114 $\pm 9\%$	0.194	0.036	0.060
ALH78132,102	309	15.6	12.4	0.067	1.15	0.87	0.225
EET79005,95	115	11.6	13.2	0.036	0.48	0.57	0.058
EET79005,93	277	22.7	18.5	0.051	0.64	0.60	0.190
EET92023,9a	299	1350	1500	6.3	40	51	16.2
EET92023,9b	298	1110	1320	4.4	53	45	15.9
LEW87004,14	305	34	71	0.072	1.15	1.21	0.26
LEW87004,19	297	41.3	76	0.116	1.28	1.86	0.433
LEW87295,7	244	97	610	0.67	10.0	12.0	2.1
TIL82403,31	349	7.7	8.7	0.026	0.75	0.64	0.074
Y790266,102	433	9.7	4.4	0.038	0.72	0.43	0.0227
Y791192,81b	309	4.6	11.8	0.0061	0.035	0.028	0.035
Y82049,65a	337	100	77	0.252	4.6	5.1	1.00
Y82052,63 howardite	500	29.0	34	0.083	0.76	1.19	0.324
Chaves	227	65	44	0.095	1.05	1.07	46.6*

* The Chaves sample (a powder kindly supplied by Señor José F. Monteiro) evidently contained Au contamination. All other siderophile elements are relatively low, for a polymict impact breccia.

References: [1] Warren P. H. & Kallemeyn G. W. (1997) *Antarct. Meteorites XXII*, 200-202. [2] Morgan J. W. et al. (1978) *GCA* 42, 27-38. [3] Warren P. H. et al. (1999) *GCA*, in press. [4] Righter K. et al. (1999), submitted to *Origin of the Earth & Moon*. [5] Wolf R. et al. (1979) *PLPSC* 10, 2107-2130. [6] Gibson E. K. et al. (1977) *PLSC* 8, 1417-1428. [7] Tschauer O. et al. (1998) in *Origin of the Earth & Moon* (abstract volume), p. 48-49. [8] Ringwood A. E. (1992) *EPS Lett.* 111, 537-555. [9] Konopliv A. S. et al. (1998) *Science* 281, 1476-1480. [10] Ruzicka A. et al. (1997) *MPS* 32, 825-840. [11] Jones J. H. (1995) in *Rock Physics and Phase Relations, A Handbook of Physical Constants* (ed. T. J. Ahrens), p. 73-104. [12] Borisov A. & Palme H. (1995) *GCA* 59, 481-485.

ZONED METAL IN THE CR CLAN CHONDRITES.

Michael K. Weisberg and Martin Prinz
Earth and Planetary Sciences, American Museum Natural Hist., NY, NY 10024, USA.

Introduction. The CR clan includes CR, CH and CB (Bencubbinite) chondrites, as well as the Acfer 182 and LEW 85332 ungrouped chondrites [1-3]. All of these chondrites are metal-rich with modal metal abundances ranging (in vol.%) from 7 in the CR and up to >70 in the CB chondrites [1-4]. The origin of metal in these primitive meteorites has been the subject of much debate. Metal compositions (Ni, Co, Cr) in CR chondrites follow the calculated compositional path for metal condensing from a solar gas, suggesting their compositions are inherited from primary condensation processes [4,5]. CB chondrite metal, which is compositionally similar to that in CR chondrites, was also interpreted to be a primitive component, preserving its nebular condensation heritage [6,7]. Additionally, zoned metal in CH and CB chondrites was recently shown to have zoning patterns consistent with a condensation origin [3,8]. The compositional trends in CR clan metal has also been interpreted to be the result of reduction during chondrule formation [9] and post-lithification metamorphism [10]. Here, we present a comprehensive study of zoned metal in the CR clan to discuss its origin and implications.

CB Metal. The CB chondrites are a new group of chondrites with four members (Bencubbin, Weatherford, QUE 94411 and Hammadah al Hamra 237 (HH 237) [2,3]. Bencubbin and Weatherford contain large, cm-sized, metal clasts that constitute about 60 vol.% and metal in QUE 94411 and HH 237 is smaller, mm-sized, and constitutes >70%. The metal in Bencubbin and Weatherford has a tight range, from 5-8% Ni, and some metal grains with 2.5% Si were found in Bencubbin [6,7]. In QUE 94411 and HH 237 the metal is more complex. It ranges (wt. %) from about 4.5-14 Ni and occurs as two major textural types; these are large mm-size metallic chondrules, and smaller, 100-300 μ m size irregular grains (Fig. 1). The large metal chondrules appear to be aggregates of smaller metal grains and contain μ m-sized blebs of Cr-bearing troilite (Fig. 1). These features are similar to those in large cm-size metal in Bencubbin and Weatherford. The troilite blebs have an average of 2- 4% Cr. Cr is homogeneously distributed in most troilite, but in some cases blebs have exsolved daubreelite. Around some troilite blebs is a fine (sub- μ m) rim of high Ni-metal. One of the distinguishing characteristics of the CB chondrites is anomalously heavy nitrogen with $\delta^{15}\text{N}$ values up to 1000‰, and one location of heavy nitrogen in Bencubbin is as rims around the troilite blebs within metal [11]. Some small metal in HH 237 and QUE 94411 is homogeneous, with compositions similar to that of large metal chondrules; others are more Ni-rich with up to 14 % Ni and many grains are zoned with Ni and Co decreasing, and Fe and Cr increasing, from core to rim (Fig. 2, 3). Ni in zoned metal ranges (wt. %) from 4.5 in the cores to 15 in the rims, with a positive Ni-Co relationship. All metal in the CB chondrites plots along the solar Ni-Co trend, predicted for metal condensation from a solar gas at 1475 through 1375 K and 10^{-4} atm, and the zoned metal grains are no exception (Fig. 4). In addition, Ni-Cr in the zoned metal follows the predicted condensation trend for metal, but at lower Cr values (Fig. 4).

CR Metal. Metal in the CR chondrites occurs in two major textural settings, inside chondrules and as isolated clasts in the matrix. Chondrule metal may be subdivided into core and rim. In many cases, the metal is spherical to sub-spherical. Metal compositions range (in wt. %) from 7-14 in the chondrule cores and 5- 12 in chondrule rims. Isolated metal ranges from 5-10, similar to that in the rims. As in the CB chondrites, most CR metal has a solar Ni-Co trend. Rim metal has lower Ni than associated core metal, consistent with rim metal as a lower temperature condensate that attached itself to the chondrule at a later stage. Some of the large, isolated metal in CR chondrites is zoned with Ni-rich cores and Ni-poor rims, similar to zoned metal in CB chondrites (Fig. 5). The zoned metal is in contact with the oxidized, aqueously altered matrix. This highly unequilibrated assemblage of reduced metal and oxidized matrix suggests that the zoning in the

metal is primary, predating the assemblage of the host chondrite. It attests to the highly primitive character of Renazzo.

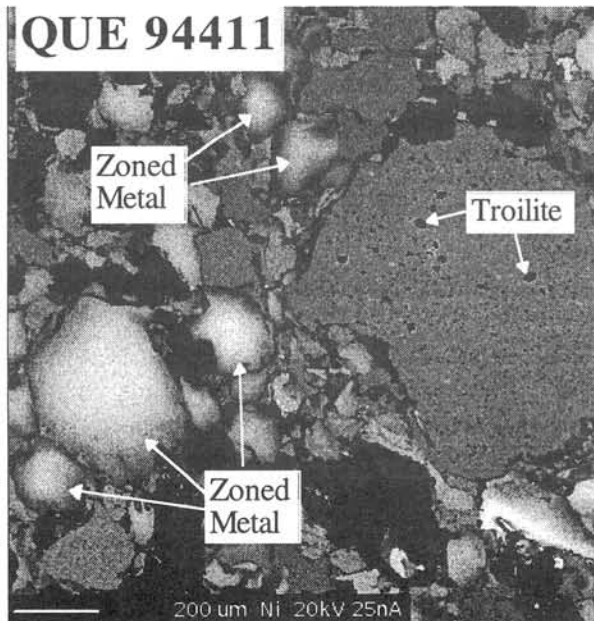


Fig. 1 Ni X-ray map of the QUE 94411 CB chondrite. Brighter areas have higher Ni. Dark areas are non-metal.

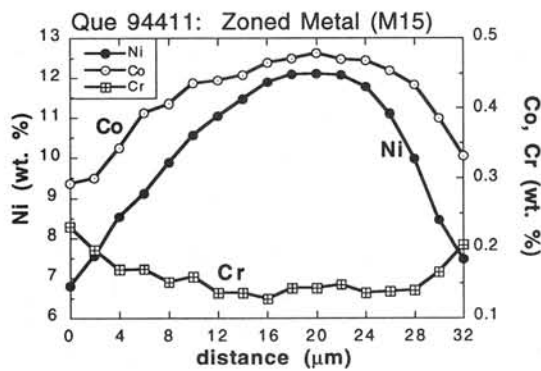


Fig. 2. Zoning profile across a metal grain in the QUE 94411 CB chondrite.

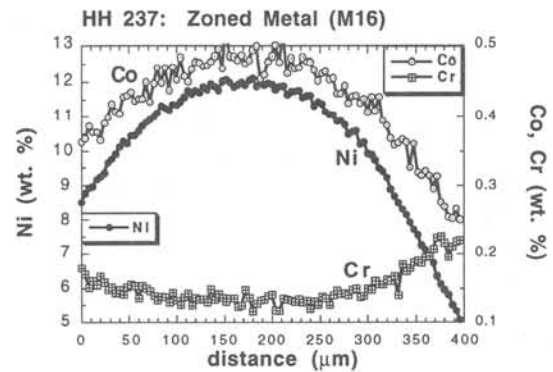


Fig. 3. Zoning profile across a metal grain in the HH 237 CB chondrite.

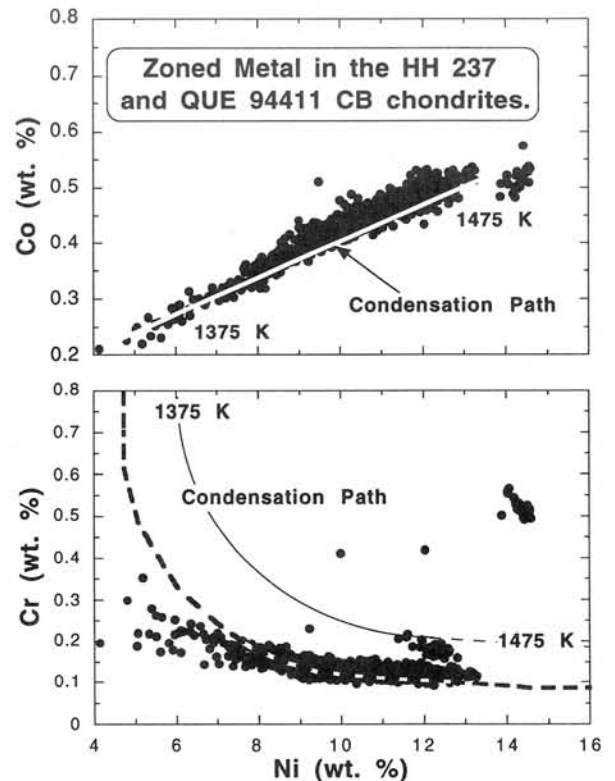


Fig. 4. Plot of Ni vs Co, Cr for 25 zoned metal grains from the QUE 94411 and HH 237 bencubbinites. Solid lines are calculated condensation paths from [8].

CH Metal. The CH chondrites contain about 20 vol.% metal [12]. The metal occurs as small (10-50μm) metallic chondrules, similar in size to the silicate chondrules, with occasional metal clasts up to 500μm in length (Fig. 6). In some CH chondrites the metal wraps around the silicate chondrules. Metal compositions range from 4-14% Ni and has a positive solar Ni-Co ratio, as in all CR clan chondrites, as discussed above. Some metal is zoned similar to that in the CB chondrites, with compositions that follow the condensation path, as recently described [8].

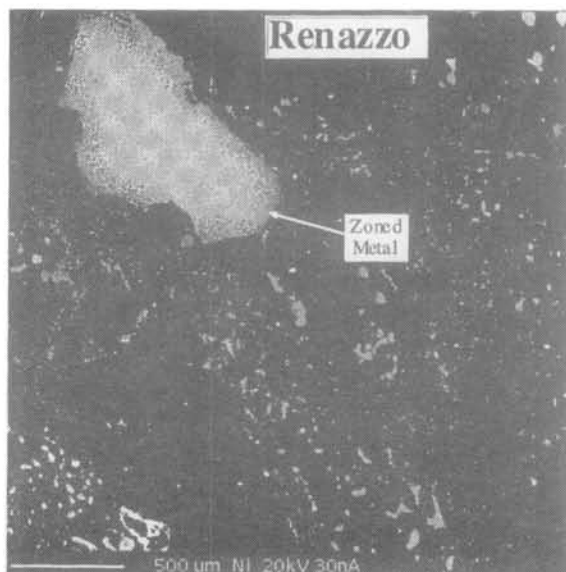


Fig. 5 Ni X-ray map of the Renazzo CR chondrite. Brighter areas have higher Ni. Dark areas are mainly silicate.

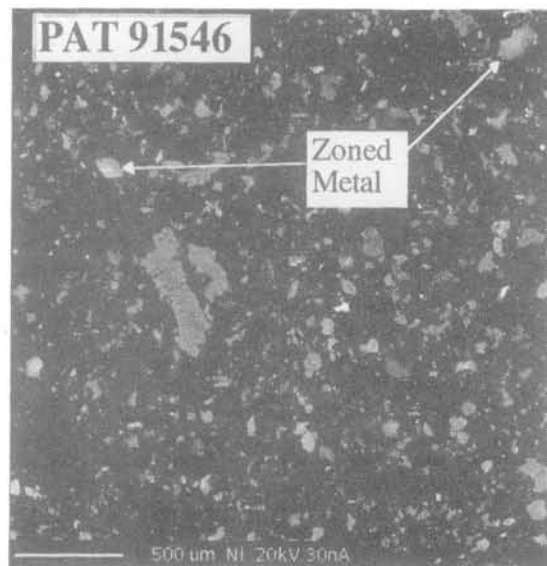


Fig. 6 Ni X-ray map of the PAT 91546 CH chondrite. Bright areas have higher Ni. Dark areas are mainly silicate.

Discussion. The heterogeneity and preservation of primary zoning in the CR clan metal indicates that it was cooled rapidly to below and not reheated above, 500°C, as in the least equilibrated ordinary chondrites [e.g., 13]. Further, the occurrence of high (up to 14%) Ni in the cores of some zoned metal suggests that these grains are metastable [e.g., 14] and would likely have decomposed to plessite structures if they were only mildly heated (above 300°C) during thermal metamorphism [8]. Therefore, the metal compositions attest to the highly unequilibrated, primitive character of the CR clan chondrites. The Ni vs. Co relationship, with a solar Ni:Co ratio, suggests a similar nebular condensation origin for all CR clan metal. Alternatively, the range of Ni and Co contents may be the result of modification of primitive metal by the reduction during or after chondrule formation [e.g., 9,10], but the data from zoned metal do not support this hypothesis. In some metal, other elemental trends cannot be used to test these competing hypotheses because they are generally unclear, obscured by redistribution of elements into other phases. For example, Cr-bearing troilite blebs in some CB and CH metal grains are apparently the sinks for subsolidus redistribution of Cr. However, zoned metal in the CH and CB chondrites do not contain troilite and show Ni-Cr relationships that are consistent with a condensation origin of the metal. One of the problems with a condensation origin for CR clan metal is the presence of troilite blebs within some CH and CB metal. Troilite forms at much lower temperatures than FeNi in equilibrium condensation models. It is possible that some CR clan metal was initially porous aggregates, allowing metal surfaces to react with gaseous H₂S at lower nebular temperatures to form troilite. This is consistent with the occurrence of troilite along boundaries of the metal grains within some large metal chondrules in CB chondrites. Ni-rich rims around some of the troilite blebs in CB chondrite metal may also be an artifact of this reaction. In summary, this detailed study of CR clan metal supports a condensation origin for the metal and attests to the highly primitive nature of the metal-rich CR clan chondrites.

References: [1] Weisberg M.K. et al. (1995) Proc. NIPR Symp. Ant. Met. 8, 11-32. [2] Weisberg M. K. et al. (1998) Meteoritics 33, A166. [3] Weisberg M. K. et al. (1999) LPSC XXX. [4] Weisberg et al. (1993) GCA 57, 1567-1586. [5] Grossman L. and Olsen E. (1974) GCA 38, 173-187. [6] Newsom H. E. and Drake M. J. (1979) GCA 43, 689-707. [7] Weisberg M. K. et al. (1990) Meteoritics 25, 269-279. [8] Meibom A. et al. (1999) LPSC XXX. [9] Zanda B. et al. (1993) Meteoritics 28, 466-467. [10] Lee M. S. et al. (1992) GCA 56, 2521-2533. [11] Sugiura N. et al. (1999) LPSC XXX. [12] Weisberg M. K. et al. (1988) EPSL 91, 19-32. [13] Nagahara H. (1982) Proc. NIPR 25, 86-96. [14] Moren A. E. and Goldstein J.I. (1979) EPSL 43, 182-196.

The collection of micrometeorites in Yamato Meteorite Ice Field of Antarctica in 1998.

YADA T.¹ and KOJIMA H.²

¹ Dept. Earth & Planet. Sci., Kyushu Univ., Fukuoka 812-8581

² Natl Inst. Polar Res., Kaga, Itabashi-ku, Tokyo 173-8515

Introduction

Yamato meteorite bare ice field is one of the most enriched places in meteorites in the world. In the past, several researches of meteorites were done there by the traverse parties of the Japanese Antarctic Research Expedition (JARE), shown as YANAI, 1976; KOJIMA and YANAI, 1981. Between October 1998 and February 1999, the traverse party of the 39th JARE performed a research of meteorites in the Yamato and Belgica bare ice fields. In this research, we tried to collect micrometeorites by melting blue ice around the Yamato Mountains. At bare ice of the edge of the Antarctic Continent, MAURETTE et al. (1991) successfully collected micrometeorites. But, at a bare ice inside the Continent, there were no research for micrometeorites. The purpose of this research was to collect micrometeorites and to estimate the density of micrometeorites at bare ice inside the Antarctic Continent.

Method

The sampling process of micrometeorites from blue ice was basically divided into two parts, melting ice and filtering the melted water. For the former, we used three boilers for heating unfrozen liquid, a storage tank for keeping the unfrozen liquid, a water pump for circulation of the unfrozen liquid, and a radiator for heating and melting ice (Fig. 1). The latter part was composed of sieve holders, an eliminator and a vacuum pump for pull up the melted water through the sieves. The openings of the stainless steel sieves

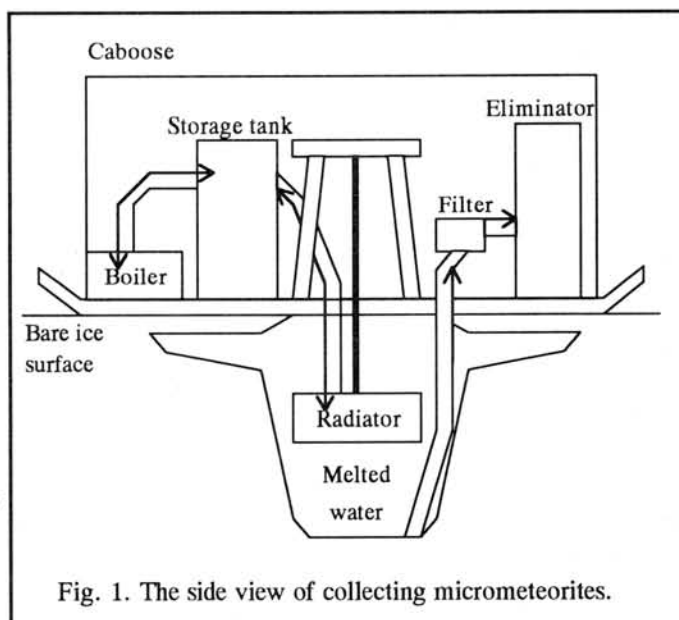


Fig. 1. The side view of collecting micrometeorites.

were $10\ \mu\text{m}$, $40\ \mu\text{m}$, $100\ \mu\text{m}$, and $238\ \mu\text{m}$. It took about seven hours for melting 2~3 tons of ice and an hour for filtering glacier sand settled down the bottom of the melted water. We didn't mix

the water completely, so the shape of the cross section of the melted water hole was like an upside down hat, shown in Fig. 1. Captured particles were immediately preserved in sealed sacks still on the stainless steel and frozen until the experimental work in NIPR, Japan.

Sampling Site

We performed the collection in three areas of the bare ice field around the Yamato Mountains; south end of the Yamato bare ice field, the western area from the Kuwagata Nunatak which is located in South Yamato Nunataks, and the southeast area from JARE IV Nunataks. In the first area, three times of the collections were done between November 20 and 22, 1998. This area is 30 km southern away from the south end of the South Yamato Nunataks. In the second, we carried out the collections at eleven places between December 3 and 9, 1998. This area is located at side flow of the glacier against Kuwagata Nunatak and 2 km to the Nunatak. The third, we did the collection at ten places between January 5 and 12, 1999. This area is upper side of the glacier flow against JARE IV Nunataks and 2 km to the nearest Nunatak.

Throughout the collection in three areas, the weather was 15 m/s in wind and -20 °C in temperature on the average.

Gained Samples

The total amounts of the water we have melted in seventeen days were estimated about 60 tons. Based on the *in situ* observation of three or four sieves by a stereo microscope, 100~200 black irregular-shaped particles were on the 100 μ m sieves and about 500 of them on the 40 μ m sieves. So it is estimated that about 10,000 of micrometeorites were totally collected on the 24 sets of sieves. These collected samples are now under observation for description of Antarctic Micrometeorite Catalog.

Acknowledgements

We are very grateful to Msr. Y. SATO, G. OHNO, H. HANDA, H. KIRIYAMA, H. KAIDEN, and K. MEKI, the members of the 39th JARE meteorite and cosmic dust search traverse party. We would express special thanks to Prof. K. SHIBUYA, the leader of the JARE-39, and all other members of the JARE-39, for supporting our traverse cordially.

References

- KOJIMA H. and YANAI K. (1981) *Mem. Natl Inst. Polar Res.*, Spec. Issue, 20, 69.
- MAURETTE M. et al. (1991) *Nature*, 351, 44.
- YANAI K. (1978) *Mem. Natl Inst. Polar Res.*, Spec. Issue, 8, 1.

Petrological comparison between chondrules of Sahara 97096 (EH3) and Allende (CV3)

Tatsuya Yamanouchi and Hirokazu Fujimaki

Institute of Mineralogy, Petrology, and Economic Geology,
Tohoku University, Sendai, Miyagi 980-8578, Japan

Introduction

Sahara 97096 (SAH 97096) is an EH3 chondrite based on the presence of niningerite, absence of alabandite, the high Si content in kamacite and the wide compositional ranges of silicates (Weisberg and Prinz, 1998). This type of meteorite is considered to have been formed under extremely reduced condition and to preserve the most primitive features.

Allende is a CV3 chondrite. As known by many studies of this meteorite, it consists of varied materials which include high temperature condensates to low temperature ones. Its matrix consists mainly of olivines with high FeO contents. In contrast, silicates of type I chondrules (McSween, 1977), which are most common in this meteorite, have very low FeO contents. Most of these chondrules contain troilite or metal. Thus, the chondrules were probably formed in more reduced condition than the matrix were formed.

Accordingly, most of chondrules in both the E and C chondrites are thought to have been formed under highly reduced condition. The purpose of this study is to compare petrological features of them and to clarify analogies and differences between them. For this purpose, SAH 97096 and Allende are the most appropriate samples because they suffered very low degree of metamorphism. In this study, a thin section of SAH 97096 (10×10 mm) and one of Allende (30×20 mm) have been used, and we have carried out observations by a scanning electron microscope and chemical analyses of minerals and glasses by an electron probe microanalyzer.

Sample Description

SAH 97096 is a highly primitive EH3 chondrite. The shapes of the chondrules are clear and their rims are sharp in the matrix. Most of the chondrules have porphyritic texture; this differs from chondrules in Yamato-691 whose main type of texture is radial pyroxene (Ikeda, 1989). Radial pyroxene and cryptocrystalline chondrules are minor type in SAH 97096. No chondrule has barred texture in our thin section. The main constituents of chondrules are low-Ca orthopyroxene and clinoenstatite that forms polysynthetic twinning. The other constituents are olivine, high-Ca pyroxene, silica mineral, transparent glass, metal and sulfide. Olivines exist mostly in the core of low-Ca pyroxenes. High-Ca pyroxenes are relatively small in size (less than 10 μ m) and appear in the glass. Silica minerals appear inside the chondrules or along the chondrule rims, and they are anhedral. Nearly all the groundmasses of the chondrules are clear glass. Devitrification of glass scarcely occurs. Although the amounts of metal and sulfide in the chondrules are generally small, one of the chondrules includes a large aggregate of metal and sulfide (about 50 μ m in diameter). Most

of sulfides are troilite, though small amounts of oldhamite and niningerite are recognized. This is different feature from the chondrules in Qingzhen, in which troilite and oldhamite are always found (Grossman et al., 1985).

Chondrules in Allende also have sharp rims. They have mainly porphyritic texture similar to those in SAH 97096. Barred texture is also common in Allende as well. Only a chondrule has radial pyroxene texture. The main mineral in Allende chondrules is olivine. In the most cases, low-Ca pyroxene occupies little volume of a chondrule. In a few chondrules, its amount is larger than that of olivine and some olivines appear to be enclosed in low-Ca pyroxene. Nearly all of low-Ca pyroxene are clinoenstatite indicated by polysynthetic twinning under an optical microscope. High-Ca pyroxene is also recognized in these chondrules and closely associated with low-Ca pyroxene and groundmass glass. This is similar to that in SAH 97096 chondrules. Groundmass in Allende chondrules is mostly devitrified glass. Clear glass was not observed. Opaque phases appear both in chondrules and along chondrule rims, but the amounts of them in chondrules are considerably small. Most of them are troilite. Around the most of chondrules, the rims consisting of olivine with high FeO contents are also observed.

Result of chemical analyses

Olivine in SAH 97096 chondrules is nearly pure forsterite, and that in Allende chondrules generally has very high Mg# (higher than 90). In Allende, one chondrule consisting mainly of olivine with relatively low Mg# (about 65~80), called type II chondrule (McSween, 1977), is recognized (Fig. 1). The forms of olivines in the type II chondrule are mostly euhedral differing from ones in the type I chondrules. We found that one of olivines in the type II have an extremely magnesian core (Mg#=99). Ca contents of olivine in Allende chondrules are somewhat higher than those in SAH 97096 (Fig. 4).

Pyroxene in chondrules in both of the chondrites has very high Mg#. In a pyroxene-rich porphyritic chondrule in Allende, Mg# of pyroxene is somewhat lower than those in the other chondrules. The range of Ca contents of pyroxene in Allende chondrules is wider than that in SAH 97096 (Fig. 2). Cr contents of the pyroxene in Allende chondrules are slightly higher than that in SAH 97096. In the chondrules in both of the meteorites, Al contents of high-Ca pyroxene seem to be higher than those of most of low-Ca pyroxene (Fig. 3).

Chemical composition of groundmass considerably differs between Allende and SAH 97096 (Table 1). The difference of SiO₂ contents is clearly distinct. In Allende, although CaO and Al₂O₃ contents of groundmass have wide range, most of them are higher than those in SAH 97096. Na₂O contents of groundmass in Allende have wider range than those in SAH 97096. It is a noticeable feature that groundmass in SAH 97096 contains minor amounts of S and Cl.

References

- M. K. Weisberg and M. Prinz (1998) Lunar Planet. Sci. XXIX, Abstract #1741
- H. Y. McSween, Jr (1977) Geochim. Cosmochim. Acta 41, 1777-1790
- Y. Ikeda (1989) Proc. NIPR Symp. Antarct. Meteorites, 2, 75-108
- J. N. Grossman et al. (1985) Geochim. Cosmochim. Acta 49, 1781-1795

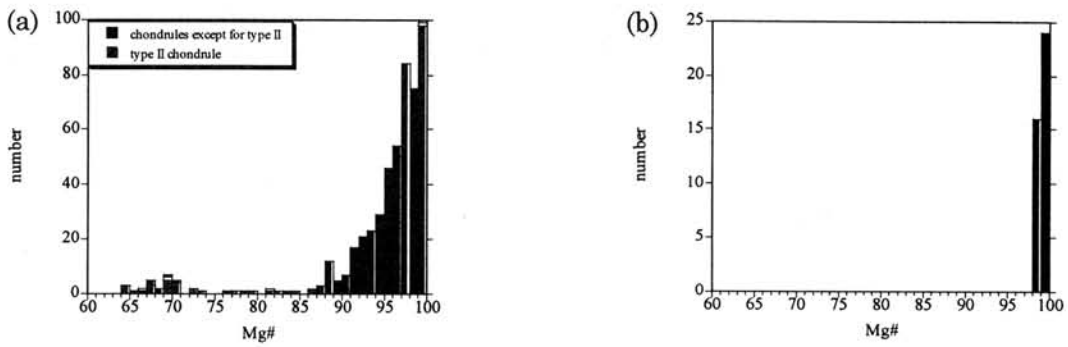


Fig. 1 Frequency diagram of olivine in chondrules (a) Allende (b) SAH 97096

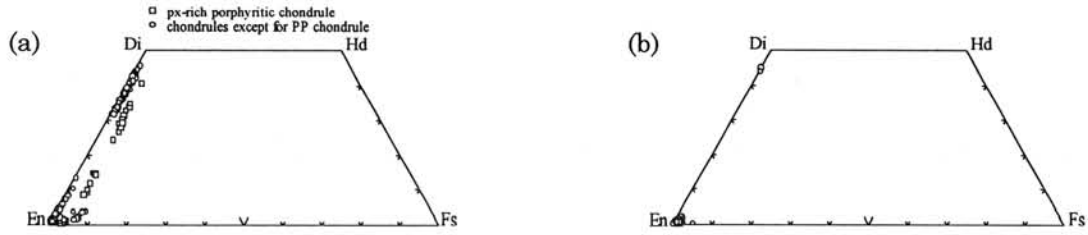


Fig. 2 Quadrilateral of pyroxene in chondrules (a) Allende (b) SAH 97096

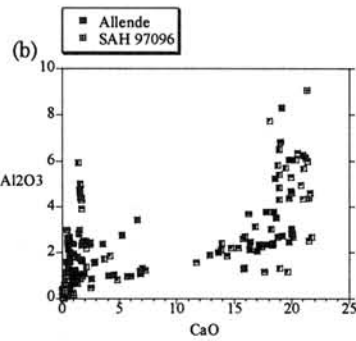
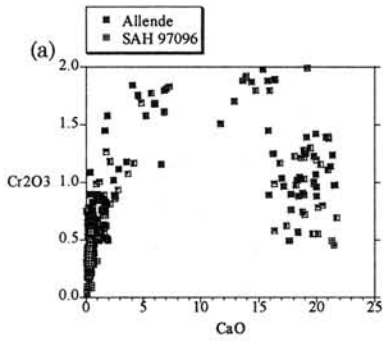


Fig. 3 Plot of pyroxene (wt%) (a) Cr₂O₃ vs CaO (b) Al₂O₃ vs CaO

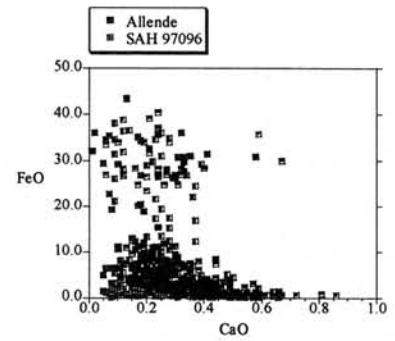


Fig. 4 Plot of CaO vs FeO in olivine (wt%)

Groundmass of Allende chondrules													
SiO ₂	46.25	45.36	44.35	45.09	43.16	47.00	46.03	47.89	43.29	42.39	44.91	46.39	47.17
TiO ₂	1.07	0.56	0.03	0.45	0.09	0.37	0.21	0.83	0.02	0.46	0.05	1.13	0.05
Al ₂ O ₃	26.96	31.16	34.63	21.56	32.49	27.05	30.54	22.82	33.73	33.06	32.81	23.45	33.08
FeO	0.71	0.30	0.64	3.57	0.90	0.85	0.71	3.16	0.84	1.07	0.61	0.58	0.62
MnO	0.05	0.05	0.02	0.15	0.08	0.06	0.03	0.13	0.01	0.12	0.04	0.08	0.05
MgO	4.40	3.24	0.64	9.16	1.92	5.38	3.14	4.26	0.65	0.62	0.59	10.06	0.43
CaO	17.87	17.02	2.50	7.86	2.82	9.61	18.64	14.09	1.42	3.25	8.28	17.87	17.77
Na ₂ O	2.12	2.62	15.31	9.56	14.20	8.03	0.56	5.33	16.02	13.37	9.27	0.91	1.54
K ₂ O	0.18	0.06	1.93	0.89	1.81	0.81	0.02	0.53	1.85	1.74	1.10	0.03	0.03
S													
Cl													
total	99.61	100.37	100.04	98.29	97.46	99.14	99.88	99.03	97.83	96.06	97.65	100.50	100.75
Groundmass of SAH 97096 chondrules													
SiO ₂	62.01	67.77	65.21	60.84	56.70	63.72	69.29	54.20	70.99				
TiO ₂	0.54	0.21	0.28	0.31	0.16	0.41	0.22	0.32	0.09				
Al ₂ O ₃	23.49	18.49	18.61	17.82	23.95	18.95	20.13	21.27	14.84				
FeO	0.49	0.23	0.19	0.90	0.50	0.19	0.20	1.79	0.53				
MnO	0.00	0.02	0.06	0.07	0.05	0.02	0.02	0.05	0.04				
MgO	0.49	1.53	2.72	5.65	4.66	3.69	0.06	10.12	3.27				
CaO	4.82	6.21	0.76	1.36	7.74	0.75	0.42	7.26	0.74				
Na ₂ O	4.29	4.19	9.82	8.55	5.65	9.77	4.42	4.22	8.02				
K ₂ O	0.47	0.43	0.90	0.90	0.41	1.14	0.66	0.36	0.79				
S	0.26	0.46	0.66	0.70	0.26	0.36	0.72	0.37	0.50				
Cl	0.56	0.45	1.10	0.99	0.48	0.91	1.22	0.35	0.21				
total	97.43	99.98	100.32	98.09	100.56	99.91	97.34	100.32	100.00				

Table 1. Chemical composition of groundmass

Purely physical separation of the phase enriched in noble gases from the Allende meteorite.

Shiho Zaizen, Eiji Nakasyo, Teruyuki Maruoka, Jun-ichi Matsuda

Department of Earth and Space Science, Graduate School of Science,

Osaka University, Toyonaka, Osaka 560-0043, Japan

INTRODUCTION

Noble gases were concentrated in a very small fraction (named "Q") of the chondrites [1]. Lewis *et al.* [1] obtained the "original residue" of the Allende CV3 meteorite by HCl-HF (and CS₂) treatment. Then they etched the original residue with oxidizing acids like HNO₃, and obtained the "oxidized residue". The phase Q is the fraction dissolved in the oxidization procedure, in which heavy noble gases (Ar to Xe) are strongly enriched.

Matsuda *et al.* [2] reported that noble gases were greatly enriched in the fine black material which floated on the water during freeze-thaw disaggregation of the Allende meteorite. This material had noble gas compositions similar to the original residues. This new separation technique allows us to obtain a fraction highly enriched in primordial noble gases without the chemical treatment in which more than 99% of precious meteoritic matter was dissolved. Absence of ¹²⁹Xe excess indicated that the physical separation should be free from the re-adsorption. Therefore, the physical separation is more proper than the chemical separation to obtain the pure primordial noble gases.

Matsuda *et al.* [2] also reported that the Xe-Q/Xe-HL ratio in one floating fraction (A1) was different from that in the other (A1A). Therefore, they thought that Q was not completely tightly combined with the presolar diamond, although Q- and HL- components are closely associated during the chemical treatment.

In this study, we attempt to check the reproducibility of this purely physical separation method, and to examine whether the abundance ratio of Q- and HL- components is uniform or not among different samples.

SAMPLE AND EXPERIMENTAL PROCEDURE

The Allende meteorite was immersed in distilled water, which was frozen in a freezer and then put into an ultrasonic bath for 40 min. The meteorite gradually began to disintegrate after several such cycles. The chondrules and inclusions sank, whereas the black matrix suspended in the water for a while after ultrasonic vibration. The matrix material sank usually in a day or so. We scooped up very fine black material floated on the water surface with aluminum foil and dried it at 120°C for 1hr. We could prepared 2.55mg as a total amount from 3.846g bulk Allende, and designated one of these samples as C1-7 (0.23mg).

The sample C1-7 was loaded into a molybdenum crucible and heated in vacuum by a tantalum heater at 800, 1200 and 1600°C for noble gas analyses.

RESULT AND DISCUSSION

We compare here C1-7 with the bulk [3], the original residue (3C1 [1]), the oxidized residue (3C2 [1]), and the floating fractions (A1 and A1A which were prepared previously [2]).

Elemental Abundance

The elemental concentrations of C1-7 are about two orders of magnitude higher than those of bulk Allende (Fig.1). The elemental abundance pattern of C1-7 is very similar to that of the

original residue.

Isotopic Ratios

In $^{134}\text{Xe}/^{132}\text{Xe}$ vs. $^{136}\text{Xe}/^{132}\text{Xe}$ diagram (Fig.2-a), the data points of C1-7 lie on the mixing line between Xe-Q and Xe-HL. The Q/HL ratio is larger at higher temperatures. Therefore, it is suggested that the Q component is released at higher temperatures than the HL component.

This figure also shows that the Q/HL ratio of C1-7 total fraction is different from that of A1A. We can confirm the heterogeneity of the Q/HL ratios in the floating fractions.

In $^{129}\text{Xe}/^{132}\text{Xe}$ vs. $^{136}\text{Xe}/^{132}\text{Xe}$ diagram (Fig.2-b), the data point of the original residue is not on the mixing line of Xe-Q and Xe-HL, and situated above the line. The data points of A1 and A1A fall clearly below those of the bulk and the original residue, and lie on the mixing line of Xe-Q and Xe-HL. Matsuda *et al.* [2] reported the difference of the $^{129}\text{Xe}/^{132}\text{Xe}$ ratio between their floating fractions and the original residues. However the data points of C1-7 do not lie on the mixing line, and have the tendency to the upper side from the line with increasing the extraction temperatures. It is conceivable that the sample C1-7 contains the host phase of ^{129}I .

CONCLUSION

In this study, floating fraction C1-7 is also very similar to the original residue elementally and isotopically. Thus, it is again confirmed that this physical separation is useful method for isolating the gas-rich fraction similar to the original residue. However, the Q/HL ratios and the $^{129}\text{Xe}/^{132}\text{Xe}$ ratios are different among the samples separated by this method.

REFERENCE

- [1] Lewis R. S., Srinivasan B. and Anders E. (1975) *Science* **190**, 1252-1262.
- [2] Matsuda J., Amari S. and Nagao K. (1999) *Meteorit. Planet. Sci.* **34**, 129-136.
- [3] Lewis R. S., Gros J. and Anders E. (1977) *J. Geophys. Res.* **82**, 779-792.
- [4] Wieler R. and Baur H. (1994) *Meteoritics* **29**, 570-580.
- [5] Ozima M. and Podosek F. A. (1983) *Cambridge Univ. Press* 367pp.
- [6] Huss G. R. and Lewis R. S. (1994) *Meteoritics* **29**, 791-810.

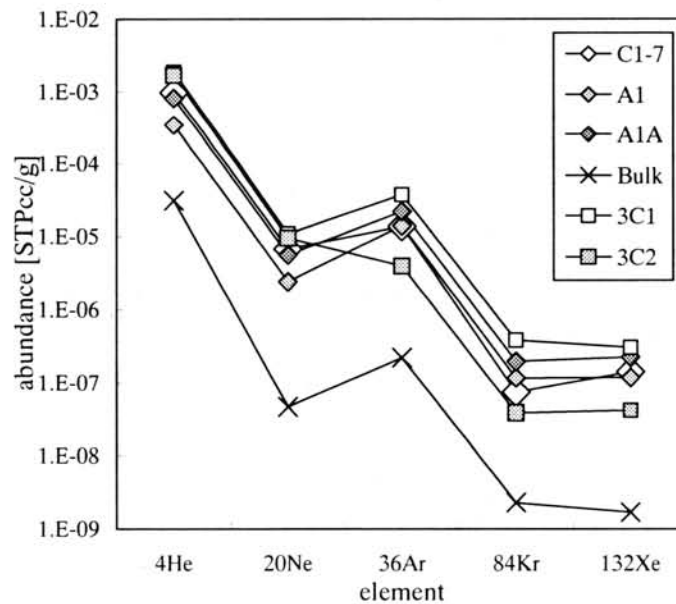


Fig.1 Elemental abundance.

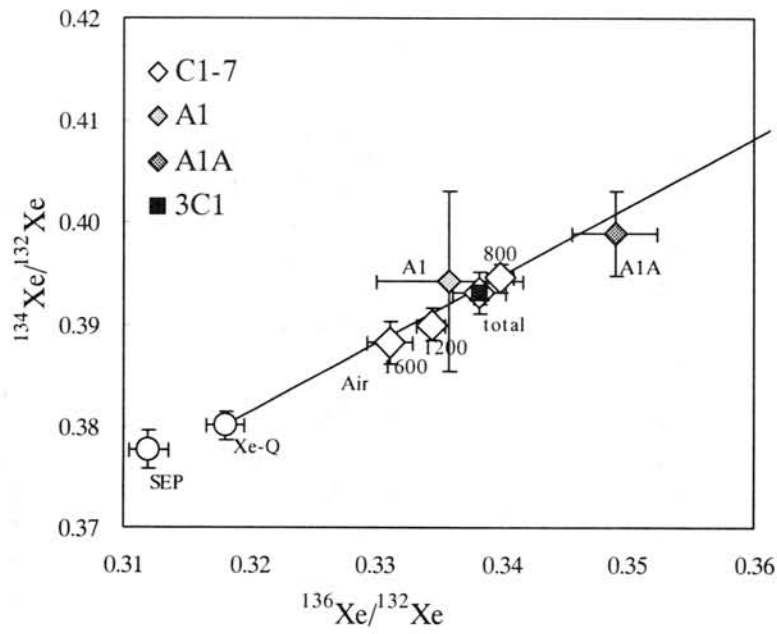


Fig. 2-a $^{134}\text{Xe}/^{132}\text{Xe}$ vs. $^{136}\text{Xe}/^{132}\text{Xe}$.

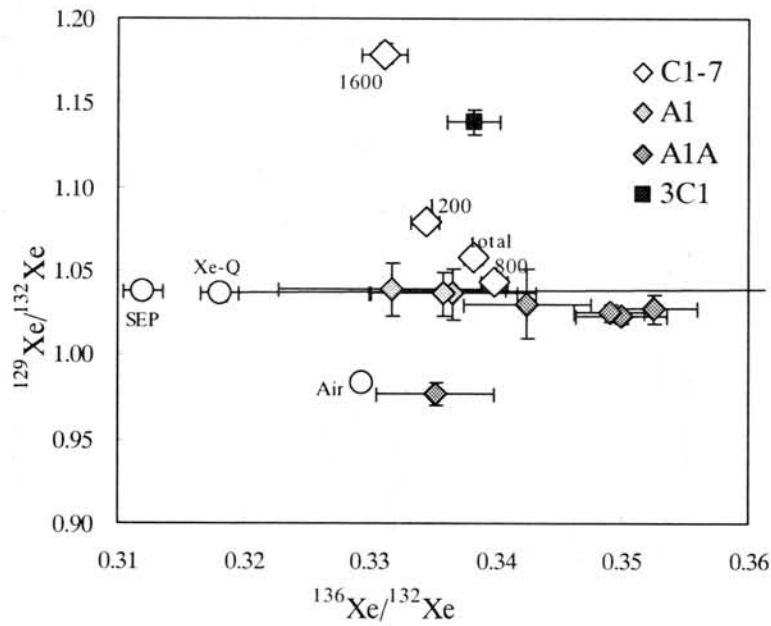


Fig. 2-b $^{129}\text{Xe}/^{132}\text{Xe}$ vs. $^{136}\text{Xe}/^{132}\text{Xe}$.

Data Source

SEP [4], Air [5], Xe-HL, Xe-Q [6]

AUTHOR INDEX

Aoki Y.	127	Kimura M.	67
Asame K.	1	Kimura S.	69
Bobrov A. V.	96	Kiss A. Z.	15
Bodó P.	15	Kita N. T.	43, 72, 111, 113
Boesenberg J. S.	43	Kitamura M.	177
Bogard D. D.	157	Kiuchi H.	75
Buchanan P. C.	4	Klandrud S. E.	62
Bérczi Sz.	6, 9	Kobatake H.	78
Chaplygin O. V.	96	Kobayashi T.	116
Chikami J.	12	Koezuka T.	28
Cielaszyk E.	62	Kojima H.	47, 81, 121, 139, 190
Clayton R. N.	121	Kojima T.	82
Cloudt S.	62	Kokubo M.	116
Crozaz G.	18	Komatsu M.	85
Detre C. H.	15	Kondo M.	64
Don G.	15	Kondo N.	24, 119, 143
Ebihara M.	154	Kondorosi G.	88, 121
El Goresy A.	67	Kurat G.	1, 99
Field M. P.	166	Kuribayashi K.	179
Floss C.	18	Kusakabe M.	59
Franchi I. A.	136	Lindstrom D. J.	4
Fujimaki H.	78, 192	Lindstrom M. M.	4, 90
Fujita T.	21	Lukács B.	6, 9
Fukuoka T.	24, 143, 175	MacPherson, G. J.	93
Funaki M.	26	Marakushev A. A.	96
Gál-Sólymos K.	6	Martinás K.	6
Hanamoto T.	28	Maruoka T.	1, 99, 130, 195
Hashimoto A.	37	Matsuda J.	1, 99, 130, 195
Herzog G. F.	166	Mayeda T. K.	121
Hirata N.	31	McKay G. A.	102
Hiroi T.	34	Mikouchi T.	102
Hirota Y.	88	Misawa K.	88
Hiyagon H.	37, 182	Mitreikina O. B.	105
Holba Á.	9	Miura Y. N.	108
Honda M.	116	Miyamoto M.	12, 85, 102
Hori K.	88	Mori T.	24, 143, 175
Hoshino H.	168	Morikawa N.	88
Hutson M.	40	Morishita Y.	72, 111, 113
Ikeda Y.	43, 72	Mostefaoui S.	111
Imae N.	24, 47, 50, 121, 139, 143, 175	Murakami T.	24, 143
Imai H.	53	Nagahara H.	111, 113
Ishii T.	172	Nagai H.	116
Itoh D.	56	Nagao K.	59, 108, 148, 151
Jabeen I.	59	Nakai I.	24, 119, 143
Japan AMM working group	175	Nakamura N.	47, 88, 121
Jull A. J. T.	62	Nakamura T.	24, 50, 59, 119, 123, 125, 141, 143, 148, 151, 175
Kaiden H.	81	Nakamuta Y.	125, 127
Kaito C.	69	Nakasyo E.	130, 195
Kallemeyn G. W.	154		
Kawabata T.	28, 64		
Kawano S.	1		
Keil K.	18, 157		

Namba M.	99	Tsujimoto Y.	28
Naraoka H.	133	Tsukamoto K.	78, 179
Nehru C. E.	43, 72	Tunyi I.	26
Newton J.	136	Tóth I.	15
Ninagawa K.	139	Ul'yanov A. A.	182
Nogami K.	24, 143	Ushikubo T.	182
Noguchi T.	24, 50, 119, 125, 141, 143, 175	Uzonyi I.	15
Nozaki W.	50, 143, 175	Wada S.	69
Ohashi H.	24, 143	Warren P. H.	185
Ohmori R.	24, 143	Wasson J. T.	28
Ohnishi I.	145	Weisberg M. K.	72, 187
Ohtani E.	67	Yada T.	81, 190
Okazaki R.	108, 148	Yamaguchi A.	18, 31
Orlicky O.	26	Yamanouchi T.	192
Osawa T.	151	Yatagai T.	82
Ozaki H.	154	Yurimoto H.	53
Ozawa K.	113	Zaizen S.	195
Pillinger C. T.	136	Zinovieva N. G.	105
Pinault L. J.	157		
Porubcan V.	26		
Prinz M.	43, 72, 187		
Ruzicka A.	40, 160		
Saiki K.	172		
Sano Y.	24, 175		
Sasaki M.	119, 143		
Sasaki S.	34		
Satoh H.	78, 163, 179		
Sawada S.	121		
Schléder Z.	15		
Schnabel C.	166		
Scott E. R. D.	157		
Sekine T.	31		
Sherrell R. M.	166		
Snyder G. A.	160		
Sugiura N.	168, 182		
Suzuki A.	67		
Tachibana S.	75, 169, 179		
Takamura Y.	179		
Takaoka N.	123, 148, 151		
Takeda H.	172		
Tamaki M.	121		
Taylor L. A.	160		
Taylor S.	166		
Tazawa Y.	24		
Terada K.	24, 119, 143, 175		
Terada Y.	119		
Togashi S.	72, 111		
Tomeoka K.	56, 82, 145		
Tomiyama T.	177		
Toyoda S.	139		
Tsuchiyama A.	28, 64, 75, 169		

